A Flexible Approach to [1]Ferrocenophanes:

Metallopolymers through a New Family of Chiral Sandwich Compounds

A Thesis Submitted to the College of

Graduate Studies and Research

in Partial Fulfillment of the Requirements

for the Degree of Doctor of Philosophy

in the Department of Chemistry

University of Saskatchewan

Saskatoon

By

SAEID SADEH

Permission to Use

In presenting this thesis in partial fulfilment of the requirements for a Postgraduate degree from the University of Saskatchewan, I agree that the Libraries of this University may make it freely available for inspection. I further agree that permission for copying of this thesis in any manner, in whole or in part, for scholarly purposes may be granted by the professor or professors who supervised my thesis work or, in their absence, by the Head of the Department or the Dean of the College in which my thesis work was done. It is understood that any copying or publication or use of this thesis or parts thereof for financial gain shall not be allowed without my written permission. It is also understood that due recognition shall be given to me and to the University of Saskatchewan in any scholarly use which may be made of any material in my thesis.

Requests for permission to copy or to make other use of material in this thesis in whole or part should be addressed to:

Head of the Department of Chemistry

University of Saskatchewan

Saskatoon, Saskatchewan (S7N 5C9), Canada

ABSTRACT

Applying known "Ugi's amine" chemistry and based on a literature procedure, (R,R,S_p,S_p)-2,2′-bis(α-N,N-dimethylaminoethyl)-1,1′-dibromoferrocene was prepared and the pathway was modified for a synthesis on a larger scale. Adding two more synthetic steps, amino groups were replaced with methyl groups which resulted in the planar-chiral (S_p,S_p)-1,1′-dibromo-2,2′-di(isopropyl)ferrocene (**120**). Starting with **120**, lithium-bromine exchange using *n*BuLi and different solvent systems was investigated and a reliable method was developed. Salt-metathesis reaction of (S_p,S_p)-1,1'-dilithio-2,2′-di(isopropyl)ferrocene (**121**) and Ar′$GaCl_2$ [Ar′ = 2-(Me_2NCH_2)C_6H_4] was performed and yielded the respective [1]ferrocenophane ([1]FCP) **122** with high conversions. This gallium-bridged [1]FCP **122** was isolated by crystallization from the reaction mixture and its molecular structure in the solid state was determined. The Differential Scanning Calorimetry (DSC) thermograph of the gallium-bridged [1]FCP **122** proved that the [1]FCP is a potential candidate for thermal ring-opening polymerization (ROP). The starting compound Ar′$InCl_2$ was reacted with **121** and yielded a mixture of an indium-bridged [1]FCP (**126_1**) and a [1.1]FCP (**126_2**). Reacting the bulkier reagent (Mamx)$InCl_2$ [Mamx = 2,4-*t*Bu_2-6-(Me_2NCH_2)C_6H_2] with **121** resulted in the selective formation of an indium-bridged [1]FCP (**125_1**). All attempts to isolate the strained indium-bridged [1]FCP were unsuccessful as it reacted further through a spontaneous ROP under conditions of its formation. DFT (Density Functional Theory) calculations were performed to investigate the structure and reactivity of synthesized indium-bridged [1]FCPs. Moreover, the effects of different substituents on the unusual reactivity of indium-bridged [1]FCP was studied.

A group of amino(dichloro)boranes with different substitutions [Et_2NBCl_2, *i*Pr_2NBCl_2, and *t*Bu(Me_3Si)$NBCl_2$] were reacted with **121** and its 3-pentyl substituted analog [(S_p,S_p)-1,1′-

dilithio-2,2′-di(3-pentyl)ferrocene] (**131**). Six bora[1]ferrocenophanes were synthesized and purified with different techniques including crystallization, sublimation, and flask-to-flask condensation. While salt-metathesis reactions with Et_2NBCl_2 were very selective toward [1]FCPs, employing the amino(dichloro)boranes iPr$_2$NBCl$_2$ and tBu(Me$_3$Si)NBCl$_2$ resulted in formation of significant amounts of bis(boryl)ferrocenes as byproducts. A systematic study was performed, which resulted in increasing the reaction temperature and controlling the rate of addition of the amino(dichloro)boranes to increase the yield of desired [1]FCPs. Thermal ROP of selected bora[1]FCPs were performed and the resulting polymers were analyzed by Gel Permission Chromatography (GPC) and Dynamic Light Scattering (DLS).

Synthesis of chiral group-14-bridged [1]FCPs were attempted by salt-metathesis reaction of **121** with tBuSnCl$_2$ and Me$_2$SiCl$_2$. The respective strained [1]FCPs (**140** and **141**) were formed in the reaction mixture quantitatively and isolated by vacuum sublimation in good yields. The molecular structures in the solid state of both [1]FCPs were determined and it was deduced that an interaction between alkyl groups increased the strain in the molecules. Measuring DSC thermographs proved these compounds to be suitable for thermal ROP.

A group of chiral phosphorus-bridged [1]FCPs (**142**, **143** and **144**) with different groups in the bridging position (Ph, iPr, and tBu) were prepared by reacting **121** with the respective phosphorus dihalides. These compounds were stable enough to be purified by column chromatography. The molecular structures of isopropyl and phenyl substituted phosphorus-bridged [1]FCPs were determined in the solid state. Potential application of these phosphorus-bridged [1]FCPs as monodentate ligands for asymmetric catalysis will be studied in the future.

ACKNOWLEDGMENTS

I would like to express my gratitude to my supervisor, Dr. Jens Müller, for his support, patience and encouragement throughout my PhD studies.

I would like to thank University of Saskatchewan and Department of Chemistry for supporting me during my PhD program; the members of my advisory committee for their assistances and the staff at the Saskatchewan Structural Science Centre and the Department of Chemistry. In particular, I am thankful to Dr. Keith C. Brown for his help for NMR measurements and Dr. Wilson J. Quail for X-ray diffraction analyses.

A big thank you is due to all past and present Müller group members for helpful discussions and the nice atmosphere in the lab.

I would like to acknowledge my parents Dr. Fazlollah Sadeh and Pouran Dehabadi for allowing me to realize my own potentials. All the support they have provided me over the years was the greatest gift anyone has ever given me.

Last, but certainly not least, I would like to thank my wife Azadeh Kosari for her understanding and love during the past few years. Her support and encouragement was in the end what made this dissertation possible.

TABLE OF CONTENTS

LIST OF FIGURES

LIST OF SCHEMES

Scheme page

LIST OF TABLES

LIST OF ABBREVATIONS

Abbrevations

Ar′.....2-(Me_2NCH_2)C_6H_4

cod.....1,5-cyclooctadiene

Cp.....cyclopentadienyl

CV.....cyclic voltammetry

dba.....dibenzylideneacetone

DLS.....dynamic light scattering

DSC.....differential scanning calorimetry

ESR.....electron spin resonance

FCP.....ferrocenophane

fc.....(C_5H_4)$_2$Fe

GPC.....gel permeation chromatography

HOMO.....highest occupied molecular orbital

LUMO.....lowest unoccupied molecular orbital

Mamx..... 2,4-*t*Bu_2-6-(Me_2NCH_2)C_6H_2

Me_2Ntsi..... $C(SiMe_3)_2SiMe_2NMe_2$

Mes.....2,4,6-trimethylphenyl

PDI.....poly dispersity index

PFS.....poly(ferrocenylsilane)

Pytsi..... $C(SiMe_3)_2SiMe_2(2\text{-}C_5H_4N)$

r.t.....room temperature

R_g.....radius of gyration

R_h.....hydrodynamic radius

ROP.....ring-opening polymerization

TGA..... thermal gravimetric analysis

tmeda.....N,N,N′,N′-tetramethylethylenediamine

CHAPTER 1

INTRODUCTION

Strained cyclic organic compounds have been studied intensely over the last few decades. These compounds are particularly interesting as they can go through ring-opening polymerization (ROP) and produce organic polymers. Metallacyclophanes are a class of strained cyclic organometallic compounds that contain sandwich moieties of transition metals. In these compounds, two π-hydrocarbon rings of the sandwich unit are connected by main group elements. These species have attracted considerable attention over the last twenty years. [n]Metallocenophanes (**1**; Figure 1) are a group of metallacyclophanes that contain a transition metal M and two η^5-cyclopentadienyl (Cp) anions, which are connected by n bridging elements. The first strained metallocenophane, a [3]ferrocenophane ([3]FCP), was reported in 1957 by Rinehart Jr. et al.[1] (**2**; Figure 1). A few years later, the first [2]FCP was reported by the same research group and the authors suggested that a [1]FCP analog would be too strained to exist.[2] Despite this assumption, 15 years later Osborne and co-workers successfully synthesized the first [1]FCP with silicon in the bridging position (**4**; Figure 1).[3]

To date, a large number of metallacyclophanes with a wide variety of transition metals, π-hydrocarbons and bridging elements, such as [n]metallarenophanes (**5**; Figure 1), where a sandwich unit is formed of two benzene rings, are known and this area of organometallic chemistry is developing very fast.

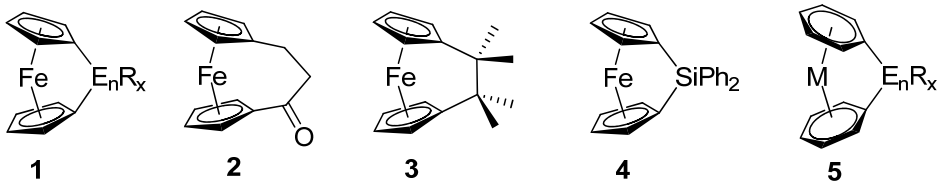

Figure 1. Metallocyclophanes.

1.1. Ferrocenophanes

Ferrocene is the text book example of metallocene compounds in which two Cp rings are oriented parallel to each other. This parallel structure is due to the overlapping of π orbitals of Cp ligands with s, p and d orbitals of the d^6 Fe(II) center. The introduction of short *ansa* [n] bridges (n = 1, 2, 3) changes the normal geometry of ferrocene to a ring-tilted structure. The dihedral angle between two Cp rings, known as α angle, is usually used to express the amount of ring tilt. There are also some other geometrical features to explain the tilted structures such as β, denotes the $Cp_{centroid}$-C_{ipso}-E angle, θ, shows C_{ipso}-E-C'_{ipso} angle, and δ, illustrates the $Cp_{centroid}$-M-$Cp'_{centroid}$ angle (Figure 2).

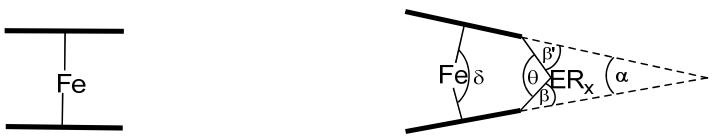

Figure 2. Illustration of ring tilt and the geometrical features for [n]ferrocenophanes.

In [n]ferrocenophanes, the tilt angle α decreases by increasing the number of same elements in the bridging position. For example, the tilt angle of dibora[2]ferrocenophanes is around 10°[4] while that of boron-bridged [1]FCPs is around 31°.[5] The tilt angle α increases by decreasing the size of the bridging element, therefore, larger α angles are expected while moving from left to right in a same row of periodic table; e.g., the α angle increases moving from aluminum (α ≈ 15° for alumina[1]ferrocenophane)[6] to silicon (α ≈ 21° for silicon-bridged [1]FCP)[7] to phosphorus (α ≈ 27° for phospha[1]ferrocenophane)[8, 9] to sulfur (α ≈ 31° for thia[1]ferrocenophane).[10, 11] For the same reason, the tilt angle α decreases by going down in a group of periodic table; e.g., the α angle decreases from silicon (α ≈ 21° for silicon-bridged [1]FCP)[7] to germanium (α ≈ 19° for germa[1]ferrocenophane)[12] to tin (α ≈ 14° for stanna[1]ferrocenophane).[13] The HOMO-LUMO

gap decreases by increasing the tilt angle in [1]FCPs and, therefore, a bathochromic shift of the lowest energy absorbance of the molecule is observed. By decreasing the size of bridging element a steady slope in the color of [1]FCPs is observable from orange (ferrocene) to red (sila- and phospha[1]ferrocenophanes, $\alpha \approx 20°$) to purple (bora- and thia[1]ferrocenophanes, $\alpha \approx 31°$).

In a tilted structure, the iron centre lies closer to the *ipso* carbon atoms and, thus, the carbon-carbon bond opposite to *ipso*-carbon atoms is shortened. In metallocenophanes, the distortion of planar Cp ligands increases the antibonding interactions and electron-electron repulsions and for metals with more than three d electrons, this results in an increase in the total energy of the molecule and introduces ring strain to the molecule. It is evidenced by density functional theory (DFT) calculations that the tilt angle α is an important factor for determining the tendency of FCPs toward ROP.[14] In the same calculation it was found that experimental values for ΔH^{ROP} is very similar to the calculated energy value for tilting Cp rings from the planar orientation. The present energy in [n]FCPs with large α angles ($\alpha \geq 12°$) and short *ansa* bridges ($n \leq 2$) can be released by ring-opening polymerization (ROP) reactions. In contrast to the other pathways toward organometallic polymers which go through polycondensation mechanism, and often do not result in high-molecular-weight metallopolymers, ROP of strained ferrocenophanes proceeds through a chain growth polymerization mechanism.[15] This method is capable of producing high-molecular-weight metallopolymers even at low levels of monomer conversion. The ROP of strained metallocenophanes is a very versatile method toward metallopolymers in which the properties of the polymers can be defined by introducing different metals and spacers in the polymer chain.

The salt-metathesis approach and the flytrap route are the two well-known synthetic pathways toward strained ferrocenophanes (Scheme 1). The salt-metathesis approach, as the most

commonly used pathway, requires the reaction of dilithioferrocene·tmeda (tmeda = N,N,N′,N′-tetramethylethylenediamine) or dilithioferrocene·ptmeda (ptmeda = N,N,N′,N′,N″,N″-pentamethyldiethylenetriamine) and an element dihalide equipped with a proper ligand system.[16, 17] This method was used for the preparation of most of elemental-bridged ferrocenophanes such as group 13 (B, Al, Ga), group 14 (Si, Ge, Sn), group 15 (P, As), group 16 (S, Se), group 4 (Ti, Zr, Hf) and group 10 (Ni, Pd, Pt). The "fly-trap" route on the other hand, is the less popular pathway which involves the synthesis of dianionic $(C_5H_4)_2(ER_x)_y$ species before reacting them with an iron(II) dihalide. This method was mostly used for the preparation of [2]FCPs. For instance, the dicarba[2]FCP **3** was prepared by fly-trap route in 1960[2] and the first [1]FCP, a silicon-bridged [1]FCP, was synthesized via salt-metathesis route.[3]

Scheme 1. Commonly Employed Synthetic Pathways for the Preparation of [n]Ferrocenophanes.

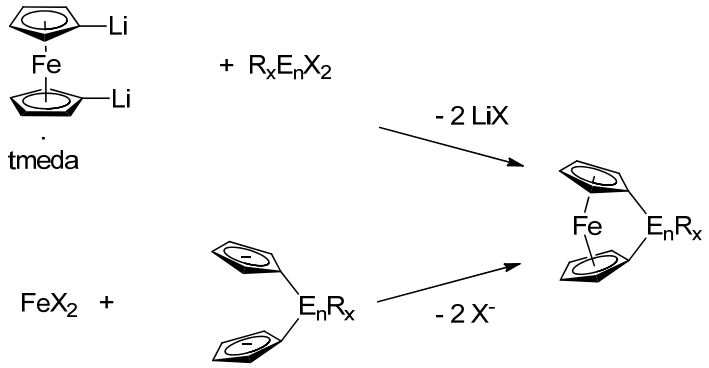

The ROP of strained ferrocenophanes was first reported by Manners et al. in 1992 where they successfully synthesized high-molecular-weight poly(ferrocenylsilane)s (PFSs) via thermal ROP of strained silicon-bridged [1]FCPs.[18] This achievement opened a new door to the area of metallocenophane chemistry and to date a large group of metallopolymers are synthesized by ROP of metallocenophanes. Among all the metallopolymers synthesized by this approach, PFSs are the most well-investigated compounds and nowadays are finding application in photonic

crystal displays,[19] precursor to ceramic materials[20] and redox-tunable capsules.[21] There are different techniques known for the ROP of ferrocenophanes and among them, those which go through a living process are the most interesting ones, as they give access to block copolymers. Block copolymers can be self-assembled in different morphologies, such as cylinders, spherical micelles, and vesicles, by being introduced to bock-selective solvents and these nanoscopic aggregated polymers have the potential to find application in nanoscience.[22-26]

Reviewing the entire published material in the area of metallocenophane chemistry is beyond the aim of this thesis and interested readers are referred to published reviews in this area where the synthesis, characterization and polymerization of different metallocenophanes are comprehensively explained.[27-29] However, in order to give an overview of importance of this contribution in the area of ferrocenophane chemistry following areas will be reviewed in the introduction chapter: ferrocenophanes with group 13, 14, and 15 and their ROP to yield poly(ferrocene)s, as well as planar-chiral ferrocenes.

1.1.1. Group-13-bridged [1]Ferrocenophanes

Boron-bridged [1]Ferrocenophanes

Boron-bridged [1]FCPs are particularly interesting as boron is the only second period element which has been successfully incorporated into the bridge of [1]FCPs. The first boron-bridged [1]FCPs (**6**) were reported by Braunschweig and Manners et al. in 1997, followed by another publication in 2000.[5, 30] However, the chemistry of boron-bridged [1]FCPs came to a halt after these two reports. In all cases, the synthesis involved the reaction of aminodichloroboranes equipped with bulky substituents on nitrogen (**6**: R = R′ = $SiMe_3$; R = $SiMe_3$, R′ = *t*Bu; R = R′ = *i*Pr) with dilithioferrocene·tmeda at room temperature (Scheme 2). It was mentioned that using

bulky amino groups on boron was absolutely essential as insoluble material were obtained when aminoboranes with less bulky amines, such as NMe_2, N(Ph)Me and N(Me)*n*Bu, were reacted with dilithioferrocene·tmeda. Boron-bridged [1]FCPs were isolated by crystallization followed by sublimation as dark red crystals.

Scheme 2. Synthesis of Boron-bridged [1]FCPs.

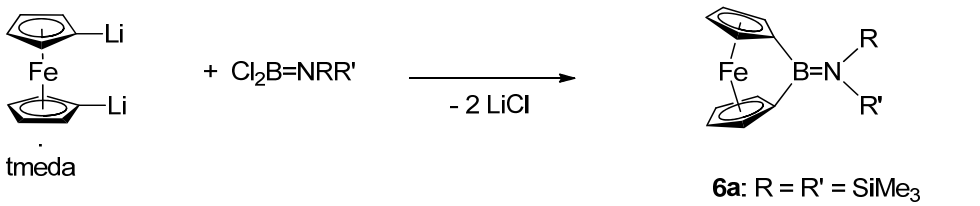

6a: R = R' = $SiMe_3$
6b: R = $SiMe_3$, R' = *t*Bu
6c: R = R' = *i*Pr

Boron is the smallest element which has been incorporated in the bridge of [1]FCPs and, consequently, boron-bridged [1]FCPs exhibited the highest tilt angle known to the date (approximately 32°). The UV/Vis absorbance of these species is also considerably red shifted [$(Me_3Si)_2$NBfc: λ_{max} = 479 nm, (Me_3Si)*t*BuNBfc: λ_{max} = 489 nm, $i Pr_2$NBfc: λ_{max} = 489 nm] [fc = $(FeC_5H_4)_2$] with respect to parent ferrocene (λ_{max} = 440 nm). The high tilt angle of boron-bridged [1]FCPs is also confirmed by the ^{13}C NMR spectroscopy of these species. In comparison to parent ferrocene (δ = 68.2), boron-bridged [1]FCPs demonstrate a considerably higher downfield shift for the *ipso*-carbon [$(Me_3Si)_2$NBfc: δ = 45.0, (Me_3Si)*t*BuNBfc: δ = 45.2, $(iPr)_2$NBfc: δ = 44.2]. However, these signals show up at a significantly lower field compared to other strained ferrocenophanes with similar or less tilt angles, thia[1]ferrocenophane (δ = 14.3). In ^1H NMR spectra, the characteristically large separation between α and β protons [$(Me_3Si)_2$NBfc: Δδ = 0.5, (Me_3Si)*t*BuNBfc: Δδ = 0.5, $(i Pr)_2$NBfc: Δδ = 0.5] confirms the tilting of the Cp moieties from planarity.

X-Ray diffraction analysis of the boron-bridged [1]FCPs revealed that the boron-bridged [1]FCPs **6** are highly strained with tilt angles of 32.4(2)° [$(Me_3Si)_2$NBfc] and 31.0(2)° [(Me_3Si)*t*BuNBfc] and 31.4(2)° [$(i$Pr$)_2$NBfc]. The boron atom is expected to adopt a trigonal planar configuration with 120° angle between the three substituents. However, the existing strain in these species reduces C-B-C angles to lower values [$(Me_3Si)_2$NBfc: 100.1°, (Me_3Si)*t*BuNBfc: 102.0°, $(iPr)_2$NBfc: 103.2°].

In order to further investigate the reactivity of these highly strained species, the boron-bridged [1]FCPs **6** were reacted with metal carbonyl compounds (Scheme 3). The photochemical reaction of $Fe(CO)_5$ and (iPr$)_2$NBfc (**6c**) in thf at low temperature resulted in the insertion of an iron carbonyl fragment into the Fe-Cp bond. The resulted red crystalline compound **7** is a boron-bridged analogue of the well-known dimer $[Cp(CO)Fe(\mu\text{-}CO)]_2$.

Scheme 3. The Reaction of Boron-bridged [1]FCPs with Metal Carbonyl Compounds.

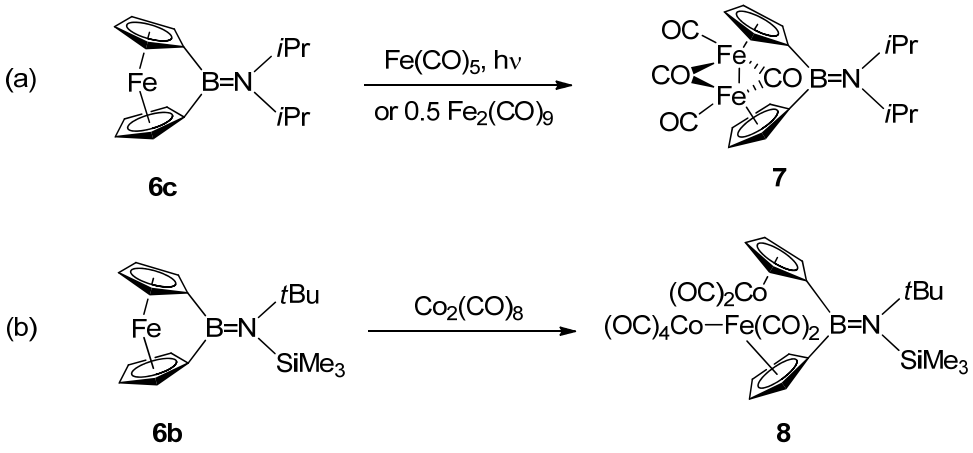

Similarly, the reaction of **6c** with $Fe_2(CO)_9$ in a 2:1 ratio resulted in formation of **7** with a better isolation yield. The reaction of (Me_3Si)*t*BuNBfc (**6b**) with $Co_2(CO)_8$ in a 1:1 ratio resulted in the unusual trimetallic compound **8**. The resulting complex **8** contains a $Cp(CO)_2Fe\text{-}Co(CO)_4$ fragment and a $CpCo(CO)_2$ fragment bridged by a boron linker. The mechanism of this reaction

is not clear, however, it can be assumed that the reaction goes through the breakage of Fe-Cp bond followed by the subsequent insertion of metal carbonyl fragments.

Aluminum- and Gallium-bridged [1]Ferrocenophanes

All the aluminum- and gallium-bridged [1]FCPs in the literature were reported by Müller's group.[6, 31-34] While bulky π-donor ligands were required to prepare boron-bridged [1]FCPs, the *first generation* of aluminum- and gallium-bridged [1]FCPs were synthesized by applying bulky trisyl-based ligands [trisyl = tris(trimethylsilyl)methyl]. These ligands provide both steric protection from the trimethysilyl groups and intramolecular stabilization via a pendant N donor. The synthesis of these species was performed by addition of intramolecularly stabilized aluminum and gallium dihalide complexes to dilithioferrocene·tmeda. The first aluminum-bridged [1]FCP (**9a**) was synthesized in 2005.[6] The synthesis was accomplished by the reaction of (Pytsi)$AlCl_2$ [Pytsi = $C(SiMe_3)_2SiMe_2(2\text{-}C_5H_4N)$] with dilithioferrocene·tmeda (Scheme 4).

Scheme 4. Synthesis of Aluminum- and Gallium-bridged [1]FCPs.

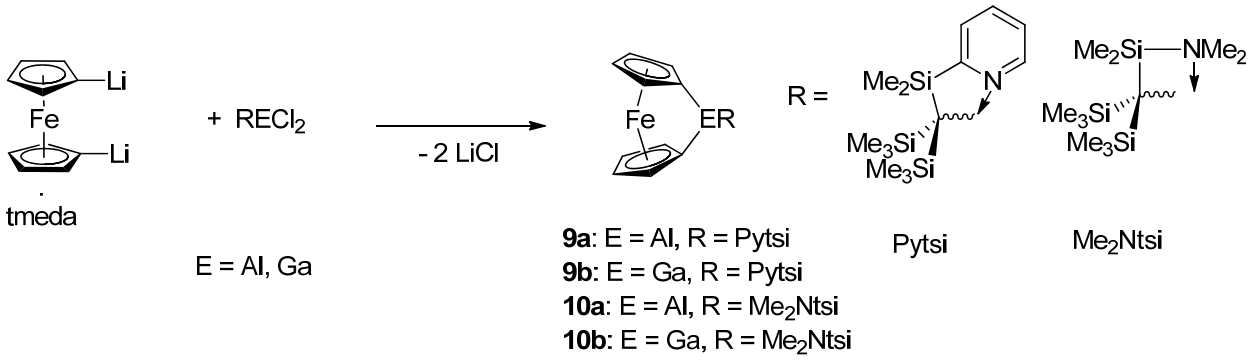

Soon after, the first gallium-bridged [1]FCPs (**9b**) was synthesized by applying the same ligand on the bridging element.[31] The second pair of aluminum- and gallium-bridged [1]FCPs (**10a** and **10b**; Scheme 4) were prepared one year later by employing the similarly bulky and

intramolecularly coordinating Me_2Ntsi [Me_2Ntsi = $C(SiMe_3)_2SiMe_2NMe_2$] ligand.[32] All these compounds were isolated in moderate to high yields by crystallization at low temperature from organic solvents.

Since elements with a larger covalent radius than that of boron are introduced in the bridge, smaller tilt angles are observed for these compounds [(Pytsi)Alfc: α = 14.9°,[6] (Pytsi)Gafc: α = 15.7°,[31] (Me_2Ntsi)Alfc: α = 14.3°, (Me_2Ntsi)Gafc: α = 15.8°)].[32] The ^{13}C NMR spectra of these species demonstrate the presence of strain in the molecules through the upfield shift of the *ipso*-carbon resonances [(Pytsi)Alfc: δ = 52.9, (Pytsi)Gafc: δ = 47.2, (Me_2Ntsi)Alfc: δ = 53.0, (Me_2Ntsi)Gafc: δ = 47.3)] with respect to parent ferrocene (δ = 68.2). The use of sterically demanding ligands for the preparation of heavier group-13-bridged [1]FCPs is considerably important and this was evidenced by applying less bulky intramolecularly stabilizing ligands in the bridging position. As shown in Scheme 5, attempts for the preparation of aluminum- and gallium-bridged [1]FCPs by applying the flat Ar′ ligand (Ar′ = 2-[(dimethylamino)methyl]phenyl) did not result in the intended products and instead yielded [1.1]ferrocenophanes, which are the formal dimers of [1]FCPs and this was attributed to the lack of steric protection in the bridge.[35, 36] The formation of [1.1]FCPs instead of [1]FCPs was attributed to the lack of steric protection on the bridging elements.

Scheme 5. Synthesis of Aluminum- and Gallium-bridged [1.1]Ferrocenophanes.

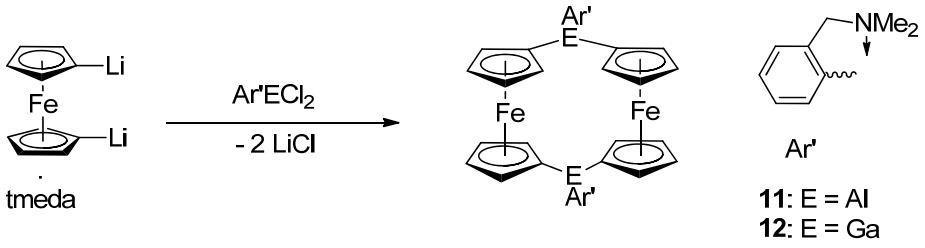

In respective ^{1}H NMR spectra, the difference between [1]FCPs and [1.1]FCPs can be identified by studying the Cp proton patterns. In [1.1]FCP species, the two signals related to β protons fall between the two signals of α protons whereas for [1]FCPs, both signals related to α protons move upfield and show up at a lower chemical shift with respect to β protons.

The *second generation* of aluminum- and gallium-bridged [1]FCPs were attempted by our group in 2010.[33] The reaction of (Mamx)$GaCl_2$ [Scheme 6; Mamx = 2,4-*t*Bu_2-6-(Me_2NCH_2)C_6H_2] with dilithioferrocene·tmeda resulted in formation of the gallium-bridged [1]FCP **13**, which was not isolable from the reaction mixture and polymerized under the condition of its formation.[33] Similarly, attempts to synthesize aluminum-bridged [1]FCP equipped with the Mamx ligand resulted in polymeric materials (Scheme 6).[34]

Scheme 6. Synthesis of Aluminum- and Gallium-bridged [1]FCPs Applying Mamx Ligand.

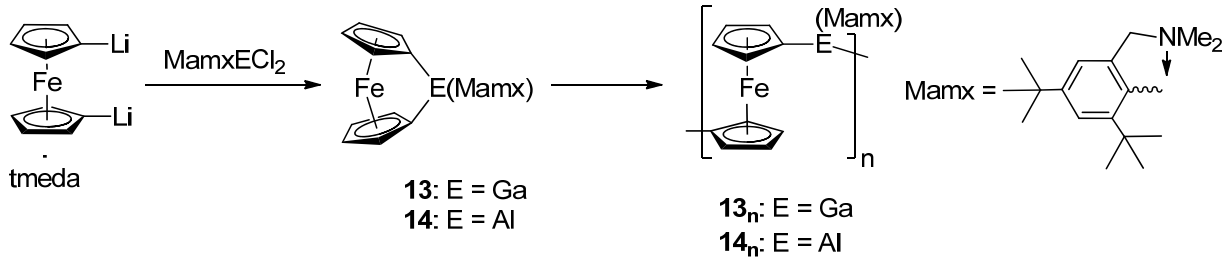

In both cases the presence of strained species was detected by measuring ^{1}H NMR spectra of an aliquot taken from the reaction mixture. DFT calculations revealed the geometric parameters of the aluminum- and gallium-bridged [1]FCPs. The calculated tilt angle α for both aluminum- and gallium-bridged [1]FCPs [(Mamx)Alfc: α = 12.36°, (Mamx)Gafc α = 15.80°) were similar to other similar known species. Interestingly, it was shown that the steric interactions between *ortho t*Bu group of the Mamx ligand and the ferrocene moiety induced additional strain in these molecules.

Indium-bridged [1]Ferrocenophanes

Before our investigations, there was no report of indium-bridged [1]FCPs in the literature. The reaction of indium dichloride $Ar'InCl_2$ with dilithioferrocene·tmeda resulted in the diinda[1.1]FCP **15** (Scheme 7).[36] This result was in agreement with what was observed in the case aluminum and gallium species. Surprisingly, the salt-metathesis reaction of dilithioferrocene·tmeda with $(Me_2Ntsi)InCl_2$ resulted in diinda[1.1]FCP.[37] This result was in contrast with the case of aluminum and gallium species where applying the same ligand system yielded [1]FCPs.[32] This unexpected result was rationalized by the 10% longer bond length of In-C compared to Al-C and Ga-C, which leaves more space for the bulky ligand to fit in the [1.1]FCP structure.[37]

Scheme 7. Synthesis of Indium-bridged [1.1]Ferrocenophanes.

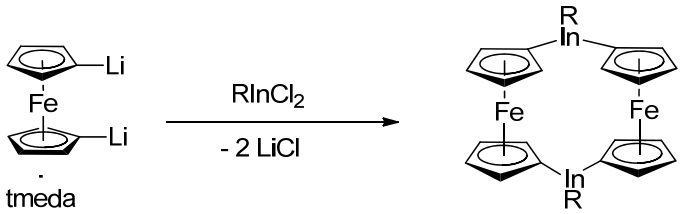

15: R = Ar'
16: R = Me_2Ntsi

The ^1H NMR spectrum of the diinda[1.1]FCP **16** exhibits only two signal for all sixteen Cp protons. This low number of Cp signals was rationalized by the fast *anti*-to-*anti* isomerization of the complex. The NOE experiment of the indium-bridged [1.1]FCP **15** revealed the same fluxional behavior by showing the exchange of Cp protons, an obvious indication of *anti*-to-*anti* isomerization.

1.1.2. Group-14-bridged [1]Ferrocenophanes

Carbon-bridged [1]Ferrocenophanes

Currently there is no record of carbon-bridged [1]FCPs in the literature. It is believed that the high expected tilt angle for carba[1]ferrocenophanes would make them too unstable to exist. However, [n]FCPs with n ≥ 2 are known in the literature. For example, carba[2]FCP **3** with a C_2Me_2 in the bridge was reported by Rinehart et al. in 1960.[2]

Silicon-bridged [1]Ferrocenophanes

Silicon-bridged [1]FCPs were first reported in 1975 by Osborne et al. and applied as agents for derivatizing surfaces via their stoichiometric ring-opening reactions.[3, 7, 38] However, the area of strained silicon-bridged [1]FCPs was quite silent for many years until Manners et al. reported on the synthesis of high-molecular-weight polymer via ROP of silicon-bridged [1]FCPs in 1992.[18] The potential application of PFSs triggered an intensive research in this area and, consequently, a vast number of silicon-bridged [1]FCPs were synthesized in order to modify the properties of the resulting polymers. The reaction of diorganodichlorosilanes with dilithioferrocene·tmeda have resulted in numerous symmetrically and unsymmetrically substituted silicon-bridged [1]FCPs (Scheme 8).[7, 16, 39-42]

Scheme 8. Synthesis of Silicon-bridged [1]FCPs.

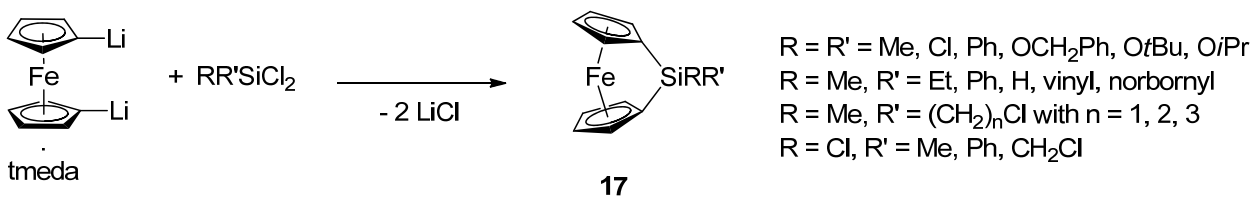

In addition, chlorine replacement in dichlorosila[1]ferrocenophanes with alkoxy-, aryloxy- or amino- groups by using alcohols, phenols and amines in the presence of a base is another route to silicon-bridged [1]FCPs (Scheme 9).[39, 42]

Scheme 9. Substitution Reaction on Dichlorosila[1]ferrocenophanes.

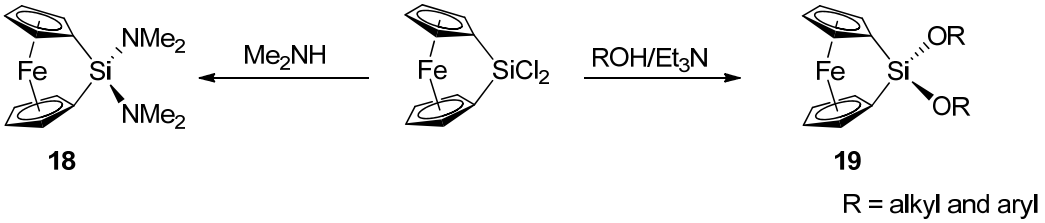

18 **19**

R = alkyl and aryl

Despite the propensity of silicon-bridged [1]FCPs to ring-open with alkyl lithium reagents, the reaction of chloro-substituted silicon-bridged [1]FCPs with lithium reagents at low temperature can lead to the synthesis of different silicon-bridged [1]FCPs (Scheme 10).[43]

Scheme 10. Reaction of Chloro-substituted Silicon-bridged [1]FCPs with Lithium Reagents.

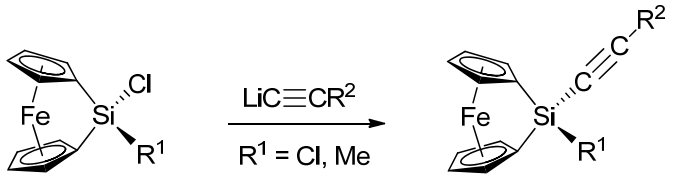

20: R^1 = Me, R^2 = *n*Bu
21: R^1 = Me, R^2 = Ph
22: R^1 = CCPh, R^2 = Ph

Following the same strategy, Manner et al. synthesized the first hypercoordinated silicon-bridged [1]FCP (**23**) in 2000 through reacting unsymmetrically substituted silicon-bridged [1]FCP with Ar′Li at –78 °C (Scheme 11a).[44] The solid state structure of **23**, measured by single crystal X-ray diffraction, revealed the distorted trigonal bipyramidal geometry of the five coordinate silicon center with elongation of Si-Cp bonds. Five years later, Hatanaka et al. synthesized the

pentacoordinate silicon-bridged [1]FCP **24**, where the Si-Cp bond is weakened by the donation of oxygen to the silicon center (Scheme 11b).[45] Pentacoordinate silicon-bridged [1]FCPs can be used as models for studying the unknown mechanism of the thermal ROP process and also that of the nucleophilic ROP of tin-bridged [1]FCPs.

Scheme 11. Synthesis of Pentacoordinate Silicon-bridged [1]FCPs.

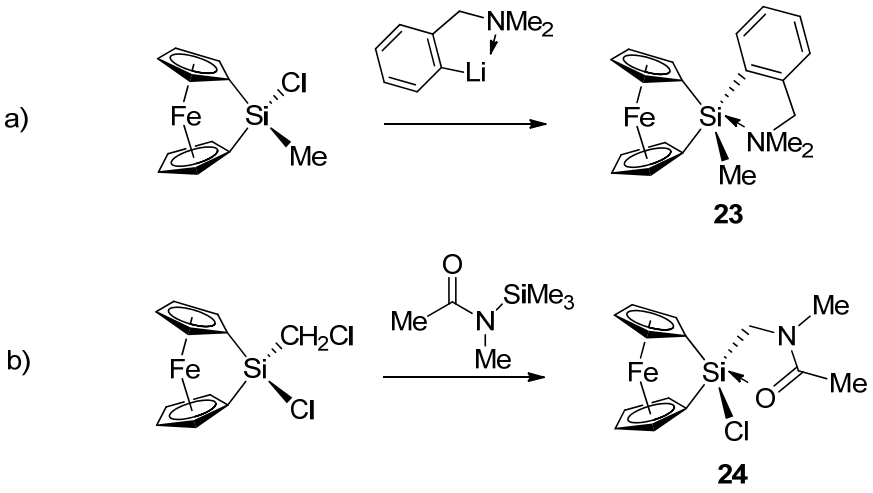

Preparation of the first [1]ferrocenophanium ion, a one-electron oxidized species of [1]FCP, was an interesting development in the chemistry of [1]FCPs. The reversibility of the one electron oxidation process of ferrocene has led to its widespread application as a standard for electrochemical studies. The first example of stable one-electron oxidized [1]FCP was reported in 2009, where the silicon-bridged [1]FCP **25** was chemically oxidized by $[N(C_6H_4\text{-}4\text{-}Br)_3][SbF_6]$, the so-called "magic blue" (Scheme 12).[46] It was assumed that the presence of electron donating *t*Bu substituents on the Cp units facilitated the oxidation process and increased the stability of the cationic product. The resulting [1]ferrocenophanium ion **26** has a larger tilt angle compared to its 18-electron precursor [**25**, $\alpha = 18.69(9)°$ and **26**, $\alpha = 28.9(13)°$]. This increased tilt angle of **26** compared to that of **25** enhances the reactivity of **26** toward hydrolysis and methanolysis reactions and results in ring-opened products. [1]Ferrocenophanium ion **26** can

be ring-opened at a significantly lower temperature compared to **25**, however, a polymer is not produced.

Scheme 12. Synthesis of Silicon-bridged [1]Ferrocenophanium Ion.

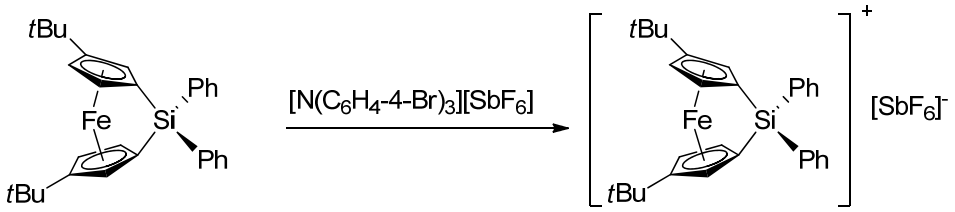

25 **26**

The first spirocyclic [1]FCP (**27**) was reported by Osborne et al. in 1980 in a very low yield (7%) by the reaction of dilithioferrocene·tmeda with $SiCl_4$.[47] However, in the 1990s Manners et al. reported on a modified procedure for the preparation of **27**, as well as on the synthesis of the new spirocyclic species **28** (Figure 3).[48] The reported tilt angles α and bond angle distortions (β, δ and θ angles) for [1]FCPs **27** and **28** are comparable to other silicon-bridged [1]FCPs in the literature.[27] Due to the steric shielding around the silicon bridge, provided by four Cp rings, compound **27** is exceptionally air and moisture stable. In contrast, the lack of steric protection causes silicon-bridged [1]FCP **28** to be considerably air and moisture sensitive.[48]

27 **28**

Figure 3. Spirocyclic silicon-bridged [1]FCPs.

A number of silicon-bridged [1]FCPs with substituted Cp rings are reported in the literature (Figure 4).[49-52] Due to the introduction of steric protection from the Cp units these silicon-bridged [1]FCPs, these species exhibit an enhanced air and moisture stability. The alkyl-substituted Cp

rings in these compounds demonstrate a stronger electron-donor property compared to the non-substituted Cp rings, resulting in a decreased Fe-Cp bond distance. Interestingly, compound **32** shows an unusual large tilt angle of 26.3° and it is attributed to the steric repulsion between bulky trimethylsilyl groups which are stacking on the top of each other. However, this steric repulsion is not observed for compound **29** with the tilt angle of 20.3° and this is due to the orientation of *t*Bu substituents which are laying between each other (Figure 4).

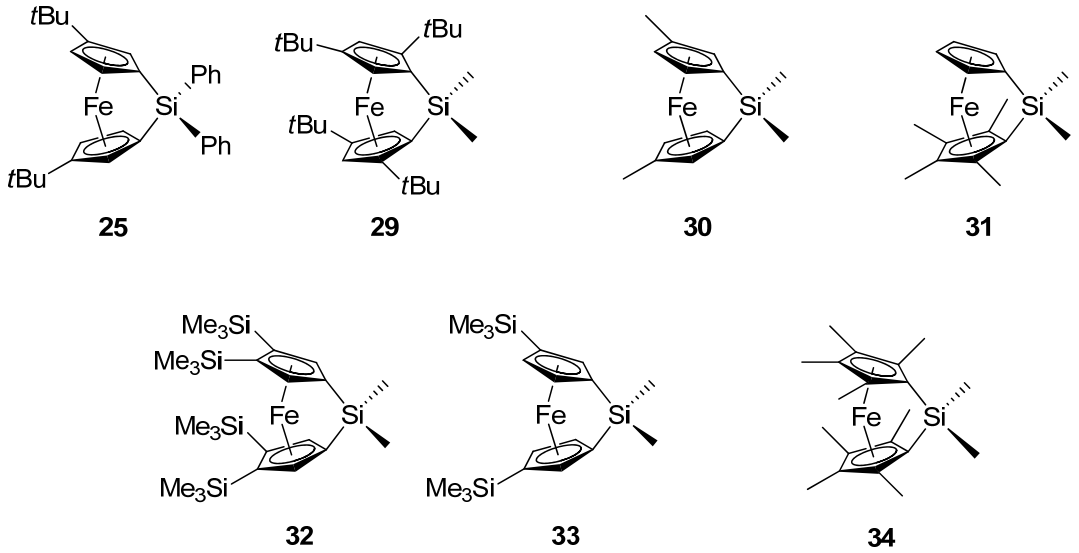

Figure 4. Silicon-bridged [1]FCPs with substituted Cp rings.

Germanium-bridged [1]Ferrocenophanes

A number of germanium-bridged [1]FCPs have been reported in the literature and they were prepared by using the traditional salt-metathesis routes (Scheme 13).[12, 47, 53, 54]

Scheme 13. Synthesis of Germanium-bridged [1]FCPs.

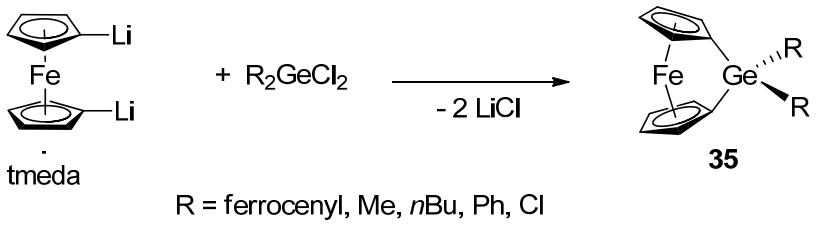

Tin-bridged [1]Ferrocenophanes

However, the unusual spirocyclic germanium-bridged bis[1]FCP **36** was prepared by the reaction of $GeCl_4$ and dilithioferrocene·tmeda (Scheme 14).[48] Compared to silicon-bridged [1]FCPs, the larger radius of germanium causes a smaller tilt angle ($\alpha \approx 18°$) for germa[1]ferrocenophanes, which is intermediate between those of stanna- and sila[1]ferrocenophanes. Germa[1]ferrocenophanes can go through ring-opening polymerization and yield high-molecular-weight polymers.[12, 53, 55]

Scheme 14. Synthesis of Spirocyclic Germanium-bridged Bis[1]FCP.

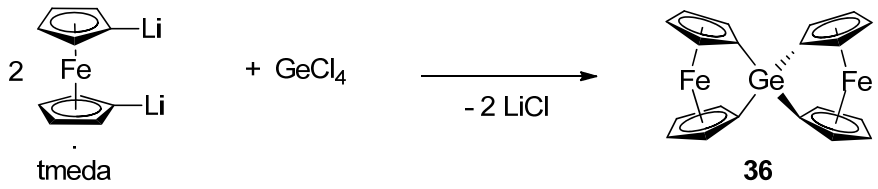

Tin-bridged [1]FCPs were first reported in 1996 by Manners et al. and, a few years later, Pannell et al. introduced another example of these compounds (Scheme 15).[13, 56, 57]

Scheme 15. Synthesis of Tin-bridged [1]FCPs.

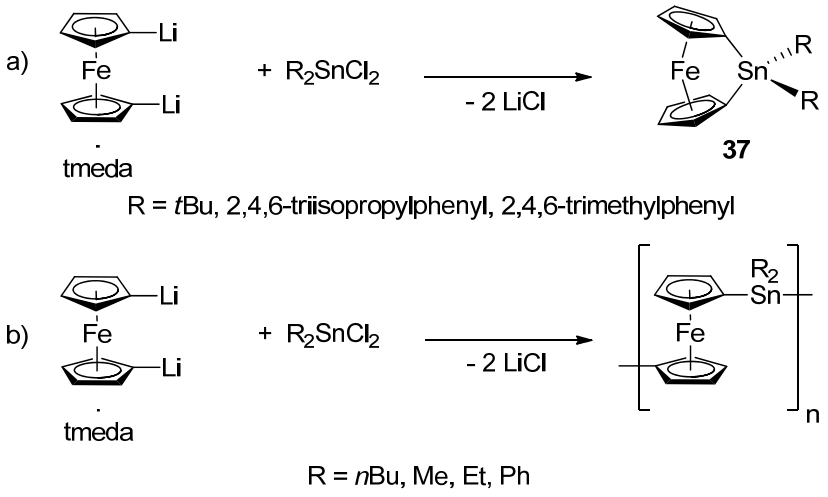

To date, there are only three stanna[1]ferrocenophanes known in the literature. In all cases, the presence of sterically demanding groups on the tin bridge, such as *t*Bu, 2,4,6-trisopropylphenyl or 2,4,6-trimethylphenyl, seemed to be necessary in order to produce isolable strained species. This was evidenced by the salt-metathesis reaction of R_2SnCl_2 (R = Me, Et, Ph, *n*Bu) with dilithioferrocene·tmeda where oligomeric products and cyclic dimers were obtained instead of the intended stanna[1]ferrocenophanes (Scheme 15).[58]

The reaction of stanna[1]ferrocenophanes with metal carbonyl reagents resulted in the insertion of metal center into a C_{ipso}-Sn bond (Scheme 16).

Scheme 16. Reactivity of Tin-bridged [1]FCPs.

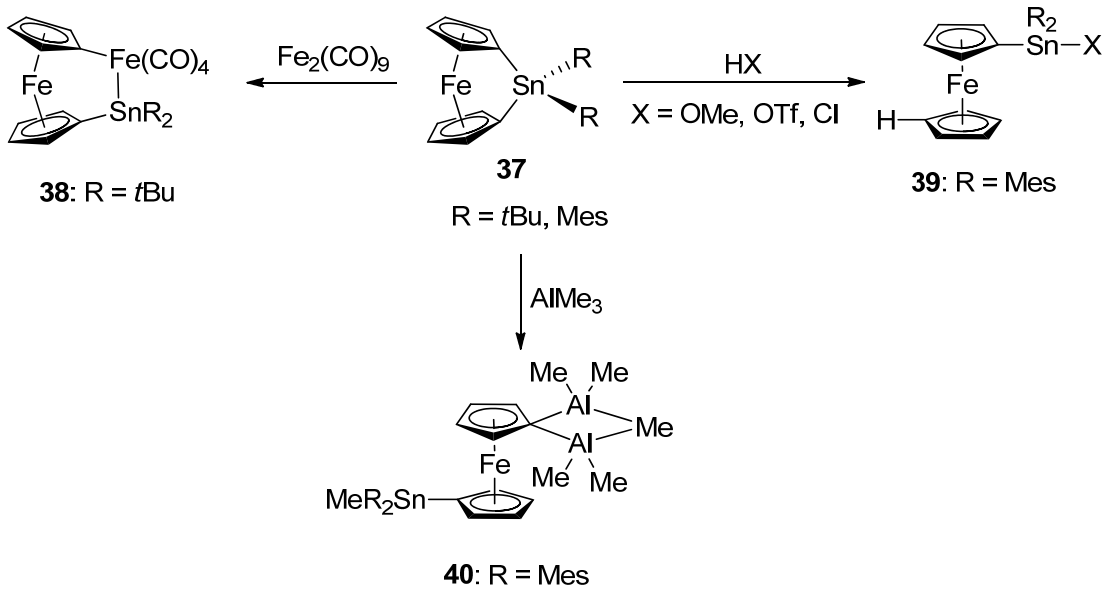

This result was in contradiction with what had been observed for the highly tilted boron-bridged [1]FCPs, where the cleavage happened on the Fe-Cp bond upon reacting with $[Fe_2(CO)_9]$.[59] Similar to silicon-bridged [1]FCPs, stanna[1]ferrocenophanes go through ring-opening reactions upon being exposed to protic species such as HOTf, MeOH and HCl. In another example, the

reactivity of stanna[1]ferrocenophanes with the Lewis acid $AlMe_3$ was studied and the ring-opened compound **40** was identified (Scheme 16).[60]

1.1.3. Group-15-bridged [1]Ferrocenophanes

Phosphorus-bridged [1]Ferrocenophanes

While there is no example of nitrogen-, antimony- and bismuth-bridged [1]FCPs, phosphorus and arsenic-bridged [1]FCPs are well-known in the literature. In most cases, a salt-metathesis approach was applied to prepare phospha- and arsa[1]FCPs, meaning dilithioferrocene·tmeda was reacted with phosphorus or arsenic organodihalides. Phosphorus-bridged [1]FCPs **41** (Scheme **17**) were first prepared in the eighties by Osborne et al.[47] and Seyferth et al.[8] In all examples, phospha[1]ferrocenophanes demonstrated a narrow range of tilt angle α (26.9-27.9°).[8, 47, 61-64]

Scheme 17. Synthesis of Phosphorus-bridged [1]FCPs.

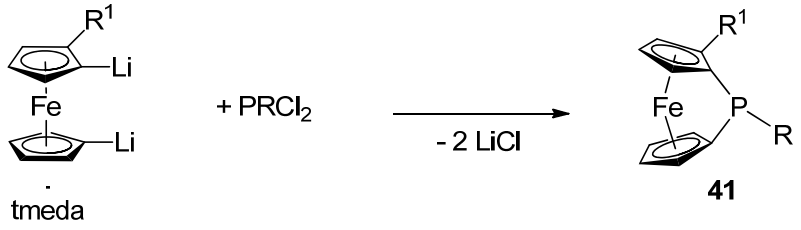

R^1 = H, R = N*i*Pr$_2$, Ph, Cl, *p*-*t*BuC$_6$H$_4$
R^1 = CH(Me)NMe$_2$, R = Ph

In another example, enantiomerically resolved dichloroorganophosphines were used to synthesize chiral phosphorus-bridged [1]FCPs. These phospha[1]ferrocenophanes were applied as chiral ligands in the Rh-catalyzed diastereoselective hydrogenation of folic acid (Scheme 18). It was also described that poly(ferrocenylphophine)s yielded from ROP of

phospha[1]ferrocenophanes can be used as both ligands or support in transition-metals catalysts.[62]

Scheme 18. Synthesis of Chiral, Phosphorus-bridged [1]FCPs.

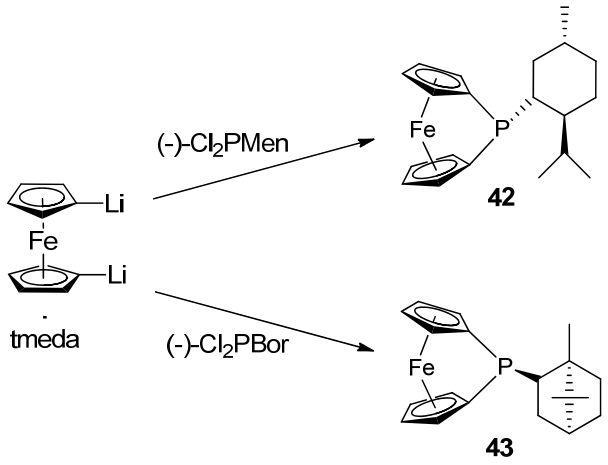

Phospha[1]ferrocenophanes can coordinate to the metal center via the lone pair on the phosphorus atom and the subsequent 1,2-shift will result in the insertion of metal into P-C bond (Scheme 19).[65, 66] Stable phosphonium-bridged [1]FCPs, borane adducts, and sulfurized P(v) derivatives, of (phenyl)phospha[1]ferrocenophane are reported in the literature and some of these species are prone to thermal or transition-metal-catalyzed ROP.[67, 68] To explore the thermal polymerization behavior of (phenyl)phospha[1]ferrocenophane, a Differential Scanning Calorimetry (DSC) study was undertaken. The measured enthalpy (DSC thermogram) for the thermal ROP of (phenyl)phospha[1]ferrocenophane (–68 ± 5 kJ mol^{-1}) is reported be smaller than the expected value for the amount of strain existing in the molecule. The authors explained this discrepancy by assuming that the bulky phenyl substituent on the bridge hinders the ROP process and causes the low exothermic values.[67]

Scheme 19. Insertion of Iron into P-C Bond in Phosphorus-bridged [1]FCPs.

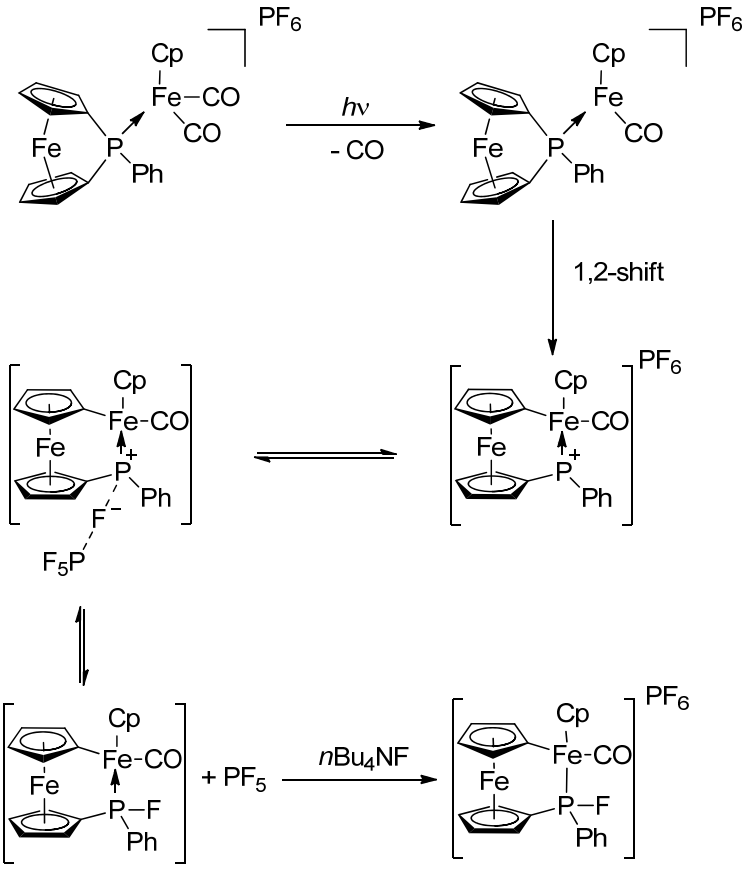

Arsenic-bridged [1]Ferrocenophanes

To date, there are only two arsa[1]FCPs known in the literature (Scheme 20).[61] The crystal structure of **43** was determined by single crystal X-ray diffraction and a tilt angle α of 22.9° was revealed for this compound, which is higher than the expected value for arsa[1]FCPs.

Scheme 20. Synthesis of Arsenic-bridged [1]FCPs.

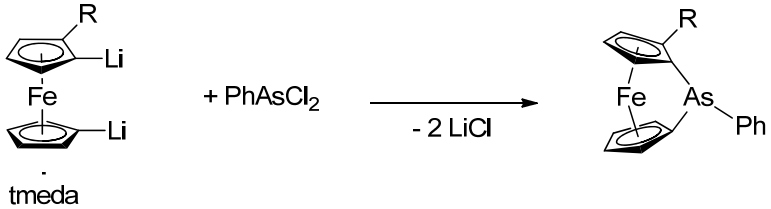

42: R = H
43: R = $CH(Me)NMe_2$

Despite the nearly identical covalent radius between arsenic- and germanium-bridged species (P 1.10 Å; As 1.21 Å; Ge 1.22 Å),[69] the geometrical parameters of arsa-bridged [1]FCPs are more similar to phospha[1]ferrocenophanes. It is suggested that in Ge-bridged [1]FCPs, strain is absorbed in other parts of structure, as it was evidenced by their larger β and θ angle.[47]

1.1.4. Group-16-bridged [1]Ferrocenophanes

The first chalcogen-bridged *ansa* ferrocene, sulfur-bridged [3]FCP (**44**), was prepared by the reaction of elemental sulfur with dilithioferrocene·tmeda in the 70s (Scheme 21).[70] Triselena- and tritellura[3]FCPs were also synthesized by following the same synthetic method.[70] These compounds are nearly unstrained and have low tilt angles (less than 4.5º).

Scheme 21. Synthesis of Sulfur-bridged [3]FCP.

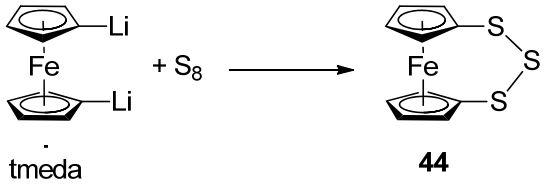

Surprisingly, the sulfur-bridged [1]FCP **45** was obtained in low yields when a [2]FCP species was aimed at (Scheme 22).[10] Selenium- and sulfur-bridged [1]FCPs **45** and **46** were synthesized by following the typical salt-metathesis reactions by using dilithioferrocene·tmeda and doing workup at low temperature.[11] The solid-state structure of the sulfur-bridged [1]FCP **45** revealed a high tilt angle α of 31º, as expected by the small atomic radius of sulfur.

Scheme 22. Synthesis of Selenium- and Sulfur-bridged [1]FCPs.

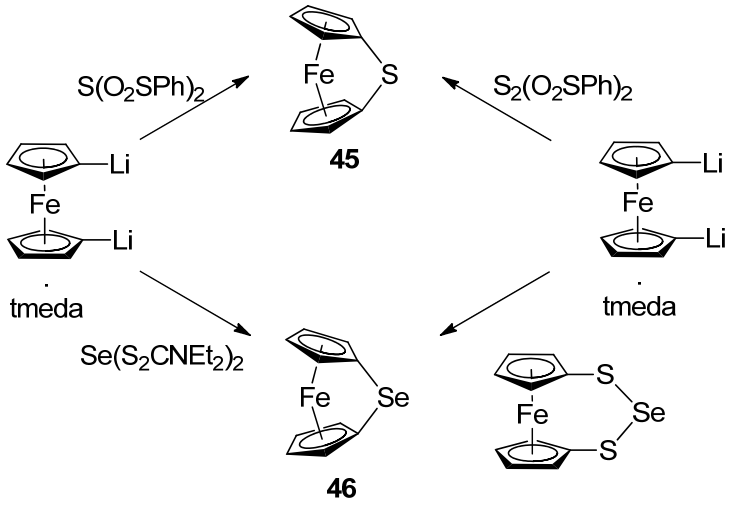

1.2. Poly(ferrocene)s via Ring-opening Polymerization of [1]Ferrocenophanes

1.2.1. Background of Metallopolymers

For centuries, natural occurring polymers, such as cellulose, amber and natural rubber, have been used widely in human societies. Over the last 100 years, synthetic organic polymers, such as polyethylene, polypropylene, polystyrene, polyvinyl chloride, polyvinyl butyral, nylon, neoprene and synthetic rubber, have played a revolutionary role in the terms of necessary materials in the modern life. For the last few decades, 'value added' materials, such as polymers with special properties, have attracted researchers attention. By providing key properties and functions, metal centers have the potential to play a very crucial role in the two- or three-dimensional structures of solids. Metallopolymers are a new generation of materials, which contain metals in the repeating unit either in the backbone or as a pendant group. The first synthetic metallopolymers was synthesized by Dupont in 1955 by the radical polymerization of vinylferrocene.[71] Despite this early achievement, the area of metallopolymers was held back for 30 years because of the synthetic difficulties. Generally, metallopolymers cannot be synthesized by using the established methods for the preparation of organic polymers. Applying common synthetic protocols for the

preparation of metallopolymers resulted in low-molecular-weight species which were insoluble and poorly characterized. Since the mid-1990s, most of the synthetic obstacles in this area have been overcome by different research groups through the development of synthetic strategies which are compatible with the existence of metal centers.[72-75] Nowadays, preparation of high-molecular-weight and soluble metallopolymers with a variety of structures has allowed the detailed studies of their properties and applications of these materials are emerging. A variety of metals including main group metals, such Sn and Pb, transition metals, such as Fe or Ir, and lanthanides, such as Eu, can be incorporated into metallopolymers. Despite the early preparation of polyvinylferrocene in 1950s where ferrocene units are pendant groups of the polymer chain,[71] poly(ferrocene)s containing ferrocene in the polymer backbone were reported more recently. In the early 1980's, Seyferth and Garrou et al. reported the synthesis of high-molecular-weight ferrocenylphenylphosphine polymers (**47**$_n$) with a wide range of molecular weight (M_w = 8.9-161 kDa) via treating dilithioferrocene·tmeda with $PhPCl_2$ in different organic solvents.[76] The high molecular weight of the obtained polymer was quite a surprise for such a polycondensation reaction. However, It can be assumed that the reaction of dilithioferrocene·tmeda with $PhPCl_2$ resulted in formation of phosphorus-bridged [1]FCP, which then undergoes an anionic ROP upon reacting with dilithioferrocene·tmeda. However, the authors did not provide any explanation about the probable *in situ* formation of phosphorus-bridged [1]FCP and its subsequent ROP, initiated by dilithioferrocene. In the same article,[76] Seyferth et al. reported about the unsuccessful attempts for the anionic ROP of **47** where phenyllithium, as an initiator, was reacted with **47** in different ethereal solvents and in all of the cases oligomeric materials were formed. The unsuccessful ROP of **47** can be attributed either to steric effects or to insolubility of the starting materials or to other technical problems (Scheme 23).

Scheme 23. Synthesis of Poly(ferrocenylphenylphosphine).

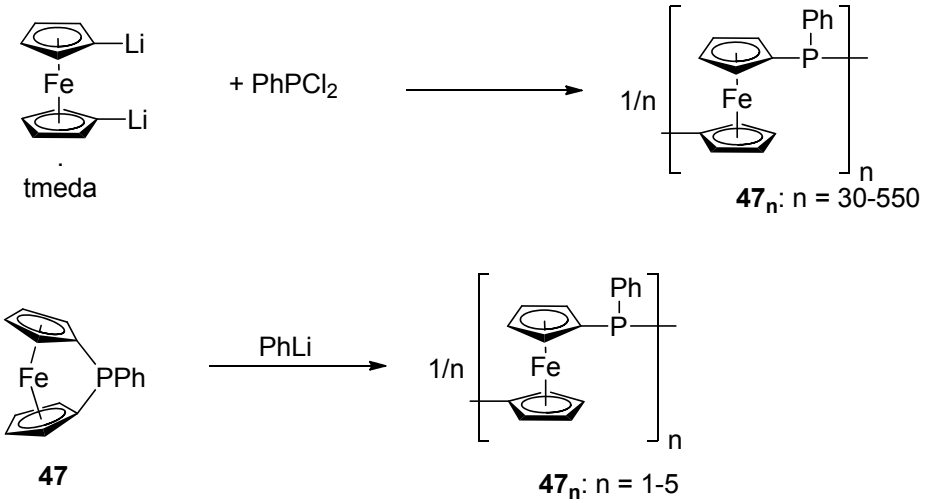

Probably as a result of this unsuccessful attempt, further investigation in this area was hindered for about 10 years until Rauchfuss and Brand et al. reported on the synthesis of high-molecular-weight poly(ferrocenylsulfide) $\mathbf{44_n}$ (Scheme 24).[77] The ROP of **44** was accomplished through chalcogen abstraction in the presence of tributylphosphine and it was suggested that sulfur-bridged [2]FCP could be the potential intermediate for this process. [77]

Scheme 24. Synthesis of Poly(ferrocenylsulfide).

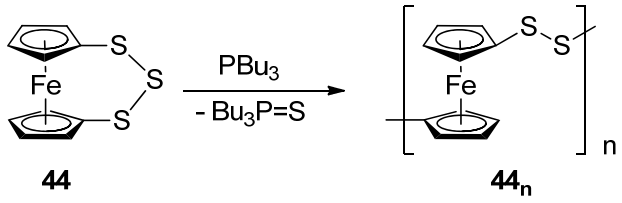

Only few months later, Manner's et al. reported the synthesis of high-molecular-weight PFSs via thermal ROP of the corresponding silicon-bridged [1]FCPs (Scheme 25).[18] This achievement was a milestone in the development of organometallic polymers and triggered a huge amount of research activities in the area of strained sandwich compounds.[27-29]

Scheme 25. Thermal ROP of Silicon-bridged [1]FCPs.

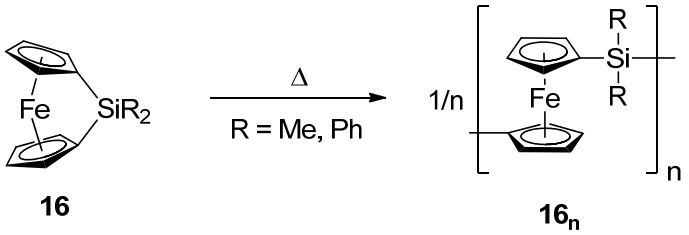

16 **16_n**

Manner's group had initially studied the thermal ROP of disilane-bridged [2]FCP and concluded that this compound is not prone to ROP.[78] During the course of these investigations, they also aimed for the synthesis of the similar [2]FCP compounds through the Wurtz coupling of [fc($SiMe_2Cl$)$_2$]. However, the reaction between one equivalent of dilithioferrocene·tmeda with two equivalents of Me_2SiCl_2 resulted in the yellow polymeric materials instead of intended disubstituted ferrocene species. The analysis of the resulting polymer revealed the 1:1 ratio between $SiMe_2$ groups and ferrocene moieties which was in contrast with the 1:2 stoichiometry of the reaction. The high-molecular-weight of the obtained polymer (300 kDa) was quite unusual and they considered the possible in situ formation of dimethylsila[1]ferrocenophane which subsequently polymerizes. In order to confirm this speculation, dilithioferrocene·tmeda was reacted with Me_2SiCl_2 in a 1:1 ratio and the isolated dimethylsila[1]ferrocenophane was ring-open polymerized thermally at 130 ºC to yield solid amber materials, characterized as high-molecular-weight PFS.[18]

1.2.2. The Importance of Ring-opening Polymerization

In linear polymers, the interesting properties of the polymers begin to exist when the polymer chains are long enough to get entangled to each other. However, efficient polymerization methods are needed to reach the desired polymer length. As described before, high-molecular-weight metallopolymers are not accessible through conventional polycondensation pathways. It

is worth to mention that poly(ferrocenyldimethysilane) was first synthesized in 1962 by a polycondensation reaction between iron dichloride and anionic dicyclopentadienyl bridged with dimethylsilicon (Scheme 26a).[79] Seven year later, PFSs with methyl and phenyl substituents were prepared by the reaction of dilithioferrocene·tmeda and the respective dialkylsilicon dichlorides (Scheme 26b).[80]

Scheme 26. Applying Polycondensation Pathway for the Synthesis of Oligo(ferrocenylsilane)s.

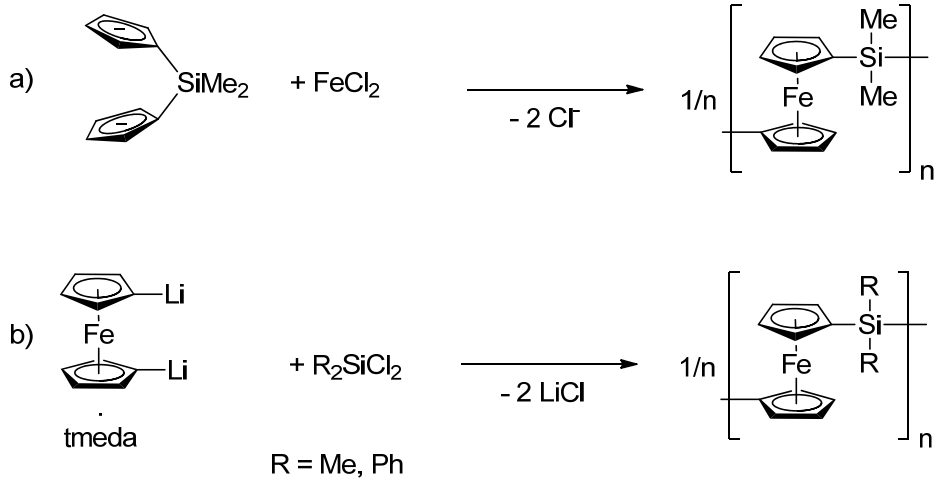

Later on, poly(ferrocenylstannane)s were synthesized through a polycondensation reaction by reacting dilithioferrocene·tmeda with dialkyltin dichlorides (Scheme 15b). In all cases, polycondensation pathways resulted in low-molecular-weight polymers.

Various polymer chains with a wide distribution of chain lengths are present in the reaction mixture of polycondensation polymerization and these polymer chains can react with each other randomly, as a result, polymers with a broad molecular weight distribution will be obtained. In a polycondensation reaction, high-molecular-weight polymers are only accessible if the stoichiometry between the reagents is well-maintained, the starting monomers are highly purified and the polymerization reaction proceeds with high conversion yields. In general, high-

molecular-weight poly(ferrocene)s are not obtainable by polycondensation reactions because of first, the difficulties with maintaining the proper stoichiometry between monomers and second, the low purity of starting monomers. For instance, dilithioferrocene·tmeda, as the main starting monomer, often contains some amount of ferrocene as its main impurity, which cannot be eliminated easily. Moreover, the ratio between dilithioferrocene and tmeda varies between 2/3 to 2 and the stoichiometry is highly disturbed by this uncertainty. Accordingly, it was not a surprise that low-molecular-weight PFSs and poly(ferrocenylstannane)s were obtained when dilithioferrocene·tmeda was applied as one of the starting material in polycondensation reactions. In contrast, high-molecular-weight polymers, at even low levels of monomer conversion, can be synthesized by chain-growth processes and this is mainly attributed to the high reactivity of the propagating chains. ROP reactions proceed through a chain-growth mechanism and, therefore, high-molecular-weight polymers are accessible via this method. Many inorganic polymers, such as polycarbosilanes, polysilazanes, polysilanes, polysiloxanes and polyphosphazenes, have been prepared by ROP reactions.[81] In 1989, Roesky and Lücke employed the ROP reactions for the synthesis of polymers containing transition metal in the backbone. They prepared $[\{(C_5Me_5)TaN(Cl)\}_n]$ and $[\{\text{-}N{=}MCl_3\text{-}N{=}P(Ph_2)\text{-}N{=}P(Ph_2)\text{-}\}_n]$ (M = Mo or W) from the corresponding metal nitride and metallophosphazenes.[82, 83] Similarly, ROP of [n]FCPs is proven to be a very effective method toward preparation of high-molecular-weight metallopolymers. This is usually the case for [n]FCPs with high tilt angles, and therefore strained and prone to release their strain through ROP.

1.2.3. Ring-opening Polymerization Methodologies

Since the first report about the thermal ROP of silicon-bridged [1]FCPs in 1992,[18] various methods have been developed for ROP of strained sandwich compounds. To date, high-

molecular-weight poly(ferrocene)s have been prepared by anionic, thermal, photo-controlled and transition-metal-catalyzed ROP methodologies. These methods are briefly discussed in the following section.

Thermal ROP

The thermal ROP of strained [1]FCPs was first introduced by Manners et al. where high-molecular-weight ($M_w \approx 10^5$) poly(ferrocenylsilane)s was synthesized (Scheme 25).[18] Thermal ROP of [n]FCPs is usually performed in either bulk or solution and results in metallopolymers with a broad distribution of molecular weight. The most common synthetic pathway is to heat the bulk monomer in a sealed Pyrex glass tube above its melting point for a certain amount of time, followed by a purification through repeated precipitations of the resulting polymer into methanol or hexanes. A wide range of strained sandwich compounds have been polymerized by thermal ROP, which is quite tolerant toward functional groups. However, there is always a risk for the degradation of starting monomers as a result of high temperatures. Despite all of the attempts to understand the mechanism of thermal ROPs, there is little known about the nature of propagating species. Manners et al. studied the thermal ROP of silicon-bridged [1]FCPs containing unsymmetrically methylated Cp rings in order to comprehend the mechanism of this polymerization reaction.[49] Si-Cp^H and Si-Cp^{Me} bonds are cleaved non-selectively during the thermal ROP process and this was evidenced by ^{1}H NMR microstructure analysis, cyclic voltammetry, as well as ESR spectroscopy of the oxidized products (Scheme 27).

The thermal ROP of monomers equipped with chlorosilyl groups yielded high-molecular-weight polymers and this result completely omitted the possibility of a carbanionic mechanism for these reactions. It is generally believed that a mechanism involving radicals is governing the thermal

ROP reactions, however, more studies are essential in order to understand the mechanism for thermal ROP of strained [n]FCPs.

Scheme 27. Synthesis of Amorphous Poly(ferrocenylsilane)s.

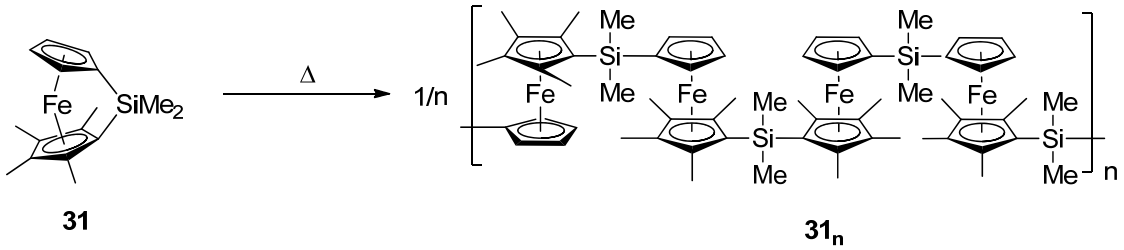

31 **31_n**

Anionic ROP

As it was discussed before, the first example of anionic ROP was investigated done by Seyferth et al. in the 1980s when phosphorus-bridged [1]FCP **47** was reacted with phenyllithium in different ethereal solvent to give the oligomerics **47_n** (Scheme 23).[76] One decade later, Manners' group introduced the first successful living carbanionic ROP. Poly(ferrocenesilane)s with a narrow molecular-weight distribution and predictable molecular weights were prepared by the reaction of silicon-bridged [1]FCPs with ferrocenyllithium as an anionic initiator.[84] Besides ferrocenyllithium, a group of other alky lithium species, such as MeLi, *n*BuLi and *t*BuLi, have been applied successfully for the anionic ROP of [n]FCPs and studies have shown that the mechanism of anionic ROP involves the cleavage of the bond between *ipso*-carbon of the Cp ring and the bridging element.[85, 86] The anionic ROP is particularly important because it can result in poly(ferrocene)s with a high degree of compositional homogeneity [polydispersity index (PDI) ≈ 1] and the molecular weight of the resulting polymers can be defined by changing the ratio between anionic initiators and monomers. Compared to thermal ROP, anionic ROP is performed at milder conditions. Despite thermal ROP, anionic ROP is confined to the monomers with functional groups, which are not reactive toward carbanions. Applying the anionic ROP

methodology, a large group block copolymers, such as **48$_n$**, **49$_n$** and **50$_n$**, with well-defined compositions and architectures have been prepared (Scheme 28).[86] However, this method is limited and exhaustive purification of reagents is required in order to avoid premature termination.

Scheme 28. Synthesis of Block Copolymers via Living Anionic ROP.

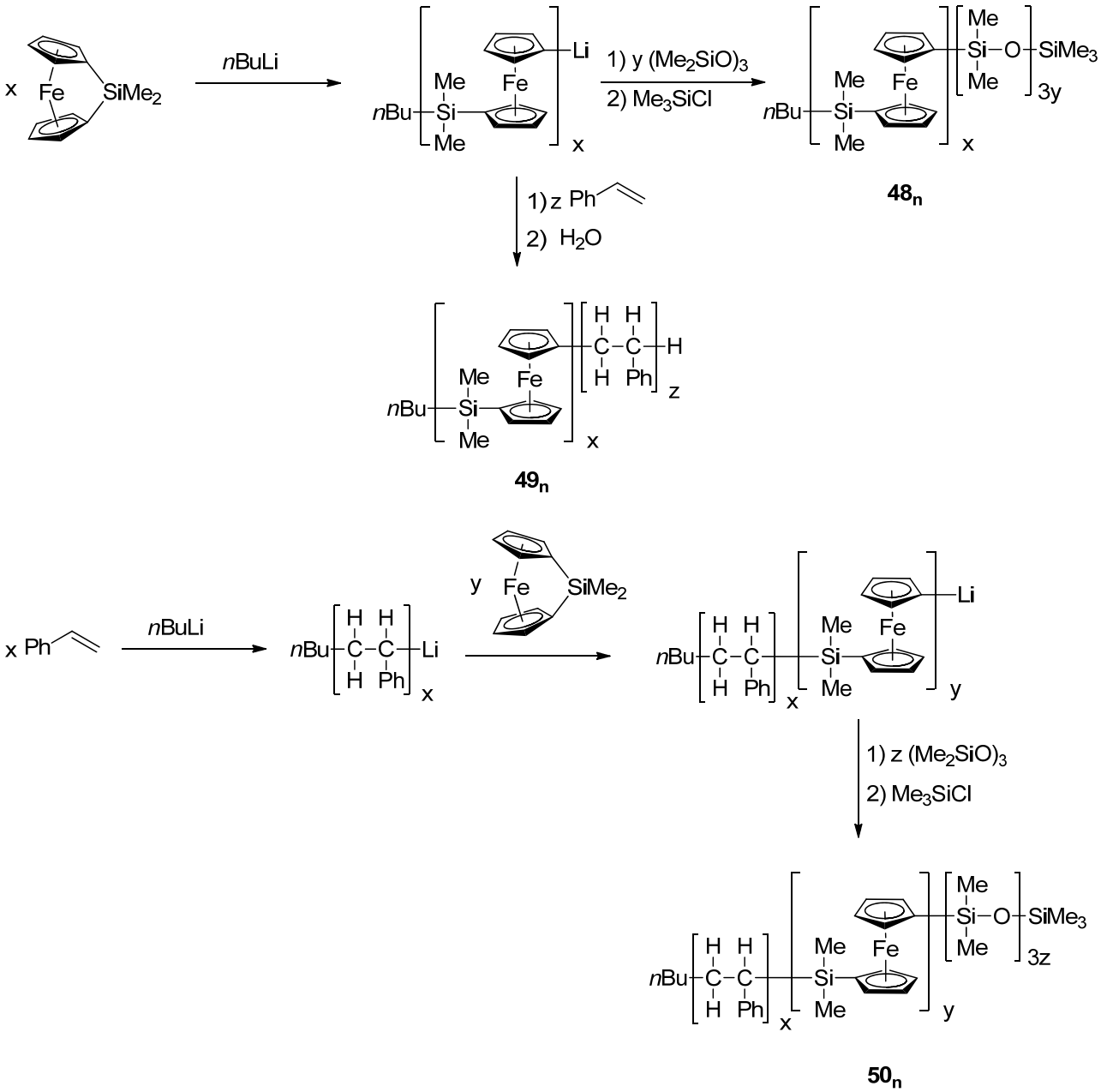

Photocontrolled ROP

The first example of photocontrolled ROP was introduced by Miyoshi et al. in 2000.[87] High-molecular-weight polymers were synthesized by UV/Vis irradiation of phosphorus-bridged [1]FCPs of the type Ph(X)P[1]FCP [X = $W(CO)_5$, $Mn(C_5H_5)(CO)_2$, $MnC_5H_4Me(CO)_2$] coordinating to an organometallic fragment in donor solvents such as acetonitrile and thf (Scheme 29).

Scheme 29. ROP of Metallized Phosphorus-bridged [1]FCPs.

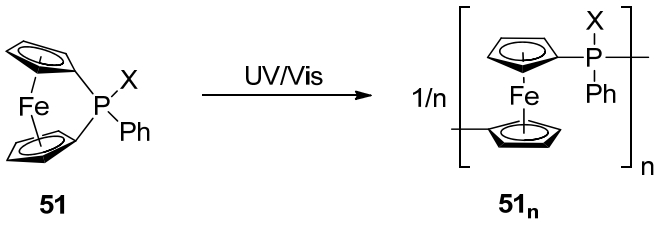

51 **51_n**

X = $W(CO)_5$, $Mn(C_5H_5)(CO)_2$, $Mn(C_5H_4Me)(CO)_2$

The single sharp peak observed in $^{31}P\{^1H\}$ NMR spectra of the resulting polymers indicated that ROP process is completely regioselective. However, this regioselectivity was only observed when non-chlorinated donor solvents were used and applying nonpolar and chlorinated solvents resulted in complicated $^{31}P\{^1H\}$ NMR spectra. This was the first and only report about the ROP of metallized FCPs. The important advantage of this methodology is the presence of pendant groups in the polymer chains which gives a better understanding of the polymer structure. Applying other ROP methods, such as anionic and transition-metal-catalyzed, for the polymerization of metallized monomers failed to produce high-molecular-weight polymers.

In order to understand the mechanism of photocontrolled ROP, phospha[1]ferrocenophane **52** was irradiated with UV light in presence of a large excess of $P(OMe)_3$.[88] Characterization of the resulting product **52a** by X-ray crystallography revealed that a $\eta^5 \rightarrow \eta^1$ haptotropic shift for one of

the Cp rings had occurred (Scheme 30). Further heating of the product **52a** resulted in poly(ferrocenylphosphine) $\mathbf{52_n}$. In another attempt, **52** was treated with the stronger coordinating agent PMe_3 under UV/Vis irradiation and analysis of the resulting product **52b** revealed the complete dissociation of the η^1-Cp ring from the iron center (Scheme 30).

Scheme 30. Photolysis of Phospha[1]Ferrocenophanes **52** in the Presence of $P(OMe)_3$ and PMe_3.

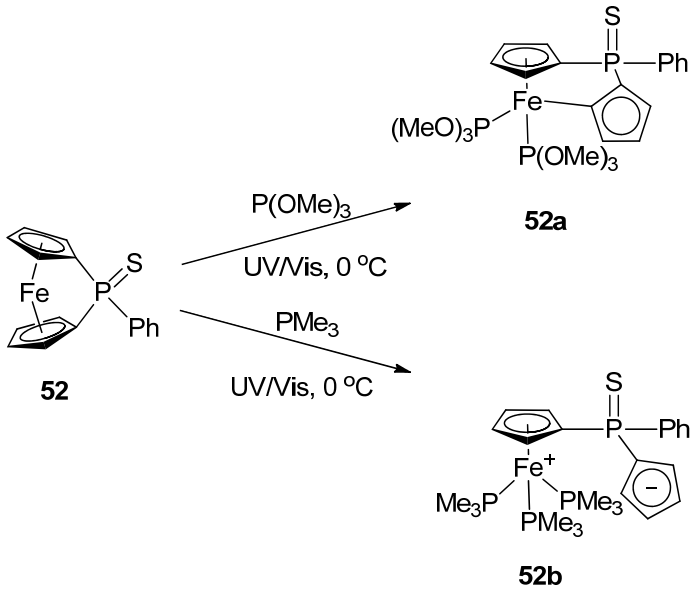

Based on these results a mechanism was proposed for the photocontrolled ROP of strained sandwich compounds in which the reactive intermediates, similar to the isolated species **52a** and **52b**, are formed initially and then react with remaining monomers for the propagation step (Scheme 31).

Scheme 31. Proposed mechanism for the Photocontrolled ROP of Phospha[1]ferrocenophane.

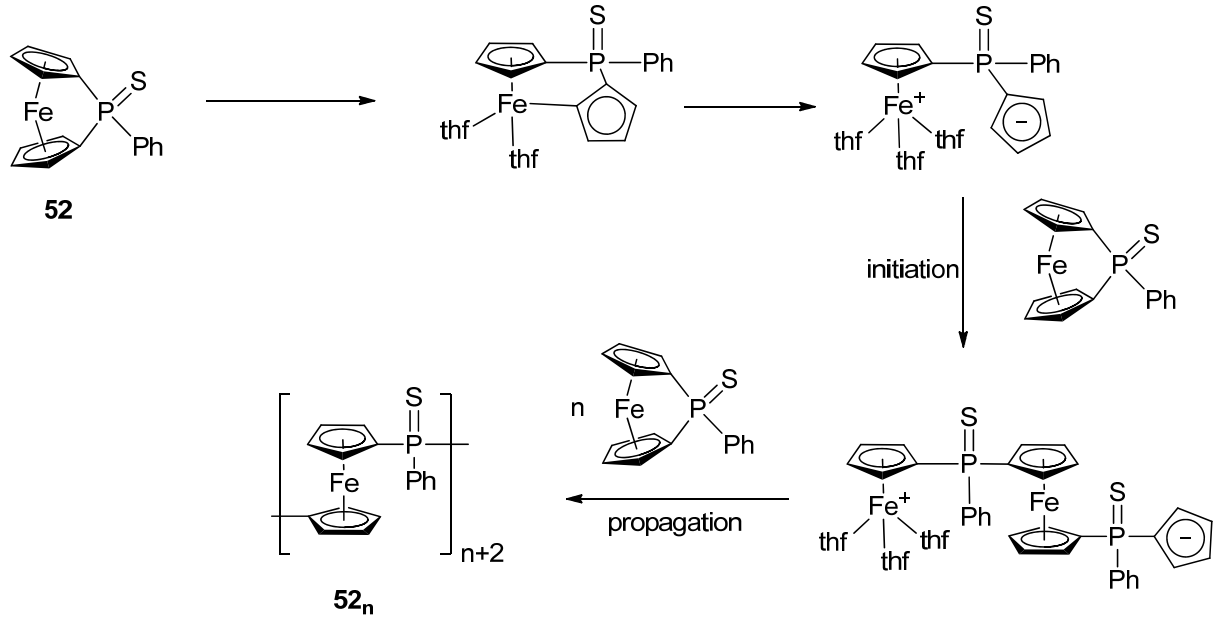

Being inspired by these results, Manners et al. investigated the photocontrolled living carbanionic ROP of silicon-bridged [1]FCPs in 2004.[89] Initial results demonstrated that neither UV/Vis irradiation (λ > 300 nm) nor $(C_5H_4Me)Li$ is solitary capable of causing a ROP on silicon-bridged [1]FCPs. However, UV/Vis irradiation of dimethylsila[1]ferrocenophane in the presence of $(C_5H_4R)Li$ (R = Me or H) results in Fe-Cp bond cleavage. The relatively weak Fe-Cp bond of strained dimethylsila[1]ferrocenophane is further weakened up on irradiation, which causes iron center to be more reactive toward nucleophilic attack and, therefore, the mechanism of photocontrolled ROP goes through the breakage of Fe-Cp bonds (Scheme 32).

In a similar reaction, high-molecular-weight PFS with a narrow molecular-weight distribution (PDI < 1.1) was obtained by living photocontrolled ROP in the presence of NaCp under UV/Vis irradiation.[90]

Scheme 32. Proposed Mechanism for the Photocontrolled ROP of Me_2Si[1]FCP.

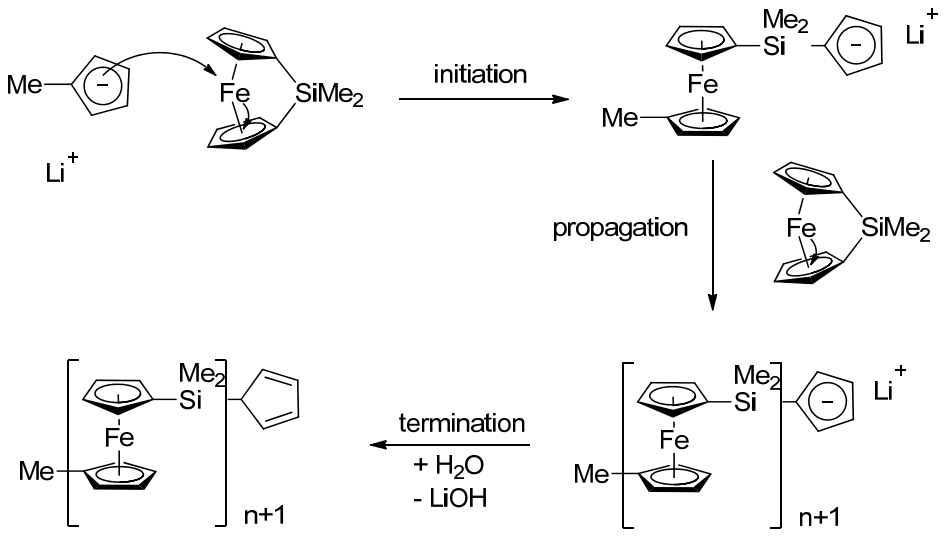

Transition-metal-catalyzed ROP

This method was employed by Tanaka et al. in 1995 for the ROP of silicon-bridged [1]FCPs.[91] Dimethylsila[1]ferrocenophane was reacted with a catalytic amount of $[Pt(cod)_2]$ (cod = 1,5-cyclooctadiene) and high-molecular-weight polymer ($M_w \approx 10^6$) with a wide range of molecular weight distribution (PDI = 2.8) was obtained. In another attempt, applying more soluble catalysts, such as $[Pt_2(dba)_3]$ and $[Pd(dba)_2]$ (dba = dibenzylideneacetone), yielded polymers of lower molecular weights ($M_w \approx 10^4$) over a shorter period of time. Using $[Pt(cod)_2Cl_2]$ as catalyst, resulted in extremely fast polymerization of dimethylsila[1]ferrocenophane and polymers with bimodal molecular weight distribution ($M_w \approx 10^4$ and 10^6) were obtained. In contrast, applying phosphine complexes of palladium and platinum, such as $[M(PPh_3)_4]$ and $[M(PPh_3)_4]$ (M = Pd and Pt), for the ROP of dimethylsila[1]ferrocenophane at ambient temperature did not yield polymers. The transition-metal-catalyzed ROP of [1]FCPs was also reported by Manners et al. in 1995 when catalytic amount of $[PtCl_2]$, $[PdCl_2]$, $[Pd(cod)Cl_2]$ and $[Rh(cyclooctene)_2(\mu\text{-}Cl)]_2$ were applied for the ROP of silicon-bridged [1]FCPs.[92] Similar to

silicon-bridged [1]FCPs, germanium-bridged [1]FCPs are also reactive with respect to transition-metal-catalyzed ROP. In contrast to living carbanionic ROP, this method does not require high purities of reagents and, therefore, it is more convenient for monomers which cannot be extensively purified. Compared to thermal ROPs, where higher temperatures are essential for polymerization, transition-metal-catalyzed ROP proceeds under milder conditions, opening opportunities for ROP of many [1]FCPs which would decompose at high temperatures. In contrast to amorphous polymers obtained from thermal ROP, the transition-metal-catalyzed ROP of silicon-bridged [1]FCPs containing unsymmetrically methylated Cp rings resulted in crystalline material with regular microstructure (Scheme 33). According to the analysis of the resulting polymer, Si-Cp^{H} bond cleavage happens exclusively during the ROP process and Si-Cp^{Me} bond is resistant toward $PtCl_2$-catalyzed ROP. This result was confirmed by the unsuccessful $PtCl_2$-catalyzed ROP of $[(C_5Me_4)_2FeSiMe_2]$.[93]

Scheme 33. Synthesis of Regioregular Poly(ferrocenylsilane).

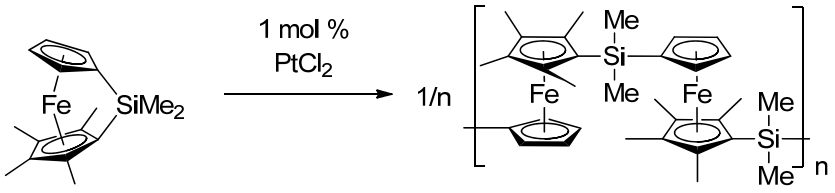

31 **31_n**

Despite the initial belief that transition-metal-catalyzed ROP goes through a homogeneous mechanism,[94] Manners et al. suggested a heterogeneous catalytic pathway where colloidal metal is the main active catalyst (Scheme 34).[95] The reaction between dimethylsila[1]ferrocenophane and $[Pt(cod)_2]$ results in platinasila[2]FCP **53** through the oxidative addition to the transition-metal fragment. It was initially believed that species **53** is the active precatalyst for the homogeneous catalytic pathway, however, further studies revealed the absence of this species in

the growing chain. In the proposed mechanism, reductive elimination of the transition-metal complex Pt(cod) from [2]FCP **53** is followed by the elimination of cod resulting in platinum colloids which act as the active catalyst species. This mechanism was also supported by observing the retardation of the reaction in presence of mercury, a well-known inhibitor for heterogeneous catalysis. However, since inhibitors for homogenous catalysts were not tried to check a relevant retardation effect on these reactions, the homogeneous pathway cannot be ruled out completely.

Scheme 34. Proposed Mechanism for the Transition-metal-catalyzed ROP.

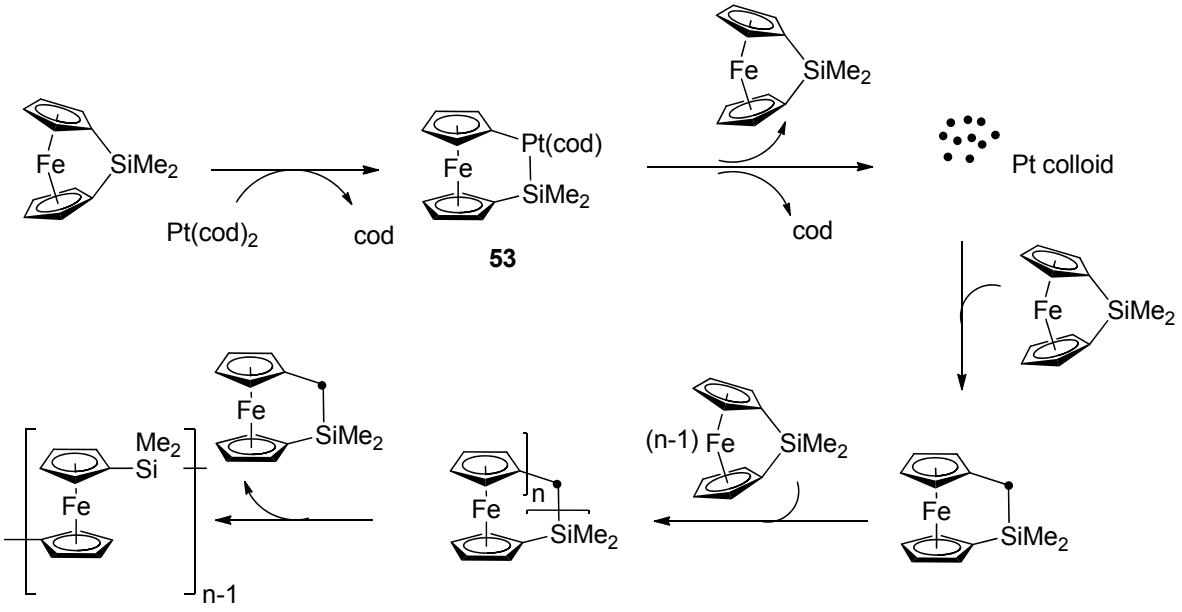

1.2.4. Poly(ferrocene)s Containing Group 13 Elements in the Bridging Position

As it was described earlier, boron-bridged [1]FCPs possess the highest known tilt angle ($\alpha \approx 32°$) among [1]FCPs known to date.[5, 30] The high tilting of Cp rings in these [1]FCPs makes them valuable candidates for the preparation of poly(ferrocenylborane)s through ROP. Compared to silicon-bridged [1]FCPs, the exothermic peak for boron-bridged [1]FCPs appears at higher temperatures in the DSC thermogram. For instance, the published DSC thermogram of

$(Me_3Si)_2$NBfc (**6a**) displayed a ROP exotherm at 190 °C with a melt endotherm at 115 °C and that of (Me$_3$Si)*t*BuNBfc (**6b**) demonstrated a melt endotherm at 150 °C which overlaps with the ROP exotherm at a slightly higher temperature. Similar to **6b**, *i*Pr$_2$NBfc (**6c**) illustrated an endothermic melting signal at 185 °C overlapping with the ROP exotherm. Due to the overlapping of the melt endotherms and ROP exotherms, the ring-opening enthalpy was only reported for $(Me_3Si)_2$NBfc (**6a**; ΔH^{ROP} = -95 kJ mol^{-1}). Although the measured ring-opening enthalpy for **6a** is higher than the measured values for silicon-bridged [1]FCPs (ΔH^{ROP} = -70-80 kJ mol^{-1}),[18] it is less than the expected value for a [1]FCPs with a tilt angle around 32° (ΔH^{ROP} of -130 ± 20 kJ mol^{-1} for sulfur-bridged [1]FCP **45** with similar tilt angle).[10, 11] The thermal ROP of $(Me_3Si)_2$NBfc (**6a**) resulted in mostly insoluble materials and the characterization of the soluble fraction with ^{1}H NMR spectroscopy indicated the presence of cyclic dimers in the mixture (Scheme 35). On the other hand, solid ^{13}C NMR spectroscopy of the insoluble material illustrated characteristic peaks such as a peak at 5.1 ppm corresponding to $SiMe_3$ substituent and peaks at 74.1 ppm and 77.6 ppm related to Cp carbons. Molecular ion peaks of the oligo(ferrocenylborane) with 2 and 3 repeating units were observed by the pyrolysis mass spectrometry of the insoluble material. Similarly, the thermal ROP of (Me$_3$Si)*t*BuNBfc (**6b**) at 200 °C yielded insoluble material. In contrast to the other two boron-bridged [1]FCPs, thermal ROP of $(iPr)_2$NBfc (**6c**) at 200 °C resulted in products which are completely soluble in common organic solvents such as CH_2Cl_2, $CHCl_3$, thf and toluene. Due to the moisture instability of **6c$_n$**, the molecular weight of the obtained polymer could not be measured by gel-permission chromatography (GPC). However, dynamic light scattering (DLS) measurement of the product in toluene did not indicate the presence of any detectable particle, which was justified by the low-molecular-weight of the resulting polymers.[96] Moreover, mass spectrometry identified the

existence of dimeric and trimeric ferrocenylboranes with cyclic structures. The cyclic dimer and trimer were also characterized by multinuclear NMR spectroscopy after being separated from the bulk polymer. In conclusion, all the attempts for ROP of the boron-bridged [1]FCPs have been unsuccessful and, at best, resulted in the formation of oligomers with 2 and 3 repeating units. Since then, there has not been any other progress in this area and this chemistry came to standstill in 2000.

Scheme 35. Thermal ROP of Boron-bridged [1]FCPs.

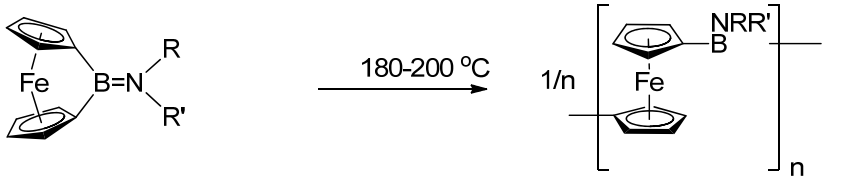

6a: R = R' = $SiMe_3$
6b: R = $SiMe_3$, R' = *t*Bu
6c: R = R' = *i*Pr

6a$_n$: R = R' = $SiMe_3$
6b$_n$: R = $SiMe_3$, R' = *t*Bu
6c$_n$: R = R' = *i*Pr

In 2006, a completely different pathway toward the preparation of poly(ferrocenylborane)s was introduced by Wagner et al. when the highly air- and moisture sensitive poly(ferrocenylborane) **54** was synthesized by the coupling reaction of $(C_5H_4BBr_2)_2Fe$, while using three equivalents of triethylsilane (Scheme 36).[97]

Scheme 36. Synthesis of the Bromine-substituted Poly(ferrocenylborane).

54

The polymer **54** is barely soluble in common organic solvents. In order to increase its solubility as well as air stability, **54** was reacted with CuMes and bromine groups on the boron were

replaced with mesityl groups. Compared to **54**, the resulting polymer **55** has the advantage of being moderately stable in air and also properly soluble in organic solvents (Scheme 37).

Scheme 37. Synthesis of the Mesityl-substituted Poly(ferrocenylborane) **55**.

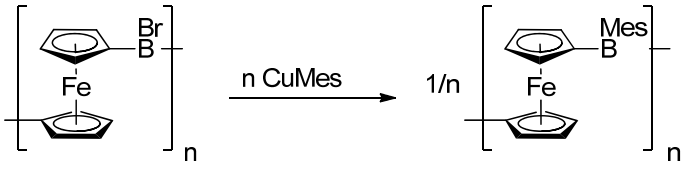

54 **55**

The polymer **54** was analyzed by different techniques such as ^{1}H NMR spectroscopy, thermogravimetric analysis (TGA), GPC and MALDI TOF mass spectroscopy. The GPC analysis of **54** showed a molecular weight of M_w = 7.5 kDa with respect to polystyrene. The highest peak in the MALDI TOF mass spectrum of **54** was correlated to 12 ferrocene units.

Compared to boron-bridged [1]FCPs, lower tilt angles were observed for heavier group-13-bridged [1]FCPs. The measured tilt angle α for the four successfully isolated aluminum- and gallium-bridged [1]FCPs **9a**, **9b**, **10a**, and **10b** were in the range of 14-16° (Scheme 4).[6, 31, 32, 98] Generally, strained [1]FCPs with α tilt angles above 12° are prone to ROP and this means these compounds are potential candidates for polymerization. The DSC thermograms of aluminum- and gallium-bridged [1]FCPs bearing the Me_2Ntsi ligand (**9a** and **9b**) displayed melt endotherms of 177 °C for the alumina[1]ferrocenophane **9a** and 183 °C for the galla[1]ferrocenophane **9a** and the ROP exotherm signals were observed at 212 °C for the alumina[1]ferrocenophane **9a** and 220 °C for the galla[1]ferrocenophane **9b**.[99] On the other hand, only exotherm ROP signals (180 °C for the alumina[1]ferrocenophane and 173 °C for the galla[1]ferrocenophane) were observed in the DSC thermogram of the aluminum- and gallium-bridged [1]FCPs equipped with Pytsi ligand (**10a** and **10b**, Scheme 4). Attempts for the thermal ROP of aluminum- and gallium-

bridged [1]FCPs **9a** and **9b** resulted in the complete conversion of monomers into oligomers with the molecular-weight of 1.5 kDa (measured by DLS). The anionic ROP of aluminum and gallium-bridged [1]FCPs (**9a** and **9b)** was attempted by treating them with the equivalent amount of alkyllithium reagents, such as MeLi, *n*BuLi and *t*BuLi, in different organic solvents at r.t. and elevated temperatures. Interestingly, **9a** and **9b** showed a complete resistance toward anionic initiators as no trace of the ring-opened products was observed in the reaction mixtures. The aluminum- and gallium-bridged [1]FCPs equipped with Pytsi ligand (**10a** and **10b**, Scheme 4) were also reacted with equivalent amount of *n*BuLi, as anionic initiator, to test their propensity toward anionic ROP. The presence of the unreacted starting materials as well as the new [1]FCP **56** was confirmed by reviewing the ^{1}H NMR spectra of the reaction mixture. Similarly, the photocontrolled ROP by using NaCp and UV/Vis irradiation did not show any promising result.[99]

Scheme 38. Reaction of *n*BuLi with (Pytsi)Alfc.

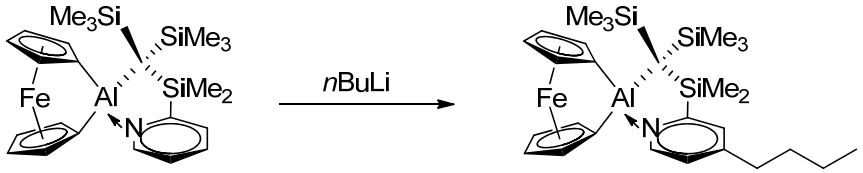

10a **56**

Despite the unsuccessful result with the thermal and anionic ROPs, the transition-metal-catalyzed ROP of aluminum- and gallium-bridged [1]FCPs (**9a**, **9b**, **10a**, **10b**) to the preparation of polymeric materials. Among all, (Pytsi)Gafc (**10b**) demonstrated the most successful result where the reaction of **10b** with 2 mol% of $Pd(dba)_2$ (dba = dibenzylideneacetone) catalyst yielded polymers with a M_w of 21.1 kDa with respect to polystyrene (measured by GPC).

The first and only fully characterized high-molecular-weight poly(ferrocenylgallane) was reported by Müller et al. in 2010 (Scheme 6).[33] All the attempts to synthesize and isolate the

gallium-bridged [1]FCP **13** resulted in formation of poly(ferrocenlylgallane) $\mathbf{13_n}$ in the reaction mixture. The resulting polymer was purified by precipitation in methanol and isolated in 45% yield. Surprisingly, $\mathbf{13_n}$ was fairly stable in air and characterized by various techniques such as GPC, DLS, DSC, TGA, CV, ^{1}H NMR and ^{13}C NMR spectroscopy (Scheme 6). The GPC analysis of $\mathbf{13_n}$ showed a M_w of 48 kDa (PDI = 3.3) with respect to polystyrene. Interestingly, the ^{1}H NMR spectrum of this poly(ferrocenylgallane) showed peaks with rich fine structures, giving information about the polymer's tacticity. Similar to the polymer $\mathbf{13_n}$, poly(ferrocenylgallane) $\mathbf{14_n}$ was synthesized by the spontaneous polymerization of aluminum-bridged [1]FCP **14** under the conditions of its formation (Scheme 6).[34] The resulting polymer $\mathbf{14_n}$ was also characterized and M_w of 106 kDa was estimated by DLS analysis.

1.2.5. Poly(ferrocene)s Containing Group 14 Elements in the Bridging Position

As it was addressed before, there is no report of carbon-bridged [1]FCPs in the literature. However, there are some known examples of carbon-bridged [n]FCPs (n > 1) (Figure 5).

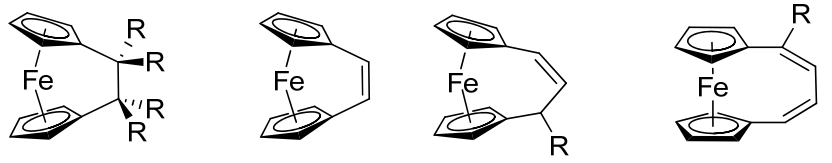

Figure 5. Carbon-bridged [n]FCPs (n = 2, 3, 4).

In contrast to the high ring strain of carbon-bridged [2]FCPs (**57**: α = 21.6° and **3**: α = 23.0°),[2, 100, 101] the ROP of these species was not very fruitful. Thermal, photocontrolled and transition-metal-catalyzed ROP techniques were applied to polymerize these species and mostly resulted in low-molecular-weight poly(ferrocenylethylene).[100] The unsaturated-carbon-bridged [2]FCP **58** has a

similar tilt angle as its saturated counterpart **57** (Figure 5).[102] Compared to the unsaturated-carbon-bridged [2]FCP **58**, olefinic-bridged [3]FCPs **59** and **60** possess lower tilt angles of around 12°.[103] Olefinic-bridged [4]FCPs (**61**, **62** and **63**) on the other hand, are not significantly tilted and the Cp ring are positioned almost parallel to each other.[104, 105] Attempts for the ROP of the unsaturated-carbon-bridged [n]FCPs (n = 2, 3 and 4) were not successful,[100] however, these species showed promising results with ring-opening metathesis polymerization (ROMP). The ROMP of the [2]FCP **58** and the [3]FCP **59** in the presence of molybdenum-based ROMP initiator ([Mo]) yielded in the formation of insoluble polymeric materials.[102, 103] However, high-molecular-weight soluble polymers ($M_w \approx 10^4$ - 10^5 kDa) were obtained by the ROMP of [4]FCPs (**61**, **62** and **63**) in the presence of tungsten-based ROMP initiator ([W]) and the resulting polymers were stable in air (Scheme 39).[105]

Scheme 39. Ring-opening Metathesis Polymerization of the Carbon-bridged [4]FCPs.

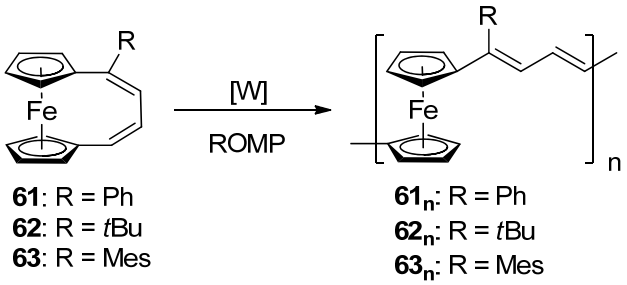

Metallopolymers with a wide range of molecular-weights ($M_w \approx 1 \times 10^5$ to 3×10^5) and polydispersities (PDI = 1.6-2.3) were obtained by changing the ratio between monomer **62** and [W]. It was observed that increasing the ratio between the catalyst and the monomers increases both the polydispersities and the molecular weights.

Currently, there is a wide range of known silicon-bridged [1]FCPs known in the literature. These compounds are highly tilted and release a considerable amount of energy upon ROP (-70-80 kJ

mol^{-1}). Silicon-bridged [1]FCPs are very flexible toward ROP techniques and their polymerization has been studied intensely by using common ROP techniques (thermal,[18] photocontrolled,[89] anionic[84] and transition-metal-catalyzed[92]). As it was described before, PFSs are the most well-known ferrocene-based metallopolymers and these polymers have a wide range of potential applications in material science. The thermal ROP of spirocyclic silicon-bridged [1]FCP **28** resulted in cross-linked poly(ferrocenylsilane) $\mathbf{28_n}$ with three different microenviroments (Scheme 40).[20]

Scheme 40. Thermal ROP of the Spirocyclic Silicon-bridged [1]FCP **28**.

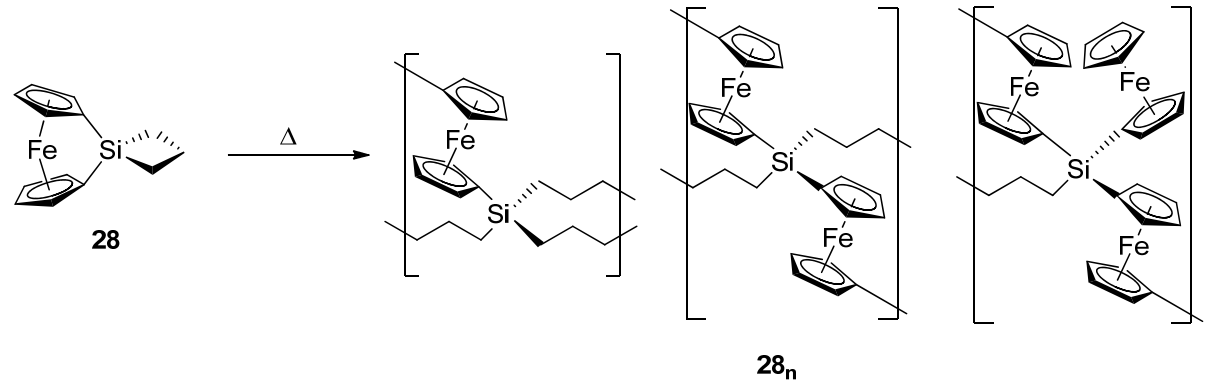

Metallopolymer $\mathbf{28_n}$ was successfully used in a reflective display technology which was based on actuation of photonic crystals.[19] Moreover, pyrolysis of the cross-linked polymer $\mathbf{28_n}$ yielded in a shape-retaining ceramic material with a very good ceramic yield (more than 90%). In contrast to neutral poly(ferrocenylsilane)s, ionic poly(ferrocenylsilane) is soluble in water. Synthesis of the ionic poly(ferrocenylsilane)s is illustrated in Scheme 41. The transition-metal-catalyzed ROP of the silicon-bridged [1]FCP **64** yielded in the metallopolymer $\mathbf{64_n}$ and the subsequent halide exchange resulted in $\mathbf{65_n}$, which was used for the preparation of the cationic and anionic poly(ferrocenylsilane)s $\mathbf{66_n}$ and $\mathbf{67_n}$.[106]

Scheme 41. Preparation of the Anionic and Cationic Poly(ferrocenylsilane)s.

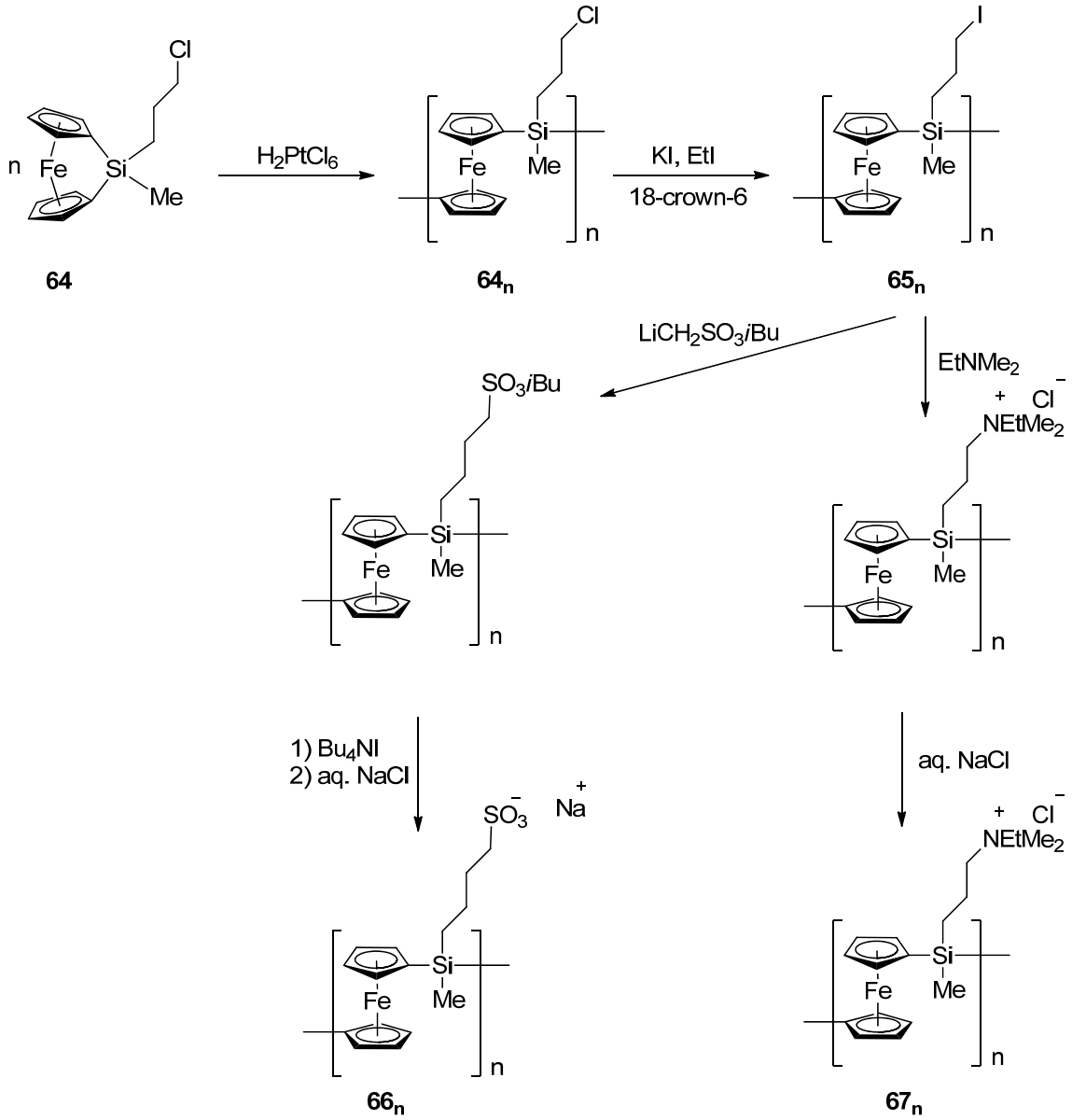

The electrostatic layer-by-layer self-assembly of the ionic ploy(ferrocenylsilane)s $\mathbf{66_n}$ and $\mathbf{67_n}$ on colloidal templates was followed by removal of templates which resulted in water-soluble poly(ferrocenylsilane)-based capsules.[21] These water soluble capsules can potentially find application in drug delivery.

In comparison to silicon-bridged [1]FCPs, germanium-bridged [1]FCPs are less strained and possess moderately tilted Cp rings (α ≈ 18°). Poly(ferrocenylgermane)s are synthesized by applying various ROP techniques such as thermal,[53] anionic[107] and transition-metal-catalyzed ROP.[108] Similar to silicon-bridged [1]FCPs, germa[1]ferrocenophanes can be polymerized in a living fashion,[107] for instance, poly(ferrocenylgermane)-based block copolymers, such as polyisoprene-block-poly(ferrocenylgermane), are prepared by employing living anionic ROP. Micelles with triblock and pentablock core, containing poly(ferrocenylsilane) and poly(ferrocenylgermane) in the core, were prepared in block selective solvents by crystallization-driven selfassembly.[109] Despite the low tilt angle of germanium-bridged [2]FCPs (α ≈ 4°), the transition-metal-catalyzed ROP of digerma[2]ferrocenophane **68**, using Pt(II), Pd(0) and Pd(II) catalysts, yielded high-molecular weight poly(ferrocenylgermane)s.[110] However, attempts for the thermal and anionic ROP of digerma[2]ferrocenophane **68** were not successful (Scheme 42).

Scheme 42. Transition-metal-catalyzed ROP of Digerma[2]ferrocenophane.

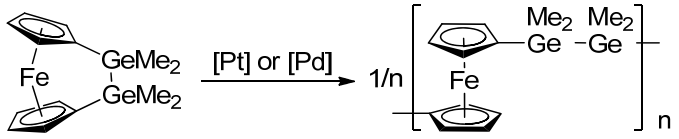

68 **68n**

The initial attempts for the synthesis of poly(ferrocenylstannane)s by the polycondensation polymerization of dilithioferrocene and R_2SnCl_2 (Me, Et, *n*Bu and Ph) resulted in low-molecular-weight polymers.[47, 58] Interestingly, stanna[1]ferrocenophanes **37a** and **37b** were unstable in solution and the spontaneous ROP of these species in organic solvents resulted in high-molecular-weight poly(ferrocenylstannane)s ($M_w \approx 10^6$, PDI = 1.3-1.6) as well as small amount of cyclic species.[13, 56] The DSC thermograms of stanna[1]ferrocenophanes **37a** and **37b** displayed exotherm peaks at 150-180 °C, confirming the potential of these species for thermal ROP. The

thermal ROP of tin-bridged [1]FCPs **37a** and **37b** resulted in high-molecular-weight polymers ($M_w \approx 10^5$) with a relatively narrow molecular weight distribution (PDI = 1.6-1.9) (Scheme 43).

Scheme 43. Thermal and Spontaneous ROP of Stanna[1]ferrocenophanes.

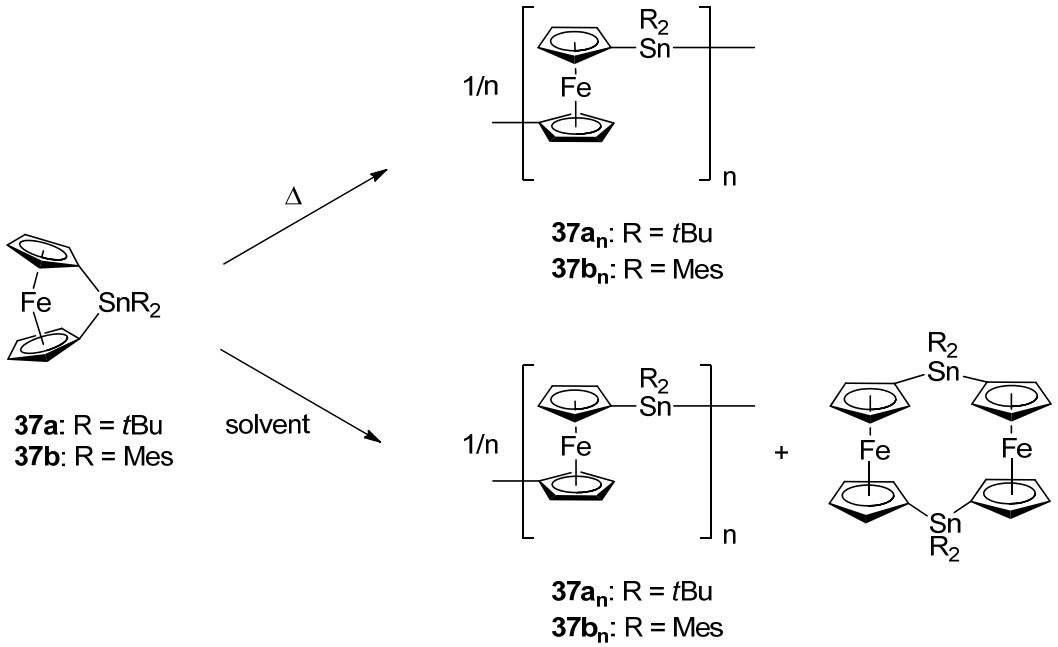

Despite the successful transition-metal-catalyzed ROP of silicon-bridged [1]FCPs and germa[1]ferrocenophanes, the transition-metal-catalyzed ROP of stanna[1]ferrocenophanes did not result in metallopolymers. For instance, employing Karstedt's catalyst, a Pt(0) species, hindered the spontaneous polymerization of **37a** and **37b** in solution.[13]

1.2.6. Poly(ferrocene)s Containing Group 15 Elements in the Bridging Position

While there is no report about the ROP of arsenic-bridged [1]FCPs, the ROP of phosphorus-bridged [1]FCPs is very well developed. Phospha[1]ferrocenophanes have been polymerized by using different ROP methods such as thermal,[63] anionic[111] and photocontrolled.[64] Block copolymers polystyrene-*b*-poly(ferrocenylphosphine) and polyisoprene-*b*-poly(ferrocenylphosphine) with a narrow molecular weight distribution (PDI = 1.1-1.2) were

synthesized by the living anionic block-copolymerization of the respective monomers (Scheme 44).[111]

Scheme 44. Anionic ROP of Phospha[1]ferrocenophane Initiated by Living Isoprene and Polystyrene.

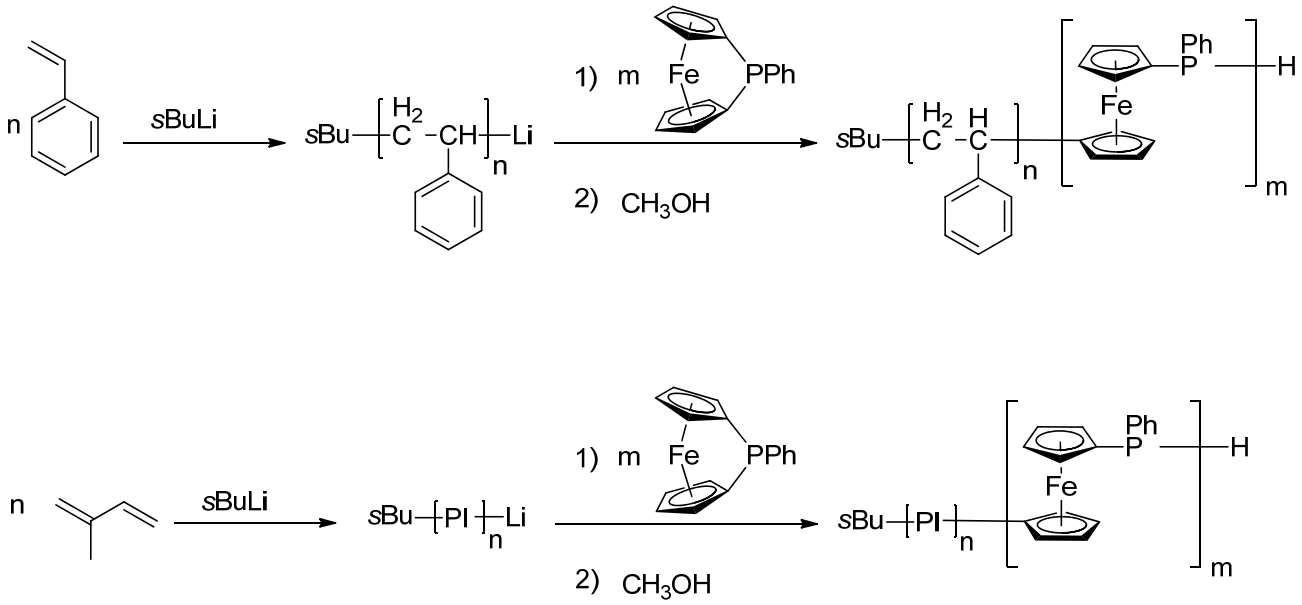

Employing NaCp as the initiator, poly(ferrocenylphosphine)s with well-defined molecular weights were synthesized through photocontrolled living anionic ROP of the phosphorus-bridged [1]FCPs **69**, **70** and **71** (Scheme 45a). Moreover, the living nature of this photocontrolled ROP allowed the preparation of the diblock copolymer polyferrocenylmethyl(3,3,3-trifluoropropyl)silane-*b*-poly(ferrocenylphosphine) through stepwise addition of monomers (Scheme 45b).[64]

Scheme 45. Photocontrolled Living Anionic ROP of Phosphorus-bridged [1]FCPs.

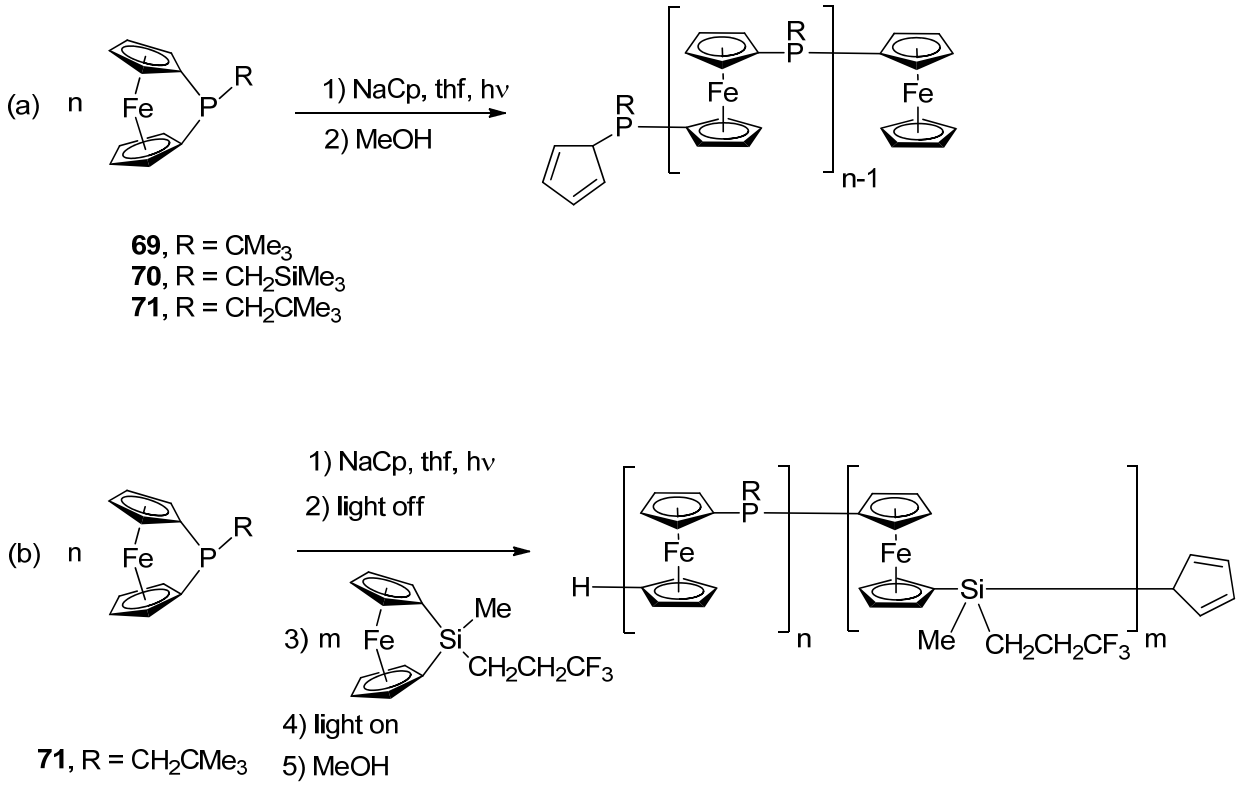

1.3. Planar-chiral Ferrocenes

Planar chiral ferrocenes are particularly important as they have widely been used in catalytic asymmetric transformations in both industry and scientific research. For instance, highly efficient Ir/Xyliphos-catalyzed enantioselective hydrogenation of imine **72** is recognized to be the largest scale enantioselective catalytic reaction (Scheme 46).[112, 113]

Scheme 46. Ir/Xyliphos Catalyzed Imine Hydrogenation.

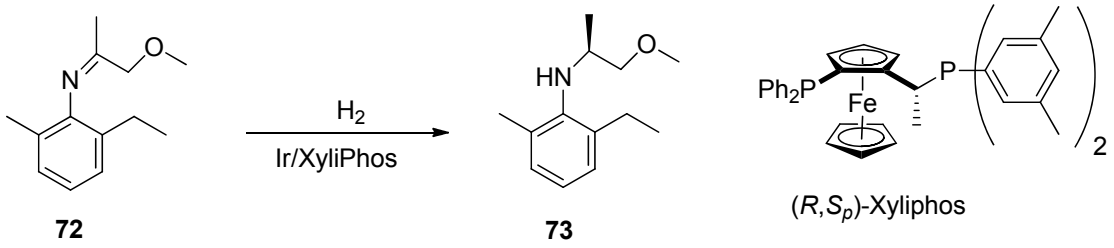

72 **73**

The obtained amine **73** is a very important intermediate for the synthesis of the herbicide (*S*)-metolachor which is prepared in a volume of more than 10000 tons per year. The three-dimensional nature of ferrocene causes the planar chirality of heterodisubstituted ferrocenes. Within this thesis, the stereodescriptors "R_p" and "S_p" are used, according to Schlögl's definition, in order to describe planar chirality (Figure 6).

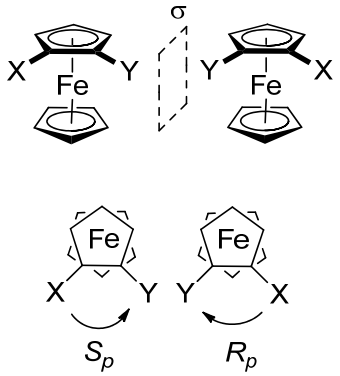

Figure 6. Enantiomeric1,2-heterodisubstituted ferrocenes (X and Y) from two different prospective and assignments of stereodescriptors according to Schlögl's definition where (X > Y).

A comprehensive overview of the synthesis and applications of planar-chiral ferrocenes in asymmetric catalysis is beyond the scope of this chapter and interested readers are referred to the excellent reviews published in this area.[114-117] However, the *ortho*-directed metalation of ferrocene species, specially the "Ugi's amine" approach, will be discussed shortly.

1.3.1. *ortho*-Directed Metalation

Lithiation by employing strong bases is one of the most common pathways for the derivatization of the ferrocene backbone. Dilithioferrocene·tmeda, which is synthesized by the treatment of ferrocene with *n*BuLi in the presence of tmeda, is the most well-known reagent for derivatization of ferrocene. Planar-chiral ferrocenes can be synthesized by the reaction of mono or 1,1′-disubstituted ferrocenes with strong bases. For instance, the treatment of isopropylferrocene **74**

with *n*Buli in ether and the subsequent reaction with trimethylchlorosilane results in four different substituted ferrocenes. By applying a ratio of 1:1 *n*BuLi and **74**, the ratio between mono- and disubstituted products is reported to be almost the same and the deporotonation happened in the order of 1′ > 3 > 2 (Scheme 47).[118]

Scheme 47. Lithiation and Subsequent Silylation of Isopropylferrocene.

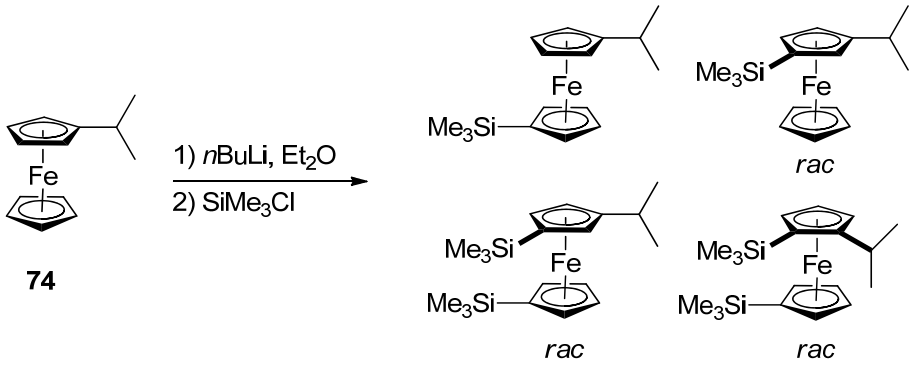

However, the presence of an *ortho*-directing group (ODG) on the Cp ring causes a significant change in the ratio between products.[119, 120] This effect was first reported by Benkeser et al. in 1961 where an ether solution of diphenylferrocenylcarbinol **75** was treated with an excess of *n*BuLi at r.t. and subsequently reacted with dry ice or methyl iodide.[121] Interestingly, the 1,2-disubstituted ferrocenes *rac*-**76a,b** were identified as the sole products and there was no trace of lithiation on the unsubsituted Cp ring or phenyl rings (Scheme 48).

Scheme 48. *ortho*-Directed Lithiation of Diphenylferrocenylcarbinol.

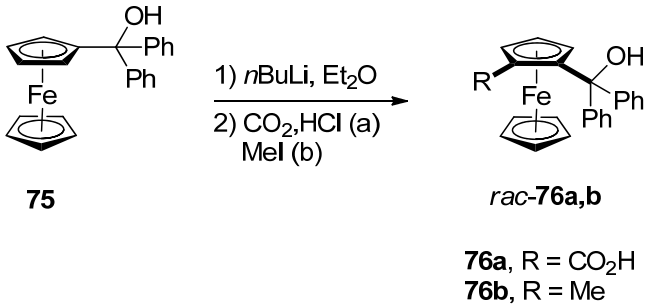

Few years later, Slocum et al. introduced the *ortho*-directed lithiation of N,N-dimethylaminomethylferrocene (**77**), which widely has been used afterward for the preparation of ferrocene-based molecules.[122] It is also described that the choice of solvent plays a crucial role in the selectivity of lithiation. Employing a solvent mixture of hexanes/ether results in the exclusive formation of the 1,2-diubstituted derivative *rac*-**78**, whereas changing the solvent to a mixture of hexanes/thf yields a mixture of different substituted ferrocenes (Scheme 49).

Scheme 49. *ortho*-Directed Lithiation of N,N-Dimethylaminomethylferrocene.

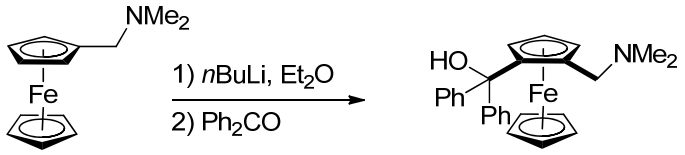

77 *rac*-**78**

The NMe_2 moiety of aminoferrocene **77** can be easily replaced through a nucleophilic substitution reaction and this is probably another reason for the widespread application of this compound. For instance, the treatment of *rac*-**78** with MeI and the subsequent addition of a nucleophilic reagent, e.g. KCN, results in the replacement of trimethylamine group by an SN1 mechanism (Scheme 50).[123, 124]

Scheme 50. Nucleophilic Substitution Reaction of *rac*-**78**.

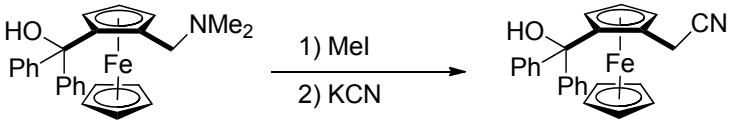

rac-**78** *rac*-**79**

A similar nucleophilic substitution reaction was performed by Weissensteiner and Widhalm for the resolution of the racemic 2-N,N-dimethylaminomethyl-1-bromoferrocenes **80**.[125] The aminoferrocene **77** is *ortho*-lithitated and subsequently brominated to obtain a racemic mixture

of **80**. Compound **80** (Scheme 51) is functionalized by the methylation of the amine group followed by the substitution reaction with (*1R*,*2S*)-ephedrine to yield a 1:1 mixture of diastereomers **81** and **82** which are separable by column chromatography. Eventually, the separated diastereomers **81** and **82** are converted to enantiomerically pure (S_p)- and (R_p)-**80** by another substitution reaction, using methyliodide and dimethylamine.

Scheme 51. Resolution of the Racemic 2-N,N-Dimethylaminomethyl-1-bromoferrocenes.

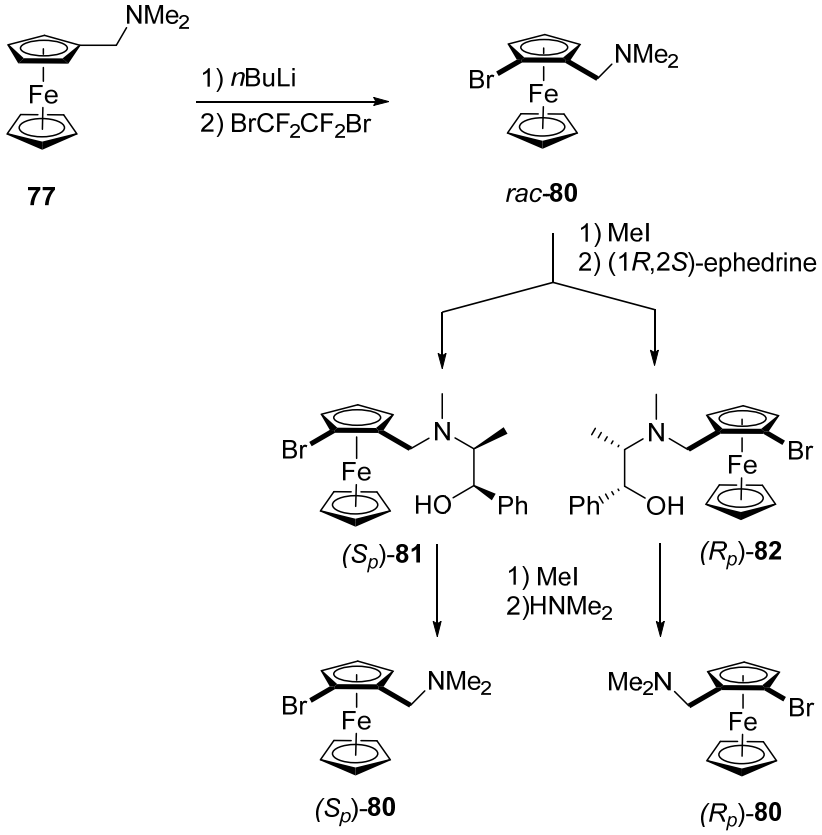

As depicted in Figure 7, the idea of *ortho*-directed metalation of ferrocene moieties has been generalized to a variety of functional groups.[126] However, different ODGs require the use of different metalation protocols such as solvents (hexanes, Et_2O, thf), bases (LDA, *n*BuLi, *t*BuLi, *s*BuLi) and reaction temperatures (-78 °C to reflux). In most of the cases, the 1,2-substituted ferrocenes are obtained with good yields and high regioselectivity.

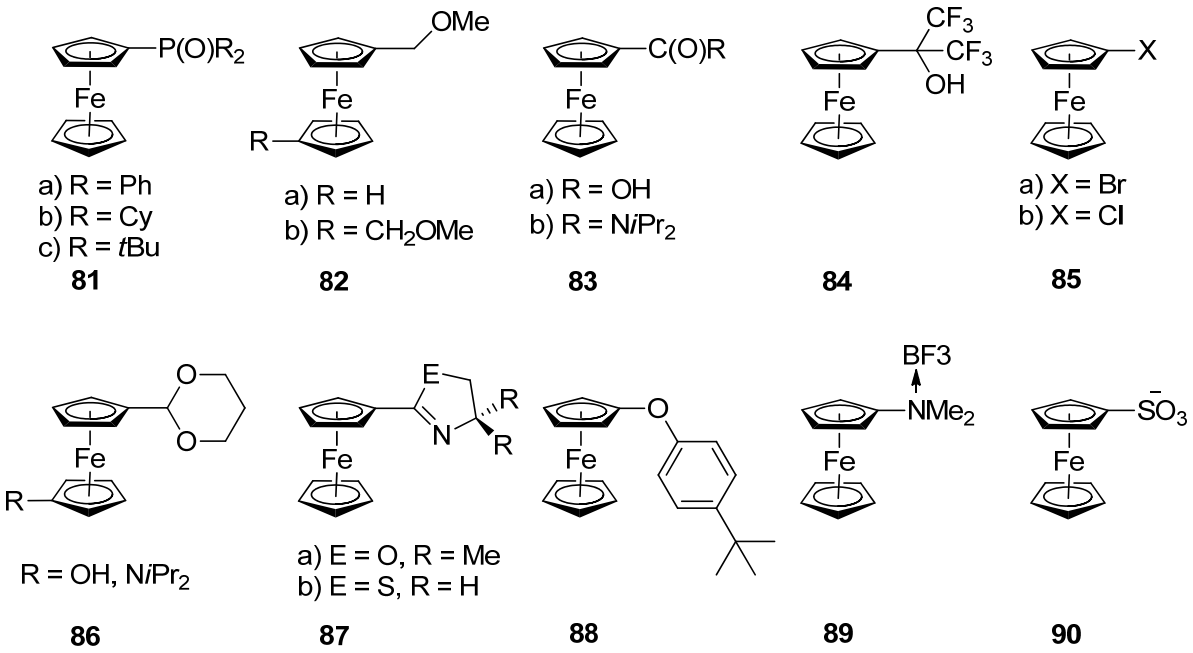

Figure 7. Ferrocene derivatives applied for *ortho*-directed metalations.

During the last few years, bimetal bases [TMPMgCl·LiCl, $(TMP)_3CdLi$ and $(TMP)_2Zn·2LiCl$ (TMP = 2,2,6,6-tetramethylpiperid-1-yl)] have been employed widely for the metalation of ferrocene moieties.[127-129] Compared to alkyl lithiums, bimetallic bases have the advantage of being more compatible with sensitive functional groups such as esters and nitriles.[130] Employing this method, Knochel et al. converted ferrocenyl carboxylic acid derivatives **91** to 1,2-disubstituted ferrocenes *rac*-**92** through metalation with TMPMgCl·LiCl and reaction with electrophiles.[131] In a similar attempt by Krishna and Mongin, an in situ generated mixture of $Zn(TMP)_2$ and LiTMP was used for the *ortho*-directed zincation of **93** and iodoferrocene *rac*-**94** was synthesized in excellent yield (Scheme 52).[132]

Scheme **52**. Using Bimetalic bases for Functionalization of Ferrocenyl Carboxolic Acid Derivatives.

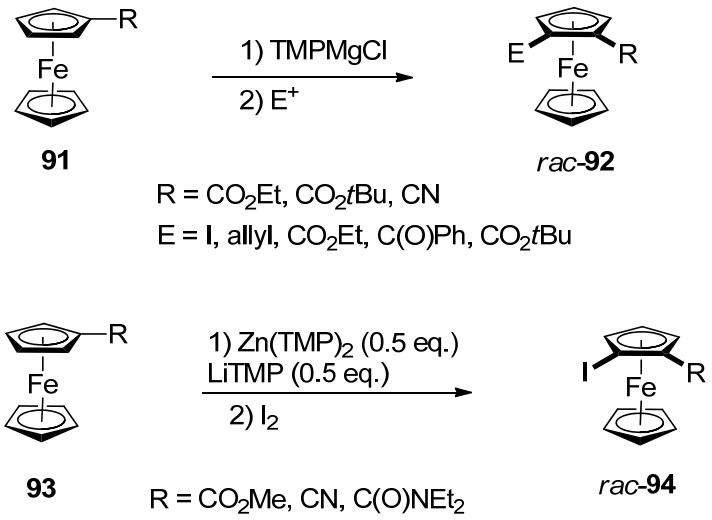

1.3.2. Diastereoselective *ortho*-Directed Metalation

In principal, the *ortho*-directed metalation of chiral ferrocenes results in a mixture of diasteromeric products which might be separable with crystallization or column chromatography. The diastereoselectivity of the metalation increases by the presence of the chirality source in neighborhood of the ferrocene backbone and in the ideal scenario, only one diastereomer is formed as the product. In contrast to the case of *rac*-**80** (Scheme 51), where the resolution was done at the last step,[125] in this method the resolution is performed at the *ortho*-directed metalation step. However, it should be noted that the starting material for the diastereoselective *ortho*-directed metalation has to be enantiomerically pure and the purity should either come from a resolution step or an enantioselective transformation.

The first example of diastereoselective *ortho*-metalation was reported by Aratani et al. in 1969 where the treatment of (*S*)-1-ferrocenylmethyl-2-methylpiperidine (**95**) with *n*BuLi is followed by the reaction with dry ice and resulted in the amino acid (R_p)-**96a**.[133, 134] The (R_p)-2-methylferrocene carboxylate **96b** is obtained in 24% yield and 94% optical purity after the

sequential reaction of (R_p)-**96a** with methyl iodide, sodium amalgam in water and diazomethane (Scheme 53).

Scheme 53. Synthesis of (R_p)-2-Methylferrocene Carboxylate **96b**.

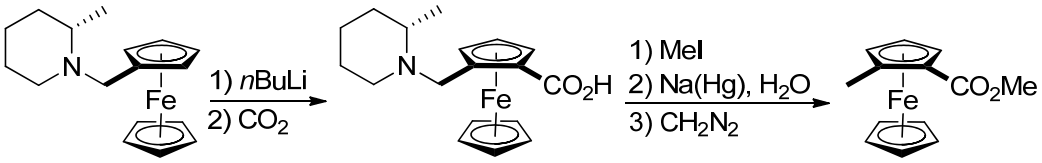

95 (R_p)-**96a** (R_P)-**96b**

In the same year, (*R*)- and (*S*)-N,N-dimethy-1-ferrocenylethylamine (**97**, known as Ugi's amine) was introduced by Ugi et al. as a starting material for diastereoselective *ortho*-directed metalation and it was a milestone in ferrocene chemistry.[135] Both enantiomers of (±)-**97** are separated in high yields by the resolution with (*R*)-(+)-tartaric acid. The lithiation of (*R*)-**97** with *n*Buli in ether at r.t. is followed by addition of an electrophile and (R,S_p)-**98** is obtained in 92% de (Scheme 54).

Scheme 54. Diastereoselective Lithiation of "Ugi's Amine" (*R*)-**97**.

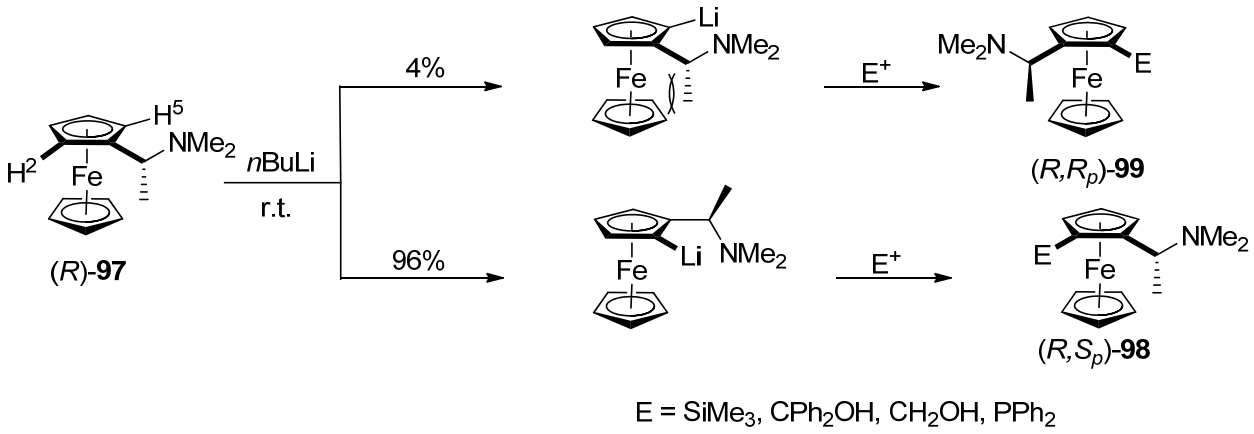

(*R*)-**97** (R,R_p)-**99** (R,S_p)-**98**

E = $SiMe_3$, CPh_2OH, CH_2OH, PPh_2

The small amount of the other diastereomer (R,R_p)-**99** is removed by column chromatography. The X-ray analysis of (R,S_p)-**98** confirmed the stereo chemical course of the metalation and the

data is in agreement with a transition state where the interaction between *C*-methyl group and the ferrocene unit is minimized.[136, 137]

The dilithiation of "Ugi's amine" (*S*)-**97** can be performed in the presence of *n*BuLi and tmeda to obtain 1,2,1′-trisubstituted ferrocenes, without any interference with the diastereoselectivity of the lithiation.[138] Similarly, (*R*,*R*,S_p,S_p)-**102** can be prepared as a single diastereomer by the sequential addition of *n*BuLi and $ClPPh_2$ to a solution of (*R*,*R*)-**101** (Scheme 55).[139-142]

Scheme 55. Diastereoselective Lithiation of "Ugi's Amine" (*S*)-**97** and (*R*,*R*)-**101**.

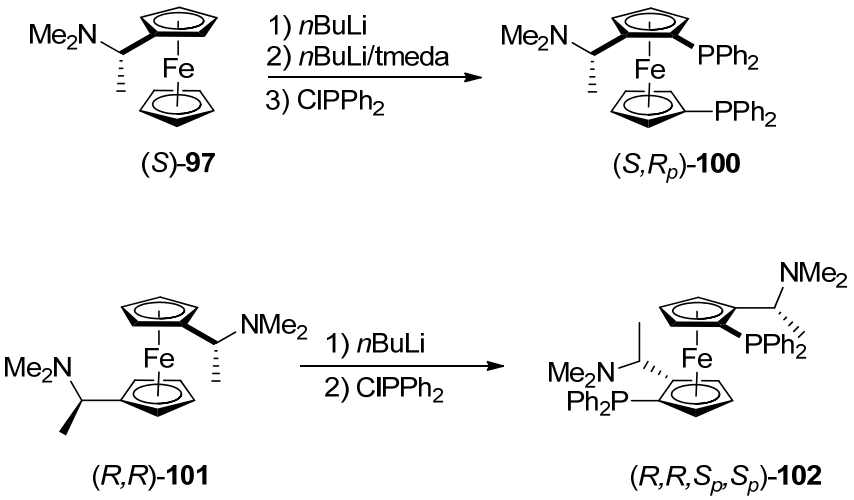

As it was mentioned for **77** (Scheme 50), the displacement of NMe_2 group in α-aminomethylferrocene can be done simply, after quaternization, by applying nucleophiles. Similarly, the dimethylamino group of "Ugi's amine" and other related ferrocenes can be substituted easily (Scheme 56). Interestingly, the nucleophilic substitution of the NMe_2 moiety occurs with a full retention of configuration. This is due to the stabilization of the cationic intermediate through the interaction with iron and, therefore, forcing the nucleophile to only attack from the exo site of ferrocene. However, applying weak nucleophiles (e.g. MeOH instead of NaOMe), which increases the life time of the cationic intermediate, results in epimerization at

the stereogenic carbon. On the other hand, applying only methiodides in the absence of any electrophiles results in the elimination of the leaving group and formation of the vinylferrocenes **104** (Scheme 56).[143, 144]

Scheme 56. Nucleophilic Substitution Reaction at Ferrocenes derived from "Ugi's Amine".

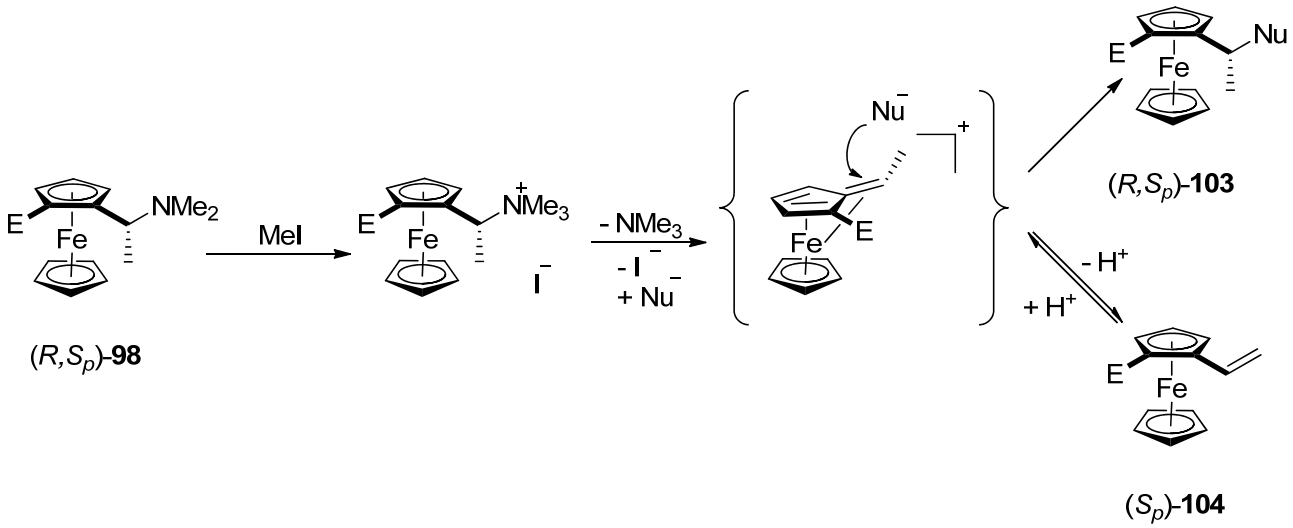

During the past few years it has been demonstrated that the "Ugi's amine" approach can be generalized to various related ferrocene substrates (**105-110;** Figure 8).

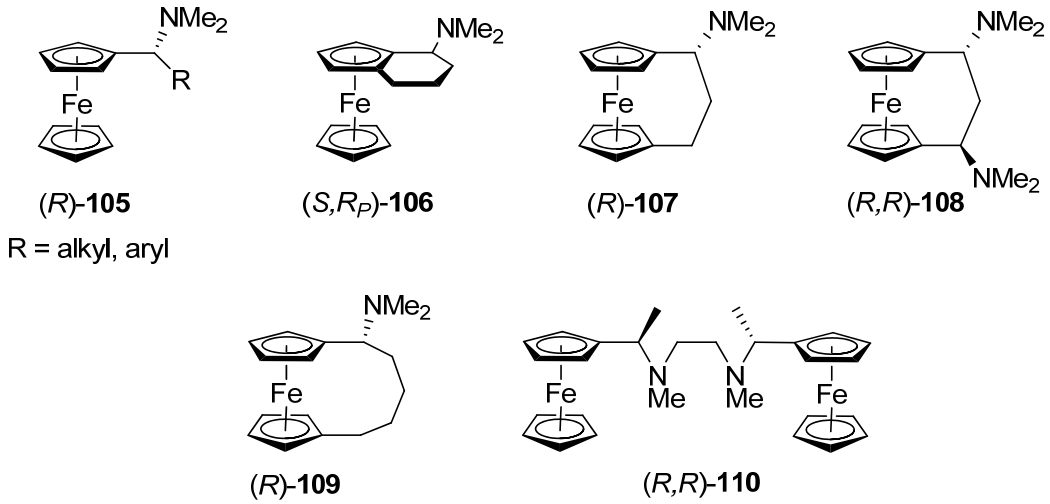

Figure 8. Chiral ferrocenes with NMe_2 substituent used for *ortho*-directed lithiation.

All of these compounds have similar stereoselectivities for *ortho*-directed lithiation and nucleophilic substitutions of the amine group. The enantiomerically pure ferrocene moieties **105-110** have been accessed through different techniques such as asymmetric reduction of imines and ketones, resolution or by applying enantiomerically pure cyclopentadienes or cyclopentadienyl ligands.[126]

Compared to "Ugi's amine" (**97**), a reversed selectivity is observed for the *ortho*-directed lithiation of ferrocene moieties **107-109** which is due to the fixed conformation of these species. For instance, while the lithiation and subsequent phosphanylation of (*S*)-**97** results in (S,R_p)-**98** as the main product, (S,S_p)-**111** is exclusively formed by applying the same reaction condition on the bridged (*S*)-**107** (Scheme 57).[145]

Scheme 57. Comparison of *ortho*-Directed Metalation between (*S*)-**97** and (*S*)-**107**.

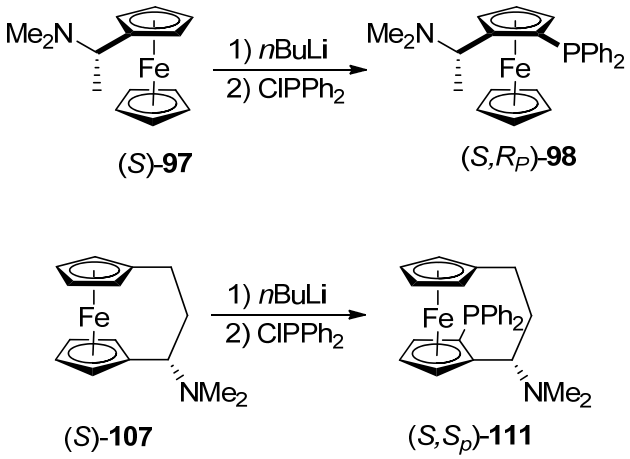

It is reported by Ugi et al. that the replacement of NMe_2 group of (*R*)-**97** with OMe group reduces the regio- and stereoselectivity of the lithiation reaction, resulting in a mixture of 1,2-, 1,3-, and 1,1′-disubstituted ferrocenes.[146] On the other hand, Knochel et al. demonstrated that α-methoxybenzylferrocenes, such as (*R*)-**112**, can be lithiated stereoselectively, yielding (R,S_p)-**113** exclusively (Scheme 58).[147, 148]

Scheme 58. *ortho*-Directed Metalation of α-methoxybenzylferrocene.

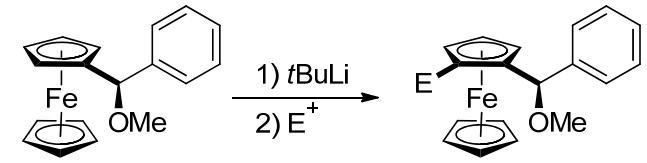

(*R*)-**112** (*R*, S_p)-**113**

Nowadays, there is a large number of publications where "Ugi's amine" **97** has been used for the preparation of starting materials for the asymmetric synthesis. In principal, three points can be addressed as the main reasons for the popularity of this pathway: (a) the high diastereoselectivity of *ortho*-directed lithiation, (b) the versatile synthetic pathway for both enantiomers of **87** and (c) the ease of substitution for amine without epimerization.

1.4. Research Objectives

As it was described in chapter 1.1.1, the bulkiness of the ligand attached to the bridging elements plays an important role for the preparation of aluminum- and gallium-bridged [1]FCPs. Both the *first generation* and the *second generation* of these species were prepared by applying bulky ligands in the bridging position. However, the *first generation* of aluminum- and gallium-bridged [1]FCPs (Scheme 4) were not reactive toward ROP and the *second generation* of aluminum- and gallium-bridged [1]FCPs (Scheme 6) polymerized under the condition of their formation. In order to perform ROP in a controlled way and prepare metallopolymers with well-defined molecular weights, strained [1]FCPs first need to be isolated and purified. The main objective of my PhD work was to prepare heavier group-13-bridged [1]FCPs which were isolable and still reactive toward ROP. My strategy for obtaining the targeted [1]FCPs was to formally move the required bulk from bridging element to ferrocene moiety.

CHAPTER 2

RESULTS AND DISCUSSION

2.1. Preamble Part 1

During the last century, organic polymers have played a very important role in the development of our modern life style. Thanks to the unique optical and electronic properties, transition-metal-containing metallopolymers have an enormous potential for application in future technologies. Since the initial report about the ROP of dimethylsila[1]ferrocenophane that resulted in high-molecular-weight metallopolymers, a tremendous amount of research activities have been devoted toward the ROP of strained [1]FCPs.[18] Nowadays, living polymerization of strained silicon-bridged [1]FCPs is one of the most efficient methods toward obtaining metallopolymers with a perfect control over the molecular weight.[28] In order to obtain new metallopolymers with well-defined molecular weights, there is a need for the development of new monomers which can be polymerized by using living polymerization methodologies. As it was described in chapter 1.1.1, our group started the synthesis of aluminum- and gallium-bridged [1]FCPs as potential monomers for the preparation of metallopolymers (Scheme 4).[6, 31, 32] These species were prepared by the salt-metathesis reaction of dilithioferrocene·tmeda and element dichlorides equipped with bulky ligands ($RECl_2$; E = Al, Ga; R = Pytsi and Me_2Ntsi; Scheme 4). However, attempts for the ROP of these compounds were not successful and, at best, resulted in low-molecular-weight polymers.[99] It was speculated that the bulkiness of the trisyl-based ligands (Pytsi and Me_2Ntsi) hinders the ROP process. It was also discovered that ligand R cannot be easily replaced by other non-bulky ligands, as applying the Ar′ ligand (Scheme 5) for the synthesis of aluminum- and gallium-bridged [1]FCPs resulted in [1.1]FCPs.[36] The resulting [1.1]FCPs do not possess ring-strain and, therefore, are not suitable candidates for ROP to

produce metallopolymers. A study of the structural data suggests that the space available for the bridging unit ER_x increases from [1.1]FCPs to poly(ferrocene)s to [1]FCPs (Figure 9).[37]

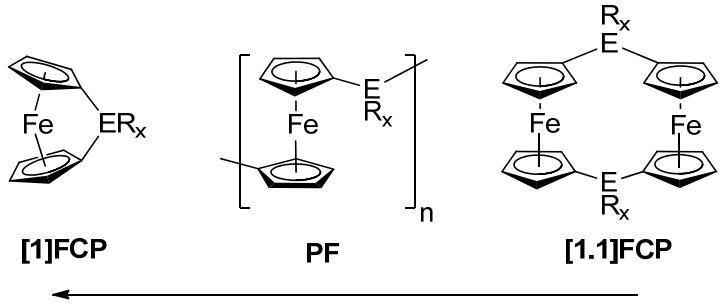

Figure 9. Illustration of the space available for the bridging unit ER_x.

Due to the existing strain in [1]FCP molecules, [1.1]FCP species are thermodynamically preferred products of salt-metathesis reactions and, if there is enough space available for the bridging ER group, [1.1]FCPs would be preferred over the targeted [1]FCPs. Since [1.1]FCPs provide the least space for the bridging unit ER, applying bulky ER groups can block their formation and, consequently, drive the reaction toward the formation of [1]FCPs. On the other hand, if the ligand R is very bulky, there would not be enough space for ER to fit in poly(ferrocene)s which explains why the *first generation* of aluminum- and gallium-bridged [1]FCPs equipped with bulky ER groups (E = Al, Ga; R = Pytsi and Me_2Ntsi) did not result in metallopolymers.

Based on the experience obtained from the *first generation* of aluminum- and gallium-bridged [1]FCPs, our group aimed to optimize steric parameters and synthesize reactive [1]FCPs. The *second generation* of aluminum- and gallium-bridged [1]FCPs were synthesized by applying the Mamx ligand in the bridging position (Scheme 6).[33, 34] The Mamx ligand is the bulky version of the Ar′ ligand due to being equipped with one *t*Bu substituent in *ortho* position of group-13 element (Schemes 5 and 6). The formation of [1.1]FCP species was blocked by applying this

strategy and the respective salt-metathesis reactions resulted in the formation of aluminum- and gallium-bridged [1]FCPs **13** and **14** (Scheme 6). However, [1]FCPs **13** and **14** were not isolable from the reaction mixture and yielded in high-molecular-weight metallopolymers under the condition of their formation. DFT calculations revealed that the amount of strain in [1]FCP species increases considerably (5.5 kcal mol^{-1} on average) due to the presence of *ortho-t*Bu group and this presumably causes the spontaneous ROP.[34] The isolation of metallopolymers $\mathbf{13_n}$ and $\mathbf{14_n}$ (Scheme 6) was an important breakthrough in this area. However, in order to perform a controlled polymerization and obtain block copolymers with a narrow molecular-weight distribution, monomers need to be isolable and still reactive.

The bulkiness of the ligands attached to the bridging element played an important role for the synthesis of both *first generation* and *second generation* of heavier group-13-bridged FCPs and, before my contribution, all the attempts in our group were focused on finding the appropriate ligand for the bridging position. Equipped with these previous experiences with heavier group-13-bridged [1]FCPs, the initial aim of my project was to develop a new method for preparing heavier group-13-bridged [1]FCPs which are isolable and also reactive toward ROP. Careful review of the previously reported structure of the $(Ar'Gafc)_2$ (**12**) shows that there is a very limited space between H atoms in α position on Cp moieties and the H atom in *ortho* position on the phenyl ring (highlighted H atoms in Figure 10).[36] If this space is occupied by a bulky substituent, the formation of [1.1]FCP will be blocked and, presumably, the respective [1]FCP will be the outcome of salt-metathesis reaction.

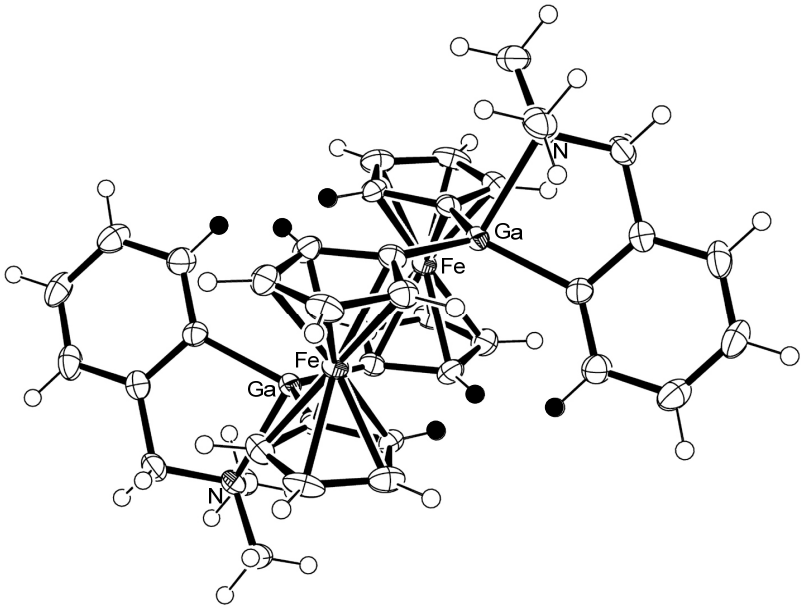

Figure 10. Illustration of the space restrictions in [1.1]FCPs. Molecular structure was reproduced based on the published single-crystal X-ray analysis of $(Ar'Gafc)_2$.[36] Reprinted with permission from Sadeh, S.; Schatte, G.; Müller, J. *Chem.–Eur. J.* **2013***, 40,* 13408-13417. Copyright 2013 Wiley VCH.

For instance, in case of the Mamx ligand, the H atom in *ortho* position on the phenyl ring was replaced by a bulky *t*Bu group and resulted in blocking the formation of the respective [1.1]FCP. For the same reason, it can be presumed that the replacement of one of the two H atoms in α positions on the Cp ring should also block the formation of [1.1]FCPs. The strategy for my PhD work, which aimed at the synthesis of the *third generation* of heavier group-13-bridged [1]FCPs, was to formally move the bulk from the bridging unit to the α position of ferrocene moiety. The aim was to introduce an appropriate amount of bulk so that the obtained [1]FCPs are stable enough to be isolable and at the same time reactive toward ROP. Generally, in salt-metathesis reactions dilithioferrocene·tmeda is commonly used to prepare [1]FCPs. The crucial part of this project was to synthesize α-substituted dilithioferrocene derivatives which can be used instead of dilithioferrocene·tmeda for the preparation of heavier group-13-bridged [1]FCPs. The ultimate aim of this project was to study the ROP of obtained [1]FCPs and eventually synthesize heavier

group-13-bridged poly(ferrocene)s. As it was mentioned earlier, the key importance for the ROP of strained [1]FCPs is to have a perfect control over the molecular weight and molecular structure and obtain metallopolymers which can be used for future technology.

Chapter 2.2 describes my research in developing a flexible method for the synthesis of α-substituted dilithioferrocene derivatives. The synthesis of heavier group-13-bridged [1]FCPs containing alkyl-substituted ferrocene units as well as ROP behavior of the resulting gallium- and indium-bridged [1]FCPs will be discussed in chapters 2.3 and 2.4.

2.2. Synthesis of (S_p,S_p)-1,1′-Dibromo-2,2′-di(isopropyl)ferrocene as a Planar-chiral Precursor for the Preparation of Chiral Ferrocenophanes

The synthetic toolbox for the preparation of α-substituted 1,1′-dilithioferrocenes is quite limited. In a retrosynthetic prospective, the presence of *ortho*-directive groups are essential in order to avoid the formation of different diastereoisomers. As it was mentioned in chapter 1.3, these types of ferrocene species are mostly utilized in the area of asymmetric catalysis for the preparation of chiral ligands which coordinate to transition metals. The preparation of nearly all of these compounds require a resolution step in order to separate the enantiomers, which limits the scope of the synthesis of these ligands. However, in 1998 Knochel et al. reported the *stereocontrolled* preparation of chiral C_2-symmetrical ferrocenes which gave an easier access to different chiral ligands for asymmetric catalysis.[142] This synthesis was based on the well-known "Ugi amine" (**97**) chemistry which utilizes C*H(Me)NMe_2 groups on Cp rings as α-directing groups for lithiation.[135] The enantiomerically pure "double Ugi amine" (*R*,*R*)-**101** (Scheme 55) is equipped with two amine groups which diastereoselectively direct the lithiation in their α positions, resulting in an enantiomerically pure dilithioferrocene unit. The key step for this four step synthesis (Schemes 59, 60, 61 and 62) is the asymmetric CBS reduction (Corey-Bakshi-Shibata

reduction) of diacetylferrocence to the *R*,*R* isomer of the diol **115** (>99% *ee*), which is transformed into the amine (*R*,*R*)-**101** with retention of configuration. Following is the preparation of "double Ugi amine" (*R*,*R*)-**101**, which I synthesized as the starting material based on the published procedure with some alteration.[142]

2.2.1. Synthesis 1,1′-Diacetylferrocene

A retrosynthetic analysis of diol **115** suggested the preparation of 1,1′-diacetylferrocene **114** as the precursor, which is accessible through Friedel-Crafts acylation of ferrocene. Shortly after the discovery of ferrocene by Pauson and Miller in 1951,[149, 150] Woodward et al. classified it to be an aromatic compound and prepared its first derivatives by acylation of ferrocene in presence of $AlCl_3$.[151] In order to access mono- or diacetylated products, the acylation of ferrocene should be controlled through the proper ratio between reagents and the sequence of addition. The 1,1′-diacetylferrocene **114** (Scheme 59) was synthesized in good yield by dropwise addition of ferrocene to a complex of $AlCl_3$ and acetyl chloride (1 : 1 ratio, 2 equiv) in dichloromethane and further purified by column chromatography. In the ^{1}H NMR spectrum of 1,1′-diacetylferrocene, the most noteworthy signal is a singlet at δ = 2.31 ppm for the six proton of acetyl groups.

Scheme 59. Synthesis of 1,1′-Diacetylferrocene.

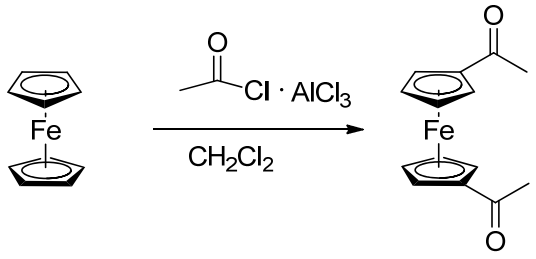

114

2.2.2. Synthesis of (*R*,*R*)-1,1′-Bis(α-hydroxyethyl)ferrocene

The reduction method developed by Corey and Itsuno has shown its broad utility during the last decade and it was selected for the reduction of 1,1′-diacetylferrocene.[152-154] The other methods for the reduction of metallocene ketones are either limited to monoacetylated systems or were reported to result in products with low optical purity.[155-158] The enantioselective preparation of α-chiral ferrocenyl alcohols can also be done by using dialkylzincs[158] to reduce ferrocenyl aldehydes or by employing tedious enzymatic resolution.[159] In 1998 Knochel et al. reported that, applying the CBS reduction gives an easy access to nearly enantiomerically pure C_2-symmetrical ferrocenyl diols with only small amount of *meso* diastereomers.[142] Following the published procedure, the 1,1′-diacetylferrocene **114** was reduced by using 60 mol% of oxazaborolidine catalyst and 2 equiv of $BH_3 \cdot SMe_2$ in thf at 0 °C (30 min) to provide a nearly quantitative yield for the *R*,*R* isomer of the diol **115** (>99% *ee*) with diastereometric ratio *dl*:*meso* of 98.5:1.5 (Scheme 60).

Scheme 60. CBS Reduction of 1,1′-Diacetylferrocene.

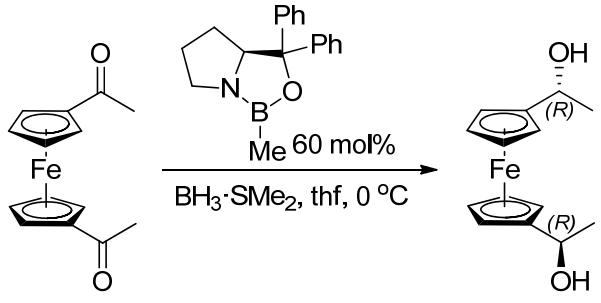

114 **115**

Diol **115** was isolated as an orange oil after the workup and further purified by column chromatography to result in a yellow solid material with good yield. However, the separation of the *meso* diastereomer from the desired diol **115** was difficult and could not be done by simple

column chromatography. The *meso* diastereomer was separated during later steps of the synthesis. The ^{1}H NMR spectrum of C_2-symmetrical diol **115** revealed a signal at δ = 3.19 ppm for two protons of the hydroxyl groups, in addition to the signals for Cp moiety and methyl protons.

2.2.3. Synthesis of (*R*,*R*)-1,1′-Bis(α-N,N-dimethylaminoethyl)ferrocene

As it was discussed in introduction (Chapter 1.2; Scheme 56), soon after the synthesis of the "Ugi amine" in 1970,[135] it was reported that by employing a wide range of heteroatom-centered nucleophiles, heteroatom in the α-position to a ferrocenyl moiety can be substituted with full retention of configuration.[144] In 1998 Knochel et al. reported the extension of this methodology to 1,1′-disubstituted C_2-symmetrical systems.[142] Accordingly, the C_2-symmetrical diol **115** was reacted with acetic anhydride in pyridine to result in the corresponding diacetate **116** (Scheme 61).

Scheme 61. Synthesis of Diacetate **116**.

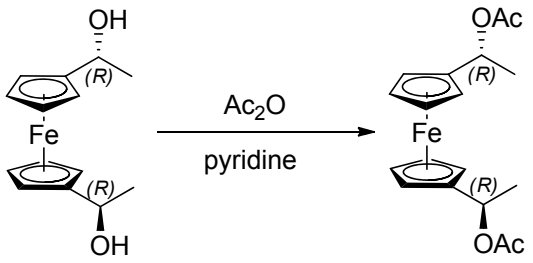

115 **116**

Interestingly, removing the volatiles in vacuum yielded pure **116** and the same reaction vessel was used for the next step. In the second step, the acetate group was replaced by amine group via dimethyl amine in a solvent mixture (MeOH/H_2O) (Scheme 62).

Knochel et al. also noted that the choice of reaction medium plays a crucial role for the outcome of the substitution reaction; using the thf/H_2O solvent mixture for the same reaction resulted in undesired products.[142] The ^{1}H NMR spectroscopy of the crude product confirmed that the reduction proceeds with full retention of configuration.

Scheme 62. Synthesis of (*R*,*R*)-1,1′-Bis(α-N,N-dimethylaminoethyl)ferrocene **101**.

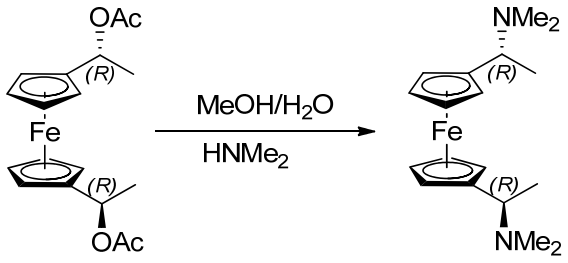

116 (*R*,*R*)-**101**

The ^{1}H NMR spectrum of the diamine **101** exhibits an intense singlet at δ = 2.09 ppm and a doublet at δ = 1.47 ppm and a quartet at δ = 3.61 ppm, assigned to protons of C*H(Me)NMe_2 groups on Cp rings.

2.2.4. Synthesis of (*R*,*R*,S_p,S_p)-2,2′-Bis(α-N,N-dimethylaminoethyl)-1,1′-dibromoferrocene

In 1970 Ugi et al. reported the diastereoselective *ortho*-lithiation of (*R*)- and (*S*)-N,N-dimethyl-1-ferrocenylethylamine (**97**) by using *n*BuLi with a selectivity of 96:4 (Scheme 54).[135] It was described that the steric repulsions place both the dimethylamino and the methyl group above the ring plane and, therefore, adjusts the nitrogen as complexation site for *n*BuLi near to H^2 (Scheme 54). Knochel et al. performed an NOE experiment with C_2-symmetrical diamine **101** and revealed the same conformational fixation of the C*H(Me)NMe_2 groups above the Cp rings for this species.[142] Following the published procedure,[160] the double deprotonation of diamine **101** was performed by using 4 equiv of *n*BuLi in diethyl ether for 16 hours at room temperature. The reaction of the resulting dilithioferrocene **117** with a brominating agent (1,2-

dibromotetrachloroethane) provided the C_2-symmetrical dibromoferrocene **118**, obtained in good yield and enantiomerically pure after column chromatography (Scheme 63).

Scheme 63. Synthesis of C_2-symmetrical Dibromoferrocene **118**.

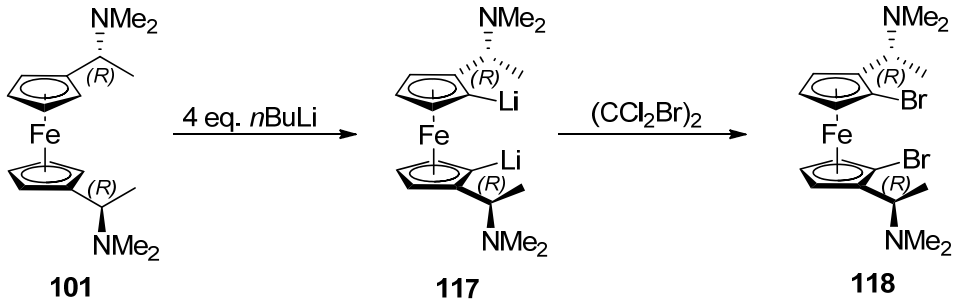

101 **117** **118**

2.2.5. Synthesis of (S_p,S_p)-1,1′-Dibromo-2,2′-di(isopropyl)ferrocene

Beside the central chirality caused by the two stereogenic centers, the dibromoferrocene **118** has a fixed planar chirality. In this stage, based on known substitution chemistry,[161] we attempted to remove the central chirality and leave the planar chirality of the ferrocene framework behind (S_p,S_p isomer; C_2 symmetry). In the first step, a mixture of the dibromoferrocene **118** with acetic anhydride was heated for 10 hours to produce the diacetoxyferrocene **119** with complete retention of configuration. Subsequently, the diacetoxyferrocene **119** was reacted with trimethylaluminum at -78 °C to afford the new planar chiral dibromoferrocene **120** (Scheme 64).

Scheme 64. Synthesis of the Planar-chiral Dibromoferrocene **120**.

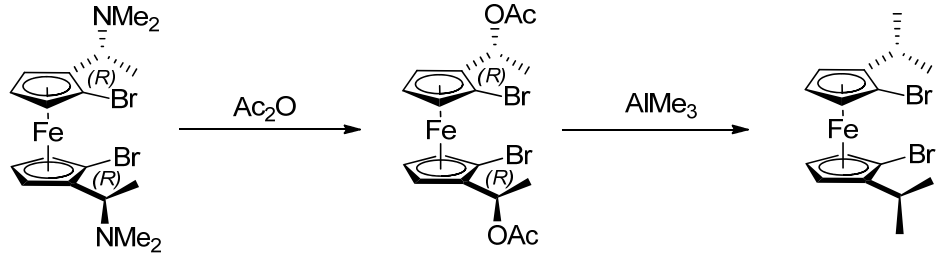

118 **119** **120**

The crude product was purified by column chromatography, followed by crystallization in a hexanes solution at -20 °C to obtain **120** as brown crystals in 85% yield. The ^{1}H NMR spectroscopy of **120** confirmed the presence of isopropyl groups, showing two doublets for methyl groups at δ = 1.06 and 1.32 ppm along with a multiplet at δ = 2.80 ppm. The molecular structure of **120** was determined by single-crystal X-ray structural analysis and confirmed the stereoselectivity of the reaction (Figure 11 and Table 1).

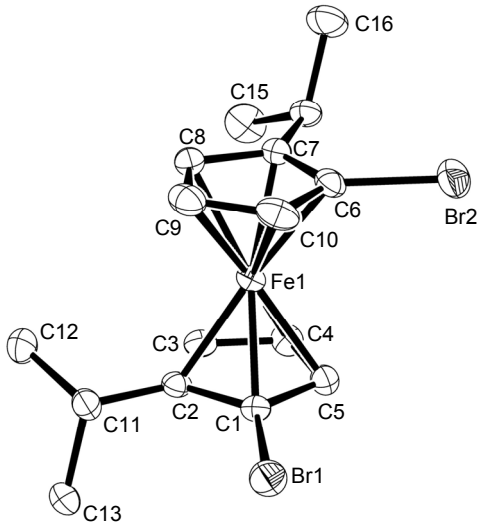

Figure 11. Molecular structure of **120** with thermal ellipsoids at the 50% probability level. Hydrogen atoms are omitted for clarity. Reprinted with permission from Sadeh, S.; Schatte, G.; Müller, J. *Chem.–Eur. J.* **2013***, 40,* 13408-13417. Copyright 2013 Wiley VCH.

Having the dibromide **120** as a proper precursor for salt-metathesis reactions prepared, the next step was to find a clean procedure for lithium-bromine exchange and to obtain the dilithioferrocene derivative. Lithiation of **120** was first attempted following the standard procedure for lithium-bromine exchange of similar species (2 equiv of *n*BuLi at -78 °C in thf) and did not result in a clean dilithiation. However, compound **120** was cleanly lithiated by using a published procedure for lithiation of aromatic bromides (thf : hexanes, 1 : 9, 0 °C).[162] It is noteworthy that, even though the solvent mixture mainly consists of hexanes, the dilithio species

121 does precipitate. The degree of lithiation of **120** was tested by using the common trapping reagent $ClSiMe_3$ and proved to be quantitative (Scheme 65).

Scheme 65. Examining the Lithiation of Dibromide **120**.

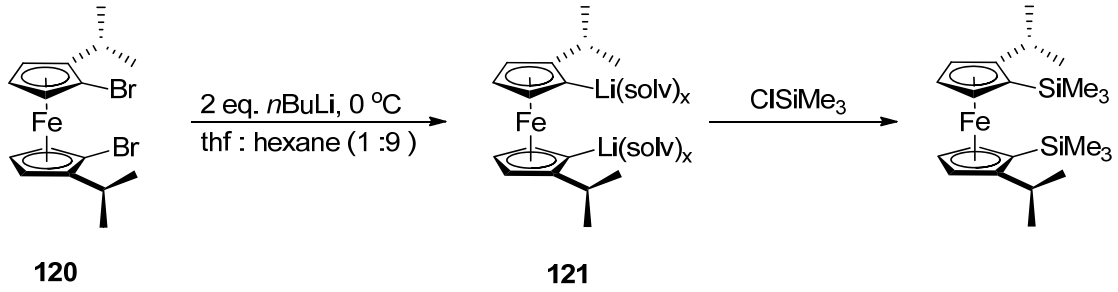

120 **121**

2.3. Gallium-bridged [1]Ferrocenophanes

2.3.1. Synthesis of the Chiral Gallium-bridged [1]Ferrocenophane 122

According to the previous results in our group, treatment of dilithioferrocene with $Ar'GaCl_2$ resulted in formation of [1.1]FCP instead of the intended strained [1]FCP.[36] In order to test our hypothesis, the dilithio derivative of **120** was reacted with $Ar'GaCl_2$ and resulted in the intended gallium-bridged [1]FCP **122**, which was isolated by crystallization from the filtrated solution of the reaction mixture at -80 °C (59%) (Scheme 66).

Scheme 66. Synthesis of Gallium-bridged [1]FCP **122**.

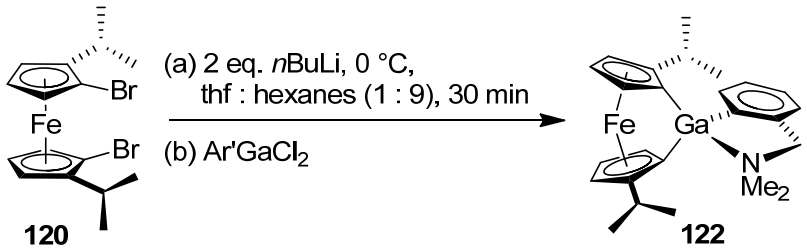

120 **122**

The formation of the targeted gallium-bridged [1]FCP **122** and not the unintended respective [1.1]FCP is evident from the NMR spectroscopy. To our surprise, the ^1H NMR spectrum taken from the reaction mixture about 5 min after the addition of $Ar'GaCl_2$ displays the complete

conversion of starting materials to the intended gallium-bridged [1]FCP **122** without formation of any byproducts such as the respective [1.1]FCP or polymeric materials. The ^{1}H NMR spectrum of the red isolated compound displays six signals in the Cp region at δ = 3.53 (1H, CH-α of Cp), 3.98 (1H, CH-α of Cp), 4.46 (1H, CH-β of Cp), 4.50 (1H, CH-β of Cp), 4.67 (1H, CH-β of Cp), 4.70 ppm (1H, CH-β of Cp). These six signals could either be caused by the intended C_1-symmetric **122** or to the respective unintended C_2-symmetric [1.1]FCP, however, the signal pattern confirms the formation of [1]FCP **122**. The ^{1}H NMR pattern of two β-protons resonating downfield with a small peak separation and α-protons displaying a significantly larger separation further upfield is typical for previously characterized heavier group-13-bridged [1]FCPs with C_s symmetry [(Pytsi)Gafc: δ = 4.08 (2H, CH-α of Cp), 4.45 (2H, CH-α of Cp), 4.61 (2H, CH-β of Cp) and 4.65 ppm (2H, CH-β of Cp);[31] (Mamx)Gafc: δ = 4.01 (2H, CH-α of Cp), 4.56 (2H, CH-α of Cp) and 4.69 ppm (4H, CH-β of Cp);[33] (Pytsi)Alfc: δ = 3.91 (2H, CH-α of Cp), 4.31 (2H, CH-α of Cp), 4.64 (2H, CH-β of Cp) and 4.68 ppm (2H, CH-β of Cp);[6] (Mamx)Alfc: δ = 3.85 (2H, CH-α of Cp), 4.51 (2H, CH-α of Cp), 4.70 (2H, CH-β of Cp) and 4.72 ppm (2H, CH-β of Cp)[34]]. In the case of **122**, there are only two α protons and there is no symmetry element present in the molecule, therefore, six signals are observed in the Cp region with the similar pattern as that of other heavier group-13-bridged [1]FCPs. The upfield shift of *ipso* carbon signals for [1]FCPs [(Pytsi)Gafc: δ = 47.2 ppm][31] compared to the unstrained [1.1]FCP analogues [(Ar′Gafc)$_2$: δ = 76.2 ppm][36] is a characteristic feature in ^{13}C NMR spectra of [1]FCPs. Expectedly, the ^{13}C NMR spectrum of **122** shows two characteristic signals for the gallium-bound carbon atom [δ = 44.23 (*ipso*-Cp, Ga), 46.43 ppm (*ipso*-Cp, Ga)]. Figure 12 displays the molecular structure of **122** derived from the X-ray diffraction data of a single crystal (see also Table 1).

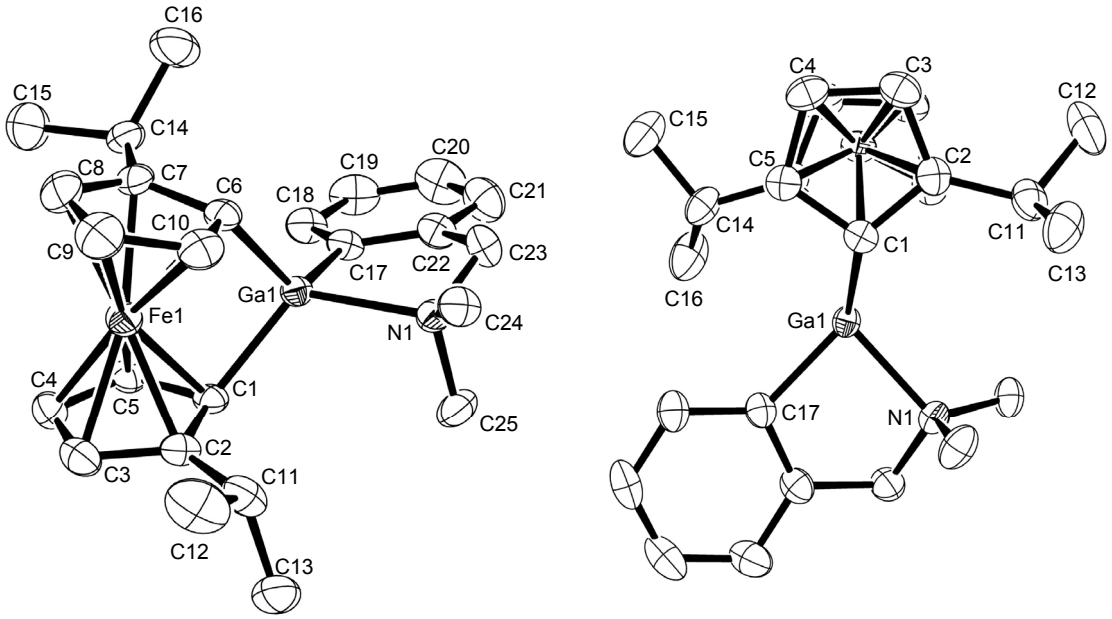

Figure 12. Molecular structure of **122** with thermal ellipsoids at the 50% probability level. Hydrogen atoms are omitted for clarity. One of two independent molecules is shown. Selected atom-atom distances [Å] and bond angles [°] for **122** (values in braces refer to the second independent molecule that is not shown): Ga1-C1 = 2.014(2) {2.020(3)}, Ga1-C6 = 2.007(3) {2.009(3)}, Ga1-C17 = 1.971(3) {1.974(3)}, Ga1-N1 = 2.083(2) {2.102(2)}, C1-Ga1-C6 = 93.44(10) {92.94(10)}, C1-Ga1-C17 = 123.87(10) {124.41(11)}, C1-Ga1-N1 = 116.45(9) {118.90(10)}, C6-Ga1-C17 = 124.55(11) {124.41(11)}, C6-Ga1-N1 = 114.48(10) {110.94(10)}, C17-Ga1-N1 = 86.08(10) {85.80(9)}. Reprinted with permission from Sadeh, S.; Schatte, G.; Müller, J. *Chem.–Eur. J.* **2013***, 40,* 13408-13417. Copyright 2013 Wiley VCH.

The gallium atom is distorted tetrahedrally surrounded by three C atoms and one N atom. The Ga-C^{Ph} bond lengths for the two independent molecules in the asymmetric unit were found in the narrow range of 1.971(3) and 1.974(3) Å, whereas the bond to the Cp groups is with 2.007(3) to 2.020(3) Å, respectively, slightly longer. As it is expected, the Ga-N bond distance with 2.083(2) and 2.102(2) Å is longer than the Ga-C bonds, however, compared to known gallium species with similar coordination the GaN bond length is on the short side of the spectrum [Ga-N bond lengths: 2.112 [(Mamx)Ga(flu)],[163] 2.153(3) [(Mamx)Gafc$_2$],[34] 2.178(3) [(Ar′Gafc)$_2$],[36] 2.192(2) ([(*p*-*t*BuAr′)Ga{1,1′-(η^6-C_6H_5)$_2$Cr}]$_2$),[32] 2.207(3) Å ([(3-*t*Bu-6-Me_2NCH_2-C_6H_3)Ga{1,1′-(η^6-C_6H_5)$_2$Mo}]$_2$)[32]].

As it was discussed before, a set of angles are commonly used to describe distortions in [1]FCPs relative to unstrained systems (Figure 2). Since the tilting of the Cp ligand alone is responsible for the major portion of the intrinsic strain, tilt angle α is the most discussed geometrical feature in [1]FCPs. Consistent with other known gallium-bridged [1]FCPs equipped with bulky trisyl-type ligands [(Pytsi)Gafc: 15.4(2) and 16.4(2)°;[31] (Me_2Ntsi)Gafc: 15.83(19)°[32]], the gallium compound **122** exhibits α angles of 16.26(9) and 16.45(10)°. Compound **122** was also characterized by mass spectrometry and elemental analysis. The measured mass spectrum showed the highest detected mass for the molecular ion of [1]FCP **122**.

Table 1. Crystal and Structural Refinement Data for Compounds **120** and **122.**

	120	**122**
empirical formula	$C_{16}H_{20}Br_2Fe$	$C_{25}H_{32}FeGaN$
fw	427.98	472.10
cryst. size / mm^3	0.15 × 0.13 × 0.13	0.23 × 0.23 × 0.18
cryst. system, space group	orthorhombic, $P2_12_12_1$	orthorhombic, $P2_12_12_1$
Z	4	8
a / Å	7.8593(2)	10.9085(2)
b / Å	8.9762(3)	11.3933(2)
c / Å	22.6090(6)	37.2000(6)
α / °	90	90
β / °	90	90
γ / °	90	90
volume / $Å^3$	1594.99(8)	4623.36(14)
ρ_{calc} / mg m^{-3}	1.782	1.356
temperature / K	173(2)	173(2)
μ_{calc} / mm^{-1}	5.940	1.803
θ range / °	3.16 to 29.99	1.09 to 29.13

reflns collected / unique	4376 / 4376	12046 / 12031
absorption correction	multi-scan	multi-scan
data / restraints / params	4376 / 0 / 177	12031 / 0 / 518
goodness-of-fit	1.080	1.045
R_1 [I > 2 σ(I)][a]	0.0361	0.0346
wR_2 (all data)[a]	0.0775	0.0694
largest diff. peak and hole	0.404 and	0.289 and
$\Delta\rho_{elect}$ / [e Å^{-3}]	-0.612	-0.327

[a] $R_1 = [\Sigma||F_o|-|F_c||]/[\Sigma|F_o|]$ for $[F_o^2 > 2\sigma(F_o^2)]$, $wR_2 = \{[\Sigma w(F_o^2-F_c^2)^2]/[\Sigma w(F_o^2)^2]\}^{1/2}$ [all data].

Table 2. Measured Distortion Angles [°] (see Figure 12).

	122 [a]
α	16.26(9) {16.45(10)}
β/β′	40.0(2) {38.9(2)} / 39.1(2) {38.4(2)}
θ	93.44(10) {92.94(10)}
δ	166.65(3) {166.78(3)}

[a] values in braces refer to the second independent molecule in the asymmetric unit.

2.3.2. Thermal Studies of the Gallium-bridged [1]FCP 122

To explore the thermal polymerization behavior of the strained gallium-bridged [1]FCP **122**, a Differential Scanning Calorimetry (DSC) study was undertaken (Figure 13). The DSC thermogram of **122** shows a melt endotherm at ca. 187 °C overlapping with the ROP exotherm at slightly higher temperature (T_{max} = 201 °C), indicative of ROP.

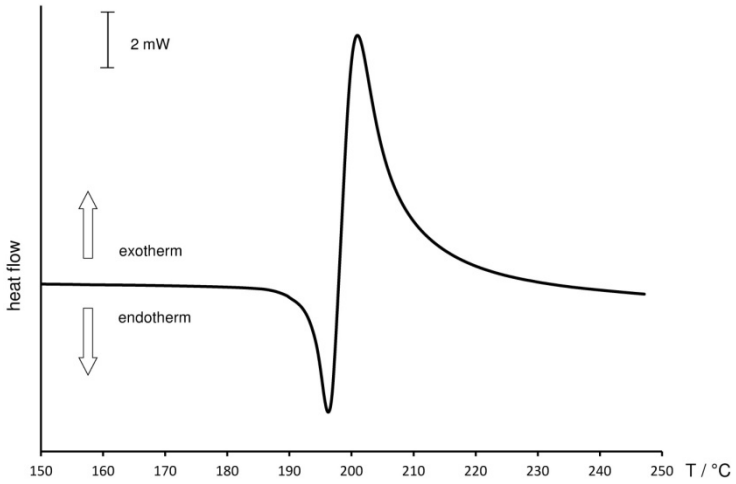

Figure 13. DSC thermogram of **122** (heating rate of 10 °Cmin^{-1}). Reprinted with permission from Sadeh, S.; Schatte, G.; Müller, J. *Chem.–Eur. J.* **2013***, 40,* 13408-13417. Copyright 2013 Wiley VCH.

The integration over the exothermic peak revealed a value of -33 kJ mol^{-1}. However, due to the overlapping of the exothermic and the endothermic peaks, it can be assumed that the ΔH^{ROP} for **122** is < -33 kJ mol^{-1}. Since the gallium-bridged [1]FCP **122** with tilt angles α of 16.26(9) and 16.45(10)° exhibits a very similar tilt angle as tin-bridged [1]FCPs,[13] a similar exotherm as tin-bridged [1]FCPs is also anticipated for **122**. Previously, a ΔH^{ROP} of -36(±9) kJ mol^{-1} was determined for *t*Bu$_2$Snfc [α = 14.1(2)°][13] and this value is comparable to the value found for the gallium-bridged [1]FCP **122**.

2.4. Indium-bridged [1]Ferrocenophanes

As it was described in the introduction (chapter 1.1.1), the bulkiness of the ligand attached to aluminum and gallium in the bridging position plays a key role for the synthesis and reactivity of aluminum- and gallium-bridged [1]FCPs. The use of bulky intramolecularly coordinating ligands Pytsi and Me$_2$Ntsi yielded in the *first generation* of aluminum- and gallium-bridged [1]FCPs (Scheme 4).[6, 31, 32] However, all the attempts for the ROP of these species either failed or resulted in sluggish polymerization.[99] On the other hand, employing the bulky Mamx ligand (Scheme 6)

gave the *second generation* of aluminum- and gallium-bridged [1]FCPs, which were highly reactive and polymerized under the conditions of their formation (scheme 6).[33, 34] In contrast to the bulky ligands, the slim ligand Ar′ gave [1.1]FCPs with aluminum and gallium in the bridging positions (Scheme 5).[36] As described in chapter 2.3, the *third generation* of heavier group-13-bridged [1]FCPs was prepared by formally moving the bulkiness from the stabilizing ligand onto the ferrocene moiety (Scheme 66).[164] The planar-chiral species **120** was synthesized as a new precursor for its dilithioferrocene derivative, and used for the preparation of new [1]FCPs. As shown in Scheme 66 for the gallium-bridged [1]FCP **122**, the *i*Pr groups of ferrocene moiety prevented the formation of [1.1]FCPs and led to the targeted [1]FCP **122**. The chiral gallium-bridged [1]FCP **122** is equipped with the non-bulky Ar′ ligand and was prepared with a complete conversion of starting materials. In contrast to the cases of aluminum and gallium, applying both slim Ar′ and bulky Me_2Ntsi ligands yielded in indium-bridged [1.1]FCPs (Scheme 7).[36, 37] This unique outcome of salt-metathesis reaction was rationalized by the 10% longer bond length of In-C compared to Al-C and Ga-C, which leaves more space for the bulky Me_2Ntsi ligand to fit into a [1.1]FCP structure.[37] Therefore, more steric protection is required in order to access indium-bridged [1]FCPs. Hence, we attempted to prepare the first indium-bridged [1]FCPs, by applying bulky alkyl groups on the ferrocene moiety as well as on the slim Ar′ ligand (using Mamx ligand).

2.4.1. Author Contribution

The results described here were published as an article and are part of a joint project with Bidraha Bagh.[164] He initiated this project and prepared (Mamx)$InCl_2$, performed the reaction of Mamx$InCl_2$ with dilithioferrocene·tmeda, and isolated the respective products. Furthermore, Bidraha Bagh obtained the initial results from the reaction of (Mamx)$InCl_2$ and (S_p,S_p)-1,1′-

dilithio-2,2′-di(isopropyl)ferrocene. I prepared (S_p,S_p)-1,1′-dibromo-2,2′-di(isopropyl)ferrocene (**120**), performed the reaction of (Mamx)$InCl_2$ and (S_p,S_p)-1,1′-dilithio-2,2′-di(isopropyl)ferrocene (**121**) and the reaction of Ar′$InCl_2$ and (S_p,S_p)-1,1′-dilithio-2,2′-di(isopropyl)ferrocene (**121**), respectively, and obtained all spectroscopic data for the latter two reactions. The structural and the thermodynamic data were obtained through DFT calculation, performed by Jennifer C. Green (Oxford) and interpreted with the help of Jens Müller.

2.4.2. Synthesis of Indium-bridged [1]Ferrocenophanes

As mentioned earlier (Chapter 1.1.1), B. Bagh had used the Mamx ligand successfully and obtained aluminum- and gallium-bridged [1]FCPs.[33, 34] Therefore, he intended to employ the same strategy for the preparation of indium-bridged [1]FCPs. (Mamx)$InCl_2$ **123** was prepared in moderate yield by the lithiation of (Mamx)Br followed by addition of 1 equiv of $InCl_3$ and characterized through using standard methods (^{1}H and ^{13}C NMR spectroscopy, mass spectrometry and elemental analysis) (Scheme 67).

Scheme 67. Synthesis of (Mamx)$InCl_2$ **123**.

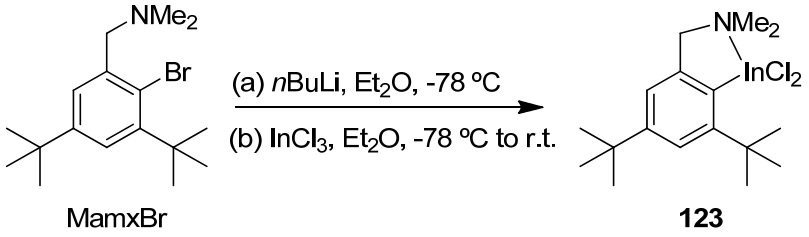

The interpretation of signal pattern for both ^{1}H and ^{13}C NMR spectra revealed the presence of a monomeric species with C_s symmetry on time average. Matching with this interpretation was the result of the mass spectrometry, displaying the highest detected mass M^+ for the molecular ion of the monomer **123**. A solution of **123** in diethyl ether was added to a suspension of

dilithioferrocene·tmeda in the same solvent and reaction control by a proton NMR spectroscopy revealed the formation of different species (Scheme 68).

Scheme 68. Reaction of (Mamx)$InCl_2$ (**123**) with Dilithioferrocene·tmeda.

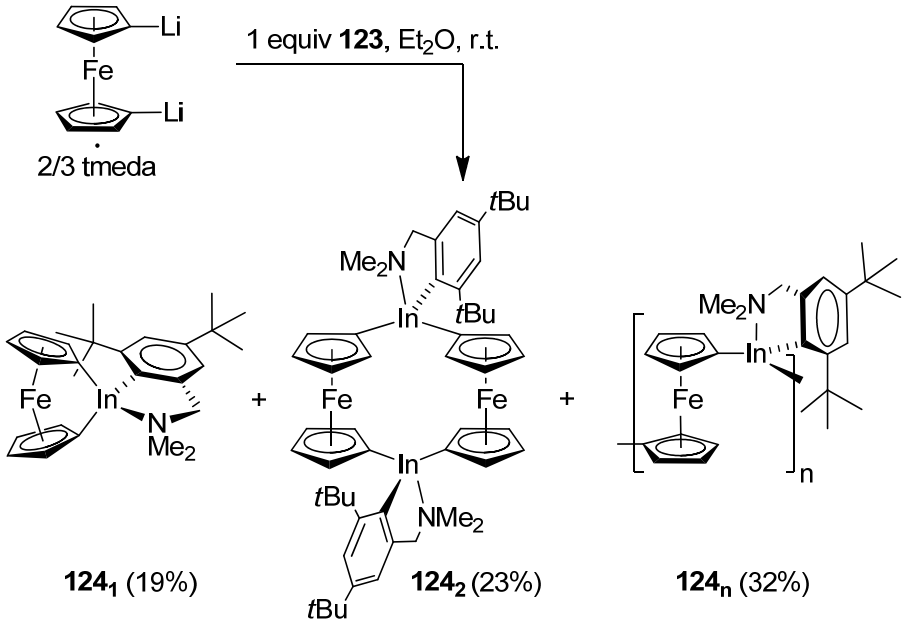

After removing LiCl by filtration, monomer $\mathbf{124_1}$, dimer $\mathbf{124_2}$ and polymer $\mathbf{124_n}$ were separated and isolated by using precipitation procedures. Species $\mathbf{124_1}$ and $\mathbf{124_2}$ were fully characterized by ^{1}H and ^{13}C NMR spectroscopy, mass spectrometry and elemental analysis. Mass spectra of $\mathbf{124_1}$ and $\mathbf{124_2}$, showed the highest detected masses for the molecular ions of [1]FCP $\mathbf{124_1}$ and $\mathbf{124_2}$ respectively. The proton spectrum of species $\mathbf{124_1}$ clearly shows the expected signal pattern for a C_s symmetry [1]FCP species. In the ^{1}H NMR spectrum, the most indicative resonances are detected in the Cp region at δ = 4.22 (2H, CH-α of Cp), 4.39 (2H, CH-α of Cp), 4.41 (2H, CH-β of Cp) and 4.46 ppm (2H, CH-β of Cp). Such a proton NMR pattern, showing two β-protons resonating downfield with a small peak separation (Δδ = 0.05 ppm) and α-protons with a significantly larger separation (Δδ = 0.17 ppm) further upfield, is typical for previously characterized heavier group-13-bridged [1]FCPs with C_s symmetry [(Pytsi)Gafc: δ = 4.08 (2H,

CH-α of Cp), 4.45 (2H, CH-α of Cp), 4.61 (2H, CH-β of Cp) and 4.65 ppm (2H, CH-β of Cp);[31] (Mamx)Gafc: δ = 4.01 (2H, CH-α of Cp), 4.56 (2H, CH-α of Cp) and 4.69 ppm (4H, CH-β of Cp);[33] (Pytsi)Alfc: δ = 3.91 (2H, CH-α of Cp), 4.31 (2H, CH-α of Cp), 4.64 (2H, CH-β of Cp) and 4.68 ppm (2H, CH-β of Cp);[6] (Mamx)Alfc: δ = 3.85 (2H, CH-α of Cp), 4.51 (2H, CH-α of Cp), 4.70 (2H, CH-β of Cp) and 4.72 ppm (2H, CH-β of Cp)[34]]. However, all of the attempts for crystallization of **124$_1$** were unsuccessful and, consequently, a molecular structure could not be obtained experimentally.

The ^{1}H NMR and ^{13}C NMR spectroscopy of [1.1]FCP **124$_2$** revealed a signal pattern, which can be correlated to a C_{2h} symmetric species. The most significant resonances are those in the Cp range of the ^{1}H NMR spectrum, displaying three signals with one signal being twice intense as the other two [δ = 3.91 (4H, CH-α of Cp), 4.26 (8H, CH-β of Cp) and 4.40 ppm (4H, CH-α of Cp)]. This characteristic signal pattern, with two signals of β protons, either with a small splitting or overlapping, positioned approximately in the middle of the two signals of α protons, is a distinctive fingerprint for heavier group-13-bridged [1.1]FCPs stabilized by "one-armed" phenyl ligands {[(Me$_2$Ntsi)Infc]$_2$: δ = 4.36 (2H, CH-α of Cp), 4.43 (2H, CH-β of Cp), 4.45 ppm (2H, CH-β of Cp) and 4.57 ppm (2H, CH-α of Cp);[37] (Ar′Infc)$_2$ δ = 4.04 (4H, CH-α of Cp), 4.45 (4H, CH-β of Cp), 4.53 ppm (4H, CH-β of Cp) and 4.97 ppm (4H, CH-α of Cp);[36] (Ar′Gafc)$_2$ δ = 3.99 (4H, CH-α of Cp), 4.37 (4H, CH-β of Cp), 4.48 ppm (4H, CH-β of Cp) and 5.07 ppm (4H, CH-α of Cp);[36] (Ar′Alfc)$_2$ δ = 3.97 (4H, CH-α of Cp), 4.42 (4H, CH-β of Cp), 4.52 ppm (4H, CH-β of Cp) and 5.17 ppm (4H, CH-α of Cp)[36]}.

The last isolated fraction from the salt-metathesis reaction contained the polymeric compound **124$_n$**, which was characterized by ^{1}H NMR spectroscopy and dynamic light scattering (DLS)

analysis. The appearance of broad peaks in the ^{1}H NMR spectrum suggested that the isolated precipitate consisted of a mixture of polymers or oligomers. This assumption is also in agreement with the data collected from DLS analyses, revealing a hydrodynamic radius (R_h) of 1.0 ± 0.1 nm for **124$_n$**. Applying the same method which was previously used for aluminum- and gallium-bridged [1]FCPs,[33, 34] an average molecular weight of 4.8 ± 0.8 kDa (about 9 repeating units) was assigned for the measured R_h (see experimental chapter for details).

The synthesis of [1]FCP **124$_1$**, which is the first indium-bridged [1]FCP, was an important achievement in the chemistry of strained sandwich compounds, however, the salt-metathesis reaction was not selective and a mixture of dimers, oligomers and polymers were obtained in the reaction mixture.

As discussed in chapter 2.3, by introducing *i*Pr groups in the α position of Cp units I was able to block the formation of unwanted [1.1]FCPs in the salt-metathesis reaction of dilithioferrocene **121** and Ar′GaCl$_2$ (Scheme 66).[164] This strategy led to the isolation of the chiral gallium-bridged [1]FCP **122**. At this stage, I joined the indium project in order to explore if *i*Pr groups on ferrocene could lead toward a selective synthesis of indium-bridged [1]FCPs. Therefore, it was hoped that the use of *i*Pr groups on the ferrocene unit as well as *t*Bu groups on the Ar′ ligand would block the formation of unwanted [1.1]FCP species and polymeric materials. As shown in Scheme 69, the enantiomerically pure ferrocene dibromide **120** was first lithiated in the hexanes/thf solvent mixture and then reacted with (Mamx)InCl$_2$ **123** to result in the targeted indium-bridged [1]FCP **125$_1$**. Monitoring the reaction mixture with ^{1}H NMR spectroscopy revealed the selective formation of the indium-bridged [1]FCP **125$_1$**. For instance, four doublets appear for the four methyl groups of the *i*Pr groups, each having an intensity of three relative to the each of the six signals of Cp protons. Moreover, the Mamx ligand results in the appearance

of two peaks in the aromatic region, two doublets at δ = 2.65 and 3.94 ppm for the CH_2 protons, two large singlets for the two *t*Bu groups, and two singlets at δ = 1.91 and 2.30 ppm for the NMe_2 group. The appearance of two peaks for the N-bound methyl groups clearly proves the existence of a nitrogen-indium donor-acceptor bond. In the absence of a nitrogen-indium bond, only one signal is anticipated for the two methyl groups, as a fast swapping between the two positions of the methyl groups would occur due to the fast inversion at the nitrogen center. It makes sense to compare the ^{1}H NMR of the indium-bridged [1]FCP **125$_1$** and that of the gallium-bridged [1]FCP **122**, as both compounds possess C_1 symmetry and contain the same ferrocene unit. Expectedly, the splitting pattern and chemical shifts of Cp protons for **122** and **125$_1$** are very similar to each other [**125$_1$**: δ = 3.68 (1H, CH-α of Cp), 4.11 (1H, CH-α of Cp), 4.47 (1H, CH-β of Cp), 4.50 (1H, CH-β of Cp), 4.67 (1H, CH-β of Cp), 4.73 ppm (1H, CH-β of Cp); **122**: δ = 3.53 (1H, CH-α of Cp), 3.98 (1H, CH-α of Cp), 4.46 (1H, CH-β of Cp), 4.50 (1H, CH-β of Cp), 4.67 (1H, CH-β of Cp), 4.70 ppm (1H, CH-β of Cp)[164]]. Similar to the case of **122**, the peak separation of Cp protons of **125$_1$** is significantly different with α protons (**125$_1$**: Δδ = 0.43 ppm; **122**: Δδ = 0.45 ppm[164]) showing a considerably larger separation compared to β protons (**125$_1$**: Δδ = 0.26 ppm; **122**: Δδ = 0.24 ppm[164]).

Scheme 69. Synthesis of Intermediate **125$_1$** and Polymer **125$_n$**.

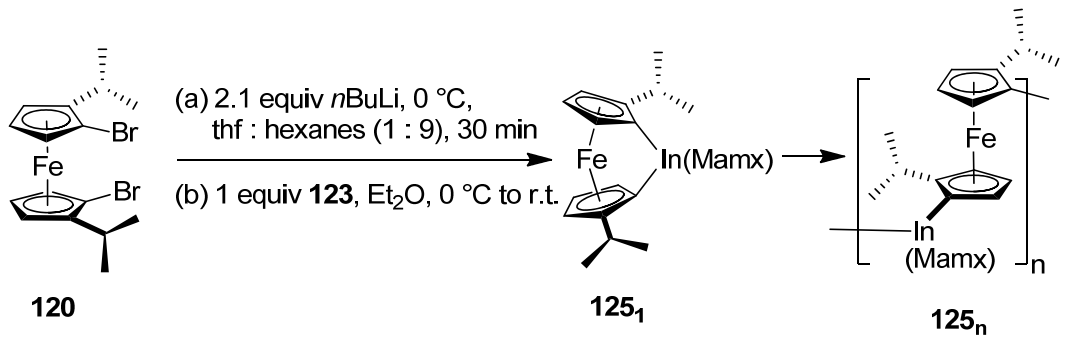

120 **125$_1$** **125$_n$**

Unfortunately, all the attempts for the isolation of the indium-bridged [1]FCP **125$_1$** were unsuccessful and this monomer polymerized spontaneously in the reaction mixture to result in poly(ferrocenylindigane) **125$_n$** (see the experimental chapter for details). According to the different types of protons, ^{1}H NMR spectrum of the isolated polymer **125$_n$** displays broad signals in the expected regions. DLS analysis of a thf solution of the polymer **125$_n$** revealed an R_h of 2.4 ± 0.1 nm, with an average molecular weight of 24 ± 2 kDa (about 38 repeating units; see experimental chapter for details). The instability of the indium-bridged [1]FCP **125$_1$** is very similar as that of the strained [1]FCPs (Mamx)Gafc (**13**)[33] and (Mamx)Alfc (**14**),[34] where both compounds spontaneously polymerized under the condition of their formation. Even though we were pleased with the synthesis of the first indium-bridged polyferrocenes (**124$_n$** and **125$_n$**), there was no control over the polymerization as monomers could not be isolated. Being inspired with the isolation of gallium-bridged [1]FCP **122**,[164] equipped with two *i*Pr groups on the ferrocenyl moiety and Ar′ ligand in the bridge, the salt-metathesis reaction of dilithio derivative of **120** and Ar′$InCl_2$ was performed with the aim to synthesize the indium-bridged [1]FCP **126$_1$** selectively (Scheme 70).

Scheme 70. Inseparable Product Mixture of **126$_1$** and **126$_2$** Identified by ^{1}H NMR Spectroscopy.

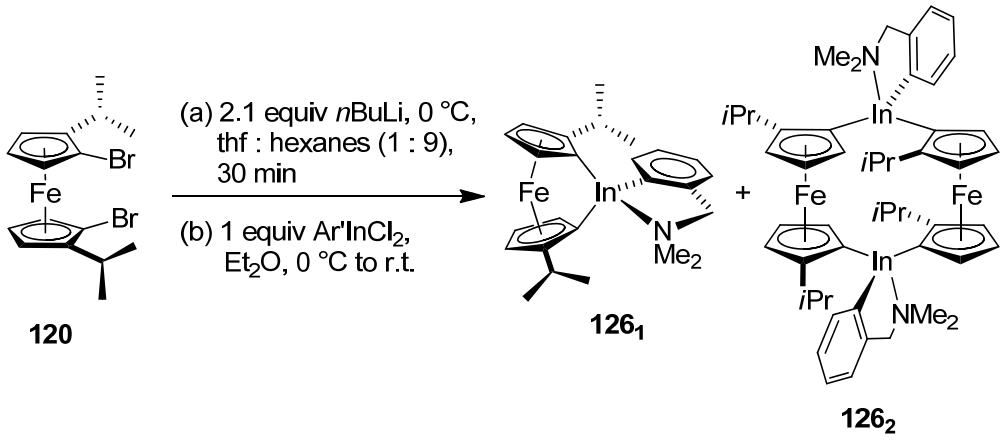

However, performing the salt-metathesis reaction resulted in a mixture of the targeted [1]FCP **126$_1$** and the unwanted [1.1]FCP **126$_2$**. According to the ^{1}H NMR spectrum of the reaction mixture, measured about 10 min after the addition of Ar′InCl$_2$, [1.1]FCP **126** formed as the major product with a ratio of 1.0 : 0.86 between [1.1]FCP and [1]FCP. Unfortunately, applying the same precipitation procedures as for species **124** did not result in separation of the new species **126$_1$** and **126$_2$**. Although all the attempts for the isolation of species **126$_1$** and **126$_2$** were unsuccessful, both compounds were clearly identified by ^{1}H NMR spectroscopy. Similar to the gallium-bridged [1]FCP **122**, the indium-bridged [1]FCP **126$_1$** is expected to have a C_1 symmetry and, therefore, six signals are expected for Cp protons. Due to the C_2 symmetry of the molecule, six signals are also expected for the twelve Cp protons of [1.1]FCP **126$_2$**. In the ^{1}H NMR spectrum, the presence of both species **126$_1$** and **126$_2$** in the reaction mixture was detected by observing two complete set of signals in the Cp region. The α proton signals for [1.1]FCP **126$_2$** appear far apart from each other at δ = 3.84 and 5.21 ppm, while those of the β protons appear in-between just spreading over a narrow range (δ = 4.28, 4.31, 4.39, and 4.48 ppm). The proton NMR signal pattern of species **126$_2$** is comparable to previously synthesized indium-bridged [1.1]FCPs. The best candidate for comparison is the known species (Ar′Infc)$_2$ with the same bridging moiety [(Ar′Infc)$_2$: δ = 4.04 (4H, CH-α of Cp), 4.45 (4H, CH-β of Cp), 4.53 ppm (4H, CH-β of Cp) and 4.97 ppm (4H, CH-β of Cp)][36] (see also the discussion for **124$_2$** for comparison with other indium-bridged [1.1]FCPs proton NMR pattern). Due to the overlapping of signals, it was only possible to assign the Cp protons of the [1]FCP **126$_1$**, however, the formation of this compound was confirmed with certainty from the pattern of the Cp protons. The signal pattern of the indium-bridged [1]FCP **126$_1$** is comparable to that of the C_1-symmetric gallium-bridged [1]FCP **122**.[164] However, the anticipated lower tilt angle of [1]FCP **126$_1$** compared to the

gallium-bridged [1]FCP **122** suggests the appearance of the Cp protons of species **126$_1$** to be in a smaller range, which is in agreement with the experimental results [**126$_1$**: δ = 3.83 (1H, CH-α of Cp), 4.16 (1H, CH-α of Cp), 4.25 (1H, CH-β of Cp), 4.29 (1H, CH-β of Cp), 4.34 (1H, CH-β of Cp), 4.53 ppm (1H, CH-β of Cp); **122**: δ = 3.53 (1H, CH-α of Cp), 3.98 (1H, CH-α of Cp), 4.46 (1H, CH-β of Cp), 4.50 (1H, CH-β of Cp), 4.67 (1H, CH-β of Cp), 4.70 ppm (1H, CH-β of Cp)[164]]. Beside the proton NMR data, the existence of [1.1]FCP **126$_2$** was also confirmed with mass spectrometry performed on a sample from the reaction mixture, which displayed the highest detected mass at m/z = 1034.2, clearly indicating the molecular ion of the [1.1]FCP **126$_2$**.

2.4.3. DFT Calculations

In order to better understand the effect of different substituents on the reactivity of indium-bridged [1]FCPs, DFT calculations were performed by Jennifer C. Green (Oxford).

Molecular Structures

The molecular structures of the indium-bridged [1]FCPs **124$_1$**, **125$_1$**, and **126$_1$** were obtained from DFT calculation. The aim was to evaluate the effect of the *i*Pr groups on the ferrocene and the *t*Bu groups on the aromatic ligand. For the calculation, we employed a similar strategy which we previously used for aluminum- and gallium-bridged [1]FCPs and [1]ruthenocenophanes equipped with Mamx ligand (**13** and **14**; Scheme 6).[33, 34] These studies previously revealed that the presence of *ortho*-*t*Bu group increases the strain of the [1]metallocenophanes on average by 5.5 kcal mol^{-1} (ΔH°). All DFT calculations were performed at the BP86/TZ2P level of theory, employing the ADF suite of programs (Experimental Section).[165, 166]

This method was successfully employed in the past for the structural calculation of different metallocenophanes.[5, 34, 167] Five species were chosen for geometry optimizations and Figure 14 illustrates an overview of these compounds.

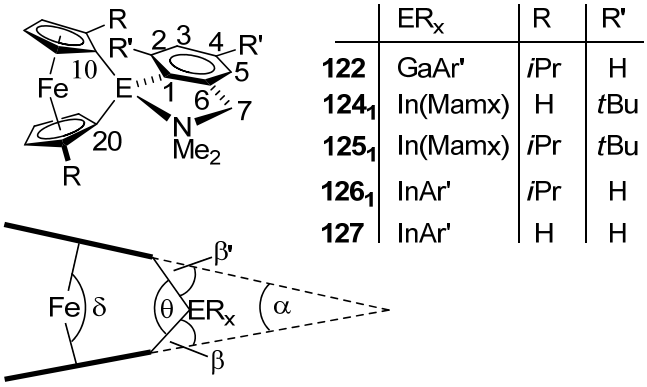

	ER_x	R	R'
122	GaAr'	*i*Pr	H
124_1	In(Mamx)	H	*t*Bu
125_1	In(Mamx)	*i*Pr	*t*Bu
126_1	InAr'	*i*Pr	H
127	InAr'	H	H

Figure 14. Calculated molecules and the set of commonly used angles in [1]FCPs.

The structural data for compounds **122**, **124_1**, **125_1**, **126_1**, and **127** can be found in Table 3. In order to validate our calculation, the geometry of the gallium-bridged [1]FCP **122** was optimized and compared to its structure, determined by single-crystal X-ray analysis.[164]

Table 3. Calculated and Measured Angles [°] and Bond Lengths [Å] in [1]FCPs [a].

	122		**124_1**	**125_1**	**126_1**	**127**
ER_x	GaAr'		In(Mamx)	In(Mamx)	InAr'	InAr'
R / R' [a]	*i*Pr / H		H / *t*Bu	*i*Pr / *t*Bu	*i*Pr / H	H / H
	calc.	exp.[b,c]	calc.	calc.	calc.	calc.
α	15.19	16.26(9) 16.45(10)	11.44	11.42	10.96	11.18
β/β′	40.28/39.84	40.0(2)/39.1(2) 38.9(2)/38.4(2)	37.60/37.62	37.62/37.79	39.03/38.85	38.42/38.27
θ	93.76	93.44(10) 92.94(10)	86.24	86.12	87.49	87.08

δ	167.87	166.65(3) 166.78(3)	169.99	170.22	170.37	170.12
E-N	2.213	2.083(2) 2.102(2)	2.430	2.462	2.448	2.432
E-C1	1.989	1.971(3) 1.974(3)	2.195	2.212	2.178	2.177
E-C10	2.020	2.007(3) 2.009(3)	2.221	2.234	2.213	2.213
E-C20	2.017	2.014(2) 2.020(3)	2.221	2.227	2.214	2.209
Fe-E-C1	145.27	140.14(8) 143.93(7)	165.70	161.48	153.76	159.32
Fe–E–C1–C2	-25.25	-14.4(3) -22.1(4)	-17.76	-37.69	-24.69	-19.21

[a] See Figure 14. [b] Experimental data taken from reference[164]. [c] Two independent molecules were found in the asymmetric unit of **122**.

In the next step, structures of the four indium-bridged [1]FCPs **124$_1$**, **125$_1$**, **126$_1$**, and **127** were optimized. All four indium-bridged [1]FCPs are formed from the possible combinations of two ferrocene moieties, $(H_4C_5)_2Fe$ (fc) and (S_p,S_p)-2,2′-(iPrH$_3$C$_5$)$_2$Fe (fc$^{i\text{Pr}2}$), with two bridging units, In(Mamx) and InAr′. As illustrated in Table 3, the experimental data of compound **122** are very similar to the calculated values for this species. Among the different angles which are used to describe the geometry of [1]FCPs, small alterations were observed for α and δ angles. For instance, a difference of about 1° is found between the calculated tilt angle value of 15.19° and the actual measured angles of 16.26(9) and 16.45(10)° (Table 1).[164] In fact, difference with this magnitude should not be a concern. Such a difference is commonly found between crystallographically independent molecules in the solid state, showing that a difference of 1° in the Cp tilt does not include a significant change in the energy of the molecule. All calculated bond lengths, with the exception of the one for the Ga-N bond, are in perfect agreement with the

experimental values. The measured value for the Ga-N donor bond of 2.083(2) and 2.102(2) Å is lower than the calculated Ga-N bond of 2.213 Å.[164] Previously, a similar difference had been found between the calculated and measured values for the aluminum- and gallium-bridged [1]FCPs equipped with intramolecularly donating ligands (Mamx ligand).[34] Table 3 illustrates the selected structural data for the four indium-bridged [1]FCPs **124_1**, **125_1**, **126_1**, and **127** and the calculated molecular structures of these species are depicted in Figure 15.

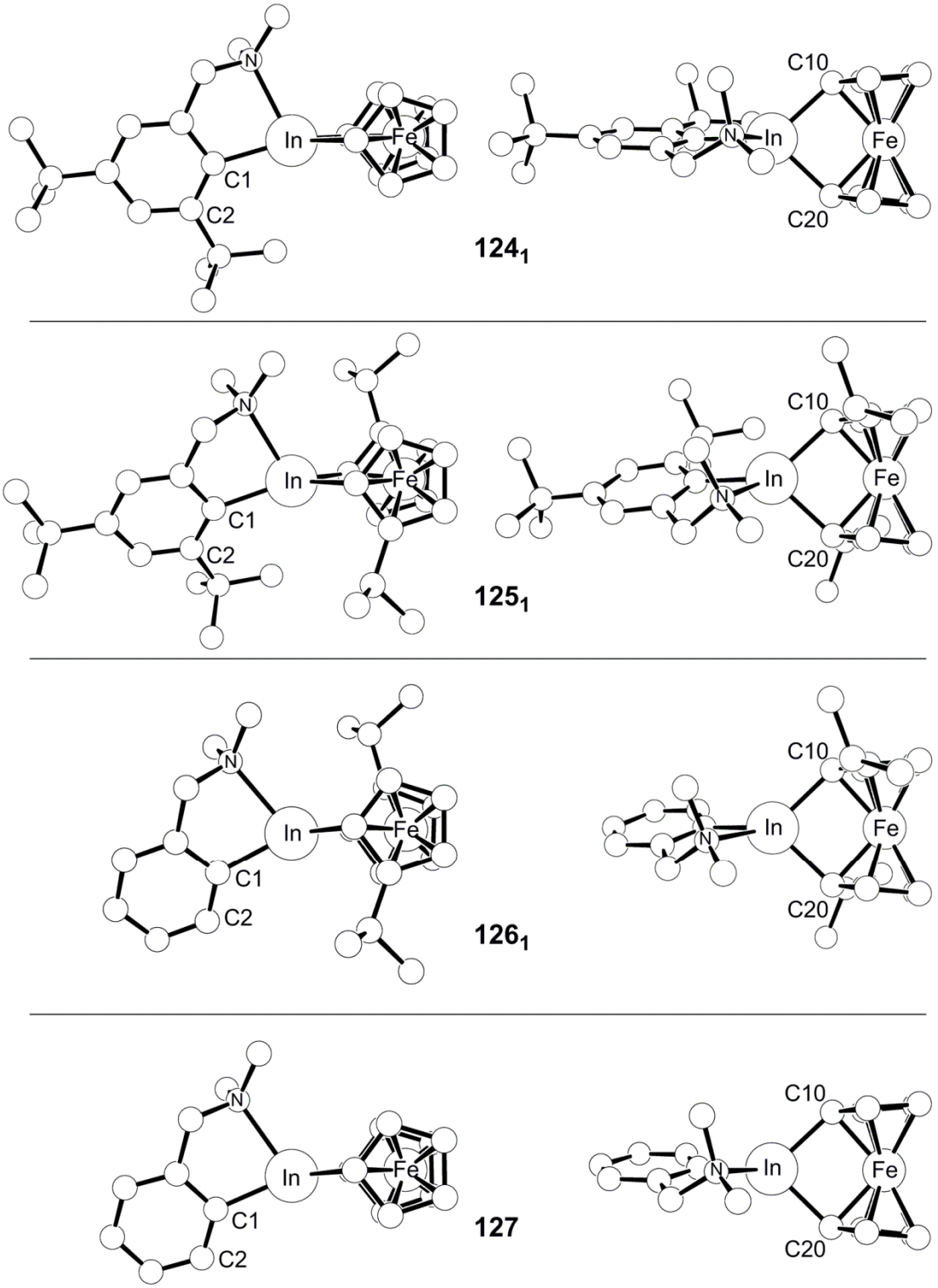

Figure 15. Calculated molecular structures of inda[1]ferrocenophanes $\mathbf{124_1}$, $\mathbf{125_1}$, $\mathbf{126_1}$, and **127**. Hydrogen atoms are omitted for clarity. Molecules are shown with views normal to the planes C10−Fe−C20 and Fe−In−C1, respectively. Reprinted with permission from Bagh, B.; Sadeh, S.; Green, J. C.; Müller, J. *Chem.–Eur. J.* **2014***, 8,* 2318-2327. Copyright 2014 Wiley VCH.

The four species **124$_1$**, **125$_1$**, **126$_1$** and **127** show similar values for the tilt angle α within a small range (10.96° for **126$_1$** and 11.4° for **124$_1$**). Based on the measured values for tilting of Cp rings in gallium-, germanium-, and tin-bridged [1]FCPs, tilt angles of around 11° are expected for indium-bridged [1]FCPs. In group-14-bridged [1]FCPs, the tilt angle α decreases by a magnitude of around 5° by descending from the 4th to the 5th period [For instance, α = 19.0(9) (Me_2Gefc),[53] 14.1(2)° ($t$$Bu_2$Snfc)[13]]. The same trend is also expected for group-13-bridged [1]FCPs. Tilt angles α of around 16° are reported for gallium-bridged [1]FCPs [α = 15.4(2) and 16.4(2)° (Pytsi)Gafc,[31] (Me_2Ntsi)Gafc,[32] 16.26(9) and 16.45(10) Ar′Gafc$^{i\text{Pr}2}$[164]] and, therefore, applying the 5° difference results in values of around 11° for indium-bridged [1]FCPs. As it can be seen in Figures 14 and 15, species **127** has the least amount of steric congestion among all species while the indium-bridged [1]FCP **125$_1$** is the most crowded one. Being equipped with either *t*Bu groups on the aromatic ligands (**124$_1$**) or *i*Pr groups on ferrocene (**126$_1$**), species **124$_1$** and **126$_1$** have an intermediate steric congestion. Comparison of the bond lengths around indium shows that the longest bonds are belonging to the most bulked-up species **125$_1$**. Within the group of four inda[1]ferrocenophanes **124$_1$**, **125$_1$**, **126$_1$**, and **127**, the differences between the shortest and the longest bonds are small: 0.032 (In-N), 0.035 (In-C1), 0.021 (In-C10), and 0.018 Å (In-C20). This amount of variation between the shortest and the longest bonds could be the result of a "steric pressure" between the Mamx and the fc$^{i\text{Pr}2}$ moiety in **125$_1$**. Previously, in the case of the aluminum- and gallium-bridged metallocenophanes, equipped with the Mamx ligand, DFT calculation revealed that the *ortho*-*t*Bu group of the Mamx moiety results in a "side shifting" of the entire ligand compared to the species where this *t*Bu group was missing and substituted by a H atom.[34] The "side shifting" of the ligand can be shown by the M-E-C1 angle, which widened between 8.08 and 12.73° in aluminum- and gallium-bridged [1]metallocenophanes equipped

with *ortho-t*Bu group of the known compounds.[34] Calculation of the molecular structure of indium-bridged [1]FCPs **124$_1$**, **125$_1$**, **126$_1$**, and **127** reveals a similar but less pronounced effect for these species (Figure 15): from **127** to **124$_1$**, the Fe-In-C1 angle increases by 6.38°; from **126$_1$** to **125$_1$**, the same angle increases by 7.72° (Table 3). Comparison of pairs of species that differ only in the presence or absence of *i*Pr groups reveals a decrease of the Fe−In−C1 angle by 4.22 (**124$_1$** to **125$_1$**) and 5.56° (**127** to **126$_1$**) when *i*Pr groups are present. On the other hand, the degree of tilting of the aromatic ligand relative to the ferrocene moiety changes depending on the steric congestion which is present in the molecules. The tilting of the aromatic ligand can be shown by the torsion angle M−E−C1−C2. An increase of between 5.26 and 6.98° was previously observed for M−E−C1−C2 angle by the presence of the *ortho-t*Bu group in the known aluminum- and gallium-bridged [1]metallocenophanes.[34] In the case of the new indium compounds **127**, the *t*Bu groups have a small influence in the Fe−In−C1−C2 angle (increasing the twist by 1.45° from **127** to **124$_1$**), however, this effect is more significant for indium-bridged [1]FCP **125$_1$** (increasing the twist by 13.00° from **126$_1$** to **125$_1$**). The most significant influence in the tilting of the aromatic ligand is observed when the effects of both alkyl groups are combined together: a comparison between the non-substituted inda[1]ferrocenophane (**127**) and the highest substituted species (**125$_1$**) reveals a difference of 18.48° in the Fe−In−C1−C2 angle. However, the importance of these structural changes should be considered with caution and over-interpretation must be avoided. For instance, the two crystallographically independent molecules of species **122** have Fe−Ga−C1−C2 angles which are different by 7.7° (Table 3).

Here is a summary of structural effects of alkyl groups in indium-bridged [1]FCPs: 1) Angles which are commonly used to describe the geometrical features of [1]FCPs, including tilt angle α (tilting of Cp moieties), do not change significantly by changing the substitution pattern of

indium-bridged [1]FCPs; 2) In all indium-bridged [1]FCPs, *ortho*-*t*Bu groups result in a widening of the Fe−E−C1 angle, however, this "side shifting" is significantly smaller than that of the similar aluminum and gallium species.[34] The lower calculated values for the Fe−In−C1 angle can be rationalized as following: In-C bonds are about 10% longer than Al−C or Ga−C bonds; therefore, the *ortho*-*t*Bu group of the Mamx ligand is further away from the ferrocene unit, resulting in reduced steric interactions; 3) The structural effect of the *ortho*-*t*Bu groups on the Ar′ ligand (**124$_1$** compared to **127**) is similarly insignificant as that of two *i*Pr groups on the ferrocene moiety (**124$_1$** compared to **127**). Surprisingly, both alkyl groups, *i*Pr and *t*Bu, result in an opposite effect with respect to the relative orientation of the aromatic ligand and the ferrocene unit (angles Fe-In-C1and Fe-In-C1-C2); and 4) Among the four indium-bridged [1]FCPs, the most sterically congested species **125$_1$** shows the highest amount of distortion, evidenced by elongation of the bonds for the fourfold-coordinated indium atom and by the amount of tilting of the Mamx ligand (Fe-E-C1-C2 = -37.69°).

Thermochemistry

DFT calculations demonstrated that *i*Pr groups as well as *t*Bu groups cause structural changes in indium-bridged [1]FCPs. In the next stage, we performed a thermodynamic study in order to understand whether these alkyl groups also increase the strain of the indium-bridged [1]FCPs. Similar to the strategy which was previously applied in our group for aluminum- and gallium-bridged [1]FCPs,[34] a hydrogenolysis reaction has been used (Scheme 71) to address this question. Table 4 shows $\Delta E^{(SCF)}$, $\Delta H°$, and $\Delta G°$ values, calculated for each indium-bridged [1]FCP (BP86/TZ2P; see Experimental Section for details). Since the hydrogenolysis reaction is non-isodesmic, the absolute values which are listed in Table 4 are meaningless. However, the thermodynamic effect of each alkyl group (*i*Pr or *t*Bu) can be understood by comparing two

reactions which are only different by the presence or absence of that particular group; the values for such a comparison are listed in Table 5.

Scheme 71. Hydrogenolysis Reaction to Evaluate Strain in [1]FCPs.

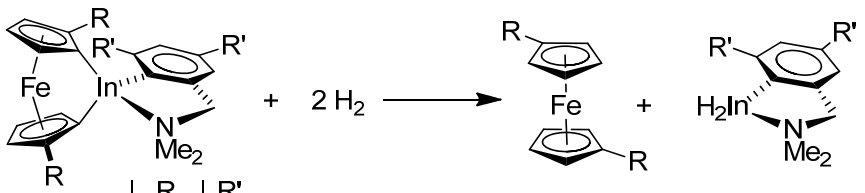

	R	R'
124$_1$	H	*t*Bu
125$_1$	*i*Pr	*t*Bu
126$_1$	*i*Pr	H
127	H	H

Table 4. Thermodynamic Data [kcal mol^{-1}] of the Hydrogenolysis Reaction (Scheme 71).

	R / R'	$\Delta E^{(SCF)}$	$\Delta H°$	$\Delta G°$
124$_1$	H / *t*Bu	-40.46	-29.93	-25.46
125$_1$	*i*Pr / *t*Bu	-43.57	-32.76	-30.42
126$_1$	*i*Pr / H	-40.48	-28.37	-25.60
127	H / H	-39.62	-28.20	-23.74

Table 5. Effects of the *i*Pr and *ortho*-*t*Bu Groups on the Hydrogenolysis Reaction (Scheme 71).[a]

	hydrogenolysis reactions of	effect of	$\Delta\Delta E^{(SCF)}$	$\Delta\Delta H°$	$\Delta\Delta G°$
1	**124$_1$** compared to **127**	*t*Bu	-0.84	-1.72	-1.72
2	**125$_1$** compared to **126$_1$**	*t*Bu	-3.09	-4.39	-4.82
3	**126$_1$** compared to **127**	*i*Pr	-0.86	-0.17	-1.86
4	**125$_1$** compared to **124$_1$**	*i*Pr	-3.11	-2.83	-4.96

[a] Values in kcal mol^{-1}. Negative values indicate that species with alkyl groups result in a larger release of energy.

In this evaluation it is assumed that the alkyl groups do not have any influence on bonds that are broken or formed in the hydrogenolysis reaction. In table 5, the thermodynamic data for two reactions are compared in such a way that a negative sign for the listed values shows an increase of strain caused by one type of alkyl substituent. Obtaining negative values for all of the comparisons in Table 5 shows that in each case an increase of strain was occurred. Entries 1 and 2 in Table 5 show the effect of the *t*Bu groups, while entries 3 and 4 indicate the effects caused by the *i*Pr groups. Moreover, entry 1 illustrates the effect of the *t*Bu groups onto the fc moiety, while entry 2 shows the effect of the *t*Bu groups onto the fc^{iPr2} unit. Likewise, entry 3 shows the effect of the *i*Pr groups onto the Ar′ ligand, while entry 4 shows the effect of the *i*Pr groups onto the Mamx ligand. Comparing the sets of ΔΔ values for entries 1 and 3 versus entries 2 and 4 shows that the ΔΔ values are much smaller for entries 1 and 3. These low values for entries 1 and 3 and high values of entries 2 and 4 are reasonable as entries 1 and 3 each illustrate the effect of one type of alkyl group (*i*Pr or *t*Bu) on to the non-bulky moiety (Ar′ or fc), while entries 2 and 4 each indicate the effect of alkyl group (*i*Pr or *t*Bu) on to the bulky moiety (Mamx or fc^{iPr2}).

To sum up, the strain effects can be ordered from the smallest to the largest as follows: the effect of *i*Pr groups toward the Ar′ ligand (nearly no effect with $\Delta\Delta H°_{298}$ = -0.17 kcal mol^{-1}), followed by the effect of *t*Bu groups toward the fc unit ($\Delta\Delta H°_{298}$ = -1.72 kcal mol^{-1}), followed by the effect of *i*Pr groups toward the Mamx ligand ($\Delta\Delta H°_{298}$ = -2.83 kcal mol^{-1}), followed by the effect of *t*Bu groups toward the fc^{iPr2} moiety ($\Delta\Delta H°_{298}$ = -4.39 kcal mol^{-1}). Among the four indium-bridged [1]FCPs, species **125_1** shows the highest increase of strain by alkyl groups ($\Delta\Delta H°_{298}$ = -2.83 and -4.39 kcal mol^{-1}). This thermodynamic data are in agreement the structural changes found for indium-bridged [1]FCPs where the most distorted structure was revealed for species **125_1**.

2.5. Preamble Part 2

Despite the large number of known [1]FCPs, living polymerization is limited to the species with silicon, germanium, and phosphorus in the bridging position. There are several problems in the area of strained [1]FCPs and their ROP, which have brought their chemistry to a standstill. In part 1 of my project it was demonstrated that using alkyl-substituted dilithioferrocenes is superior to the use of dilithioferrocene·tmeda which is commonly used as the starting material for the preparation of [1]FCPs. After the successful application of dilithioferrocene **121** for the preparation of heavier group-13-bridged [1]FCPs,[164, 168] I aimed to synthesize a new class of elemental-bridged [1]FCPs with boron, silicon, tin and phosphorus in the bridging position by using alkyl-substituted dilithioferrocenes as the starting materials. Following are some of the existing issues, which I targeted to resolve through this part of the project: 1) A number of known [1]FCPs are polymerizable, however, the insolubility of the resulting metallopolymers is a very serious issue for the characterization and processability of these species. For instance, the thermal ROPs of boron- and sulfur-bridged [1]FCPs, known as the most strained [1]FCPs, yielded insoluble polymeric materials. The existence of alkyl substituents on the Cp units would potentially increase the solubility of the [1]FCPs and their resulting metallopolymers. 2) It is known that the tmeda content of dilithioferrocene·tmeda can cause problems for the isolation of obtained [1]FCPs. For example, it was suggested that the presence of tmeda in the reaction mixture caused the spontaneous ROP tin-bridged [1]FCPs.[13] In the preparation of the alkyl-substituted dilithioferrocenes, I designed a synthetic pathway which is independent from the use of tmeda. 3) Dilithioferrocene·tmeda is poorly soluble in many organic solvents and its salt-metathesis reaction with element dichlorides R_xECl_2 is performed heterogeneously which makes it almost impossible to have a good control over the concentration of reactants. In my approach, I

developed a system where the dilithioferrocene salt is completely soluble in solvent mixture, allowing for a perfect control of the stoichiometry of the reaction and concentration of reactants.

Having alkyl-substituted dilithioferrocenes at my disposal, I synthesized a new class of chiral elemental-bridged [1]FCPs with boron, silicon, tin, and phosphorus in the bridging position. As it was mentioned before, prior to my Ph.D. work there were only three boron-bridged [1]FCPs known in the literature and the ROP of these species resulted mostly in insoluble materials. Chapter 2.6 describes my research in the preparation of boron-bridged [1]FCPs by using alkyl-substituted dilithioferrocenes as the starting material and applying different amino groups on the bridging element. The thermal ROP of the obtained boron-bridged [1]FCPs and characterization of the resulting polymers is also described in this subchapter. Chapter 2.7 and 2.8 explain the synthesis and thermal properties of the chiral silicon-, tin- and phosphorus-bridged [1]FCPs equipped with alkyl groups on the Cp units.

2.6. Chiral Bora[1]ferrocenophanes: Syntheses, Mechanistic Insights, and Ring-opening Polymerizations

During the last 20 years, there have been many progresses in the area of polymers which contain boron as a part of polymer backbone. Many research activities have been focused on the preparation of materials for optoelectronic applications which contain boron as a part of their extended π system.[169-171] Thanks to the development of new synthetic protocols as well as the use of bulky aryl ligands to protect the acidic boron center [e.g. 2,4,6-trimethylphenyl (Mes) or 2,4,6,-triisopropylphenyl (Tip)], there has been a significant amount of progress in this area of new materials. As it was described in chapter 1.2, during the last two decades, it has been demonstrated that ring-opening polymerization of strained sandwich compound is a very effective method for the incorporation of main-group elements into the polymer backbone.[28]

Silicon-bridged [1]FCPs are the most developed family of strained sandwich compound which can be applied for living polymerization and be used to produce block copolymers.[28, 84] In contrast to the developed area of silicon-bridged [1]FCPs, the polymerization chemistry of other [1]FCPs is far less advanced and only [1]FCPs bridged by germanium[107] and phosphorus[64, 67, 87, 172, 173] can be polymerized with a control over molecular-weight and molecular-weight distribution. As it was mentioned earlier, there are a number of existing problems in the area of other strained [1]FCPs, which have brought their chemistry to a halt. For example, lack of solubility is a common issue in the area of metallopolymers which is troublesome for the characterization of these species. The lack of synthetic flexibility for the preparation of strained species is another common existing problem in this area. Synthetic protocols for the preparation of strained species often require the use of bulky ligands at the bridging elements; however, the existence of these bulky ligands on monomers can cause problem for their ROP.

As it was mentioned in chapter 1.1.1, boron-bridged [1]FCPs are a very interesting class of strained sandwich compounds, as they are the only group of [1]FCPs which contain a 2nd period element in their bridging position. Moreover, these species are the current record holders for the tilting of Cp rings (tilt angle α; Scheme 2); for instance, $(Me_3Si)_2$NBfc with the α angle of 32.4(2)° is the most tilted FCP known in the literature.[5, 30]

Prior to our investigations, there were only three reported boron-bridged [1]FCPs. For the synthesis of all the three known species, $(Me_3Si)_2$NBfc, (Me_3Si)*t*BuNBfc and $(i\text{Pr})_2$NBfc, bulky amino ligands were used to protect the boron center. The thermal ROP of these boron-bridged [1]FCPs at 180-200 °C mainly resulted in insoluble material. Only for *i*Pr$_2$NBfc a soluble polymer of low molecular weight was obtained.[5] Surprisingly, the enthalpy of the thermal ROP measured by DSC was lower than the expectation. For instance a ΔH^{ROP} of -95 kJ mol^{-1} was

measured for $(Me_3Si)_2NBfc$ and this was considerably lower than the measured exothermy for the similarly tilted sulfur-bridged [1]FCP [α = 31.05(10)°; ΔH^{ROP} = -130(±20) kJ mol^{-1}].[10, 11] The lower than expected enthalpy for the ROP was rationalized by the destabilizing effect of the bulky amino groups on the resulting metallopolymer.[5] In the same report authors speculated that higher molecular-weight poly(ferrocenylborane)s can be accessed by the ROP of boron-bridged [1]FCPs with smaller substituents on the boron center. Since the publication of this article in 2000,[5] no additional progress has been reported in the area boron-bridged [1]FCPs. Being inspired by the obtained positive results for the preparation heavier group-13-bridged [1]FCPs,[164, 168] we utilized this new approach to tackle the existing problem in the area of boron-bridged [1]FCPs. The alkyl groups on the Cp units can act as solubilizing agents and increase the solubility of the resulting metallopolymers. Moreover, boron-bridged [1]FCPs with smaller substituents on boron atom can be prepared when boron in the bridge is already protected by alkyl substituents at the Cp moieties.

2.6.1. Author Contribution

I was the leading researcher of this project and prepared all the boron-bridged [1]FCPs. I developed the optimized conditions for the preparation of boron-bridged [1]FCPs. The other collaborators of this project are Hridaynath Bhattacharjee, who prepared the bis(boryl)ferrocenes, Elaheh Khozeimeh Sarbisheh, who synthesized (S_p,S_p)-1,1′-dibromo-2,2′-di(3-pentyl)ferrocene (**130**) and obtained suitable crystals for single-crystal X-ray analysis, and J. Wilson Quail, who performed the structure determinations by single-crystal X-ray analysis.

2.6.2. Synthesis of Chiral Bora[1]ferrocenophanes

The salt-metathesis reaction was preformed between iPr$_2$NBCl$_2$ and dilithio derivative of **120** (Scheme 72) and resulted in a mixture of targeted boron-bridged [1]FCP **128** and the bis(boryl)ferrocene **129**.

Scheme 72. Synthesis of Boron-bridged [1]FCP **128** and Bis(boryl)ferrocene **129**.

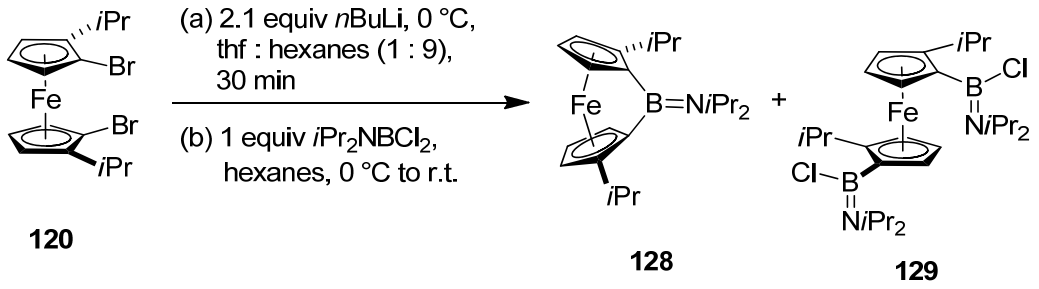

Similar reaction conditions as those applied for the gallium-bridged [1]FCP **122** (scheme 66) was applied for the preparation of boron-bridged [1]FCP **128**. The procedure involves the lithiation of dibromoferrocene **120** in a mixture of hexanes and thf (9 : 1) at 0 °C and then removal of the ice bath and addition of a solution of iPr$_2$NBCl$_2$ dropwise during 10 min through a cannula tubing from a second Schlenk flask. The ^{1}H NMR spectroscopy of the reaction mixture revealed a ratio of 1.0 to 3.5 between the species **128** and **129** respectively. The filtration of the reaction mixture to remove the LiCl was followed by removal of the solvent. The boron-bridged [1]FCP **128** has a high vapor pressure and was isolated by vacuum sublimation of the reaction mixture as a pure crystalline dark-red solid in 20% yield. The bis(boryl)ferrocene **129** was also isolated from the reaction mixture by sublimation under vacuum at a higher temperature (120 °C) and characterized by ^{1}H NMR spectroscopy. Deduced from the signal pattern of their ^{1}H NMR spectra, both species **128** and **129** are C_2-symmetric in solution. For instance, four doublets of equal intensity appear for the eight Me groups of the four iPr in **128**, while six equally intense

doublets appear for the twelve Me groups of the six *i*Pr in **129**. Each species shows three Cp signals for its six Cp signals. The signals for the Cp protons of the strained compound **128** expectedly appear over a wide range [δ = 3.50 (2H, CH-α of Cp), 4.30 (2H, CH-β of Cp), 4.53 ppm (2H, CH-β of Cp)]. In contrast, the Cp signals of the bis(boryl)ferrocene **129** resonate in a narrow range (δ = 4.25 to 4.50 ppm). The boron-bridged [1]FCP **128** shows a large splitting of Δδ = 0.92 ppm (averaged value) for the ^{1}H chemical shifts of the Cp protons. Such a splitting of the ^{1}H chemical shifts is more than twice than that of the known species *i*Pr$_2$NBfc (Δδ = 0.39 ppm, δ = 4.45 and 4.06 ppm).[5] This effect is presumably caused by the influence of the *i*Pr group on the adjacent α-H atoms. The ^{13}C NMR spectrum of species **128** shows a peak at δ = 39.9 ppm for the boron-bound carbon atom, which is similar to that of the known species *i*Pr$_2$NBfc (δ = 44.2 ppm);[174] the 4 ppm difference in the chemical shift is probably due to the shielding of C-*ipso* by *i*Pr groups on the Cp rings. The ^{11}B NMR spectroscopy of **128** shows a resonance at δ = 39.5 ppm which is very similar to the ^{11}B chemical shift of the known species *i*Pr$_2$NBfc (δ = 40.0 ppm).[174] The vacuum sublimation of species **128** resulted in suitable crystals for single-crystal X-ray analysis and the crystal structure of **128** was determined (Figure 16; Tables 6 and 7).

The X-ray analysis of **128** confirms a trigonal planar geometry for the boron atom (angle sum of 360°; Figure 16). Moreover, the short bond length of 1.387(6) Å between boron and nitrogen evidences the presence of a BN double bond (*i*Pr$_2$NBfc:[5] 1.371(6) and 1.384(6)Å).[175] A set of angles which are commonly used to describe the geometric features of [1]FCPs are listed in Table 7 for the species **128**. As described before, the highest tilting of the Cp rings among strained [1]FCPs are found for boron-bridged [1]FCPs.[5] A tilt angle α of 31.9(2)° is found for the boron-bridged [1]FCP **128** and this angle, within three estimated standard deviations, is identical

to the previously reported α angle for the known species *i*Pr$_2$NBfc [α = 31.4(2)°].[5] The bridging unit BN*i*Pr$_2$ is twisted with respect to the ferrocene moiety. This slight twist can be shown by an angle of 4.4(3)° between the two planes B1-N1-C17-C20 and C1-Fe-C6. Due to the steric interactions, the *i*Pr groups attached to the nitrogen on the bridge are twisted away from the *i*Pr groups on the Cp moieties.

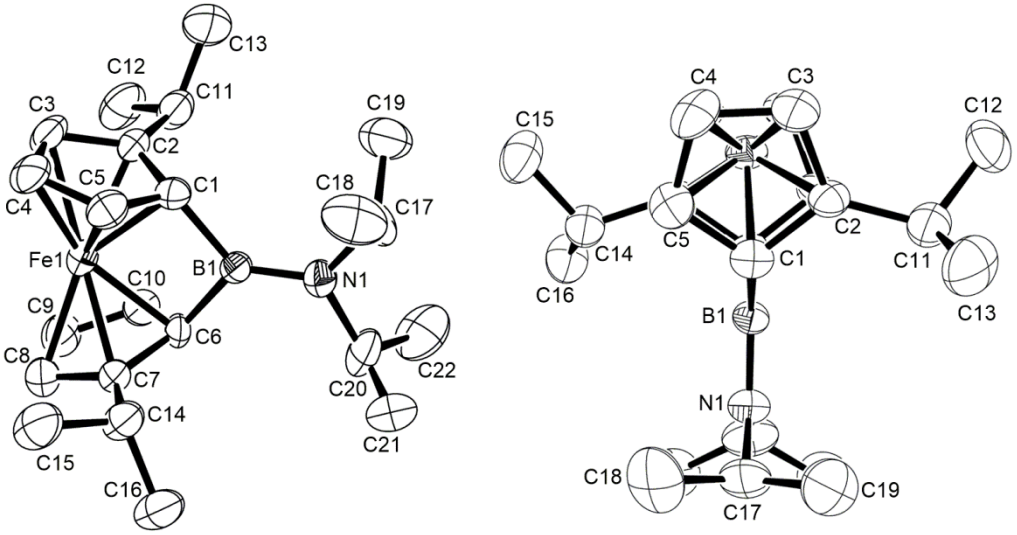

Figure 16. Molecular structure of **128** with thermal ellipsoids at the 50% probability level. Hydrogen atoms are omitted for clarity. Selected atom-atom distances [Å] and bond angles [°] for **128**: B1-C1 = 1.619(6), B1-C6 = 1.594(6), B1-N1 = 1.387(6), C1-B1-C6 = 103.0(3), C1-B1-N1 = 131.1(4), C6-B1-N1 = 125.8(4). Reprinted with permission from Sadeh, S.; Schatte, G.; Müller, J. *Chem.–Eur. J.* **2013***, 40,* 13408-13417. Copyright 2013 Wiley VCH.

Table 6. Crystal and Structural Refinement Data for **128** and **138.**

	128	**138**
empirical formula	$C_{22}H_{34}BFeN$	$C_{26}H_{42}BFeN$
fw	379.17	435.26
cryst. size / mm^3	0.08 × 0.05 × 0.05	0.200 × 0.250 × 0.300 mm
cryst. system, space group	triclinic, *P*1	triclinic, *P*1
Z	1	1
a / Å	7.3470(5)	7.3391(3)

b / Å	8.5240(7)	9.4771(3)
c / Å	9.5080(7)	9.9193(3)
α / °	106.090(4)	102.1770(12)
β / °	107.320(5)	103.3960(13)
γ / °	94.871(5)	105.9690(12)
volume / $Å^3$	537.00(7)	616.80(4)
ρ_{calc} / mg m^{-3}	1.172	1.172
temperature / K	173(2)	173(2)
μ_{calc} / mm^{-1}	0.706	0.623
θ range / °	4.36 to 27.53	3.04 to 28.28
reflns collected / unique	3881 / 3881	5988
absorption correction	multi-scan	multi-scan
data / restraints / params	3881 / 3 / 234	5988 / 35 / 338
goodness-of-fit	1.119	1.003
R_1 [I > 2 σ(I)][a]	0.0532	0.0294
wR_2 (all data)[a]	0.1209	0.0601
largest diff. peak and hole	0.477	0.287 and -0.214
$\Delta\rho_{elect}$ / e $Å^{-3}$	-0.393	0.038

[a] $R_1 = [\Sigma||F_o|-|F_c||]/[\Sigma|F_o|]$ for $[F_o^2 > 2\sigma(F_o^2)]$, $wR_2 = \{[\Sigma w(F_o^2-F_c^2)^2]/[\Sigma w(F_o^2)^2]\}^{1/2}$ [all data].

Table 7. Measured Distortion Angles [°] (see Figures 16 and 17).

	128	**138**
α	31.9(2)	31.2(1)
β/β′	36(1)/35(1)	35.2(6)/35.9(7)
θ	103.0(3)	103.3(1)
δ	155(2)	156.3(10)

The low selectivity of the described salt-metathesis reaction, which is also reflected in the low isolation yield of the species **128**, limits the potential application of this species for ROP. However, this result inspired us to optimize the reaction conditions as well as the bulkiness of the substituents in order to synthesize a new class of boron-bridged [1]FCPs (see chapter 2.6.3 for details). In addition to the previously described (S_p,S_p)-1,1′-dibromo-2,2′-di(isopropyl)ferrocene (**120**), (S_p,S_p)-1,1′-dibromo-2,2′-di(3-pentyl)ferrocene (**130**) was also used for the preparation of boron-bridged [1]FCPs. A synthetic procedure to obtain species **130** as an impure oil was already reported in the literature;[161] however, this procedure was modified by E. Khozeimeh Sarbisheh (a current group member) to obtain it as a pure crystalline solid. The multistep, diastereoselective synthesis of (S_p,S_p)-1,1′-dibromo-2,2′-di(3-pentyl)ferrocene (**130**) is very similar to that of the dibromoferrocene **120** and is based on the well-known "Ugi amine" chemistry (Scheme 73).[135]

Scheme 73. Synthesis of (S_p,S_p)-1,1′-Dibromo-2,2′-di(3-pentyl)ferrocene.

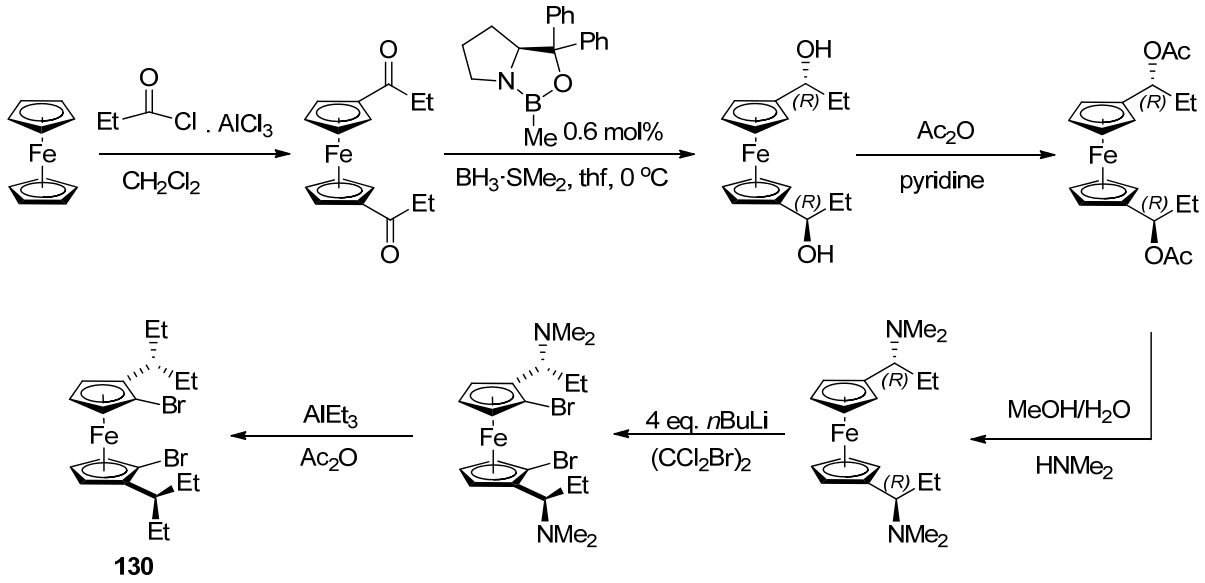

The X-Ray diffraction analysis of the obtained suitable crystals revealed the crystal structure of dibromoferrocene **130**.[176] Expectedly, the molecular structure of **130** was very similar to that of the **120** with the same orientation of alkyl groups with respect to ferrocene moiety, an important fact that will be discussed later (see chapter 2.6.3).

As it was described before, the lithium-bromide exchange of dibromoferrocene **120** can be performed cleanly by using 2.1 equivalents of *n*BuLi in a solvent mixture of hexanes : thf (9 : 1).[164] Expectedly, the lithium-bromide exchange of species **130** can be performed by using the same method to result in dilithioferrocene **131** (Scheme 74).

Scheme 74. Lithium-bromide Exchange of Dibromoferrocene **130**.

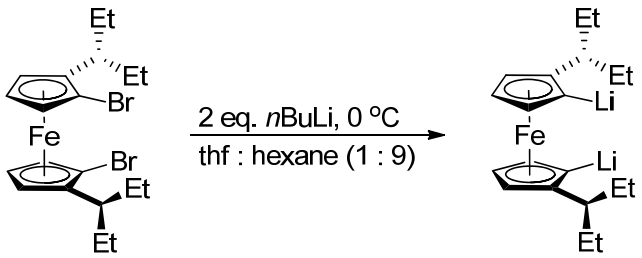

130 **131**

In addition to the species **128**, five other boron-bridged [1]FCPs were prepared by reacting the dilithio species **121** and **131** with the aminoborane Et_2NBCl_2, iPr_2NBCl_2 and tBu(Me_3Si)$NBCl_2$. All the six boron-bridged [1]FCPs were prepared by using an optimized reaction condition which was developed to increase the yield of the targeted strained species (see chapter 2.6.3).

Deduced from the ^{1}H NMR spectrum of the reaction mixture, the salt-metathesis reaction between the dilithio derivative of **120** and Et_2NBCl_2 resulted in an exclusive formation of the targeted boron-bridged [1]FCP **132** (Scheme 75). Similar to the bora[1]ferrocenophane **128**, species **132** has a high vapor pressure and was further purified by flask-to-flask condensation

under vacuum (55 °C) from the filtrated reaction mixture. All the attempts for the complete purification of species **132** were unsuccessful and this species was obtained as a red oil containing a small amount of hydrolysis byproduct $(i\text{PrH}_4\text{C}_5)_2\text{Fe}$.

Scheme 75. Synthesis of Boron-bridged [1]FCP **132**.

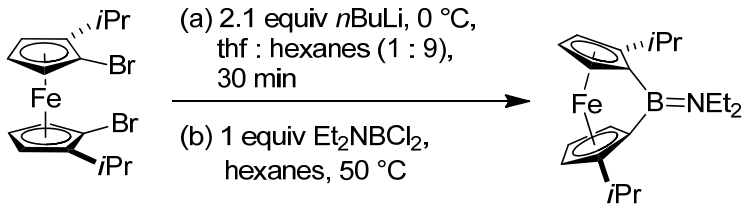

120 **132**

The boron-bridged [1]FCP **132** is C_2-symmetric and the ^{1}H NMR spectrum of this species shows three signals for the six Cp proton [δ = 3.43 (2H, CH-α of Cp), 4.28 (2H, CH-β of Cp) and 4.52 ppm (2H, CH-β of Cp)]. The signal pattern of the Cp protons is very similar to that of the bora[1]ferrocenophane **128**. Expectedly, only two signals are observed for the four Me groups of the two *i*Pr groups. In the ^{13}C NMR spectrum, the resonance of the *ipso* carbon atom bound to boron at δ = 39.9 ppm is identical to that of the species **128**. The ^{11}B NMR spectroscopy of species **132** revealed a resonance at δ = 40.0 ppm for the boron atom.

As illustrated in Scheme 76, the enantiomerically pure ferrocene dibromide **130** was first lithiated and then reacted with Et_2NBCl_2 to give the targeted boron-bridged [1]FCP **133**. Monitoring the reaction mixture with ^{1}H NMR spectroscopy revealed that the C_2-symmetric species **133** formed selectively. Species **133** was isolated by crystallization from a hexanes solution of the filtrated reaction mixture at -80 °C (63%). The ^{1}H NMR spectrum exhibits three signals in the Cp range, which could be either caused by **133** or the respective bis(boryl)ferrocene species (C_2-symmetric), however, the signal pattern indicates the formation

of the targeted [1]FCP. Similar as for other boron-bridged [1]FCPs,[5] Cp signals of species **133** spread over a wide range with the α proton appearing more toward the upfield [δ = 3.53 (2H, CH-α of Cp), 4.28 (2H, CH-β of Cp) and 4.57 ppm (2H, CH-β of Cp)].

Scheme 76. Synthesis of Boron-bridged [1]FCP **133**.

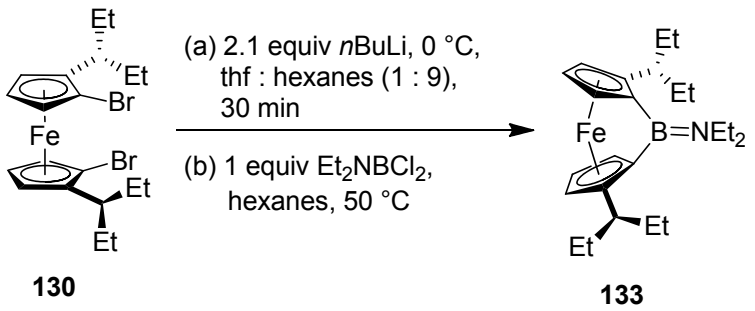

130 **133**

All the attempts for the isolation of a suitable single crystal for X-ray diffraction analysis of species **133** were unsuccessful and, therefore, the geometric features, specially the tilt angle α, were not determined. In the ^{13}C NMR spectrum the signal of *ipso* carbon atom bound to boron is found at δ = 40.7 ppm which is similar as that of **132** (δ = 40.7 ppm). The ^{11}B NMR signal appears at δ = 40.3 ppm which is comparable to the chemical shift of species **132** (δ = 40.0 ppm). Species **133** was also characterized by mass spectrometry and elemental analysis. Consistently, mass spectrometry of **133** showed the highest detected mass for M^+, confirming the formation of the strained species **133**.

The salt-metathesis reaction was performed between the dilithio derivative of **120** and bulky aminoborane *t*Bu(Me$_3$Si)NBCl$_2$ (Scheme 77). Reaction control by ^1H NMR spectroscopy confirmed the formation of the targeted bora[1]ferrocenophane **134** along with the unwanted bis(boryl)ferrocene **135**. Deduced from the ^1H NMR spectrum of the reaction mixture, species **134** and **135** are formed in an approximate ratio of 1.0 to 0.47. The boron-bridged [1]FCP **134** has a similar vapor pressure as the species **128** and was further purified by flask-to-flask

condensation, however, species **134** could not be isolated cleanly due to the presence of a small amount of the hydrolysis byproduct $(i\text{PrH}_4\text{C}_5)_2\text{Fe}$ in the condensed oil.

Scheme 77. Synthesis of Boron-bridged [1]FCP **134** and Bis(boryl)ferrocene **135**.

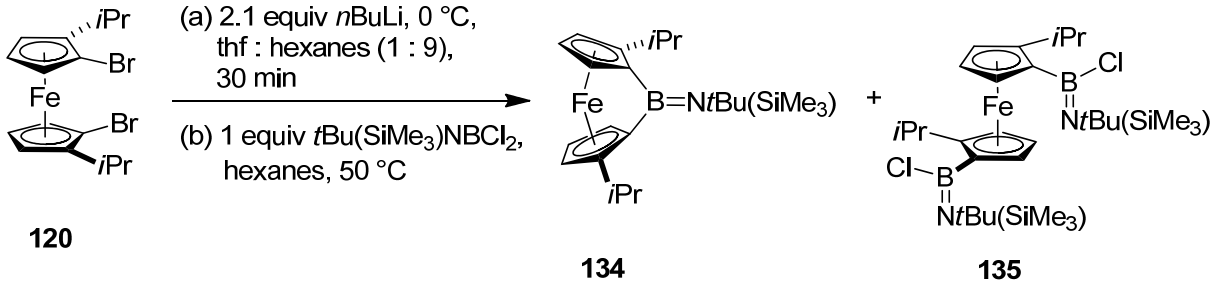

120 **134** **135**

Deduced from their ^{1}H NMR spectra, the bis(boryl)ferrocene **135** is C_2-symmetric in solution while the boron-bridged [1]FCP **134** is C_1-symmetric. The ^{1}H NMR spectrum of the asymmetric species **134** illustrates three pairs of signals for the six Cp protons with a large splitting between α and β protons [δ = 3.40 (1H, CH-α of Cp), 3.41 (1H, CH-α of Cp), 4.26 (1H, CH-β of Cp), 4.28 (1H, CH-β of Cp), 4.49 ppm (2H, CH-β of Cp)]. In the ^{13}C NMR spectrum, two characteristic peaks are found for the boron-bound *ipso*-carbon atoms at δ = 44.1 and 45.3 ppm which are similar as that of the known species *t*Bu(Me$_3$Si)NBfc (δ = 44.3 ppm).[5] The ^{11}B NMR chemical shift of δ = 46.1 ppm in **134** is higher than that of the known species *t*Bu(Me$_3$Si)NBfc (δ = 40.0 ppm).[5]

Treatment of the dilithio derivative of **130** with the bulky aminoborane *t*Bu(Me$_3$Si)NBCl$_2$ resulted in the targeted boron-bridged [1]FCP **136** as well as in the unwanted bis(boryl)ferrocene **137**. The ^{1}H NMR spectroscopy of the reaction mixture revealed a ratio of 1.0 : 0.12 between species **136** and **137** respectively (Scheme 78). Species **136** was isolated as a solid powder from hexanes solution at -80 °C (48%). Similar to the ^{1}H NMR spectrum of species **134**, three pairs of signals with a large splitting between α and β protons are observed for the six Cp protons of the

C_1-symmetric species **136** [δ = 3.43 (1H, CH-α of Cp), 3.47 (1H, CH-α of Cp), 4.25 (1H, CH-β of Cp), 4.26 (1H, CH-β of Cp), 4.50 (1H, CH-β of Cp), 4.51 ppm (1H, CH-β of Cp)].

Scheme 78. Synthesis of Boron-bridged [1]FCP **136** and Bis(boryl)ferrocene **137**.

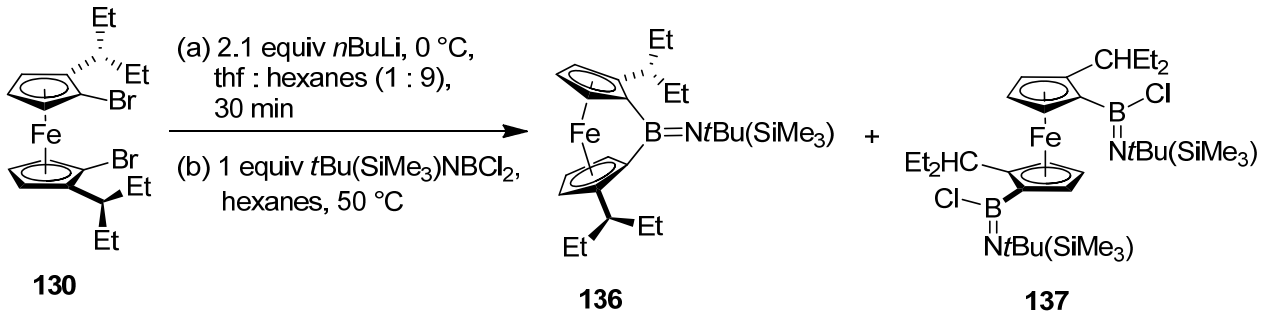

The presence of the strained compound **136** is also confirmed by ^{13}C NMR spectroscopy where the ^{13}C resonances of the *ipso*-carbon atoms bound to boron are found at δ = 42.2 and 45.5 ppm. The ^{11}B NMR signal appears at δ = 46.5 ppm which is very similar as that of boron-bridged [1]FCPs **134** (δ = 46.1 ppm). Species **136** was also characterized by mass spectrometry and elemental analysis. The measured mass spectrum showed the highest detected mass for the molecular ion of [1]FCP **136**.

As illustrated in Scheme 79, the enantiomerically pure ferrocene dibromide **130** was first lithiated, followed by reaction with aminoborane iPr$_2$NBCl$_2$ to result in the targeted bora[1]ferrocenophane **138** and the byproduct **139**. Reaction control by ^1H NMR spectroscopy revealed a ratio of 1.0 to 0.30 between the two species **138** and **139** respectively. Unlike the similar species **128** which was purified and isolated by vacuum sublimation, species **138** was isolated as small crystals from a hexane solution at -80 °C (65%). As both boron-bridged [1]FCPs **128** and **138** are C_2-symmetric and have a similar substitution pattern, the signal pattern for the Cp protons of species **138** is almost identical to that the of species **128**, with a large splitting between α and β protons [**128**: δ = 3.50 (2H, CH-α of Cp), 4.30 (2H, CH-β of Cp), 4.53

ppm (2H, CH-β of Cp); **138**: δ = 3.54 (2H, CH-α of Cp), 4.26 (2H, CH-β of Cp), 4.55 ppm (2H, CH-β of Cp)].

Scheme 79. Synthesis of Boron-bridged [1]FCP **138** and Bis(boryl)ferrocene **139**.

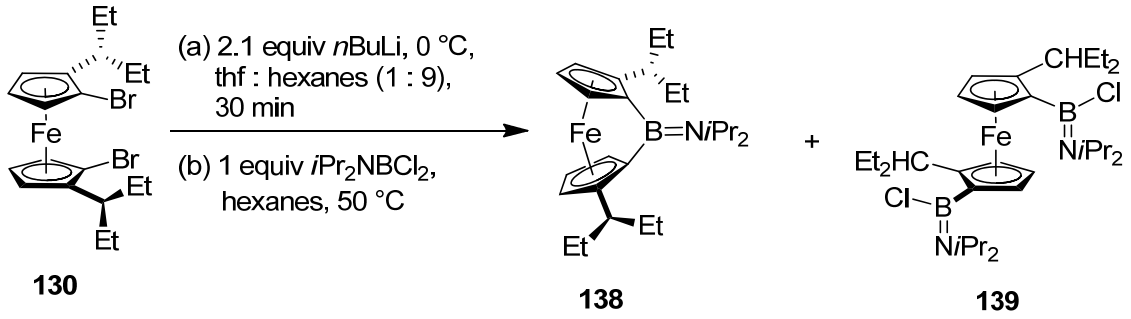

130 **138** **139**

Expectedly, the resonance of the boron-bound carbon atom in **138** at δ = 40.6 ppm is similar as that of the species **128** (δ = 39.9 ppm). The ^{11}B NMR spectroscopy of bora[1]ferrocenophane **138** revealed the resonance of the boron atom in the bridge at δ = 41.2 ppm which is slightly higher than that of the species **128** (δ = 39.5 ppm). Species **138** was also characterized by mass spectrometry and elemental analysis. In the mass spectrum, the highest detected mass matches the expected mass for M^+ of the boron-bridged [1]FCP **138**. Figure 17 displays the molecular structure of **138** derived from the X-ray diffraction data of a single crystal (see also Tables 6 and 7). The BN bond length of 1.397(11) Å for species **138** is very similar to that of **128**, confirming the presence of a BN double bond. The boron-bridged [1]FCP **138** exhibits α angles of 31.2(1)° which within three decimal standard deviations is also identical to that of species **128** [α = 31.9(2)°].

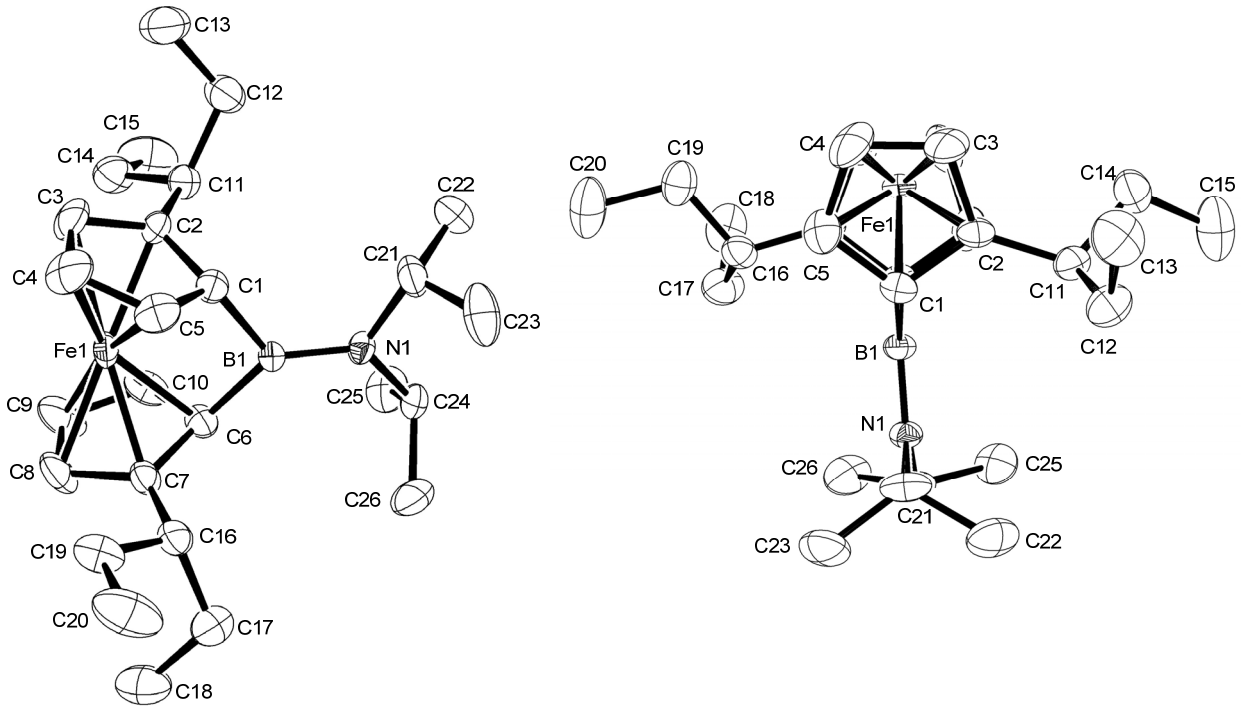

Figure 17. Molecular structure of **138** with thermal ellipsoids at the 50% probability level. Hydrogen atoms are omitted for clarity. Selected atom-atom distances [Å] and bond angles [°] for **128**: B1-C1 = 1.606(3), B1-C6 = 1.603(3), B1-N1 = 1.397(11), C1-B1-C6 = 103.20(17), C1-B1-N1 = 134.7(3), C6-B1-N1 = 122.0(3).

In summary, six chiral boron-bridged [1]FCPs were synthesized and characterized. All the six bora[1]ferrocenophanes are highly soluble in common organic solvents. The three [1]FCPs equipped with 3-pentyl groups on Cp units were isolated as solid powders or as crystalline products from hexanes solutions at -80 °C. The three bora[1]ferrocenophanes equipped with *i*Pr groups on Cp are volatile under vacuum and were further purified by sublimation (**128**) or by flask-to-flask condensation (**132** and **134**). The low tendency of boron-bridged [1]FCPs **132** and **134** to crystallize prevented further purification of these species. The two Et_2NB-bridged [1]FCPs **132** and **133** formed with high selectivity and the small peaks of the byproducts in the respective ^1H NMR spectra could not be attributed reliably to the expected bis(boryl)ferrocenes. On the other hand, applying bulkier aminoboranes iPr_2NBCl_2 and tBu(Me_3Si)$NBCl_2$ for the preparation of the respective boron-bridged [1]FCPs resulted in the formation of

bis(boryl)ferrocenes as the main byproduct. The four bis(boryl)ferrocenes **129**, **135**, **137** and **139** were identified by the ^{1}H NMR spectroscopy of the reaction mixture.

In order to fully characterize some of these bis(boryl)ferrocenes, species **129** and **135** were synthesized selectively by using a reverse order of addition; which means that, a solution of the dilithio species **121** was added to a solution of 3 equivalents of *i*Pr_2NBCl_2 and *t*$Bu(Me_3Si)NBCl_2$, respectively, at 0 °C. Nearly pure products were obtained after filtration of the reaction mixture which was followed by removal of the solvents. Species **129** and **135** were further purified and obtained in 55% and 53% yields, respectively, through crystallization from hexanes solution at -80 °C. The obtained low yields for the species **129** and **135** are due to the high solubility of these species in organic solvents, making the crystallization inefficient. Species **129** and **135** are volatile under vacuum at high temperatures and can be sublimed, however, they need higher temperatures (120 °C heating bath temperature) than their [1]FCP cousins **129** and **135**. Deduced from the signal pattern of their ^{1}H NMR and ^{13}C NMR spectra, both species **129** and **135** are C_2-symmetric in solution. The ^{11}B NMR spectra of species **129** and **135** display signals at δ = 38.0 (**129**) and 45.3 (**135**) ppm. The bis(boryl)ferrocene species **135**, having *t*$Bu(Me_3Si)N$ group, could potentially have *cis* and *trans* isomers which is caused by the BN double bonds. However, ^{1}H and ^{13}C NMR spectroscopy showed only one signal pattern for species **135** which either means that a fast *cis*-*trans* isomerization happens in solution or that only one isomer is present in the solution. However, occurrence of such a fast conversion is not feasible for species **135**. For instance, fast rotations around BN bonds were not observed for the [1]FCPs bridged by *t*Bu(MeSi)NB group (**134** and **136**) even though, due to the substitution pattern, the B atoms of these [1]FCPs are anticipated to be less Lewis acidic compared to that of the bis(boryl)ferrocene **135**.

The vacuum sublimation of species **135** resulted in suitable crystals for single-crystal X-ray analysis and the crystal structure of **135** was determined (Figure 18; Tables 8).

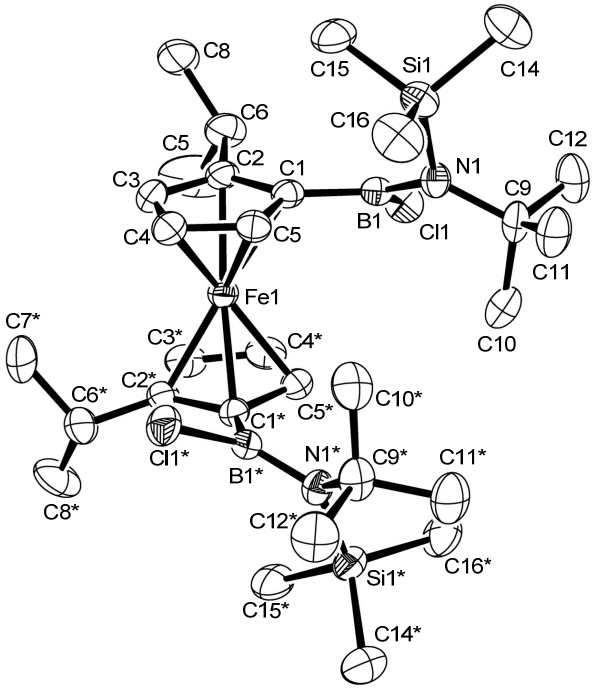

Figure 18. Molecular structure of **135** with thermal ellipsoids at the 50% probability level. Hydrogen atoms are omitted for clarity. Selected bond lengths [Å] and bond angles [º] for **135**: B1-C1 = 1.817(4); B1-Cl1 = 1.817(4); B1-N1 = 1.420(5); C1-B1-Cl1 = 116.6(3); Cl1-B1-N1 = 120.7(3); N1-B1-C1 = 122.7(3); B1-N1-Si1 = 116.9(2); Si1-N1-C9 = 120.4(2); C9-N1-B1 = 121.9(3).

Table 8. Crystal and Structural Refinement Data for Compound **135**.

	135
empirical formula	$C_{30}H_{56}B_2Cl_2FeN_2Si_2$
fw	649.29
cryst. size / mm^3	0.15 × 0.10 × 0.05
cryst. system,	orthorhombic,
space group	$C222_1$
Z	4
a / Å	8.3750(3)
b / Å	20.9020(6)
c / Å	20.3840(9)
α / °	90
β / °	90
γ / °	90

volume / $Å^3$	3568.3(2)
ρ_{calc} / mg m^{-3}	1.209
temperature / K	173(2)
$\mu_{calc.}$/ mm^{-1}	0.661
θ range / °	3.30 to 27.48
collected reflections	3881
independent reflections	4011
absorption correction	multiscan
data / restraints / params	4011 / 0 / 187
goodness-of-fit	1.061
R_1 [I > 2 σ(I)][a]	0.0393
wR_2 (all data)[a]	0.0941
largest diff. peak and hole, $\Delta\sigma_{elect}$ / e $Å^{-3}$	0.241 and -0.346
Absolute structure parameter (*Flack*)	-0.00(3)

[a] $R_1 = [\Sigma||F_o|-|F_c||]/[\Sigma|F_o|]$ for $[F_o^2 > 2\sigma(F_o^2)]$, $wR_2 = \{[\Sigma w(F_o^2-F_c^2)^2]/[\Sigma w(F_o^2)^2]\}^{1/2}$ [all data].

Chiral species **135** crystalizes in the orthorhombic space group $C222_1$ showing C_2-symmetrical molecules. The B1-N1 bond distance of 1.420(5) Å shows a slightly longer distance than a typical BN double bond of 1.41 Å.[175] An elongation is anticipated because the coordination around boron is significantly twisted to that around nitrogen [Cl1-B1-N1-Si1 = 133.3(2)°]. This can be clearly attributed to the steric congestion: twisting of the amino group to optimize the BN π-bonding is impossible due to the steric interference between the Me_3Si and the Cp ring.

2.6.3. Mechanistic Insights

As it was mentioned, we initially synthesized boron-bridged [1]FCP **128** and isolated it in a low yield of 20% through vacuum sublimation of the crude reaction mixture. The low yield of this

species was in agreement with the ^{1}H NMR spectrum of the reaction mixture, showing the 1,1′-bis(boryl)ferrocene **129** as the major product of the salt-metathesis reaction. In our first attempts to prepare new boron-bridged [1]FCPs **134**, **136** and **138** we applied similar reaction conditions as those used for the preparation of species **128**. That means, dibromoferrocene **120** and **130**, respectively, were first lithiated using a mixture of hexanes and thf (9 : 1) at 0 °C and then the ice bath was removed and a solution of aminoborane was added dropwise during 10 min through a cannula tubing from a second Schlenk flask. Table 9 lists approximate ratios between targeted [1]FCPs and the unwanted bis(boryl) species, obtained from ^{1}H NMR spectroscopy of reaction mixtures. However, during the course of these syntheses we realized that the reaction conditions could not be controlled very well. First, there is no control over the temperature during the salt-metathesis reaction in the time frame between removal of the cold bath from the solution of the dilithio species and addition of the dichlorides. Secondly, the speed of the addition of dichlorides could not be controlled perfectly by using the cannula transfer technique and, therefore, varied from experiment to experiment. In addition, we noticed that the characteristic deep red colour of strained bora[1]ferrocenophanes did not appear instantaneously with the addition of amino(dichloro)boranes and developed only at higher temperatures. Therefore, we optimized the reaction conditions in order to have a better control over addition of the reagent and the reaction temperature. This resulted in an optimized procedure where the solution of the dilithio species was immersed in a heated to 50 °C oil bath. After this warm-up period of 10 min, the solution of a respective amino(dichloro)borane was added dropwise during 10 min using a syringe pump. By applying these new conditions, we were able to have a control over the different parameters and obtained reliable ratios between targeted boron-bridged [1]FCPs and unwanted

bis(boryl)ferrocenes. Moreover, using these new conditions led to a significant change in the product ratios in favor of the targeted bora[1]ferrocenophanes.

Table 9. Measured Product Ratios Between [1]FCPs and Bis(boryl)ferrocenes.[a]

Starting Materials	Products	Reaction temperature[b]	
		0 °C to r.t.	50 °C
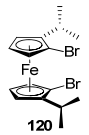 120 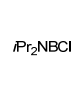 iPr$_2$NBCl$_2$,	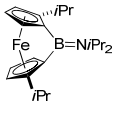 128 : 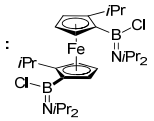 129	1.0 : 2.4[c]	1.0 : 0.59
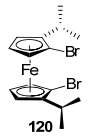 120 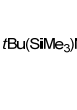 tBu(SiMe$_3$)NBCl$_2$,	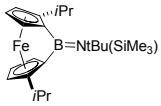 134 : 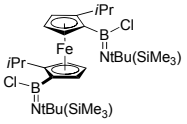 135	1.0 : 1.4	1.0 : 0.47
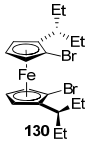 130 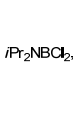 iPr$_2$NBCl$_2$,	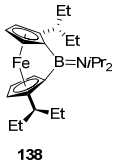 138 : 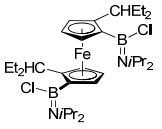 139	1.0 : 0.78	1.0 : 0.30
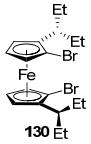 130 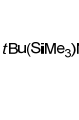 tBu(SiMe$_3$)NBCl$_2$,	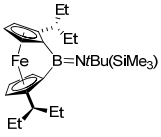 136 : 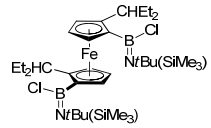 137	1.0 : 0.52	1.0 : 0.12

[a] approximate ratios determined by ^{1}H NMR spectroscopy (samples were taken from aliquots of the reaction mixture, 20 min after the addition of amino(dichloro)boranes). [b] see text for discussion. [c] A ratio of 1.0 : 3.5 was found before for allegedly the same reaction conditions used for the ratios shown here for the 0 °C → r.t conditions, which indicates that such reaction conditions cannot be reproduced well (see text for discussion).

The reaction conditions were optimized stepwise. In the first step, the speed of addition of amino(dichloro)boranes was controlled by using a syringe pump while the reaction temperature was kept in the range of 0 °C to room temperature. However, the product ratio was not affected significantly by changing the speed of the addition. In the second step, the reaction temperature was first increased to room temperature by exchanging the cold bath with a water bath and a significant change was observed in favor of the formation of boron-bridged [1]FCPs; a further increase of the bath temperature to 50 °C resulted in even higher ratios of boron-bridged [1]FCPs.

Based on these observations it can be deduced that the reaction path toward the formation of [1]FCPs has a higher activation energy than that resulting in bis(boryl)ferrocenes. It is obvious that the formation of lithium chloride in salt-metathesis reaction is an irreversible process, therefore, the formation of products must be controlled by kinetics. A feasible reaction mechanism is depicted in Scheme 80 and will be used in the following to discuss the effect of reaction conditions on the ratios of products.

The monoborylated species **A** which is the obvious intermediate in salt-metathesis reactions can either react intermolecularly with a second equivalent of amino(dichloro)borane to result in a bis(boryl)ferrocene (**C**) or intramolecularly to form a strained [1]FCP (**B**). While the reaction path of the intramolecular ring-closure to [1]FCP (**B**) is independent from the concentration of $R^1R^2NBCl_2$, the rate of formation of bis(boryl)ferrocenes (**C**) will be increased by higher concentrations of $R^1R^2NBCl_2$. Therefore, lower concentrations of $R^1R^2NBCl_2$ in reaction mixture will favor the formation of [1]FCP (**B**) which means that the solution of $R^1R^2NBCl_2$ should be added slowly to the solution of dilithioferrocene.

Scheme 80. Reaction Mechanism for the Synthesis of Boron-bridged [1]FCPs.

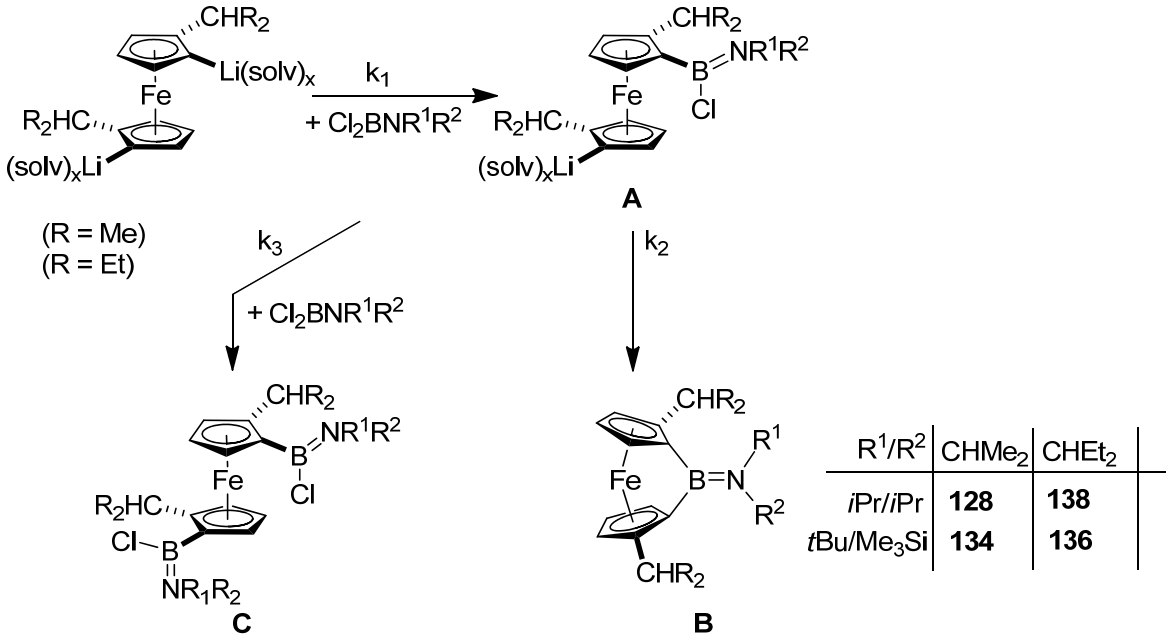

On the other hand, the rate of the intramolecular ring-closure reaction has the highest activation energy for the two following reasons. First, a significant amount of strain is introduced in this step and it can be assumed that some amount of this strain is already established in the transition state. Secondly, there should be a correlation between the electrophilicity of the borane species and the rate of the salt-metathesis reaction. Since the electrophilicity of the boryl group of the intermediate **A** which has only one chloride substituent is lower than that of the borane reagent $R^1R^2NBCl_2$, a higher activation energy is anticipated for the intramolecular ring-closure path and formation of strained [1]FCPs. However, one has to be careful as this conclusion holds true only if both intra- and intermolecular paths have the same steric influences. Applying low temperatures (e.g. 0 °C) for salt-metathesis reaction will result in a low rate of ring-closure reaction toward [1]FCPs **B** so that considerable amounts of the intermediate **A** will remain

unreacted in the reaction mixture and can compete with dilithioferrocene for reacting with $R^1R^2NBCl_2$. Due to the higher expected activation energy for intramolecular ring-closure, the rate of this path is increased stronger by increasing the reaction temperature to 50 °C, and consequently, results in a reduced concentration of intermediate **A** which, additionally, decreases the rate of the formation of bis(boryl)ferrocenes **C**. As shown in Table 9, the ratios between boron-bridged [1]FCPs and bis(boryl)ferrocenes changed significantly by increasing the reaction temperature to 50 °C. For example, bis(boryl)ferrocenes were obtained as the major products at lower temperatures for the cases with *i*Pr groups on the ferrocene moiety, while applying a higher temperature (50 °C) resulted in formation of [1]FCPs as the major products. The temperature effect is also reflected in the isolated yields. For instance, bora[1]ferrocenophane **128** was initially synthesized by applying the "low temperature" (0 °C to r.t.) procedure in a low yield of 20%. Applying the improved procedure for the same salt-metathesis reaction resulted in an isolation yield of 53% for the bora[1]ferrocenophane **128**.

Alkyl groups on the ferrocene also have a significant effect on the product ratios. This influence can be seen by comparing the respective product ratios obtained from dibromoferrocene **121** with those from dibromoferrocene **131** (Table 9). Applying 3-pentyl substituted ferrocene units resulted in higher conversions of starting materials to the targeted [1]FCPs. For instance, in the case of $i\text{Pr}_2\text{N}$-substituted species, the product ratios between [1]FCPs and bis(boryl)ferrocenes were 1.0 : 0.59 (**128** : **129**) and 1.0 : 0.30 (**138** : **139**). An analysis of the conformation of the alkyl groups on the ferrocene units can explain this ratio of the products. In the most stable conformation of the alkyl groups CHR_2 (Scheme 80, R = Me, Et) on the ferrocene units one the R groups is perpendicular to a Cp moiety and oriented away from iron atom, while the other R group is approximately in the same plane as a Cp ring. Such an orientation of alkyl groups can be

found in the all known molecular structures of [1]FCPs equipped with the fc$^{i\text{Pr2}}$ moiety,[164] and the structures of the dibromides **120** (Figure 11) and **130**. The thermodynamically preference of this conformation is probably due to the minimized interactions of the alkyl groups (R = Me or Et) with iron by orienting the small H atoms toward iron center. As a first approximation, for a particular amino(dichloro)borane the rate constant k_2 for the intramolecular ring-closure (Scheme 80) is not dependent on the type of substitution pattern on the ferrocene unit: for the both *i*Pr as well as 3-pentyl, the R groups (R = Me or Et) point to the outer part of sandwich where the ring-closure does not happen. However, the type of the R groups will affect the rate constants k_1 and k_3 for the following reasons. It can be assumed that a lithiated Cp ring will be approached by the borane $R^1R^2NBCl_2$ from the least crowded side, which is the opposite side to Fe atom. Therefore, the incoming $R^1R^2NBCl_2$ will be directed toward one R group of CHR_2 and due to the steric reasons, R = Et should result in lower rate constants than R = Me. To sum up, the rate of formation of bis(boryl)ferrocene derivatives (k_3; Scheme 80) is suppressed more effectively by using 3-pentyl groups rather than *i*Pr groups. The rate for the formation of the intermediate **A** (k_1) should also be influenced by the similar effect. However, the rate constant k_2 which leads to the formation of [1]FCPs is not dependent on the type of alkyl group.

2.6.4. Improved Synthesis of the Known Bora[1]ferrocenophane *i*Pr$_2$NBfc

Being equipped with these new insights about the mechanistic aspect of boron-bridged [1]FCPs we started to reinvestigated the synthesis of the known bora[1]ferrocenophane *i*Pr$_2$NBfc. The synthesis of *i*Pr$_2$NBfc was described in 2000 and authors did not mention anything about the formation of byproducts.[5] This reinvestigation intended to find out if the respective bis(boryl)ferrocene form as the major byproduct of this salt-metathesis reaction and if the isolation yield of *i*Pr$_2$NBfc can be improved by using higher temperatures. Compound *i*Pr$_2$NBfc

had been synthesized by dropwise addition of a hexanes solution of iPr$_2$NBCl$_2$ to a slurry of dilithioferrocene·tmeda in hexanes at room temperature, followed by filtration of LiCl and crystallization at low temperature (isolation yield of 38%).[5] First we attempted to reproduce the old results for the synthesis of iPr$_2$NBfc by following the publish reaction procedure. Expectedly, monitoring the reaction mixture by ^{1}H NMR spectroscopy revealed the formation of the bis(boryl)ferrocene species 1,1′-[Cl(iPr$_2$N)B]$_2$fc as the major product with a ratio of 2.4 : 1.0 with respect to the targeted iPr$_2$NBfc. In the next step, we tried to utilize the optimized procedure (syringe pump / 50 °C) to see if it has any positive influence on the selectivity of the salt-metathesis reaction. The ^{1}H NMR spectroscopy on a sample of the reaction mixture showed the formation of the targeted [1]FCP as the major product, with very small amount of bis(boryl)ferrocene species 1,1′-[Cl(iPr$_2$N)B]$_2$fc. The bora[1]ferrocenophane iPr$_2$NBfc was isolated in 74% yield by crystallization at low temperature, which is significantly more than the reported yield (38%). It is worth to mention that the bora[1]ferrocenophane iPr$_2$NBfc is volatile under vacuum at high temperatures (70 °C) and, similar to the boron-bridged [1]FCP **128**, can be purified by sublimation.

2.6.5. Thermal Properties of Boron-bridged [1]FCPs

A Differential Scanning Calorimetry study was performed in order to discover the thermal polymerization behavior of bora[1]ferrocenophane **128**, **133**, **136** and **138**. However, we could not measure the enthalpy of ring-opening polymerization (ΔH^{ROP}) of **128**. All attempts for measuring the DSC thermogram of **128** showed a broad jagged endothermic peak around the compound's melting point (m.p. = 68-70 °C) (Figure 19). The broad endothermic peak can be correlated to the evaporation of the sample from the aluminum crucibles. This was evidenced by observation of some leaked out materials on the edges of aluminum crucibles at the end of each

DSC run. Unfortunately, despite multiple attempts, we could not seal the aluminum crucibles properly and measure a useful DSC thermogram for the boron-bridged [1]FCP **128**.

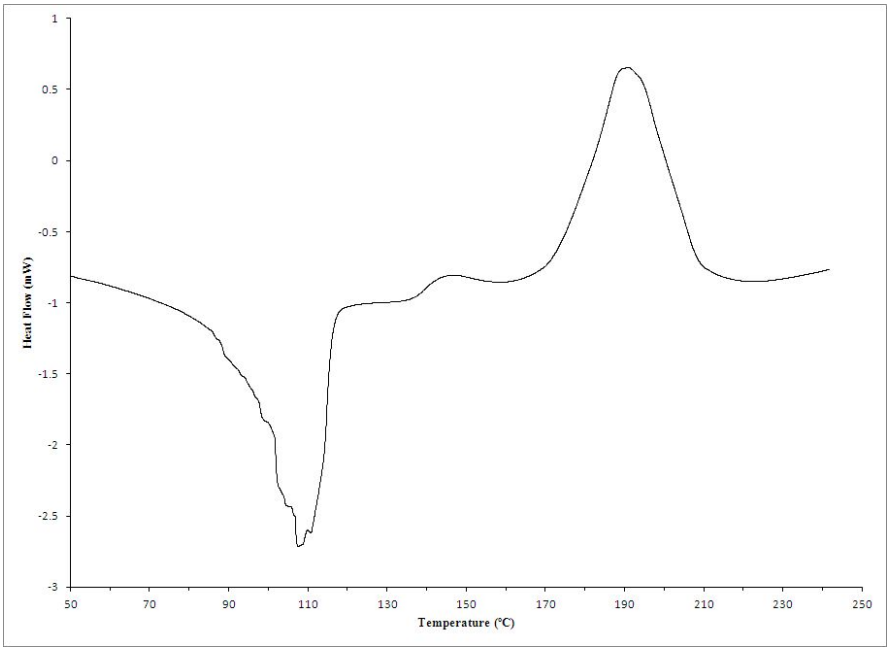

Figure 19. DSC thermogram of **128** (heating rate of 10 °Cmin^{-1}). Reprinted with permission from Sadeh, S.; Bhattacharjee, H.; Khozeimeh Sarbisheh, E.; Quail, J. W.; Müller, J. *Chem.–Eur. J.* **2014** DOI: 10.1002/chem.201404222. Copyright 2014 Wiley VCH.

In contrast to the case **128**, no leakage of the species was observed for the DSC measurement of 3-pentyl substituted boron-bridged [1]FCPs **133**, **136** and **138**. The DSC measurement of **133** shows a melt endotherm at approximately 100 °C (onset) followed by a ROP exotherm at about 205 °C (onset) (Figure 20). The enthalpy for the ROP of **133** was determined to be -75 ± 5 kJ mol^{-1}.

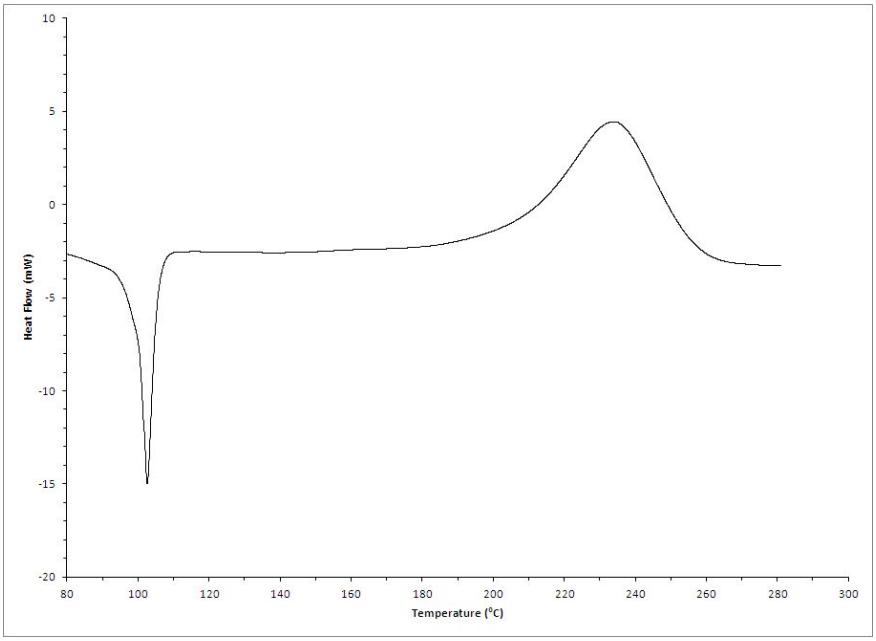

Figure 20. DSC thermogram of **133** (heating rate of 10 °Cmin^{-1}). Reprinted with permission from Sadeh, S.; Bhattacharjee, H.; Khozeimeh Sarbisheh, E.; Quail, J. W.; Müller, J. *Chem.–Eur. J.* **2014** DOI: 10.1002/chem.201404222. Copyright 2014 Wiley VCH.

A similar DSC thermogram was found for compound **138**, which shows a melt endotherm at ca. 140 °C (onset) and a ROP exotherm at about 222 °C (onset) (Figure 21). Integration over the exothermic peak area revealed a ΔH^{ROP} of -63 ± 5 kJ mol^{-1} for the bora[1]ferrocenophane **138**.

In contrast to the DSC thermograms of species **133** and **138** which show defined exothermic peaks, the DSC measurement of boron-bridged [1]FCP **136**, equipped with bulky bridging group *t*Bu(Me$_3$Si)NB-, exhibits a number of broad exothermic peaks (Figure 22).

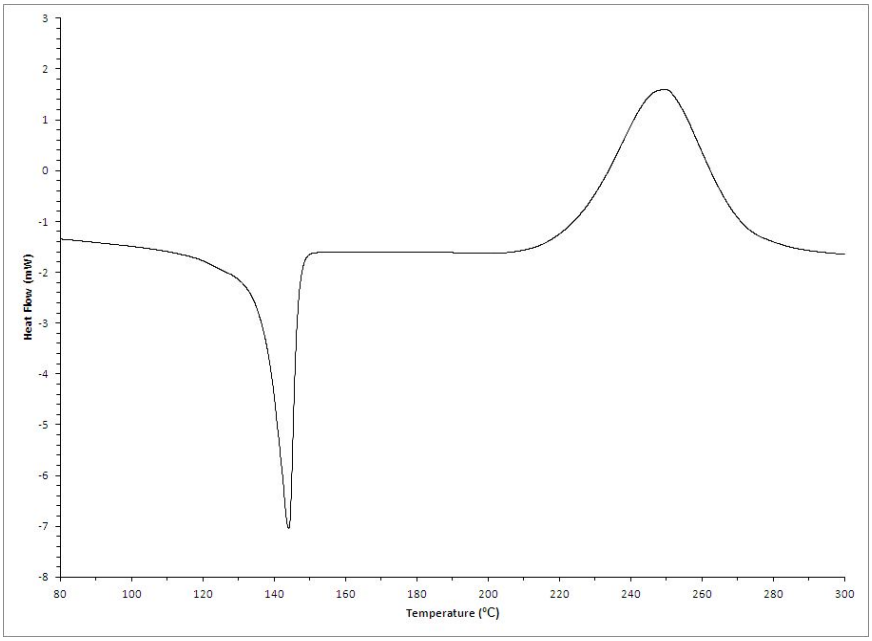

Figure 21. DSC thermogram of **138** (heating rate of 10 °Cmin^{-1}). Reprinted with permission from Sadeh, S.; Bhattacharjee, H.; Khozeimeh Sarbisheh, E.; Quail, J. W.; Müller, J. *Chem.–Eur. J.* **2014** DOI: 10.1002/chem.201404222. Copyright 2014 Wiley VCH.

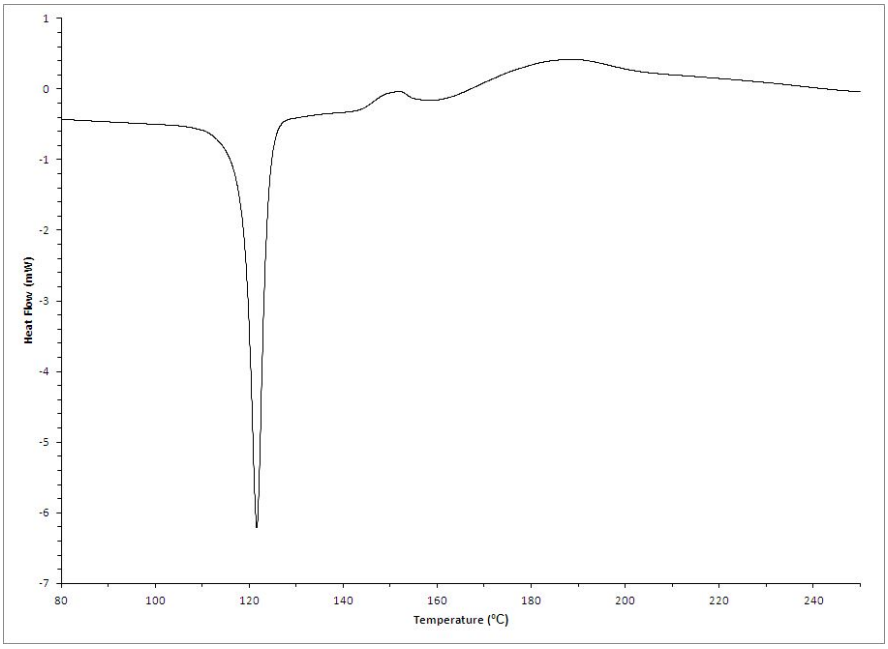

Figure 22. DSC thermogram of **136** (heating rate of 10 °Cmin^{-1}). Reprinted with permission from Sadeh, S.; Bhattacharjee, H.; Khozeimeh Sarbisheh, E.; Quail, J. W.; Müller, J. *Chem.–Eur. J.* **2014** DOI: 10.1002/chem.201404222. Copyright 2014 Wiley VCH.

The measured enthalpies for the boron-bridged [1]FCPs **133** and **138** (ΔH^{ROP} = -75 ± 5 and -63 ± 5 kJ mol^{-1}) are considerably lower than the expected values. Comparisons can be made with similarly tilted [1]FCPs for example, sulfur-bridged [1]FCP[11] with an α angle of 31.05(5)° showed ΔH^{ROP} -130(±20) kJ mol^{-1} and dimethylsila[1]ferrocenophane with an α angle of 20.85(5)° showed ΔH^{ROP} of -80 kJ mol^{-1}.[18] Boron-bridged [1]FCPs with tilt angle α of around 30° are similarly tilted as sulfur-bridged [1]FCP and, therefore, a similar ΔH^{ROP} of is expected for these species. Among the three known bora[1]ferrocenophanes, ΔH^{ROP} was only determined for one of the species [$(Me_3Si)_2$NBfc, ΔH^{ROP} = -95 kJ mol^{-1}] and it was significantly lower than expected.[5] The low value of the ROP exotherm was rationalized by the existence of "side group interactions" between the bulky amino groups, which probably caused substantial destabilization of the polymer relative to the monomer.

We analyzed the remaining materials of the DSC run of species **138** as following: The aluminum crucible was opened after the DSC run and the contents were extracted in C_6D_6 to result in a yellow solution with black floating particles. Interestingly, the floating particles were attracted toward a magnet and it can be assumed that those are made of iron. This result is in agreement with what we observed for the thermal ROP of species **133** and **138**, where magnetic particles were detected after the polymerization reaction (see chapter 2.6.6). The thermal extrusion of iron is probably either a slightly exothermic or even an endothermic process, which proceeds through a radical mechanism. Therefore, the measured values for the ROP exothermy in DSC thermograms are not the representative of the existing amount of strain in boron-bridged [1]FCPs, as a clean ROP process is not happening for these species. The three known boron-bridged [1]FCPs[5] and also the new four boron-bridged [1]FCPs **128**, **133**, **136** and **138** all show exothermic peaks in DSC thermograms. As the onset temperatures for all of the exothermic

peaks are very close to each other (around 200 °C), it can be speculated that iron extrusion also occurs for the known boron-bridged [1]FCPs. This speculation was confirmed when we measured a DSC thermogram of *i*Pr$_2$NBfc (Figure 23). Similar to the reported data,[5] the DSC thermogram of *i*Pr$_2$NBfc illustrates a melt endotherm at ca. 150 °C (onset) overlapping with the ROP exotherm at slightly higher temperature. The overlapping between the endothermic and exothermic peaks does not allow a precise integration over the peak area. However, a ΔH^{ROP} of -73 kJ mol^{-1} was estimated for the boron-bridged [1]FCP *i*Pr$_2$NBfc. Expectedly, inspection of the products of the DSC run confirmed the presence of iron particles.

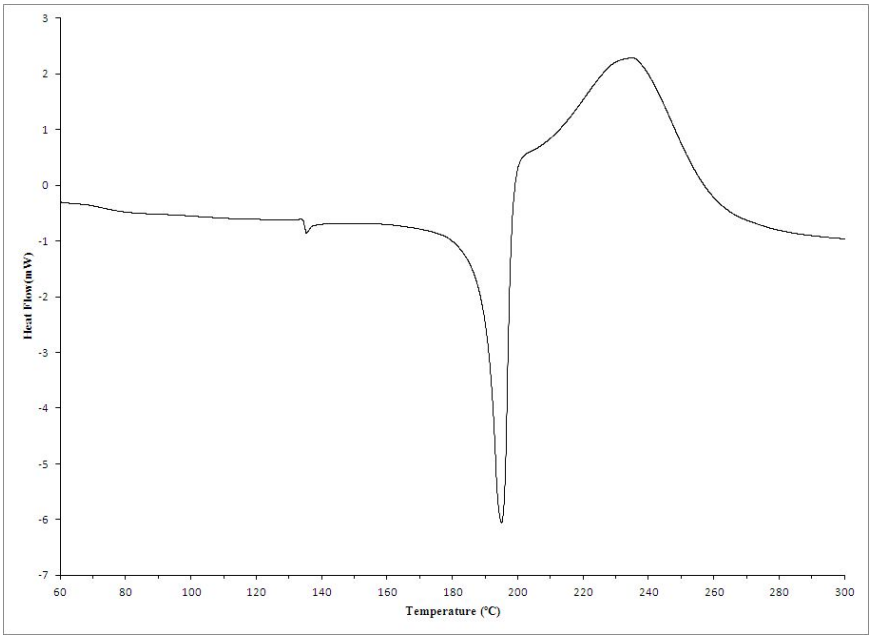

Figure 23. DSC thermogram of *i*Pr$_2$NBfc (heating rate of 10 °Cmin^{-1}). Reprinted with permission from Sadeh, S.; Bhattacharjee, H.; Khozeimeh Sarbisheh, E.; Quail, J. W.; Müller, J. *Chem.–Eur. J.* **2014** DOI: 10.1002/chem.201404222. Copyright 2014 Wiley VCH.

2.6.6. Thermal ROP of Boron-bridged [1]FCPs

On the basis of their promising results with DSC analysis, species **133** and **138** were selected for thermal ROP experiment. Heating the boron-bridged [1]FCPs **133** and **138** in flame-sealed NMR tubes for 1.5 h resulted in a color change of the monomers from red to orange (Scheme 81).

Scheme 81. Thermal ROP of Boron-bridged [1]FCPs **133** and **138**.

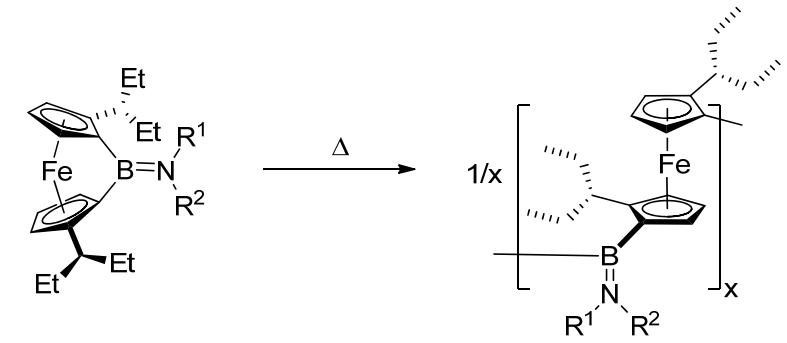

133: $R^1 = R^2 = Et$
138: $R^1 = R^2 = i$Pr

133$_x$: $R^1 = R^2 = Et$
138x: $R^1 = R^2 = i$Pr

The resulting viscous liquids obtained from thermal ROP were cooled down to room temperature and turned into orange glassy solids. These obtained materials were extracted with thf, leaving undissolved particles of iron behind. Expectedly, the ^{1}H NMR spectroscopy of the soluble products showed broad peaks in the expected areas for the different types of protons. The Gel Permission Chromatography (GPC) analysis of the products **133$_x$** and **138$_x$** showed one main fraction accompanying with other smaller fraction of lower molecular weights which interfered with system peaks of the GPC instrument. The main fractions of both species showed molecular weights (M_w) relative to polystyrene of ca. 10 kDa (Figures 24 and 25; Tables 10 and 11).

Both products **133$_x$** and **138$_x$** were characterized by elemental analysis and showed carbon values which were considerably lower than the expected values. According to these results, the boron-bridged [1]FCPs **133** and **138** were polymerized thermally; however, applying the required high temperatures for ROP resulted in unavoidable extrusion of iron. Moreover, extrusion of iron must be governed by a radical mechanism and, thus, it is feasible that the growing polymer chains were terminated by reacting with the radicals present in the reaction mixture which inhibited the formation of high-molecular-weight polymers.

Table 10. GPC Analysis of Polymer $\mathbf{133_x}$.

	$\mathbf{133_x}$
M_n (Daltons)	3578
M_w (Daltons)	9926
M_z (Daltons)	19961
M_p (Daltons)	7988
M_w / M_n	2.744

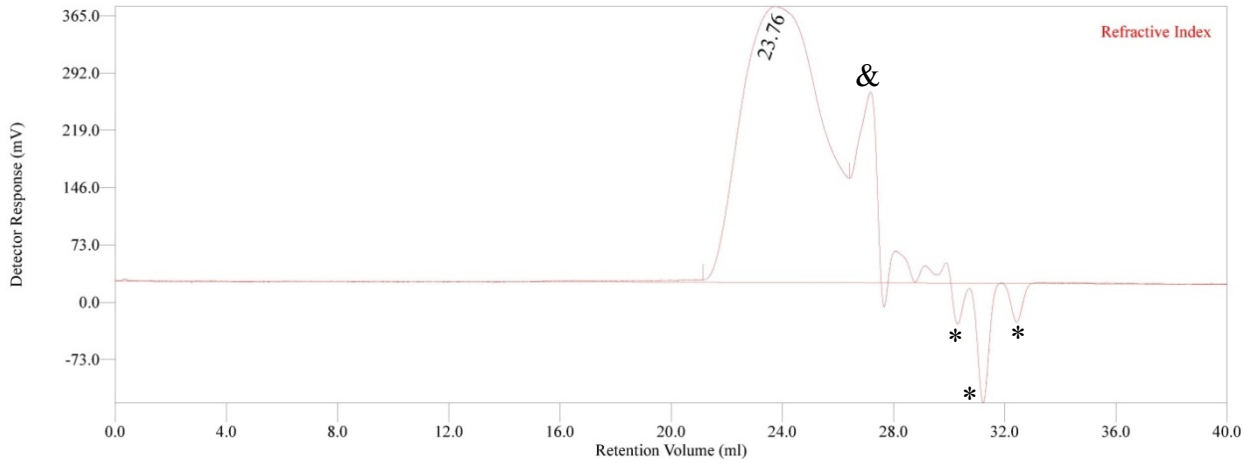

Figure 24. GPC trace of polymer $\mathbf{133_x}$ (obtained from thermal ROP) (c = 14.1 mg/ 6.0 mL thf). System peaks are indicated with *. The first system peak overlaps with the peak for oligomers indicated with &. Reprinted with permission from Sadeh, S.; Bhattacharjee, H.; Khozeimeh Sarbisheh, E.; Quail, J. W.; Müller, J. *Chem.–Eur. J.* **2014** DOI: 10.1002/chem.201404222. Copyright 2014 Wiley VCH.

Table 11. GPC Analysis of Polymer $\mathbf{138_x}$.

	$\mathbf{138_x}$
M_n (Daltons)	5506
M_w (Daltons)	9722
M_z (Daltons)	15687
M_p (Daltons)	8012
M_w/M_n	1.766

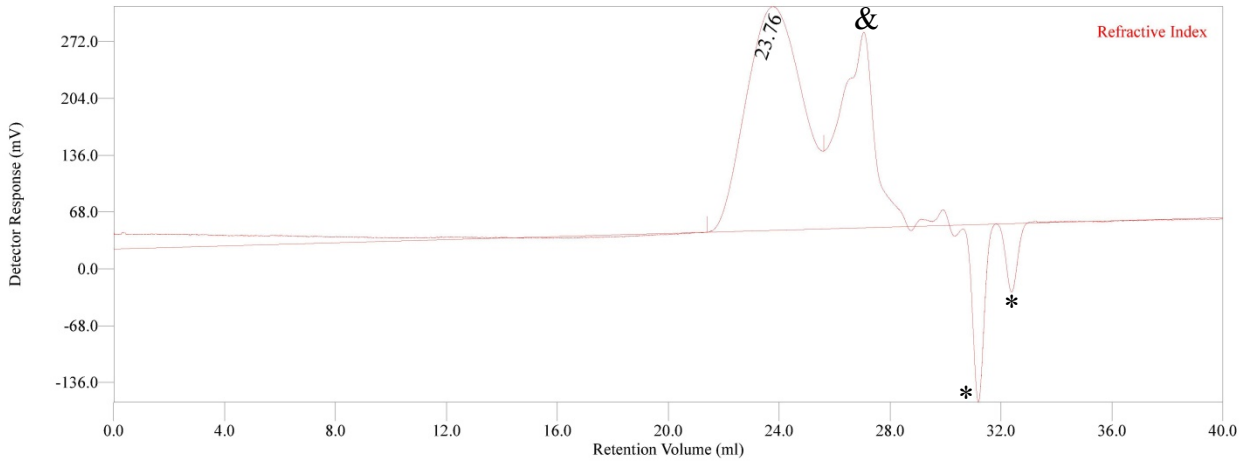

Figure 25. GPC trace of polymer $\mathbf{138_x}$ (obtained from thermal ROP) (c = 11.5 mg/ 6.0 mL thf). System peaks are indicated with *. The first system peak overlaps with the peak for oligomers indicated as &. Reprinted with permission from Sadeh, S.; Bhattacharjee, H.; Khozeimeh Sarbisheh, E.; Quail, J. W.; Müller, J. *Chem.–Eur. J.* **2014** DOI: 10.1002/chem.201404222. Copyright 2014 Wiley VCH.

2.7. Chiral Silicon- and Tin-bridged [1]Ferrocenophanes

As it was mentioned before, silicon-bridged [1]FCPs are the most developed group of strained sandwich compounds which can undergo living polymerization and consequently allow the preparation of block copolymers.[28] A vast number of silicon-bridged [1]FCPs were synthesized by different research groups (Scheme 8). Silicon-bridged [1]FCPs are generally prepared by the salt-metathesis reaction of dichlorodiorganosilanes with dilithioferrocene·tmeda. As it was mentioned in chapter 1.1.2, a number of silicon-bridged [1]FCPs with substituted Cp rings are reported in the literature (Figure 4).[49-52] These species are prepared by applying the two common synthetic strategies for the preparation of [1]FCPs (salt-metathesis and fly-trap approach; Scheme 1). Being equipped with the enantiomerically pure dibromoferrocene **120**, we attempted to prepare a Cp-substituted chiral silicon-bridged [1]FCP through salt-metathesis reaction.

2.7.1. Synthesis of Chiral Silicon-bridged [1]Ferrocenophanes

Treatment of the dilithio derivative of **120** with Me_2SiCl_2 (Scheme 82) resulted in quantitative formation of the target silicon-bridged [1]FCP in the reaction mixture, showing the indicative red color of strained [1]FCPs.

Scheme 82. Synthesis of the silicon-bridged [1]FCP **140**.

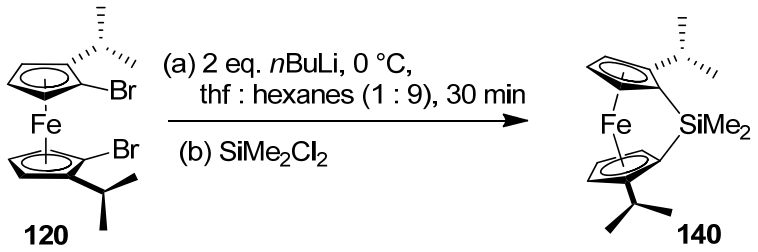

Monitoring the reaction mixture by measuring a ^{1}H NMR spectrum approximately 5 min after the addition of the dichloride confirmed the formation the silicon-bridged [1]FCP **140**. Similar to the parent dimethylsila[1]ferrocenophane, species **140** is volatile and was isolated in 80% yield by sublimation under vacuum at 55 °C. Expectedly, the ^{1}H NMR spectrum shows three Cp signals for the six protons of the C_2-symmetric for silicon-bridged [1]FCP **140**. Moreover, the *i*Pr groups on the Cp units give rise to two doublets and one multiplet, having the expected relative intensities with respect to the Cp protons. One singlet with the intensity of six with respect to the Cp protons is also observed for the methyl groups of the bridging silicon. A splitting of $\Delta\delta$ = 0.86 ppm (averaged value) is observed between the α and β Cp protons of the silicon-bridged [1]FCP **140** [δ = 3.53 (2H, CH-α of Cp), 4.31 (2H, CH-β of Cp) and 4.46 ppm (2H, CH-β of Cp)]. This splitting is significantly wider than that of the parent dimethylsila[1]ferrocenophane with $\Delta\delta$ = 0.47 ppm [δ = 3.94 (4H, CH-α of Cp) and 4.41 ppm (4H, CH-β of Cp)].[177] Comparison of the chemical shifts of α and β proton between the two species revealed that the α protons in **140** are highly shielded. It can be assumed that the observed extra shielding is due to

the close proximity of *i*Pr groups on the Cp moieties to the α-H protons. In the ^{13}C NMR spectrum, the resonance of the silicon-bounded carbon atom at δ = 31.77 ppm is similar as that of the parent dimethylsila[1]ferrocenophane at δ = 33.5 ppm.[177] Species **140** was also characterized by mass spectrometry and elemental analysis. The measured mass spectrum showed the highest detected mass for the molecular ion of [1]FCP **140**. The molecular structure of the silicon-bridged [1]FCP **140** was determined by single-crystal X-ray analysis (Figure 26; Tables 12 and 13).

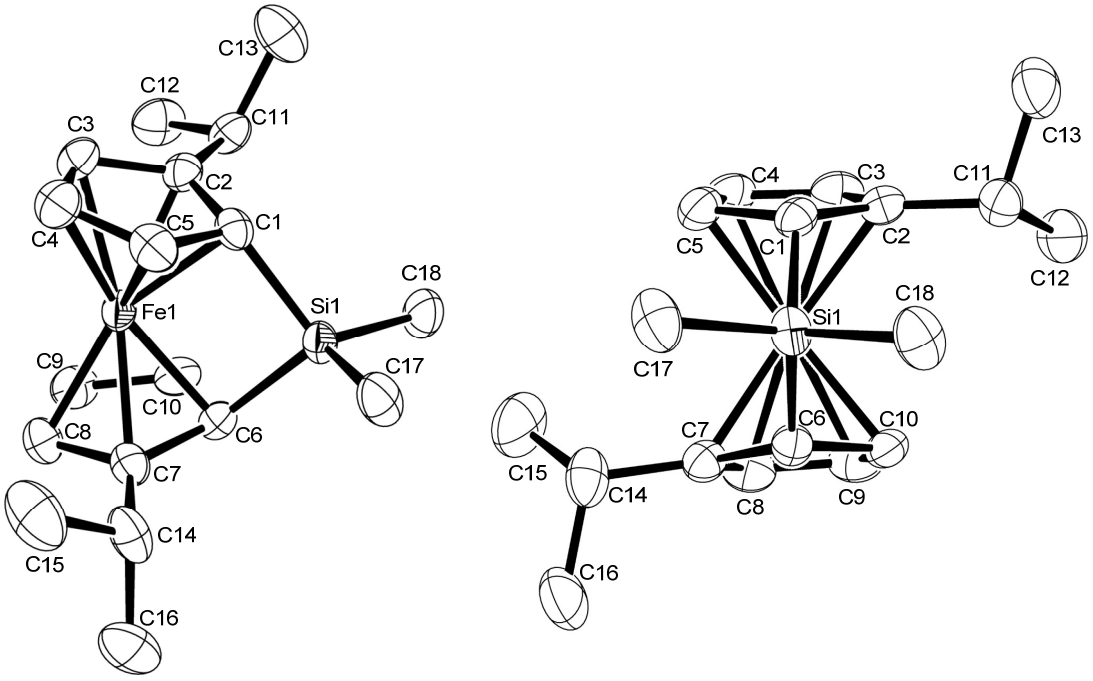

Figure 26. Molecular structure of **140** with thermal ellipsoids at the 50% probability level. Hydrogen atoms are omitted for clarity. Selected atom-atom distances [Å] and bond angles [°] for **140**: Si1-C1 = 1.892(2), Si1-C6 = 1.899(2), Si1-C17 = 1.862(2), Si1-C18 = 1.859(2), C1-Si1-C6 = 95.90(7), C1-Si1-C17 = 110.54(10), C1-Si1-C18 = 114.65(10), C6-Si1-C17 = 115.35(9), C6-Si1-C18 = 112.06(10), C17-Si1-C18 = 108.14(11). Reprinted with permission from Sadeh, S.; Schatte, G.; Müller, J. *Chem.–Eur. J.* **2013***, 40,* 13408-13417. Copyright 2013 Wiley VCH.

As it was mentioned before, a set of angles are commonly used to describe the distortion of strained [1]FCPs relative to unstained species (Figure 2). The tilt angle α, which is the dihedral angle between the two Cp rings, is generally used to express the amount of strain in FCPs. The

silicon-bridged [1]FCP **140** shows an α angle of 19.85(13)° which is similar as that for the known dimethylsila[1]ferrocenophane with α angle of 20.85(5)°.[177] Similarly, species **140** exhibits expected values the other distortion angles (β, θ and δ; Figure 26; Tables 13), based on the known data for the parent species dimethylsila[1]ferrocenophane.[177]

Table 12. Crystal and Structural Refinement Data for Compounds **140** and **141**.

	140	**141**
CCDC No.	940648	940649
empirical formula	$C_{18}H_{26}FeSi$	$C_{24}H_{38}FeSn$
fw	326.33	501.11
cryst. size / mm^3	0.20 × 0.18 × 0.08	0.23 × 0.18 × 0.08
cryst. system, space group	orthorhombic, $P2_12_12_1$	monoclinic, $P2_1$
Z	4	4
a / Å	10.2719(2)	9.77040(10)
b / Å	7.35830(10)	13.4722(2)
c / Å	22.5357(3)	18.0028(3)
α / °	90	90
β / °	90	96.1719(8)
γ / °	90	90
volume / $Å^3$	1703.33(5)	2355.95(6)
ρ_{calc} / mg m^{-3}	1.273	1.413
temperature / K	173(2)	173(2)
μ_{calc} / mm^{-1}	0.945	1.681
θ range / °	2.91 to 27.88	2.59 to 30.05
reflns collected / unique	6812 / 4062	36450 / 11843
absorption correction	multi-scan	multi-scan

data / restraints / params	4062 / 0 / 188	11843 / 1 / 489
goodness-of-fit	1.063	1.045
R_1 [I > 2 σ(I)][a]	0.0296	0.0331
wR_2 (all data)[a]	0.0688	0.0813
largest diff. peak and hole	0.245	1.329
$\Delta\rho_{elect}$ / e Å^{-3}	-0.302	-1.175

[a] $R_1 = [\Sigma||F_o|-|F_c||]/[\Sigma|F_o|]$ for $[F_o^2 > 2\sigma (F_o^2)]$, $wR_2 = \{[\Sigma w(F_o^2-F_c^2)^2]/[\Sigma w(F_o^2)^2]\}^{1/2}$ [all data].

Table 13. Measured Distortion Angles [°] (see Figures 26 and 27).

	140	**141**[a]
α	19.85(13)	13.46(11) {14.6(2)}
β/β′	37.94(13)/38.23(12)	37.3(4) {36.2(3)}/36.9(4){36.7(3)}
θ	95.90(7)	86.78(13) {86.43(12)}
δ	165.30(2)	168.97(4) {168.5(4)}

[a] values in braces refer to the second independent molecule in the asymmetric unit.

2.7.2. Synthesis of Chiral Tin-bridged [1]Ferrocenophanes

As mentioned before, there are only three tin-bridged [1]FCPs known in the literature (Scheme 15). All of the known species were prepared by the use of sterically demanding groups on the tin bridge.[13, 56, 57] On the other hand, attempts for the preparation of tin-bridged [1]FCPs equipped with smaller ligands (Me, Et, Ph, *n*Bu) in the bridging position resulted in formation of oligomeric materials and cyclic dimers.[58] The chemistry of tin-bridged [1]FCPs is reminiscent of heavier group-13-bridged [1]FCPs where bulky ligands where required to block the formation of dimers.[6, 31, 32] The salt metathesis of tBu$_2$SnCl$_2$ with dilithio derivative of **120** (Scheme 83) resulted in selective formation of the tin-bridged [1]FCP **141** which was evidenced by the ^{1}H NMR control of the reaction mixture.

Scheme 83. Synthesis of the Tin-bridged [1]FCP **141**.

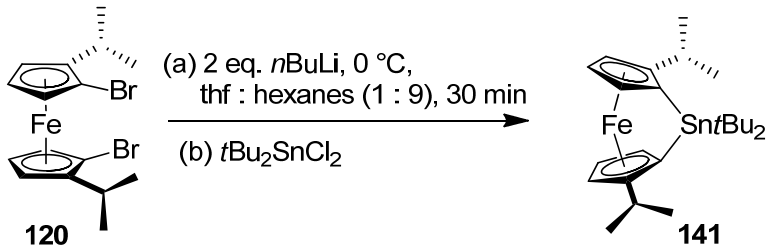

The tin-bridged [1]FCP **141** is volatile and was isolated in 88% yield by sublimation under vacuum at 55 °C. The ^{1}H NMR spectrum reveals the expected pattern for the C_2-symmetric tin-bridged [1]FCP **141**, exhibiting three signals for the six Cp protons [δ = 4.02 (2H, CH-α of Cp), 4.27 (2H, CH-β of Cp) and 4.45 ppm (4H, CH-β of Cp)]. The α and β protons show a splitting of 0.34 ppm (averaged value) which is significantly higher than that of the parent *t*Bu$_2$Snfc with Δδ = 0.22 ppm [δ = 4.22 (4H, CH-α of Cp) and 4.44 ppm (4H, CH-β of Cp)].[56] As it was explained for the silicon-bridged [1]FCP **140**, this effect is probably due to the shielding of the α-H atoms by *i*Pr groups on the Cp moieties. The measured ^{13}C NMR chemical shift of the *ipso* carbon atoms bound to tin at δ = 36.7 ppm is comparable to that found for the known tin-bridged [1]FCP equipped with the same bridging unit [*t*Bu$_2$Snfc: δ = 34.9 ppm].[56] The stanna[1]ferrocenophane **141** was also characterized by mass spectrometry and elemental analysis. In the mass spectrum, the highest detected mass matches the M^+ for the tin-bridged [1]FCP **141**.

Suitable crystals of **141** for single-crystal X-ray analysis were obtained by vacuum sublimation (Figure 27; Tables 12 and 13). The measured tilt angles α of 13.46(11) and 14.6(2)° for stanna[1]ferrocenophane **141** are comparable to that of the known *t*Bu$_2$Snfc [α = 14.1(2)°].[56] The other distortion angles of the tin-bridged [1]FCP **141** (β, θ and δ; Figure 27; Tables 13) are also similar as that of the species *t*Bu$_2$Snfc.[56]

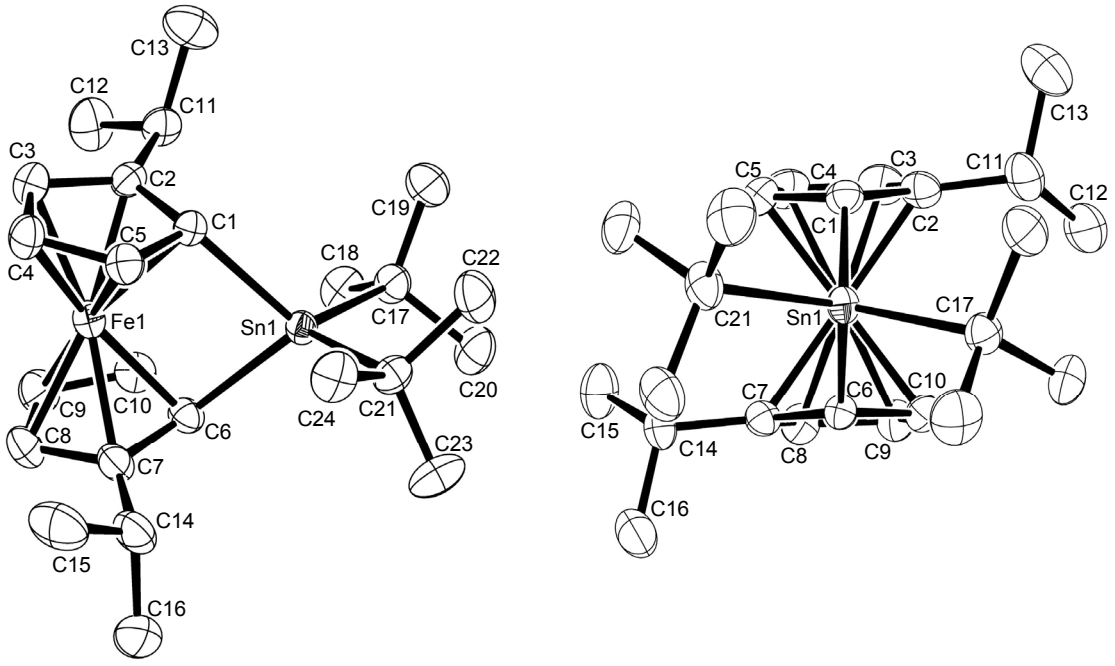

Figure 27. Molecular structure of **141** with thermal ellipsoids at the 50% probability level. Hydrogen atoms are omitted for clarity. One of two independent molecules is shown. Selected atom-atom distances [Å] and bond angles [°] for 1**41** (values in braces refer to the second independent molecule that is not shown): Sn1-C1 = 2.189(5) {2.182(4)}, Sn1-C6 = 2.195(5) {2.183(4)}, Sn1-C17 = 2.209(5) {2.209(4)}, Sn1-C21 = 2.208(4) {2.213(5)}, C1-Sn1-C6 = 86.78(18) {86.43(16)}, C1-Sn1-C17 = 119.24(18) {121.51(17)}, C1-Sn1-C21 = 107.80(17) {108.48(17)}, C6-Sn1-C17 = 110.9(2) {108.66(17)}, C6-Sn1-C21 = 121.05(19) {120.74(16)}, C17-Sn1-C21 = 109.9(2) {110.06(18)}. Reprinted with permission from Sadeh, S.; Schatte, G.; Müller, J. *Chem.–Eur. J.* **2013***, 40,* 13408-13417. Copyright 2013 Wiley VCH.

The only unusual structural feature of species **141** is a twisting of bridging unit tBu$_2$Sn with respect to the ferrocene moiety. This unexpected feature can be seen by looking along the Sn-Fe axis in the molecular structure of **141** (Figure 27). The angles 79.82(11) and 81.25(12)° between the two planes of C17-Sn-C21 and C1-Sn-C6 can reveal the degree of twisting in the stanna[1]ferrocenophane **141**. This twisting is clearly the result of steric repulsions between the *t*Bu groups bound to tin and the *i*Pr groups in α position of the Cp moieties. It is worth to mention that a similar but less pronounced repulsion of alkyl groups can be observed for the silicon-bridged [1]FCP **140** showing an angle of 87.10(9)° between the two planes of C17-Si-C18 and C1-Si-C6.

2.7.3. Thermal Properties of the Silicon- and Tin-bridged [1]Ferrocenophanes 140 and 141

Similar to the case of the boron-bridged [1]FCP **128**, we were not able to measure the ΔH^{ROP} of the species **140** by DSC. This was due to the leakage of samples from aluminum crucibles during DSC measurements. Despite multiple attempts, we were not able to seal aluminum crucibles well enough for **140**. However, the DSC measurements of the species **141** was not accompanied with any loss of samples and its DSC thermograms were measured reproducibly (Figure 28). The DSC thermogram of **141** exhibited a melt endotherm at 135 °C (onset), followed by a ROP exotherm at approximately 175 °C (onset). The onset temperature of polymerization for the known species *t*Bu_2Snfc was found at about 170 °C. The enthalpy for ROP **141** was determined to be -33 kJ mol^{-1} which is comparable to the value found for *t*Bu_2Snfc [-36(±9) kJ mol^{-1}].[13]

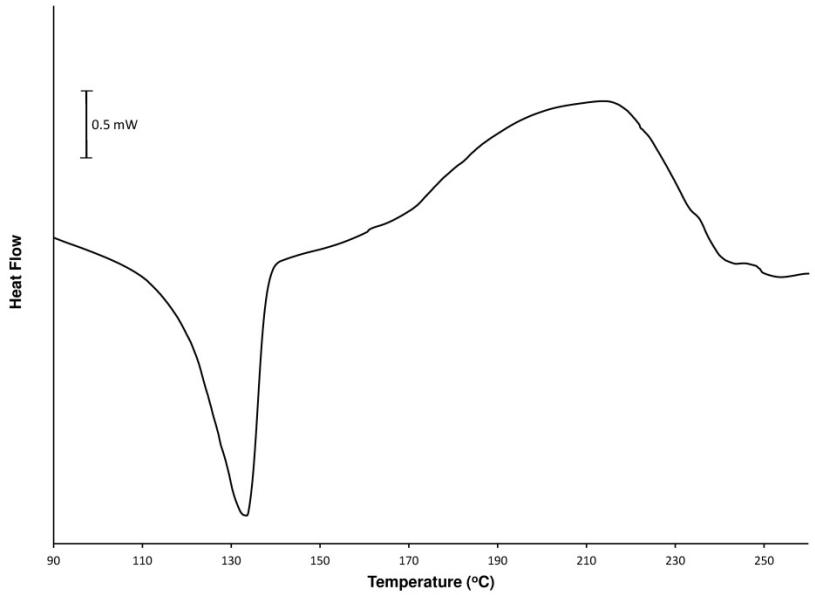

Figure 28. DSC thermogram of **141** (heating rate of 10 °Cmin^{-1}). Reprinted with permission from Sadeh, S.; Schatte, G.; Müller, J. *Chem.–Eur. J.* **2013***, 40,* 13408-13417. Copyright 2013 Wiley VCH.

2.8. Phosphorus-bridged [1]Ferrocenophanes

As it was described in chapter 1.1.3, phosphorus-bridged [1]FCPs are a well-developed group of strained sandwich compounds. However, compared to their silicon cousins, phosphorus-bridged [1]FCPs are much less studied. During the last two decades phosphorous-bridged [1]FCPs have been polymerized by using different ROP techniques such as thermal, anionic, transition-metal-catalyzed and photocontrolled.[63, 64, 111] As shown in Scheme 18, chiral phosphorous-bridged [1]FCPs **42** and **43** were prepared by applying enantiomerically resolved dichloroorganophosphines.[62] Chiral phosphorous-bridged [1]FCPs can be applied as monodentate chiral ligands in asymmetric catalysis. In this part of the my PhD work, I targeted a group of enantiomerically pure phosphorous-bridged [1]FCPs where the chirality comes from a planar-chiral ferrocene moiety.

2.8.1. Synthesis of Phosphorus-bridged [1]Ferrocenophanes

The dilithio derivative of **120** was reacted with $PhPCl_2$ (Scheme 84) and monitoring the reaction mixture with ^1H NMR spectroscopy showed the formation of the target phosphorous-bridged [1]FCP **142** as the major product. Moreover, that the conversion of the staring materials to the targeted phosphorus-bridged [1]FCP had occurred was confirmed by observing a distinctive color change of the reaction mixture, from orange to dark-red, after the addition of $PhPCl_2$. The phosphorous-bridged [1]FCP **142** was purified by flash chromatography to remove the hydrolysis byproduct $(i\text{PrH}_4\text{C}_5)_2\text{Fe}$ as well as other byproducts. The collected dark-red oil from column chromatography was further purified by vacuum sublimation at 80 °C to obtain **142** as dark-red crystals (56%).

Scheme 84. Synthesis of the Phosphorus-bridged [1]FCP **142**.

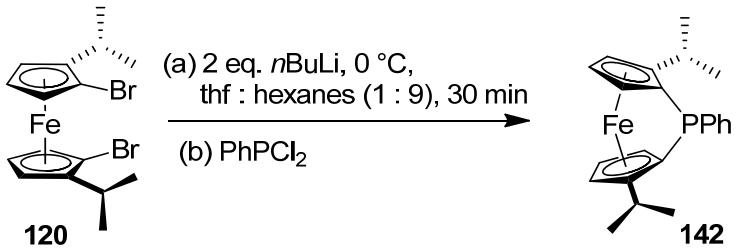

In the ^{1}H NMR spectrum of the isolated product four signals appear for the six Cp protons of this C_1-symmetric species [δ = 4.11 (2H, CH of Cp), 4.17 (1H, CH of Cp), 4.26 (2H, CH of Cp), 4.38 ppm (1H, CH of Cp)]. The Cp protons in species **142** appear in a narrower range compared to those of the parent species PhPfc [δ = 4.20 (2H, CH of Cp), 4.35 (2H, CH of Cp), 4.55 ppm (4H, CH of Cp)].[178] The ^{13}C NMR spectroscopy of **142** revealed two signals for the phosphorus-bounded carbon atom at δ = 15.86 and 18.65 ppm. The ^{31}P NMR signal appears at δ = 8.77 ppm which is comparable to that of PhPfc (δ = 12.9 ppm).[178] Species **142** was also characterized by mass spectrometry and elemental analysis. The mass spectrum was consistent with the assigned empirical formula and showed the highest detected mass for the molecular ion. To further characterize the molecular structure of **142**, dark-red single crystals suitable for X-ray crystallography were grown by vacuum sublimation. The molecular structure of **142**, obtained from single crystal X-ray diffraction studies, is depicted in Figure 29 (see also Tables 14 and 15). Species **142** crystallizes in the orthorhombic space group $P2_12_12_1$. The tilt α in **142** was found to be 26.21(13)° and, therefore, slightly lower than the narrow range of 26.9-27.9°,[8, 47, 61-64] known for other phosphorus-bridged [1]FCPs. It is worth to mention that the tilt angle of phosphorous-bridged [1]FCPs are much higher than those of the silicon-bridged [1]FCPs, which indicates the increased amount of ring strain existing in phosphorous-bridged [1]FCPs due to the smaller size of the bridging phosphorus.

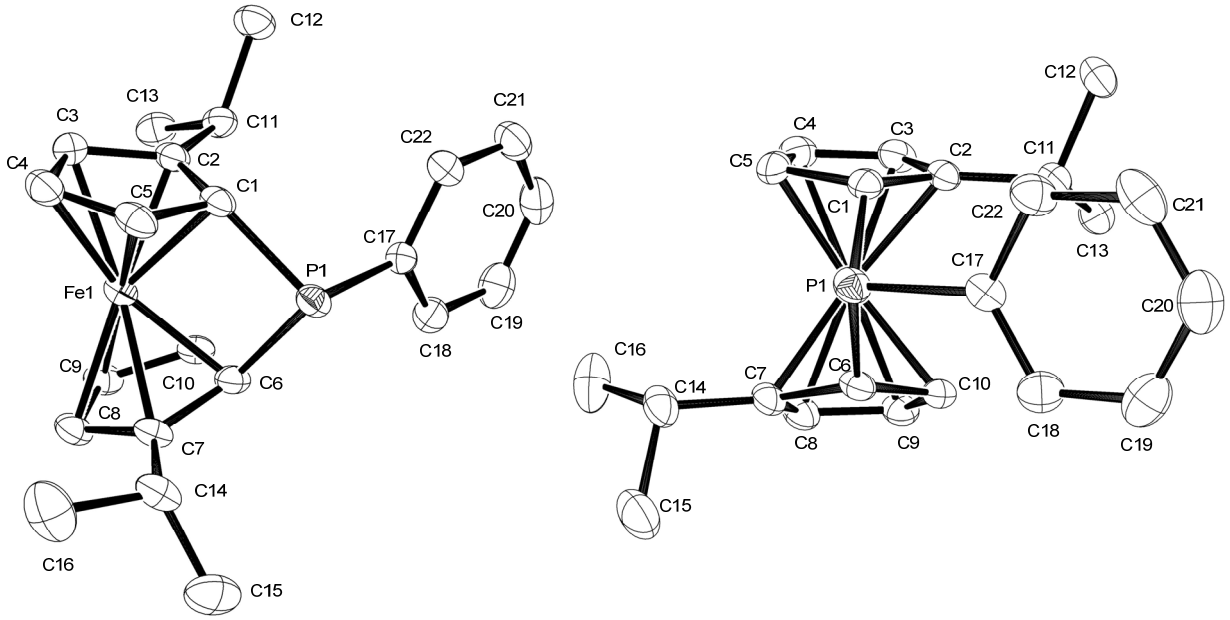

Figure 29. Molecular structure of **142** with thermal ellipsoids at the 50% probability level. Hydrogen atoms are omitted for clarity. Selected atom-atom distances [Å] and bond angles [°] for **142**: P1-C1 = 1.857(2), P1-C6 = 1.855(2), P1-C17 = 1.821(2), C6-P1-C1 = 92.09(10), C17-P1-C1 = 105.21(11), C17-P1-C6 = 104.40(11).

As illustrated in Scheme 85, the enantiomerically pure ferrocene dibromide **120** was first lithiated and then reacted with *i*PrPCl$_2$ to give the targeted phosphorus-bridged [1]FCP **143**. Monitoring the reaction mixture with ^{1}H NMR spectroscopy revealed that the C_1-symmetric species **143** formed as the major product. Similar to the case of species **142**, phosphorous-bridged [1]FCP **143** was first purified by flash column chromatography and then isolated as dark-red crystals through vacuum sublimation at 60 °C (52%). The ^{1}H NMR spectrum of the C_1-symmetric phosphorous-bridged [1]FCP **143** exhibits six separate resonances in the Cp region [δ = 3.93 (1H, CH of Cp), 3.95 (1H, CH of Cp), 4.16 (1H, CH of Cp), 4.22 (1H, CH of Cp), 4.25 (1H, CH of Cp), 4.37 ppm (1H, CH of Cp)]. The methyl protons of the three *i*Pr groups resonate in the range of δ = 1.08-1.34 ppm. The ^{31}P NMR spectrum of **143** shows a resonance at δ = 18.66 ppm which is considerably higher than that of the phosphorous-bridged [1]FCP **142**. Presumably, the extra shielding in species **142** is caused by the proximity between phenyl group and

phosphorus atom. Similarly, the measured ^{13}C chemical shift of the *ipso* carbon atoms bound to phosphorus in **143** of δ = 18.28 and 19.78 ppm is higher than that of the phosphorous-bridged [1]FCP **142**. The phosphorous-bridged [1]FCP **143** was also characterized by elemental analysis and mass spectrometry. The mass spectrum of the isolated product shows the highest detected mass for the molecular ion of the phosphorous-bridged [1]FCPs **143**.

Scheme 85. Synthesis of the Phosphorus-bridged [1]FCP **143**.

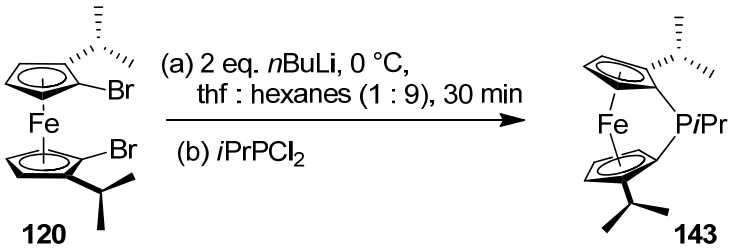

The vacuum sublimation of species **143** resulted in suitable crystals for single-crystal X-ray analysis and the crystal structure of **143** was determined (Figure 30; Tables 14 and 15). Species **143** crystallized in a triclinic space group *P*1 with two independent molecules per asymmetric unit. The tilt angles α of 25.82(13) and 25.70(15)° (for the two independent molecules in the asymmetric unit) are slightly lower than those of the known phosphorus-bridged [1]FCPs.[8, 47, 61-64] The other distortion angles (β, θ and δ; Table 15; Figures 29 and 30) determined for **143** are very similar as those of the phosphorus-bridged species **142**.

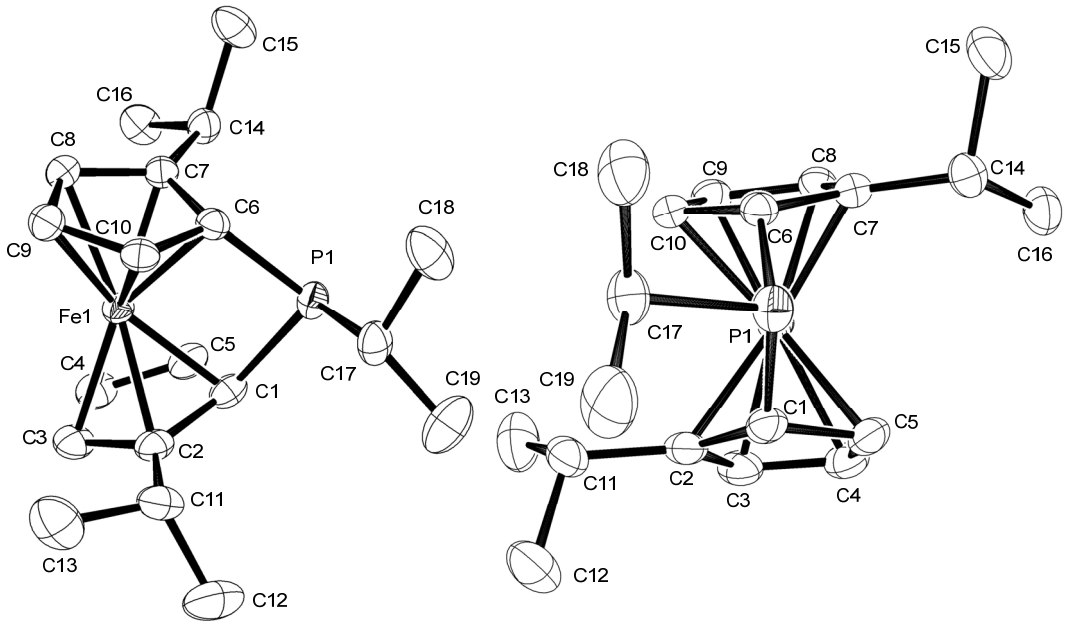

Figure 30. Molecular structure of **143** with thermal ellipsoids at the 50% probability level. Hydrogen atoms are omitted for clarity. Selected atom-atom distances [Å] and bond angles [°] for **143** (values in braces refer to the second independent molecule that is not shown): P1-C1 = 1.868(2) {1.868(2)}, P1-C6 = 1.854(2) {1.854(2)}, P1-C17 = 1.849(2) {1.843(3)}, C6-P1-C1 = 91.25(9) {91.35(10)}, C17-P1-C1 = 108.99(11) {108.64(11)}, C17-P1-C6 = 103.13(10) {103.20(11)}.

Table 14. Crystal and Structural Refinement Data for Compounds **142** and **143**.

	142	**143**
empirical formula	$C_{22}H_{25}FeP$	$C_{19}H_{27}FeP$
fw	376.24	342.22
cryst. size / mm^3	0.15 × 0.15 × 0.15	0.15 × 0.20 × 0.25
cryst. system, space group	orthorhombic, $P2_12_12_1$	triclinic, $P\bar{1}$
Z	4	2
a / Å	8.18100(10)	9.3595(3)
b / Å	11.7137(2)	9.9292(3)
c / Å	19.8518(3)	10.8017(3)
α / °	90	76.2510(12)
β / °	90	74.6300(12)

γ / °	90	70.1650(12)
volume / Å^3	1902.39(5)	898.34(5)
ρ_{calc} / mg m^{-3}	1.314	1.265
temperature / K	173(2)	173(2)
μ_{calc} / mm^{-1}	0.876	0.921
θ range / °	3.21 to 30.52	2.36 to 28.28
reflns collected / unique	25854 / 5808	34305 / 8892
absorption correction	multi-scan	multi-scan
data / restraints / params	5808 / 0 / 221	8892 / 3 / 392
goodness-of-fit	1.027	1.035
R_1 [I > 2 σ(I)][a]	0.0325	0.0230
wR_2 (all data)[a]	0.0710	0.0524
largest diff. peak and hole	0.282	0.234
$\Delta\rho_{elect}$ / e Å^{-3}	-0.292	-0.186

[a] $R_1 = [\Sigma||F_o|-|F_c||]/[\Sigma|F_o|]$ for $[F_o^2 > 2\sigma (F_o^2)]$, $wR_2 = \{[\Sigma w(F_o^2-F_c^2)^2]/[\Sigma w(F_o^2)^2]\}^{1/2}$ [all data].

Table 15. Measured Distortion Angles [°] (see Figures 29 and 30).

	142	**143**[a]
α	26.21(13)	25.82(13) {25.70(15)}
β/β'	34.61(16) / 33.52(17)	34.99(31) {32.88(37)} / 35.33(30) {32.84(31)}
θ	92.09(10)	91.25(9) {91.35(10)}
δ	160.83(2)	160.77(47) {160.90(48)}

[a] values in braces refer to the second independent molecule in the asymmetric unit.

The salt-metathesis reaction was performed between the dilithio derivative of **120** and *t*BuPCl$_2$ (Scheme 86). Reaction control by ^{1}H NMR spectroscopy revealed five signals for the six Cp protons of the C_1-symmtric phosphorous-bridged [1]FCP **144** [δ = 4.00 (m, 1H, CH of Cp), 4.08

(m, 1H, CH of Cp), 4.18 (m, 1H, CH of Cp), 4.22 (m, 2H, CH of Cp), 4.40 ppm (m, 1H, CH of Cp)].

Scheme 86. Synthesis of the Phosphorus-bridged [1]FCP **144**.

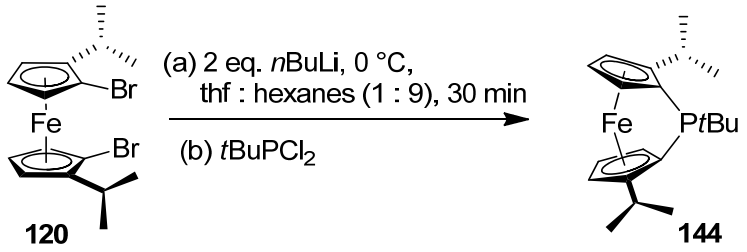

Similar to the work up procedure applied for species **142** and **143**, the reaction mixture was first purified by column chromatography to remove the hydrolysis byproduct $(i\text{PrH}_4\text{C}_5)_2\text{Fe}$ and other byproducts. The obtained dark-red oil after column chromatography was further purified by flask-to-flask condensation under vacuum at 80 °C (67%). The presence of the strained compound **144** was also confirmed by ^{13}C NMR spectroscopy where the ^{13}C resonance of the *ipso*-carbons bound to phosphorus was found at δ = 21.08 and 25.24 ppm which are comparable to that of the parent *t*BuPfc (δ = 19.4 ppm).[64] The ^{31}P NMR signal for species **144** appears at δ = 29.02 ppm, which is similar as that of the parent *t*BuPfc (δ = 26.1 ppm).[64] It is worth to mention that a small signal at δ = 16.00 ppm was observed in the ^{31}P NMR spectrum of the isolated product with an amount of around 3% with respect to the main product **144**. This signal can be correlated to the C_s-symmetric species **145** (Scheme 87) which forms through isomerization of the C_1-symmetric species **144** to its C_s-symmetric isomer **145** in the reaction mixture. The isomerization of the enantiomerically pure species **144** to its C_s-symmetric isomer is reminiscent of a similar isomerization reaction reported for the C_1-symmetic species **146** (Scheme 88).[179] Recently, our group reported the preparation of the phosphorous-bridged [1]FCP **146** through a salt-metathesis reaction between *t*BuPCl$_2$ and dilithioferrocene **131**. Interestingly, the chiral

species **146** isomerized in the reaction mixture thermally to yield C_s-symmetric phosphorous-bridged [1]FCP **147**. This thermal isomerization went through haptotropic η^5 to η^1 shifts of Cp rings.

Scheme 87. Isomerization of the Phosphorous-bridged [1]FCPs **144** and **145**.

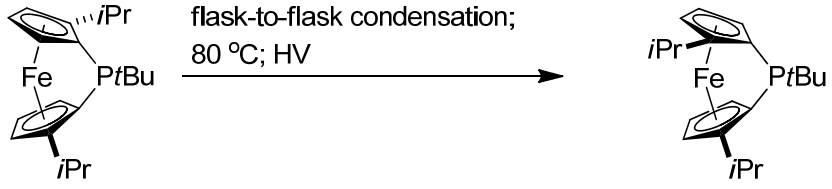

144 **145**

The ^{31}P NMR spectrum of the phosphorous-bridged [1]FCP **147** showed a resonance at δ = 16.2 ppm which is very similar to that of the C_s-symmetric isomer **145** (δ = 16.0 ppm). It can be assumed that a small amount species **144** isomerized in the mixture during the flask-to-flask condensation step to produce the C_s-symmetric isomer **145**.

Scheme 88. Isomerization of the Phosphorous-bridged [1]FCPs **146** and **147**.

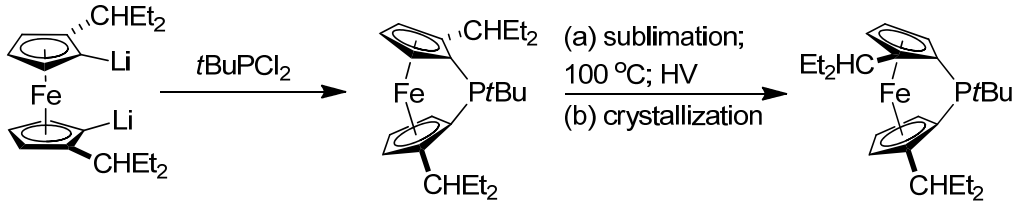

131 **146** **147**

CHAPTER 3

SUMMARY AND CONCLUSION

The new C_2-symmetric dibromoferrocene derivative **120** was synthesized as a precursor for the preparation for chiral [1]FCPs. I prepared the dibromoferrocene **120** which can quantitatively be lithiated and produce the chiral dilithioferrocene **121** (Figure 31).

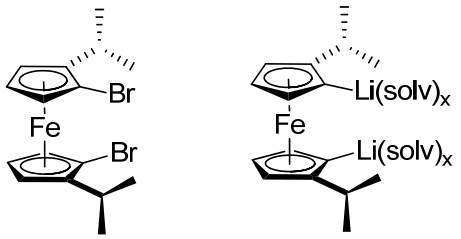

120 **121**

Figure 31. The C_2-symmetric dibromoferrocene **120** and dilithioferrocene **121**.

The gallium-bridged [1]FCP **122** was synthesized by the salt-metathesis reaction between the dilithioferrocene **121** and Ar′$GaCl_2$ (Figure 32). It was previously reported by our group that the salt-metathesis reaction of dilithioferrocene·tmeda with the non-bulky Ar′$GaCl_2$ results in the respective [1.1]FCP (Scheme5).[36] The gallium-bridged [1]FCP **122** was prepared by formally moving the bulk from the bridging element to the ferrocene unit. Performing DSC measurements confirmed that species **122** is a potential candidate for thermal ROP for the preparation of new metallopolymers.

The first indium-bridged [1]FCPs $\mathbf{124_1}$, $\mathbf{125_1}$, and $\mathbf{126_1}$ (Figure 32) were prepared by salt-metathesis reactions between dilithioferrocene·tmeda or the chiral dilithioferrocene **121** and the Ar′$InCl_2$ and (Mamx)$InCl_2$, respectively The preparation of the indium-bridged [1]FCPs $\mathbf{124_1}$ and $\mathbf{126_1}$, in which only either the ferrocenediyl moiety or the stabilizing ligand at indium is sterically demanding (fc$^{i\text{Pr2}}$ or Mamx), went along with the formation of unwanted [1.1]FCPs.

Interestingly, the indium-bridged [1]FCP **125** formed exclusively in the reaction mixture by applying bulky groups on the ferrocene moiety as well as on the ligand at indium. It was previously reported by our group that the salt-metathesis reaction of dilithioferrocene·tmeda with non-bulky Ar′$InCl_2$ results in the respective [1.1]FCP exclusively. This kind of selectivity for [1]FCPs over [1.1]FCPs by increasing the steric bulk of reagents had been previously observed in the case of related aluminum- and gallium-bridged compounds. For instance, gallium-bridged [1]FCPs are accessible either by applying bulky Mamx ligand on the bridging moiety[33] or by introducing *i*Pr groups on the ferrocene unit (using fc$^{i\text{Pr}2}$ moieties).[164] In [1.1]FCP, the space available in the bridging position increases when the bridging unit ER_x is moved slightly away from the sandwich moiety by increasing the E-C bond distance. Introducing indium as the bridging element, with In-C bonds being around 10% longer than the respective Al-C or Ga-C bonds, creates more space available in the bridging position of indium-bridged [1.1]FCPs.[37] Therefore, suppressing the formation of [1.1]FCPs requires introducing bulky groups on both moieties: the bridging ligand and the ferrocene unit. While the use of the bulky Me_2Ntsi ligand in the bridging position yielded in formation of respective aluminum- and gallium-bridged [1]FCPs (Scheme 4),[32] applying the same ligand system for the preparation of indium-bridged [1]FCPs yielded the non-strained [1.1]FCP [(Me_2Ntsi)Infc]$_2$ (Scheme 7).[37]

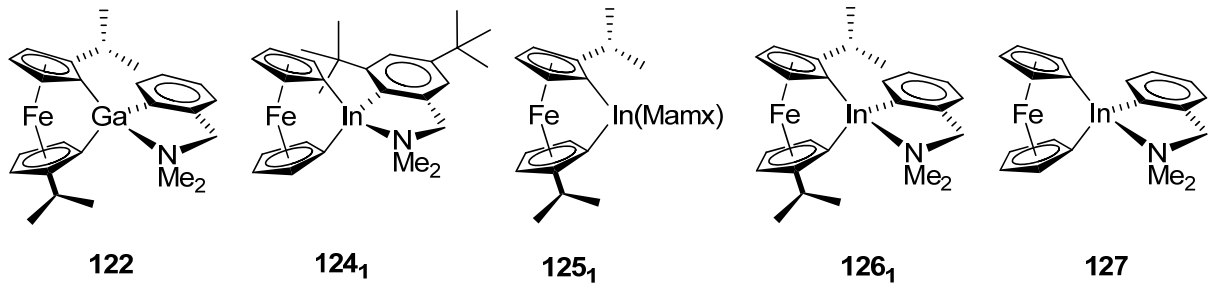

122 **124$_1$** **125$_1$** **126$_1$** **127**

Figure 32. Gallium- and indium-bridged [1]FCPs.

DFT calculations were performed for the prepared indium-bridged [1]FCPs **124$_1$**, **125$_1$**, **126$_1$**, and also the hypothetical species **127**. These studies revealed similar tilt angles for all for species in the range of 10.96-11.44° (Table 3). The relative orientation of the aromatic ligand with respect to the ferrocene unit changes significantly by introducing alkyl groups on the ferrocene unit as well as the aromatic ligand. These structural changes are caused by the interactions between alkyl groups at the sandwich and ligand moieties and have a significant influence on the overall amount of strain in [1]FCPs. Among the four indium-bridged [1]FCPs **124$_1$**, **125$_1$**, **126$_1$**, and **127**, species **125$_1$** with substituents on both the Ar′ ligand and the ferrocene moiety shows the highest amount of strain effects with strain increases of -2.83 kcal mol^{-1} (effect of *i*Pr groups) and -4.39 kcal mol^{-1} (effect of *t*Bu groups). Unfortunately, attempts for the isolation of the indium-bridged [1]FCP **125$_1$** were unsuccessful and species **125$_1$** polymerized spontaneously in the reaction mixture to give the polymer **125$_n$**. As the tilt angle of 11.42° is considered to be insufficient for ROP, the high reactivity of the strained [1]FCP **125$_1$** is quite unexpected. Based on the DFT calculations, it can be speculated that the high reactivity of species **125$_1$** is caused by the interactions between alkyl groups attached to the ferrocene moiety and the Ar′ ligand. The high reactivity of species **125$_1$** is reminiscent of aluminum- and gallium-bridged [1]FCPs **13** and **14** equipped with Mamx ligands, where the additional strain caused by the presence of *ortho*-*t*Bu groups on the Mamx ligand was reported for the first time.[33, 34]

A class of chiral boron-bridged [1]FCPs was synthesized by salt-metathesis reactions of enantiomerically pure dilithioferrocenes **121** and **131** and the three amino(dichloro)boranes Et_2NBCl_2, *i*Pr_2NBCl_2, and *t*Bu(Me_3Si)$NBCl_2$ (Figure 33). In case of the amino(dichloro)borane Et_2NBCl_2, the salt-metathesis reactions proceeded with nearly complete conversion of starting materials to the targeted boron-bridged [1]FCPs **132** and **133**, respectively. In contrast to this

result, salt-metathesis reactions did not proceed with selectivity in case of the bulky amino(dichloro)boranes iPr$_2$NBCl$_2$ and tBu(Me$_3$Si)NBCl$_2$ and ^{1}H NMR spectra of reactions mixtures revealed that significant amounts of bis(boryl)ferrocenes formed as the major byproduct.

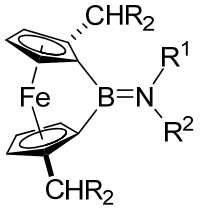

R^1/R^2	$CHMe_2$	$CHEt_2$
Et/Et	**132**	**133**
*i*Pr/*i*Pr	**128**	**138**
*t*Bu/Me$_3$Si	**134**	**136**

Figure 33. Boron-bridged [1]FCPs.

The product ratios between the targeted [1]FCPs and the bis(boryl)ferrocenes depend on the speed of addition of amino(dichloro)boranes, the bulkiness of the groups attached to the Cp moieties, the bulkiness of amino groups and, most importantly, on the reaction temperature. As salt-metathesis reactions are governed by kinetics, the ratio between the targeted [1]FCPs and the unwanted bis(boryl)ferrocenes can be interpreted as the relative rate between the ring-closure reaction of the intermediate **A** to produce [1]FCPs and the reaction of another amino(dichloro)borane with intermediate **A** to form bis(boryl)ferrocenes (Scheme 80). The fact that elevated reaction temperature favors the formation of [1]FCPs more strongly reveals that the highest activation barriers belongs to the formation of [1]FCPs. This seems logical as some of the strain present in [1]FCPs must be established in the transition state. In addition, increasing the reaction temperature to 50 °C improved the reported yield of the known bora[1]ferrocenophane iPr$_2$NBfc by almost 100%. To the best of our knowledge, this is the first report of using elevated temperatures for the preparation of strained sandwich compounds. This is probably due to the fact that strained sandwich compounds are generally considered to be

thermally reactive and, therefore, mostly prepared by applying low temperatures. Based on our successful results with boron-bridged [1]FCPs, we strongly recommend using high temperatures for future syntheses of [1]FCPs.

The substitution pattern of the alkyl groups CHR_2 attached to the Cp moieties has a significant influence on the selectivity of the salt-metathesis reactions (Scheme 80). In general, the formation of [1]FCPs is favored stronger by the presence of $CHEt_2$ than $CHMe_2$ groups. The bulkiness of the CHR_2 groups has a significant influence on the rate of intermolecular reactions (Scheme 80, k_1 and k_3). However, the rate of the intramolecular ring-closure (k_2), which results in formation of [1]FCPs, is not affected by the choice of CHR_2 groups.

Soluble metallopolymers were obtained from thermal ROP of selected boron-bridged [1]FCPs. However, applying the required high temperature for thermal ROP resulted in extrusion of elemental iron. The observation of elemental iron can explain the low measured exothermy in DSC thermograms of these highly strained boron-bridged [1]FCPs.

The two new chiral silicon- and tin-bridged [1]FCPs were synthesized and isolated in high yields. Evidenced by the ^{1}H NMR spectroscopy of the reaction mixtures, the targeted compounds **140** and **141** formed quantitatively in the reaction mixtures (Figure 34). The stanna[1]ferrocenophane **141** exhibited an increased air and moisture stability compared to the known tin-bridged [1]FCP *t*Bu_2Snfc.[56] This is presumably due to the steric protection of the bridging element by the *i*Pr groups on the Cp moiety. The fact that species **140** and **141** can be purified by sublimation makes them promising candidates for living anionic polymerization, as this method of polymerization requires high purity of monomers.

I prepared three enantiomerically pure phosphorous-bridged [1]FCPs through the salt-metathesis reaction of dilithio derivative of **120** with three dichlorophosphines (Figure 34). All three chiral phosphorus-bridged [1]FCPs (**142**, **143**, and **144**) are volatile under vacuum at high temperatures (60-80 °C) and were isolated in moderate yields by sublimation (**142** and **143**) or flask-to-flask condensation (**144**). The crystal structures of the phosphorous-bridged [1]FCPs **142** and **143** were determined by single crystal X-ray diffraction analysis. The tilt angles α of 26.21(13) (**142**) and 25.82(13) and 25.70(15)° (**143**) are slightly below the narrow range of 26.9-27.9° known for a variety of phosphorous-bridged [1]FCPs. The phosphorous-bridged [1]FCP **144** was isolated as a dark-red viscous oil which was contaminated with a small amount of its C_s-symmetric isomer.

One of the motivations behind this project was to investigate the application of these enantiomerically pure phosphorous-bridged [1]FCPs as chiral ligands in asymmetric catalysis in collaboration with Professor Andrew Evans's group at Queens University. Samples of the chiral phosphorous-bridged [1]FCPs **142**, **143**, and **144** were sent to Evans's group for further investigations in asymmetric catalysis.

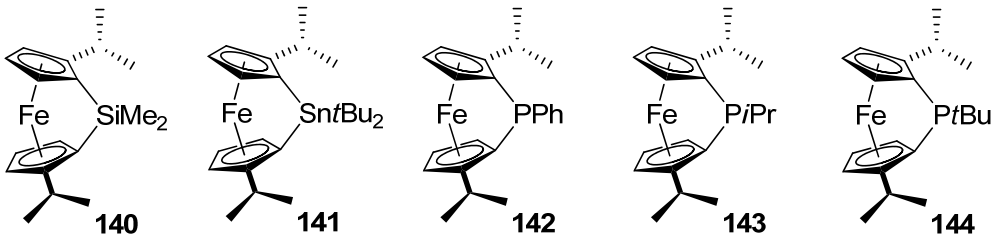

Figure 34. Silicon-, tin-, and phosphorus-bridged [1]FCPs.

Applying my new approach resulted in the syntheses of group of chiral [1]FCPs with boron, gallium, indium, silicon, tin, and phosphorus in bridging positions. Based on the following reasons it can be concluded that applying **120** as a precursor for dilithioferrocenes is superior to

the use of dilithioferrocene·tmeda which is the common starting material for preparation of strained [1]FCPs. 1) In contrast to dilithioferrocene·tmeda, this approach does not require the use of tmeda, which is reported to initiate the ROP of tin-bridged [1]FCPs. 2) Dilithioferrocene·tmeda is insoluble in most of the organic solvent and this hinders a perfect control over its concentration in the reaction which this reagent is involved. The dibromoferrocene **120** can be lithiated quantitatively in a solvent mixture of thf/hexanes (1 : 9) and remains dissolved in the solvent mixture; therefore, its salt-metathesis reaction with element dichlorides R_xECl_2 can be performed homogeneously, giving a perfect control over the concentration of the reactants and stoichiometry of the reaction. 3) The solvent mixture of thf/hexanes (1 : 9) which is applied for this approach allows the precipitation of LiCl during in salt-metathesis reactions and, thus, facilitates the formation of [1]FCPs. 4) In this approach the bridging elements are protected with *i*Pr groups which permits the use of "less-protective" ligands on the bridging elements. This is an important aspect as it is known that bulky groups on bridging elements can hinder the ROP of strained [1]FCPs. 5) All the chiral [1]FCPs prepared by this approach are highly soluble in common organic solvents. The high solubility of these species is mainly attributed to the presence of the two solubilizing *i*Pr groups on ferrocene units. It can be assumed that the solubility of the respective metallopolymers will be increased for the same reason. The low solubility of metallopolymers is one of the most critical problems existing in the area of metal-containing polymers. For instance, the thermal ROP of bora[1]ferrocenophanes resulted in mostly insoluble materials.[5] I produced highly soluble metallopolymers by thermal ROP of the chiral bora[1]ferrocenophanes obtained from my approach. 6) Monomers with a high level of purity are required for living anionic ROP. One of the main reasons behind the successful chemistry of dimethylsila[1]ferrocenophane is the high volatility of this species,

which allows extensive purification of this species by repeated vacuum sublimation. The fact that most of the [1]FCPs obtained through my approach are volatile under vacuum at elevated temperatures (50-80 °C) and were purified by vacuum sublimation makes these species potential candidates for living ROP. Moreover, the synthetic approach, which I developed for the preparation of **120**, is very flexible and can be extended to introduce substituents other than *i*Pr on the ferrocene unit. Efforts in our group are currently focused on preparing dibromoferrocenes with different substitution patterns on ferrocene unit.

CHAPTER 4

EXPERIMENTAL

4.1. General Procedures

If not mentioned otherwise, all syntheses were carried out using standard Schlenk and glovebox techniques. Solvents were dried using an MBraun Solvent Purification System and stored under nitrogen over 3 Å molecular sieves. All solvents for NMR spectroscopy were degassed prior to use and stored under nitrogen over 3 Å molecular sieves. ^{1}H and ^{13}C NMR spectra were recorded on a 500 MHz Bruker Avance NMR spectrometer at 25 °C. ^{1}H chemical shifts were referenced to the residual protons of the deuterated solvents (δ = 7.15 ppm for C_6D_6; 7.26 ppm for $CDCl_3$); ^{13}C chemical shifts were referenced to the C_6D_6 signal at δ = 128.00 ppm, the $CDCl_3$ signal at δ = 77.00 ppm, and the [D_8]toluene signal at δ = 20.43 ppm. ^{11}B chemical shifts were referenced to F_3B-OEt_2 (external standard in C_6D_6). Polymer **125$_n$** was isolated using inert gas techniques. Polymer **125$_n$** can be handled under air for a short amount of time; however, overnight exposure of solution of NMR samples of **125$_n$** to air resulted in intense signals of the $FeCp_2$ and (iPrC_5H_4)$_2$Fe, respectively. Assignments for **120**, **122**, **128**, **129**, **132**, **133**, **134**, **135**, **136**, **137**, **138**, **139**, **140**, **141**, **142**, **143**, and **144** were supported by additional NMR experiments (DEPT, HMQC, COSY). As signals of Cp protons show a fine structure, all signals were called multiplets. Mass spectra were measured on a VG 70SE and were reported in the form *m/z* (rel intens) [M^+] where *m/z* is the observed mass. The intensities are reported relative to the most-intense peak and $[M]^+$ is the molecular-ion peak or a fragment; only characteristic mass peaks are listed. For isotopic pattern, only the mass peak of the isotopoloque or isotope with the highest natural abundance is listed. Elemental analyses were performed on a Perkin Elmer 2400 CHN Elemental Analyzer using V_2O_5 to promote complete combustion. UV/Vis spectra were

measured at ambient temperature with dry, degassed solvents, using a Varian Cary 50 Bio UV/Visible Spectrophotometer.

4.2. Reagents

The compounds Ar′$GaCl_2$,[180] Ar′$InCl_2$,[181] dilithioferrocene·tmeda,[182] Et_2NBCl_2,[183] and *t*Bu(Me_3Si)$NBCl_2$[184] were prepared as described in the literature. Species (*R,R,S$_p$,S$_p$*)-2,2′-bis(α-N,N-dimethylaminoethyl)-1,1′-dibromoferrocene (**118**) and (*R,R,S$_p$,S$_p$*)-2,2′-bis(α-acetoxyethyl)-1,1′-dibromoferrocene (**119**) are described in reference[160] but experimental procedures and spectroscopic data were not published. Species **101**, **114**, **115** and **116** were prepared according to literature procedure[142] with some alternations. Therefore, we report on the preparation of these known compounds below. Ferrocene (98%), *n*BuLi (2.5 M in hexanes), Me_2SiCl_2 (98%), *i*Pr_2NBCl_2, $AlEt_3$ (1.9 M in toluene), $AlMe_3$ (2.5 M in hexanes) dichloroisopropylphosphine (97%), and *tert*-butyldichlorophosphine (1.0 M solution in diethyl ether) were purchased from Sigma Aldrich. 1,2-Dibromotetrachloroethane (Alfa Aesar; 98%) and *t*Bu_2SnCl_2 (Alfa Aesar; 98%) were purchased from VWR. Silica gel 60 (EMD, Geduran, particle size 0.040–0.063 mm) were used for column chromatography.

4.3. Thermal Studies

DSC analyses were performed on a TA Instruments Q20 at a heating rate of 10 °C/min. Samples were sealed in hermetic aluminum pans, and their mass determined by a AB204-S Mettle Toledo balance (amounts of sample: 2-5 mg). DSC data was analyzed with TA Instruments Universal Analysis 2000 software.

4.4. Dynamic-light Scattering (DLS)

Dynamic-light scattering experiments were performed using a nano series Malvern zetasizer instrument equipped with a 633 nm red laser. Samples were filtered through 0.2 μm syringe

PTFE filters before they were analyzed in 1 cm glass cuvettes at concentrations of 5.0 and 2.5 mg/mL in thf at 25 °C. The refractive index of the polymers was assumed to be 1.5. For each polymer, two samples were prepared at each concentration. Every sample was measured three times. For poly(ferrocenyldimethylsilane) (PFS) the absolute molecular weights (M_w) in the range of 10 to 100 kDa and radii of gyration (R_g) are known in the literature.[185] Assuming that polymers **124$_n$** and **125$_n$** can be described as random coils, with thf being a good solvent, hydrodynamic radii R_h (**124$_n$**: 1.0 ± 0.1 nm; **125$_n$**: 2.4 ± 0.1 nm) gave radii of gyration (R_g) by using the equation $R_g/R_h = 2.05$.[186] Applying the published relation between log(R_g) and log(M_w) for poly(ferrocenyldimethylsilane) (PFS),[185] molecular weights were calculated (**4$_n$**: M_w = 4.8 ± 0.8 kDa; **5$_n$**: M_w = 24 ± 2 kDa).

Table 16. DLS Data of Poly(ferrocenylindigane) **124$_n$**[a]

Concentration (mg/mL)	5		2.5	
sample #	1	2	1	2
R_h (nm)	0.981	1.056	0.963	0.883
	1.059	0.973	0.926	1.018
	0.879	1.114	1.033	1.154
Average (nm)	1.010		0.996	
SD (nm)	0.083		0.096	
Overall Average (nm)	1.003			
Overall SD (nm)	0.086			

[a] based on the size distribution by number

Table 17. DLS Data of Poly(ferrocenylindigane) **125$_n$**[a]

Concentration (mg/mL)	5		2.5	
sample #	1	2	1	2
R_h (nm)	2.204	2.327	2.465	2.533
	2.334	1.564[b]	2.453	2.525
	2.362	2.493	2.415	2.408
Average (nm)	2.344		2.467	
SD (nm)	0.103		0.053	
Overall Average (nm)	2.411			
Overall SD (nm)	0.099			

[a] based on the size distribution by number
[b] outlier not taken into account

4.5. Computational Details

The following paragraph was adopted from reference 168. Theoretical calculations were carried out using the Amsterdam Density Functional package (version ADF2010.02).[165, 166, 187] The Slater-type orbital (STO) basis sets were of triple-ζ quality augmented with a two polarization functions (ADF basis TZ2P). Core electrons were frozen (C, N 1s; Fe 2p; Ga 3d; In 4d) in our model of the electronic configuration for each atom. Relativistic effects were included by virtue of the zero order regular approximation (ZORA).[188, 189] The local density approximation (LDA) by Vosko, Wilk and Nusair (VWN)[190] was used together with the exchange correlation corrections of Becke[191] and Perdew (BP86). Tight optimization conditions were used for all compounds. Frequency calculations were used to confirm minima and provide thermodynamic information. The product of the hydrogenolysis reaction (Mamx)InH_2 (Scheme 6) showed a small imaginary frequency (-*i*27 cm^{-1}) corresponding to barrierless rotation of a *t*Bu groups. The notation used for $\Delta H°_{298}$ and $\Delta G°_{298}$ indicate standard condition (p = 10^5 Pa and T = 298.15 K).

Graphical illustrations of calculated results were done with the help of *ORTEP-3 for Windows* (version 2.02);[192] extraction of structural parameters (see Table 3) from the calculated coordinates of [1]FCPs were done with the help of *Mercury* (version 3.1.1).

4.6. GPC Analyses

Chromatograms were recorded on a Viscotek 350 HT-GPC system (Malvern) that was used at low temperature (column temperature of 37.5 ºC; thf; flowrate = 1.0 mL min^{-1}; calibrated for polystyrene standards). The instrument was equipped with the following Viscotek components: autosampler (Model 430 Vortex), degasser (model 7510), two pumps (model 1122), 7° and 90° light scattering detectors, refractometer, and viscometer. GPC columns cover the range of M_w of 500 to 10,000,000 g/mol (three main columns: Plgel 10 μM MIXED-B LS 300 x 7.5 mm; one guard column: 10 μM GUARD 50 x 7.5 mm; Agilent Technologies). Samples were dissolved in thf and filtered through 0.2 μm syringe PTFE filters before GPC analysis.

4.7. Synthesis of 1,1′-diacetylferrocene (114)[142]

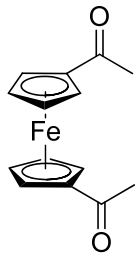

114

Acetyl chloride (6.25 mL, 88.0 mmol) was added to a suspension of aluminum chloride (10.6 g, 80.0 mmol) in CH_2Cl_2 (40 mL) at 0 °C. Ferrocene (6.00 g, 32.4 mmol) in CH_2Cl_2 (400 mL) was added dropwise within 20 min. The reaction mixture was warmed up to r.t. and stirred for 2 h. Hydrolysis was done at 0 °C by dropwise addition of ice-cold water (200 mL). The reaction mixture was diluted with CH_2Cl_2 (200 mL) and washed with saturated $NaHCO_3$ (100 mL) and

brine (100 mL). The organic phase was dried over $MgSO_4$, concentrated and purified with column chromatography (hexanes/EtOAc 1:1) to yield in a brown-red solid (85%, reported: 85%). ^1H NMR ($CDCl_3$): δ = 2.31 (s, 6H), 4.46 - 4.47 (m, 4H), 4.72 - 4.73 (m, 4H).

4.8. Synthesis of (*R*,*R*)-1,1′-bis(α-hydroxyethyl)ferrocene (115)[142]

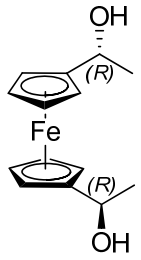

115

Oxazaborolidine (0.330 g, 1.20 mmol) was dissolved in thf (12 mL) and cooled down to 0 °C under nitrogen. From a syringe charged with $BH_3 \cdot SMe_2$ (4 mL, 1M in thf) 20% of the final amount (0.8 mL) was added to the catalyst solution. After 5 min stirring, the remaining $BH_3 \cdot SMe_2$ and a solution of **114** (0.540 g, 2.00 mmol) in thf (5.0 mL) were added simultaneously within 20 min. The red color of the ketone turned to yellow on reduction. After 15 min at 0 °C the excess $BH_3 \cdot SMe_2$ was quenched by dropwise addition of methanol (2.0 mL). After the hydrolysis was complete, the mixture was poured into a saturated aqueous solution of NH_4Cl (150 mL) and extracted with ether (200 mL). The organic phase was washed with water (100 mL) and brine (100 mL), dried over $MgSO_4$, and then the volatiles were removed to give an oil which was purified by column chromatography (hexanes/EtOAc 6:1), resulting in a yellow solid (0.535 g, 98%). ^1H NMR ($CDCl_3$): δ = 1.39 (s, 6H), 3.19 (s, 2H), 4.02 - 4.26 (m, 8H), 4.59 - 4.65 (q, 2H).

4.9. Synthesis of (*R*,*R*)-1,1′-bis(α-acetoxyethyl)ferrocene (116)[142]

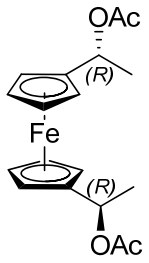

116

Metallocenyldiol **115** (0.805 g, 2.92 mmol) was treated with acetic anhydride (2.0 mL, 21.0 mmol) and pyridine (5 mL) under nitrogen and the reaction mixture was stirred for 12 h at r.t. All Volatiles were removed in high vacuum resulting in a brown oil as the crude product which was already >95% pure, as indicated by NMR analysis. The yield was quantitative and the compound was used in the next step without further purification. ^{1}H NMR ($CDCl_3$): δ = 1.51 - 1.55 (d, 6H), 2.04 (s, 6H), 4.13 - 4.23 (m, 8H), 5.78 - 5.82 (q, 2H).

4.10. Synthesis of (*R*,*R*)-1,1′-bis(α-N,N-dimethylaminoethyl)ferrocene (101)[142]

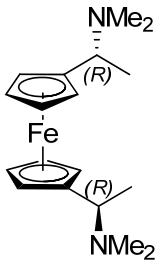

(*R*,*R*)-**101**

The metallocenyl acetate **116** (0.390 g, 1.09 mmol) was dissolved in MeOH (10 mL). An excess of dimethylamine (2.0 mL, 40% in water, 15.8 mmol) was added. After stirring for 12 h at r.t., the reaction mixture was poured into a saturated aqueous solution of NH_4Cl (50 mL). The aqueous phase was separated and neutralized by dropwise addition of 1M KOH and extracted with ether (100 mL). After washing with water (50 mL) and brine (50 mL) the organic layer was dried over $MgSO_4$ and all volatiles were removed to yield a brown oil as the product (0.323 g,

90%) which was used in the next step without further purification. ^{1}H NMR ($CDCl_3$): δ = 1.45 - 1.49 (d, 6H), 2.09 (s, 12H), 3.59 - 3.63 (q, 2H), 4.05 - 4.08 (m, 8H).

4.11. Synthesis of (*R,R,S*$_p$,*S*$_p$)-2,2′-bis(α-N,N-dimethylaminoethyl)-1,1′-dibromoferrocene (118)[160]

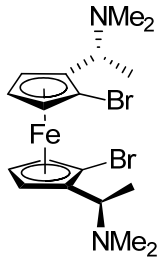

118

To a stirred solution of (*R,R,*)-1,1′-bis(α-N,N-dimethylaminoethyl)ferrocene (**101**) (1.96 g, 6.01 mmol) in diethyl ether (20 mL) under inert atmosphere, *n*BuLi (2.50 M in hexanes, 9.60 mL, 24.0 mmol) was added dropwise over 15 min at r.t. After several minutes, the color of the mixture changed from orange to red. The reaction mixture was stirred overnight (16 h) and then cooled down to -78 °C. A solution of 1,2-$Br_2Cl_4C_2$ (8.80 g, 27.0 mmol) in thf (13.5 mL) was added dropwise via syringe over 15 min. The resulting dark brown suspension was allowed to warm to r.t. over a period of 90 minutes, stirred at r.t. for 1 h, and then quenched with saturated aqueous $Na_2S_2O_3$ solution at 0 °C. From this point on the manipulation was done under air. The mixture was diluted with diethyl ether (200 mL), the organic layer was separated, and the aqueous layer was extracted with diethyl ether (2 × 75 mL). The combined organic phases were poured into a saturated aqueous NH_4Cl solution (200 mL). The aqueous phase was separated, neutralized with dropwise addition of 1M KOH, and extracted with diethyl ether (200 mL). After washing with water (100 mL) and saturated aqueous NaCl solution (100 mL), the organic layer was dried over $MgSO_4$, and all volatiles were removed to give the product as a yellow solid (2.21 g, 76%), which was used in the next step without further purification. ^{1}H NMR ($CDCl_3$): δ =

1.48 (d, 6H, CH_3), 2.12 (s, 12H, NMe_2), 3.74 (q, 2H, CH), 4.13 (m, 4H, CH of Cp), 4.27 ppm (m, 2H, CH of Cp).

4.12. (*R,R,S$_p$,S$_p$*)-2,2'-bis(α-acetoxyethyl)-1,1′-dibromoferrocene (119)[160]

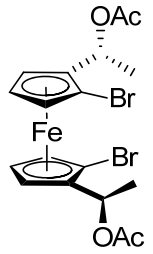

119

A mixture of **118** (1.09 g, 2.26 mmol) and acetic anhydride (7.39 g, 72.4 mmol) was thoroughly degassed and stirred for 10 h at 70 °C. All volatiles were removed at 40 °C under high vacuum to give the product as a dark brown oil (1.00 g, 85%). ^{1}H NMR ($CDCl_3$): δ = 1.62 (d, 6H, CH_3), 2.01 (s, 6H, OAc), 4.18 (m, 2H, CH of Cp), 4.32 (m, 2H, CH of Cp), 4.38 (m, 2H, CH of Cp), 5.93 ppm (q, 2H, CH).

4.13. Synthesis of (*S$_p$,S$_p$*)-1,1′-dibromo-2,2'-di(isopropyl)ferrocene (120)[164]

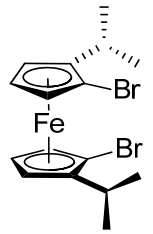

120

A solution of $AlMe_3$ (12.2 mL, 2.0 M solution in hexanes, 24.2 mmol) was added dropwise to a solution (-78 °C) of (*R,R,S$_p$,S$_p$*)-2,2′-bis(α-acetoxyethyl)-1,1'-dibromoferrocene (2.50 g, 4.85 mmol) in CH_2Cl_2 (48.5 mL). The reaction mixture was stirred for 60 min at -78 °C and then warmed up to r.t. and stirred for additional 20 min. The mixture was transferred into an saturated aqueous $NaHCO_3$ solution (25 mL) at 0 °C via cannula, followed by addition of a saturated

aqueous sodium potassium tartrate solution (25 mL). From this point on the manipulation was done under air. The solvent was removed under high vacuum and the residue was dissolved in diethyl ether (25 mL). The resulting solution was stirred vigorously for 15 min and then acidified with 1M HCl. The organic layer was separated and the aqueous layer was extracted with diethyl ether (2 × 50 mL). The combined organic phases were washed with saturated aqueous $NaHCO_3$ solution, water, and brine. After the organic layer was dried over $MgSO_4$, all volatiles were removed to yield a brown oil, which was further purified by column chromatography (hexanes/ethyl acetate, 100:1). The resulting brown powder was crystallized from hexanes at ca. -22 °C (1.76 g, 85%). ^{1}H NMR ($CDCl_3$): δ = 1.06 (d, 6H, CH$\underline{Me}_2$), 1.32 (d, 6H, CH$\underline{Me}_2$), 2.80 (sept, 2H, C$\underline{H}Me_2$), 4.01 (m, 2H, CH of Cp), 4.07 (m, 2H, CH of Cp), 4.23 ppm (m, 2H, CH of Cp); ^{13}C NMR ($CDCl_3$): δ = 21.52 [CH($\underline{C}H_3$)$_2$], 24.20 [CH($\underline{C}H_3$)$_2$], 25.96 [$\underline{C}H(CH_3)_2$], 64.62 ($\underline{C}$H of Cp), 67.86 ($\underline{C}$H of Cp), 73.94 ($\underline{C}$H of Cp), 80.54 (*ipso*-Cp), 95.16 ppm (*ipso*-Cp); MS (70 eV): *m/z* (%): 428 (100) [M^+], 384 (20) [M^+ - *i*Pr], 348 (7) [M^+ - Br], 268 (5) [M^+ - 2Br], 182 (5) [M^+ - 2*i*Pr - 2Br]; HRMS (70 eV): *m/z* calcd for $C_{16}H_{20}Br_2Fe$: 427.9261; found: 427.9264; elemental anal. calcd (%) for $C_{16}H_{20}Br_2Fe$ (427.983): C 44.90, H, 4.71; found: C 45.63, H, 4.55.

4.14. Synthesis of the [1]FCP 122[164]

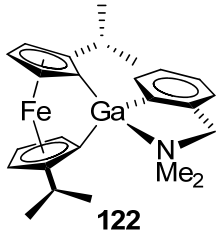

122

Species **120** (0.450 g, 1.05 mmol) was dissolved in a solvent mixture (10 mL of hexanes : thf, 9 : 1) and cooled to 0 °C. A solution of *n*BuLi (2.5 M in hexane, 0.88 mL, 2.20 mmol) was added dropwise and the reaction was stirred at this temperature for 30 min. Ar′$GaCl_2$ (0.300 g, 1.09

mmol) was dissolved in toluene (9 mL; r.t.) and added dropwise within 1 min via cannula tubing. The cold bath was removed after 5 min and the color of the reaction mixture changed from orange to red along with a formation of a colorless precipitate. All solids were removed by filtration and the product was isolated through crystallization (16 h at -80 °C) as red solid (0.290 g, 59%). Suitable crystals for X-ray analysis were obtained from Et_2O solutions at ca. -22 °C. ^{1}H NMR (C_6D_6): δ = 1.10 (d, 3H, CH$\underline{Me}_2$), 1.20 (d, 3H, CH$\underline{Me}_2$), 1.49 (d, 6H, CH$\underline{Me}_2$), 2.00 (s, 3H, NMe_2), 2.23 (s, 3H, NMe_2), 2.34 (sept, 1H, C$\underline{H}Me_2$), 2.75 (d, 1H, CH_2), 3.13 (sept, 1H, C$\underline{H}Me_2$), 3.53 (m, 1H, CH-α of Cp), 3.76 (d, 1H, CH_2), 3.98 (m, 1H, CH-α of Cp), 4.46 (m, 1H, CH-β of Cp), 4.50 (m, 1H, CH-β of Cp), 4.67 (m, 1H, CH-β of Cp), 4.70 (m, 1H, CH-β of Cp), 6.89 (d, 1H, Ar), 7.22 (t, 1H, Ar), 7.30 (t, 1H, Ar), 8.02 ppm (d, 1H, Ar); ^{13}C NMR (C_6D_6): δ = 21.89 [CH($\underline{C}H_3$)$_2$], 22.25 [CH($\underline{C}H_3$)$_2$], 28.02 [CH($\underline{C}H_3$)$_2$], 28.08 [CH($\underline{C}H_3$)$_2$], 30.75 [$\underline{C}H(CH_3)_2$], 32.42 [$\underline{C}H(CH_3)_2$], 44.23 (*ipso*-Cp, Ga), 45.64 (NMe_2), 46.43 (*ipso*-Cp, Ga), 47.12 (NMe_2), 67.64 (CH_2), 70.17 (C-β of Cp), 70.24 (C-β of Cp), 74.89 (C-β of Cp), 75.31 (C-β of Cp), 79.95 (C-α of Cp), 82.14 (C-α of Cp), 104.54 (*ipso*-Cp, *i*Pr), 105.24 (*ipso*-Cp, *i*Pr), 124.64 (CH, Ar), 127.78 (CH, Ar), 128.04 (CH, Ar), 136.23 (CH, Ar), 142.42 (*ipso*-C, Ar), 149.31 ppm (*ipso*-C, Ar); UV/Vis (toluene): λ_{max} (ε) = 468 nm (118 L mol^{-1} cm^{-1}); MS (70 eV): *m/z* (%): 471 (100) [M^+], 429 (32) [M^+ - *i*Pr], 268 (40) [M^+ - Ar´Ga], 188 (5) [M^+ - 2*i*Pr - Ar´Ga]; HRMS (70 eV): *m/z* calcd for $C_{25}H_{32}FeGaN$: 471.1140; found: 471.1130; elemental anal. calcd (%) for $C_{25}H_{32}FeGaN$ (472.096): C 63.60, H 6.83, N 2.97; found: C 63.44, H 6.81, N, 2.94.

4.15. Synthesis of the Poly(ferrocenylindigane) 125_n[168]

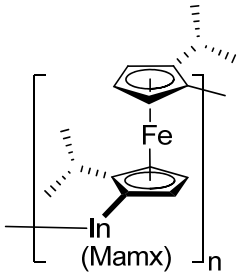

125_n

*n*BuLi (2.5 M in hexanes, 0.85 mL, 2.1 mmol) was added dropwise to a cold (0 ºC) solution of **120** (0.432 g, 1.01 mmol) in a mixture of thf (1 mL) and hexanes (9 mL). The reaction mixture was stirred at 0 ºC for 30 min, resulting in an orange solution. A solution of **123** (0.438 g, 1.01 mmol) in Et_2O (20 mL; r.t.) was added dropwise within 1 min to the solution. The resulting reaction mixture was warmed to r.t. and stirred for 30 min, resulting in a red solution with a white precipitate. All volatiles were removed under vacuum, yielding a red solid. Et_2O (25 mL) was added to the red solid and the mixture was stirred for 30 min, yielding a red solution with a white precipitate. The solid was filtered off and the filtrate was stirred for 3 h, resulting in an orange-red solution with orange gelatinous material. All volatiles were removed under vacuum, yielding an orange-red paste, which was dissolved in toluene (5 mL). The toluene solution was added dropwise to hexanes (20 mL) which was stirred vigorously, yielding an orange precipitate with a red solution. The precipitate (0.438 g) was filtered off, washed with hexanes (3 x 5 mL) and dried under vacuum to give the poly(ferrocenylindigane) **125_n** (0.211 g, 33%). ^{1}H NMR (C_6D_6): δ = 1.24-1.38 (br peaks, 9 H, *t*Bu), 1.48-1.66 (br m, 9 H, *t*Bu), 2.15-2.77 (br m, 6 H, NMe_2), 3.40-3.69 (m, 2 H, CH_2), 3.84-4.62 (m, 8H, Cp), 6.86-7.04 (m, 1 H, C_6H_2), 7.38-7.55 (m, 1 H, C_6H_2) ppm.

4.16. Identification of the Inda[1]ferrocenophane 125_1[168]

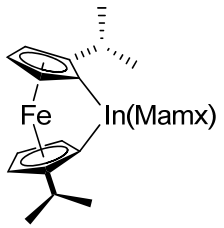

125_1

Inda[1]ferrocenophane **125_1** is an intermediate in the preparation of **5_n** and was identified via ^{1}H NMR spectroscopy. All attempts to isolate pure the inda[1]ferrocenophane **5_1** were unsuccessful. ^{1}H NMR (C_6D_6; taken from an aliquot of the reaction mixture after 30 min): δ = 1.16 (d, 3H, CH$\underline{Me}_2$), 1.19 (d, 3H, CH$\underline{Me}_2$), 1.39 (s, 9H, *t*Bu), 1.50 (d, 3H, CH$\underline{Me}_2$), 1.53 (d, 3H, CH$\underline{Me}_2$), 1.65 (s, 9H, *t*Bu), 1.91 (s, 3H, NMe_2), 2.30 (s, 3H, CH_3 of NMe_2), 2.38 (sept, 1H, C$\underline{H}Me_2$), 2.65 (d, 1H, CH_2), 2.86 (sept, 1H, C$\underline{H}Me_2$), 3.68 (m, 1H, CH-α of Cp), 3.94 (d, 1H, CH_2), 4.11 (m, 1H, CH-α of Cp), 4.47 (m, 1H, CH-β of Cp), 4.50, (m, 1H, CH-β of Cp) 4.67 (m, 1H, CH-β of Cp), 4.73 (m, 1H, CH-β of Cp), 6.93 (s, 1H, C_6H_2), 7.71 (s, 1H, C_6H_2) ppm; ^{13}C NMR (C_6D_6): δ = 21.74 [CH($\underline{C}H_3)_2$], 22.73 [CH($\underline{C}H_3)_2$], 28.07 [CH($\underline{C}H_3)_2$], 28.14 [CH($\underline{C}H_3)_2$], 31.67 [C($\underline{C}H_3)_3$], 32.15 [$\underline{C}H(CH_3)_2$], 32.82 [$\underline{C}H(CH_3)_2$], 33.11 [C($\underline{C}H_3)_3$], 34.81 [$\underline{C}(CH_3)_3$], 36.54 [$\underline{C}(CH_3)_3$], 44.46 (NMe_2), 48.28 (NMe_2), 50.53, 52.28 (*ipso*-Cp, In, tentative), 69.18 (CH_2), 69.73 (C-β of Cp), 69.93 (C-β of Cp), 74.31 (C-β of Cp), 74.86 (C-β of Cp), 80.84 (C-α of Cp), 80.89 (C-α of Cp), 104.33 (*ipso*-Cp, *i*Pr), 105.69 (*ipso*-Cp, *i*Pr), 121.44, 122.23, 128.51, 143.63, 150.45, 159.64 (C_6H_2) ppm. Note: The *ipso*-C-In was not detected. Assignments were done along the lines of the known gallium compound **122**.

4.17. Synthesis of a Mixture of 126_1 and 126_2[168]

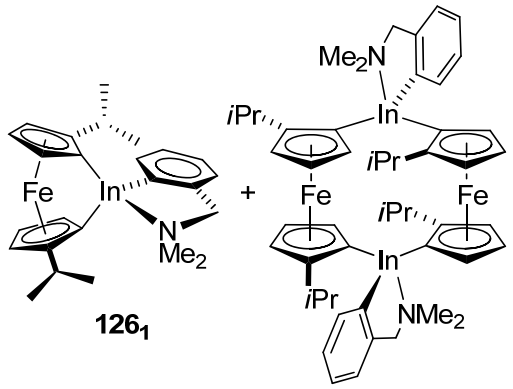

126_1 **126_2**

*n*BuLi (2.5 M in hexanes, 0.86 mL, 2.2 mmol) was added dropwise to a cold (0 ºC) solution of **120** (0.437 g, 1.02 mmol) in a mixture of thf (1 mL) and hexanes (9 mL). The reaction mixture was stirred at 0 ºC for 30 min, resulting in an orange solution. A solution of Ar′$InCl_2$ (0.340 g, 1.06 mmol) in Et_2O (20 mL; r.t.) was added dropwise within 1 min to the solution. The cold bath was removed after 5 min and the color of the reaction mixture changed from orange to light-red along with a formation of a colorless precipitate. The reaction was stirred for another 5 min, all volatiles were removed, and the resulting red residue was dissolved in hexanes (10 mL). After removal of all solids through filtration, solvent was removed under vacuum. The mixture was analyzed by ^{1}H NMR spectroscopy and MS. As many signals overlap with other smaller signals, the measured intensities are imprecise. The signals for the aromatic protons above 8 ppm do not overlap significantly with other peaks and, therefore, were used to calculate the approx molar ratio of 0.86 : 1.0 for **126_1** : **126_2**. As the intensity of the peaks for species **126_1** is approx half of that of respective peaks of species **126_2**, only certain peaks could be assigned for **126_1**. ^{1}H NMR (C_6D_6) for **126_2**: δ = 1.08 (d, 6H, CH$\underline{Me}_2$, tentative), 1.21 (d, 6H, CH$\underline{Me}_2$, tentative), 1.24 (d, 6H, CH$\underline{Me}_2$, tentative), 1.60 (d, 6H, CH$\underline{Me}_2$, tentative), 1.65 (s, 6H, NMe_2), 2.12 (s, 6H, NMe_2), 2.41 (sept, 2H, C$\underline{H}Me_2$), 3.22 (d, 2H, CH_2), 3.34 (sept, 2H, C$\underline{H}Me_2$), 3.59 (d, 2H, CH_2), 3.85 (m, 2H,

CH-α of Cp), 4.28 (m, 2H, CH-β of Cp), 4.31 (m, 2H, CH-β of Cp), 4.39 (m, 2H, CH-β of Cp), 4.49 (m, 2H, CH-β of Cp), 5.22 (m, 2H, CH-α of Cp), 7.02 (d, 2H, Ar), 7.22 (t, 2H, Ar), 7.42 (t, 2H, Ar), 8.36 (d, 2H, Ar); ^{1}H NMR (C_6D_6) for **126$_1$** (partial assignment): δ = 3.83 (m, 2H, CH-α of Cp), 4.16 (m, 2H, CH-α of Cp), 4.25 (m, 2H, CH-β of Cp), 4.29 (m, 2H, CH-β of Cp), 4.34 (m, 2H, CH-β of Cp), 4.53 (m, 2H, CH-β of Cp), 8.49 (d, 2H, Ar). MS (70 eV) of the reaction mixture showed the highest peak at *m/z* at 1034.2 (M^+ of **126$_2$**).

4.18. Synthesis of the [1]FCP 128[176]

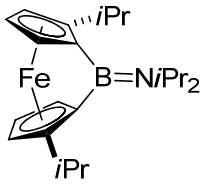

128

Species **120** (0.428 g, 1.00 mmol) was dissolved in a solvent mixture (10 mL of hexanes : thf, 9 : 1) and cooled to 0 °C. A solution of *n*BuLi (2.5 M in hexanes, 0.84 mL, 2.10 mmol) was added dropwise and the reaction mixture was stirred at 0 °C for 30 min. The cold bath was removed and *i*Pr$_2$NBCl$_2$ (0.182 g, 1.04 mmol) was dissolved in hexanes (10 mL) and added dropwise within 10 min via cannula tubing. The color of the solution changed from orange to red, along with formation of a colorless precipitate. The reaction was strirred for 15 min at r. t. All volatiles were removed and the resulting red residue was dissolved in hexanes (10 mL). All solids were removed by filtration, solvents were removed under vacuum, and the product sublimed (80 °C oil bath temperature; p ~ 10^{-2} mbar) to give red-purple crystals (0.076 g, 20%), which were suitable for X-ray analysis. ^{1}H NMR (C_6D_6): δ = 1.20 (d, 6H, CH_3), 1.23 (d, 6H, CH_3), 1.28 (d, 6H, CH_3), 1.39 (d, 6H, CH_3), 2.40 (sept, 2H, CH), 3.50 (m, 2H, CH-α of Cp), 3.99 (sept, 2H, CH), 4.30 (m, 2H, CH-β of Cp), 4.53 ppm (m, 2H, CH-β of Cp); ^{13}C NMR ([D_8]toluene): δ =

22.42 [CH($\underline{C}H_3)_2$], 24.37 [CH($\underline{C}H_3)_2$], 24.50 [CH($\underline{C}H_3)_2$], 27.30 [CH($\underline{C}H_3)_2$], 30.05 [$\underline{C}H(CH_3)_2$], 39.9 (*ipso*-Cp, B), 48.03 [N$\underline{C}H(CH_3)_2$], 71.16 (C-β of Cp), 76.26 (C-β of Cp), 79.82 (C-α of Cp), 101.25 ppm (*ipso*-Cp, *i*Pr). ^{11}B NMR (C_6D_6): δ = 39.5 ppm; UV/Vis (toluene): λ_{max} (ε) = 495 nm (347 L mol^{-1} cm^{-1}); MS (70 eV): *m/z* (%): 379 (100) [M^+], 278 (8) [M^+ - N*i*Pr$_2$], 237 (10) [M^+ - N*i*Pr$_2$ - *i*Pr]; HRMS (70 eV): *m/z* calcd for $C_{22}H_{34}BFeN$: 379.2134; found: 379.2123; elemental anal. calcd (%) for $C_{22}H_{34}BFeN$ (379.168): C 69.69, H 9.04, N 3.69; found: C 69.71, H 8.71, N 3.55.

4.19. Optimized Synthesis of the [1]FCP 128[176]

*n*BuLi (2.5 M in hexanes, 0.85 mL, 2.1 mmol) was added dropwise to a cold (0 ºC) solution of **120** (0.433 g, 1.01 mmol) in a mixture of thf (1.0 mL) and hexanes (9.0 mL). The reaction mixture was stirred at 0 ºC for 30 min, resulting in an orange solution. The cold bath was removed and replaced with a preheated oil bath (50 ºC), followed by stirring of the solution for 10 min. A solution of *i*Pr$_2$NBCl$_2$ (0.190 g, 1.04 mmol) in hexanes (10 mL) was added dropwise within 10 min applying a syringe pump. The reaction color changed from orange to dark-red along with formation of a white precipitate. After the reaction mixture was stirred at r.t. for 20 min, all volatiles were removed, and the resulting red residue was dissolved in hexanes (10 mL). All solids were removed by filtration, solvents were removed under vacuum, and the product sublimed (80 °C oil bath temperature; p ~ 10^{-2} mbar) to give red-purple crystals (0.202 g, 53%).

4.20. Synthesis of the [1]FCP 132[176]

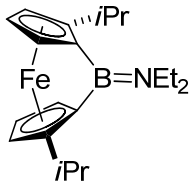

132

*n*BuLi (2.5 M in hexanes, 0.88 mL, 2.2 mmol) was added dropwise to a cold (0 ºC) solution of **120** (0.447 g, 1.04 mmol) in a mixture of thf (1.0 mL) and hexanes (9.0 mL). The reaction mixture was stirred at 0 ºC for 30 min, resulting in an orange solution. The cold bath was removed and replaced with a preheated oil bath (50 ºC), followed by stirring of the solution for 10 min. A solution of Et_2NBCl_2 (0.167 g, 1.09 mmol) in hexanes (10 mL) was added dropwise within 10 min applying a syringe pump. The reaction color changed from orange to dark-red along with formation of a white precipitate. After the reaction mixture was stirred at r.t. for 20 min, all volatiles were removed, and the resulting red residue was dissolved in hexanes (10 mL). After the removal of LiCl by filtration, the solvent was removed under vacuum, followed by a flask-to-flask condensation (55 °C oil bath temperature; p ~ 10^{-2} mbar) to yield **132** as a red oil, which was contaminated with approx 7% of $(iPrH_4C_5)_2Fe$ (0.256 g of total mass; 0.241g (calc) of pure **132**; 66% yield). ^{1}H NMR (C_6D_6): δ = 1.04 (t, 6H, $NCH_2C\underline{H}_3$), 1.17 [d, 6H, $CH(C\underline{H}_3)_2$], 1.31 [d, 6H, $CH(C\underline{H}_3)_2$], 2.34 [sept, 2H, $C\underline{H}(CH_3)_2$], 3.41 (m, 4H, $NC\underline{H}_2CH_3$), 3.43 (m, 2H, CH-α of Cp), 4.29 (m, 2H, CH-β of Cp), 4.52 (m, 2H, CH-β of Cp) ppm; ^{13}C NMR (C_6D_6): δ = 15.83 ($NCH_2\underline{C}H_3$), 21.87 [$CH(\underline{C}H_3)_2$], 27.57 [$CH(\underline{C}H_3)_2$], 30.20 [$\underline{C}H(CH_3)_2$], 39.9 (br., *ipso*-Cp, B), 41.78 ($N\underline{C}H_2CH_3$), 71.33 (C-β of Cp), 76.13 (C-β of Cp), 80.03 (C-α of Cp), 101.03 (*ipso*-Cp, *i*Pr); ^{11}B NMR (C_6D_6): δ = 40.0 ppm.

4.21. Synthesis of the [1]FCP 133[176]

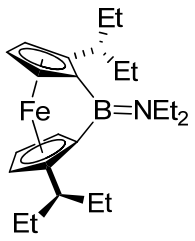

133

*n*BuLi (2.5 M in hexanes, 0.85 mL, 2.1 mmol) was added dropwise to a cold (0 ºC) solution of **130** (0.490 g, 1.01 mmol) in a mixture of thf (1.0 mL) and hexanes (9.0 mL). The reaction mixture was stirred at 0 ºC for 30 min, resulting in an orange solution. The cold bath was removed and replaced with a preheated oil bath (50 ºC), followed by stirring of the solution for 10 min. A solution of Et_2NBCl_2 (0.161 g, 1.05 mmol) in hexanes (10 mL) was added dropwise within 10 min applying a syringe pump. The reaction color changed from orange to dark-red along with formation of a white precipitate. After the reaction mixture was stirred at r.t. for 20 min, all volatiles were removed, and the resulting red residue was dissolved in hexanes (10 mL). After the removal of LiCl by filtration, the resulting solution was concentrated to around 4 mL and left at -80 °C for 48 h, resulting in **133** as a dark-red precipitate (0.260 g, 63%). ^{1}H NMR (C_6D_6): δ = 0.83 [t, 6H, $CH(CH_2C\underline{H}_3)_2$], 1.02 [t, 6H, $CH(CH_2C\underline{H}_3)_2$ or $NCH_2C\underline{H}_3$], 1.05 [t, 6H, $NCH_2C\underline{H}_3$ or $CH(CH_2C\underline{H}_3)_2$], 1.50 – 1.70 [m, 6H, $CH(C\underline{H}_2CH_3)_2$], 2.11 [m, 2H, $C\underline{H}(CH_2CH_3)_2$], 2.19 [m, 2H, $CH(C\underline{H}_2CH_3)_2$], 3.45 (m, 2H, $NC\underline{H}_2CH_3$) 3.53 (m, 2H, CH-α of Cp), 3.56 (m, 2H, $NC\underline{H}_2CH_3$), 4.28 (m, 2H, CH-β of Cp), 4.57 (m, 2H, CH-β of Cp) ppm; ^{13}C NMR (C_6D_6): δ = 9.74 $[CH(CH_2\underline{C}H_3)_2]$, 12.99 $[CH(CH_2\underline{C}H_3)_2]$, 15.64 ($NCH_2\underline{C}H_3$), 25.51 $[CH(\underline{C}H_2CH_3)_2]$, 29.16 $[CH(\underline{C}H_2CH_3)_2]$, 40.7 (br., *ipso*-Cp, B), 41.60 ($N\underline{C}H_2CH_3$), 42.52 $[\underline{C}H(CH_2CH_3)_2]$, 73.31 (C-β of Cp), 76.38 (C-β of Cp), 79.98 (C-α of Cp), 100.13 (*ipso*-Cp, 3-pentyl) ppm; ^{11}B NMR (C_6D_6): δ = 40.3 ppm; MS (70 eV): *m/z* (%): 407 (100) [M^+]; HRMS (70 eV; *m/z*): calcd for $C_{24}H_{38}BFeN$:

407.2441; found: 407.2444; UV/Vis (hexanes): λ_{max} (ε) = 496 nm (478 $Lmol^{-1}cm^{-1}$); elemental analysis calcd (%) for $C_{24}H_{38}BFeN$ (407.22): C 70.79, H 9.41, N 3.44; found: C 70.06, H 9.68, N 3.45.

4.22. Synthesis of the [1]FCP 134[176]

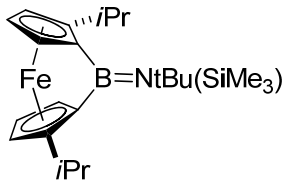

134

*n*BuLi (2.5 M in hexanes, 0.89 mL, 2.2 mmol) was added dropwise to a cold (0 ºC) solution of **120** (0.451 g, 1.05 mmol) in a mixture of thf (1.0 mL) and hexanes (9.0 mL). The reaction mixture was stirred at 0 ºC for 30 min, resulting in an orange solution. The cold bath was removed and replaced with a preheated oil bath (50 ºC), followed by stirring of the solution for 10 min. A solution of [*t*Bu(Me_3Si)N]BCl_2 (0.238 g, 1.05 mmol) in hexanes (10 mL) was added dropwise within 10 min applying a syringe pump. The reaction color changed from orange to red along with formation of a white precipitate. After the reaction mixture was stirred at r.t. for 20 min, all volatiles were removed, and the resulting red residue was dissolved in hexanes (15 mL). After the removal of LiCl by filtration, solvents were removed under vacuum. Flask-to-flask condensation (95 °C oil bath temperature; p ~ 10^{-2} mbar) resulted in condensation of **134** contaminated with (*i*Pr$H_4C_5)_2$Fe and small amounts of other unknown impurities (0.192 g). ^{1}H NMR (C_6D_6): δ = 0.46 (s, 9H, $SiMe_3$), 1.23 [2d, 6H, $CH(C\underline{H}_3)_2$], 1.38 [2d, 6H, $CH(C\underline{H}_3)_2$], 1.57 (s, 9H, *t*Bu), 2.40 [m, 2H, $C\underline{H}(CH_3)_2$], 3.40 (m, 1H, CH-α of Cp), 3.41 (m, 1H, CH-α of Cp), 4.26 (m, 1H, CH-β of Cp), 4.28 (m, 1H, CH-β of Cp), 4.49 (m, 2H, CH-β of Cp) ppm;^{13}C NMR (C_6D_6): δ = 7.77 ($SiMe_3$), 22.77 [$CH(\underline{C}H_3)_2$], 22.84 [$CH(\underline{C}H_3)_2$], 26.88 [$CH(\underline{C}H_3)_2$], 27.14

[CH($\underline{C}H_3)_2$], 29.75 [$\underline{C}H(CH_3)_2$], 30.02 [$\underline{C}H(CH_3)_2$], 34.77 [C($\underline{C}H_3)_3$], 44.1 (br., *ipso*-Cp, B), 45.3 (br., *ipso*-Cp, B), 57.86 [$\underline{C}(CH_3)_3$], 71.10 (C-β of Cp), 71.22 (C-β of Cp), 75.75 (C-β of Cp), 75.86 (C-β of Cp), 78.12 (C-α of Cp), 79.34 (C-α of Cp), 98.80 (*ipso*-Cp, *i*Pr), 99.47 (*ipso*-Cp, *i*Pr) ppm; ^{11}B NMR (C_6D_6): δ = 46.1 ppm.

4.23. Synthesis of the [1]FCP 136[176]

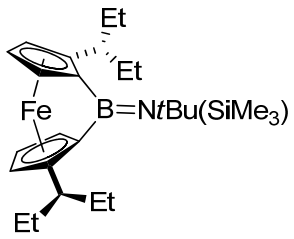

136

*n*BuLi (2.5 M in hexanes, 0.85 mL, 2.1 mmol) was added dropwise to a cold (0 ºC) solution of **130** (0.488 g, 1.01 mmol) in a mixture of thf (1.0 mL) and hexanes (9.0 mL). The reaction mixture was stirred at 0 ºC for 30 min, resulting in an orange solution. The cold bath was removed and replaced with a preheated oil bath (50 ºC), followed by stirring of the solution for 10 min. A solution of [*t*Bu(Me_3Si)N]BCl_2 (0.237 g, 1.05 mmol) in hexanes (10 mL) was added dropwise within 10 min applying a syringe pump. The reaction color changed from orange to dark-red along with formation of a white precipitate. After the reaction mixture was stirred at r.t. for 20 min, all volatiles were removed, and the resulting red residue was dissolved in hexanes (15 mL). After the removal of LiCl by filtration, the resulting solution was concentrated to around 8 mL and left at -80 °C for 16 h, resulting in **136** as a dark-red precipitate (0.234 g, 48%). ^{1}H NMR (C_6D_6): δ = 0.47 (s, 9H, $SiMe_3$), 0.80 [t, 6H, CH($CH_2C\underline{H}_3)_2$], 1.02 [t, 3H, CH($CH_2C\underline{H}_3)_2$], 1.06 [t, 3H, CH($CH_2C\underline{H}_3)_2$], 1.60 [s, 9H, C($C\underline{H}_3)_3$], 1.69 [m, 4H, CH($C\underline{H}_2CH_3)_2$], 1.82 [m, 2H, CH($C\underline{H}_2CH_3)_2$], 2.13 – 2.34 [m, 4H, CH($C\underline{H}_2CH_3)_2$ and

C<u>H</u>(CH_2CH_3)$_2$], 3.43 (m, 1H, CH-α of Cp), 3.47 (m, 1H, CH-α of Cp), 4.25 (m, 1H, CH-β of Cp), 4.26 (m, 1H, CH-β of Cp), 4.50 (m, 1H, CH-β of Cp), 4.51 (m, 1H, CH-β of Cp) ppm; ^{13}C NMR (C_6D_6): δ = 7.70 ($SiMe_3$), 8.86 [CH(CH_2<u>C</u>H_3)$_2$, 9.00 [CH(CH_2<u>C</u>H_3)$_2$], 13.08 [CH(CH_2<u>C</u>H_3)$_2$], 13.20 [CH(CH_2<u>C</u>H_3)$_2$], 24.70 [CH(<u>C</u>H_2CH_3)$_2$], 25.10 [CH(<u>C</u>H_2CH_3)$_2$], 27.47 [CH(<u>C</u>H_2CH_3)$_2$], 27.95 [CH(<u>C</u>H_2CH_3)$_2$], 34.73 [C(<u>C</u>H_3)$_3$], 41.82 [<u>C</u>H(CH_2CH_3)$_2$], 42.01 [<u>C</u>H(CH_2CH_3)$_2$], 42.2 (br., *ipso*-Cp, B), 45.5 (br., *ipso*-Cp, B), 57.87 [<u>C</u>(CH_3)$_3$], 73.61 (C-β of Cp), 73.81 (C-β of Cp), 75.71 (C-β of Cp), 75.75 (C-β of Cp), 78.75 (C-α of Cp), 79.13 (C-α of Cp), 97.10 (*ipso*-Cp, 3-pentyl), 98.24 (*ipso*-Cp, 3-pentyl) ppm; ^{11}B NMR (C_6D_6): δ = 46.5 ppm; MS (70 eV): *m/z* (%): 479 (100) [M^+], 423 (12) [M^+ - *t*Bu + H]; HRMS (70 eV; *m/z*): calcd for $C_{27}H_{46}BFeNSi$: 479.2842; found: 479.2842; UV/Vis (hexanes): λ_{max} (ε) = 487 nm (507 $Lmol^{-1}cm^{-1}$); elemental analysis calcd (%) for $C_{27}H_{46}BFeNSi$ (479.40): C 67.64, H 9.67, N 2.92; found: C 66.64, H 9.78, N 2.87.

4.24. Synthesis of the [1]FCP 138[176]

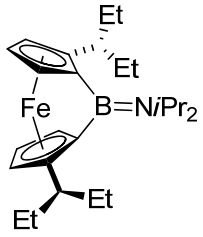

138

*n*BuLi (2.5 M in hexanes, 0.84 mL, 2.1 mmol) was added dropwise to a cold (0 ºC) solution of **130** (0.485 g, 1.00 mmol) in a mixture of thf (1.0 mL) and hexanes (9.0 mL). The reaction mixture was stirred at 0 ºC for 30 min, resulting in an orange solution. The cold bath was removed and replaced with a preheated oil bath (50 ºC), followed by stirring of the solution for 10 min. A solution of *i*Pr_2NBCl_2 (0.190 g, 1.04 mmol) in hexanes (10 mL) was added dropwise

within 10 min applying a syringe pump. The reaction color changed from orange to dark-red along with formation of a white precipitate. After the reaction mixture was stirred at r.t. for 20 min, all volatiles were removed, and the resulting red residue was dissolved in hexanes (10 mL). After the removal of LiCl by filtration, the resulting solution was concentrated to around 8 mL and left at -80 °C for 16 h, resulting in **138** as dark-red crystals (0.289 g, 65%). ^{1}H NMR (C_6D_6): δ = 0.78 [t, 6H, CH($CH_2C\underline{H}_3$)$_2$], 1.03 [t, 6H, CH($CH_2C\underline{H}_3$)$_2$], 1.25 [d, 6H, CH_3 of CH($C\underline{H}_3$)$_2$], 1.30 [d, 6H, CH_3 of CH($C\underline{H}_3$)$_2$], 1.64 [m, 4H, CH($C\underline{H}_2CH_3$)$_2$], 1.77 [m, 2H, CH($C\underline{H}_2CH_3$)$_2$], 2.24 [m, 4H, CH($C\underline{H}_2CH_3$)$_2$ and C$\underline{H}$(CH_2CH_3)$_2$], 3.54 (m, 2H, CH-α of Cp), 4.03 [sept, 2H, C$\underline{H}$(CH_3)$_2$], 4.26 (m, 2H, CH-β of Cp), 4.55 (m, 2H, CH-β of Cp) ppm; ^{13}C NMR (C_6D_6): δ = 8.78 [$CH_2\underline{C}H_3$)$_2$], 13.13 [$CH_2\underline{C}H_3$)$_2$], 24.40 [CH($\underline{C}H_3$)$_2$], 24.66 [CH($\underline{C}H_3$)$_2$], 25.00 [CH($\underline{C}H_2CH_3$)$_2$], 27.98 [CH($\underline{C}H_2CH_3$)$_2$], 40.6 (br., *ipso*-Cp, B), 41.75 [$\underline{C}$H(CH_2CH_3)$_2$], 48.06 [$\underline{C}$H(CH_3)$_2$], 73.59 (C-β of Cp), 76.39 (C-β of Cp), 79.70 (C-α of Cp), 99.64 (*ipso*-Cp, 3-pentyl) ppm; ^{11}B NMR (C_6D_6): δ = 41.2 ppm; MS (70 eV): *m/z* (%): 435 (100) [M^+], 326 (18) [M^+ - BN*i*Pr_2 + 2H]; HRMS (70 eV; *m/z*): calcd for $C_{26}H_{42}BFeN$: 435.2760; found: 435.2759; UV/Vis (hexanes): λ_{max} (ε) = 494 nm (457 $Lmol^{-1}cm^{-1}$); elemental analysis calcd (%) for $C_{26}H_{42}BFeN$ (435.27): C 71.74, H 9.73, N 3.22; found: C 70.91, H 9.77, N 3.19.

4.25. The 0 → r.t. (low temperature) Procedure that Gave the Approximate Product Ratios 138 : 139 as Shown in Table 9[176]

*n*BuLi (2.5 M in hexanes, 0.86 mL, 2.1 mmol) was added dropwise to a cold (0 ºC) solution of **130** (0.495 g, 1.02 mmol) in a mixture of thf (1.0 mL) and hexanes (9.0 mL). The reaction mixture was stirred at 0 ºC for 30 min, resulting in an orange solution. The cold bath was removed and a solution of *i*Pr_2NBCl_2 (0.190 g, 1.04 mmol) in hexanes (10 mL) was added dropwise via cannula tubing over 10 minutes. The reaction color changed from orange to dark-

red along with formation of a white precipitate. After the reaction mixture was stirred at r.t. for 20 min, all volatiles were removed, and the resulting red residue was dissolved in hexanes (10 mL). After the removal of LiCl by filtration, the resulting solution was concentrated to around 8 mL and left at -80 °C for 16 h, resulting in **138** as dark-red crystals (0.192 g, 43%).

4.26. Synthesis of the Bis(boryl)ferrocene 129[176]

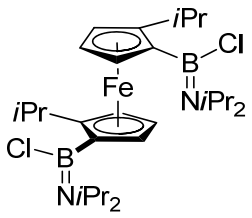

129

*n*BuLi (2.5 M in hexanes, 0.88 mL, 2.2 mmol) was added dropwise to a cold (0 ºC) solution of **120** (0.447 g, 1.04 mmol) in a mixture of thf (1.0 mL) and hexanes (9.0 mL). The reaction mixture was stirred at 0 ºC for 30 min, resulting in an orange solution, and added to a solution (0 ºC) of iPr$_2$NBCl$_2$ (0.570 g, 3.13 mmol) in hexanes (10 mL) within 5 min via a cannula. The reaction mixture was stirred at 0 ºC for 30 min, warmed to r.t., and stirred for another 30 min. All volatiles were removed and the resulting yellow residue was dissolved in hexanes (10 mL). LiCl was removed by filtration and washed with hexanes (2 × 5.0 mL), followed by removal of solvents under vacuum to leave a crystalline orange solid behind. This solid was dissolved in hexanes (2.0 mL) and the solution was left at -22 ºC for 6 days to give a small amount of crystals. The flask with the partly crystallized product was then left for 8 days at -80 ºC to yield orange crystals of **129** (0.324 g, 55%). Note that the high solubility of **129** in hexanes causes a mediocre yield. ^{1}H NMR (C_6D_6): δ = 0.73 [d, 6H, CH(C$\underline{H}_3$)$_2$], 0.96 [d, 6H, CH(C$\underline{H}_3$)$_2$], 1.13 [d, 6H, CH(C$\underline{H}_3$)$_2$], 1.34 [d, 6H, CH(C$\underline{H}_3$)$_2$], 1.48 [d, 6H, CH(C$\underline{H}_3$)$_2$], 1.54 [d, 6H, CH(C$\underline{H}_3$)$_2$], 3.16 [sept, 2H, C$\underline{H}$(C$\underline{H}_3$)$_2$], 3.40 [sept, 2H, C$\underline{H}$(C$\underline{H}_3$)$_2$], 4.23 [sept, 2H, C$\underline{H}$(C$\underline{H}_3$)$_2$], 4.25 (m, 2H, CH

of Cp), 4.29 (m, 2H, CH of Cp), 4.50 (m, 2H, CH of Cp) ppm; ^{13}C NMR (C_6D_6): δ = 21.23 [CH(<u>C</u>H$_3$)$_2$], 21.60 [CH(<u>C</u>H$_3$)$_2$], 22.05 [CH(<u>C</u>H$_3$)$_2$], 23.66 [CH(<u>C</u>H$_3$)$_2$], 23.71 [CH(<u>C</u>H$_3$)$_2$], 27.09 [CH(<u>C</u>H$_3$)$_2$], 27.16 [<u>C</u>H(CH$_3$)$_2$], 46.22 [<u>C</u>H(CH$_3$)$_2$], 51.88 [<u>C</u>H(CH$_3$)$_2$], 67.82 (<u>C</u>H of Cp), 71.19 (<u>C</u>H of Cp), 75.92 (<u>C</u>H of Cp), 76.8 (br., *ipso*-Cp, B), 102.28 (*ipso*-Cp, *i*Pr) ppm; ^{11}B NMR (C_6D_6): δ = 38.0 ppm; MS (70 eV): *m/z* (%): 560 (100) [M^+]; HRMS (70 eV; *m/z*): calcd for $C_{28}H_{48}B_2Cl_2FeN_2$: 560.2759; found: 560.2759; UV/Vis (hexanes): λ_{max} (ε) = 450 nm (216 L mol^{-1} cm^{-1}); elemental analysis calcd (%) for $C_{28}H_{48}B_2Cl_2FeN_2$ (561.07): C 59.94, H 8.62, N 4.99; found: C 60.13, H 8.95, N 4.95.

4.27. Synthesis of the Bis(boryl)ferrocene 135[176]

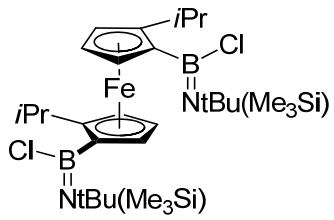

135

*n*BuLi (2.5 M in hexanes, 0.86 mL, 2.1 mmol) was added dropwise to a cold (0 ºC) solution of **120** (0.435 g, 1.02 mmol) in a mixture of thf (1.0 mL) and hexanes (9.0 mL). The reaction mixture was stirred at 0 ºC for 30 min, resulting in an orange solution, and added to a solution (0 ºC) of [*t*Bu(Me$_3$Si)N]BCl$_2$ (0.689 g, 3.05 mmol) in hexanes (10 mL) within 5 min via a cannula. The reaction mixture was stirred at 0 ºC for 30 min, warmed to r.t., and stirred for another 30 min. All volatiles were removed and the resulting yellow residue was dissolved in hexanes (10 mL). LiCl was removed by filtration and washed with hexanes (2 × 5.0 mL), followed by removal of solvents under vacuum to leave a crystalline orange solid behind. This solid was dissolved in hexanes (2.0 mL) and the solution was left at -22 ºC for 6 days to give a small amount of crystals. The flask with the partly crystallized product was then left for 8 days at -80

ºC to yield orange crystals of **135** (0.351 g, 53%, after two batches of crystallization). Note that the high solubility of **135** in hexanes causes a mediocre yield. ^{1}H NMR (C_6D_6): δ = 0.20 (s, 18H, $SiMe_3$), 1.12 [d, 6H, $CH(C\underline{H}_3)_2$], 1.31 [d, 6H, $CH(C\underline{H}_3)_2$], 1.64 (s, 18H, *t*Bu), 1.60 (s, 9H, *t*Bu), 3.56 [sept, 2H, $C\underline{H}(CH_3)_2$], 4.33 (m, 2H, CH of Cp), 4.55 (m, 2H, CH of Cp), 4.56 (m, 2H, CH of Cp) ppm; ^{13}C NMR (C_6D_6): δ = 6.64 ($SiMe_3$), 22.57 [$CH(\underline{C}H_3)_2$], 26.55 [$CH(\underline{C}H_3)_2$], 26.84 [$\underline{C}H(CH_3)_2$], 33.45 [$C(\underline{C}H_3)_3$], 57.07 [$\underline{C}(CH_3)_3$], 74.13 (C of Cp), 75.28 (C of Cp; two peaks overlapping), 77.4 (br., *ipso*-Cp, B), 102.08 (*ipso*-Cp, *i*Pr) ppm; ^{11}B NMR (C_6D_6): δ = 45.3; MS (70 eV): *m/z* (%): 648 (69) [M^+], 459 (22) [M^+ – $BClN(SiMe_3)(t\text{Bu})$ + H], 403 (14) [M^+ – $BClN(SiMe_3)(t\text{Bu})$ – *t*Bu + 2H]; HRMS (70 eV; *m/z*): calcd for $C_{30}H_{56}B_2Cl_2FeN_2Si_2$: 648.2896; found: 648.2897; UV/Vis (hexanes): λ_{max} (ε) = 463 nm (474 $Lmol^{-1}cm^{-1}$); elemental analysis calcd (%) for $C_{30}H_{56}B_2Cl_2FeN_2Si_2$ (648.32): C 55.49, H 8.69, N 4.31; found: C 55.52, H 9.14, N, 4.19.

4.28. Optimized Synthesis of *i*Pr$_2$NBfc[176]

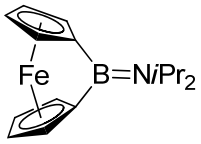

A solution of iPr_2NBCl_2 (0.577 g, 3.17 mmol) in hexanes (10 mL) was added dropwise within 10 min applying a syringe pump to a slurry dilithioferrocene·2/3tmeda (0.876 g, 3.18 mmol) in hexanes (40 mL). The reaction mixture was stirred at this temperature for another 15 min. After the removal of LiCl by filtration, the resulting solution was concentrated to around 40 mL and left at -80 °C for 16 h, resulting in ***i*Pr$_2$NBfc** as a dark-red precipitate (0.691 g, 74%). ^{1}H NMR data matches the reported data.[5]

4.29. Thermal Ring-opening Polymerization of the [1]FCP 133[176]

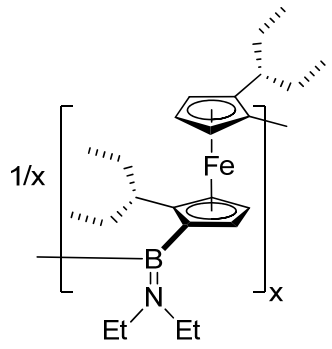

133$_x$

Monomer **133** (110 mg) was heated to 240 ºC for 90 min in a flame-sealed Pyrex NMR tube. The dark-red crystalline powder turned into a dark-orange immobile solid, which was partially soluble in toluene, benzene, and thf. From this part on all manipulations were done under ambient atmosphere. The resulting compound was dissolved in thf (1.0 mL) and precipitated into dry methanol (20 mL) in a Schlenk flask. The methanol phase was syringed off, and the precipitate was taken-up in thf (1.0 mL). This resulted in a suspension that contained particles that were attracted toward an external magnet. This suspension was precipitated into dry methanol (20 mL), the organic phase was syringed off, and the precipitate was taken-up in thf (1.0 mL). This process was repeated one more time. The pre-purified product was taken-up in thf (1.0 mL), and magnetic particles were filtered off by using a 0.2 μm syringe PTFE filter (diameter of 25 mm). This filtration procedure was repeated two more time. After all volatiles were removed, and the product was obtained as an orange solid **133$_x$** (80 mg; ~73%). ^{1}H NMR (C_6D_6): δ = 0.55 - 1.25 [m, 12H, $NCH_2C\underline{H}_3$ and $CH(CH_2C\underline{H}_3)_2$], 1.44 - 1.91 [m, 6H, $CH(C\underline{H}_2CH_3)_2$], 2.05 - 2.53 [m, 4H, $C\underline{H}(CH_2CH_3)_2$ and $CH(C\underline{H}_2CH_3)_2$], 3.21 - 3.77 [m, 6H, $NC\underline{H}_2CH_3$) and CH-α of Cp], 3.86 - 4.31 (m, 4H, CH-β of Cp) ppm; UV/Vis (thf): λ_{max} = 455

nm; elemental analysis calcd (%) for $C_{24}H_{38}BFeN$ (407.24): C 70.79, H 9.41, N 3.44; found: C 68.92, H 9.49, N 2.87 (see main text for discussion on purity).

4.30. Thermal Ring-opening Polymerization of 138[176]

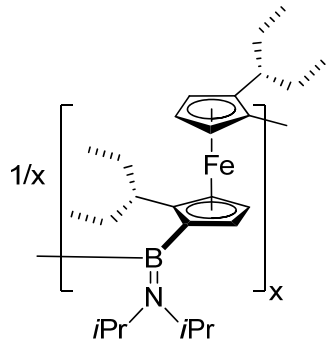

138_x

Monomer **138** (103 mg) was heated to 260 ºC for 90 min in a flame-sealed Pyrex NMR tube. The dark-red crystalline powder turned into a dark-orange immobile solid, which was partially soluble in toluene, benzene, and thf. The crude product was purified as described for **138** (3 times precipitation; 3 times filtration; removal of volatiles) to afford the product as an orange solid **138_x** (72 mg; ~70%). ^{1}H NMR (C_6D_6): δ = 0.53 – 2.10 [m, 30H, $CH(CH_2C\underline{H}_3)_2$ and CH_3 of $CH(C\underline{H}_3)_2$ and $CH(C\underline{H}_2CH_3)_2$], 2.23 – 2.43 [m, 4H, $CH(C\underline{H}_2CH_3)_2$ and $C\underline{H}(CH_2CH_3)_2$], 3.54 [m, 8H, CH-$\alpha$ of Cp and $C\underline{H}(CH_3)_2$] ppm; UV/Vis (thf): λ_{max} = 460 nm; elemental analysis calcd for $C_{26}H_{42}BFeN$ (435.27): C 71.74, H 9.73, N 3.22; found: C 67.25, H 9.51, N 2.49 (see main text for discussion on purity).

4.31. Synthesis of the [1]FCP 140[164]

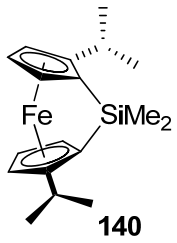

140

Species **120** (0.428 g, 1.00 mmol) was dissolved in a solvent mixture (10 mL of hexanes : thf, 9 : 1) and cooled to 0 °C. A solution of *n*BuLi (2.5 M in hexanes, 0.84 mL, 2.10 mmol) was added dropwise and the reaction mixture was stirred at 0 °C for 30 min. Freshly distilled Me_2SiCl_2 (0.134 g, 1.04 mmol) was added dropwise via syringe within 1 min and the cold bath was removed. The color of the solution immediately changed from orange to red, along with formation of a colorless precipitate. The cold bath was removed and the reaction was stirred for 5 min at r. t. All volatiles were removed under vacuum and the resulting red residue was dissolved in hexanes (10 mL). All solids were removed by filtration, solvents were removed under vacuum, and the product sublimed (55 °C oil bath temperature; p ~ 10^{-2} mbar) to give deep red crystals of **140** (0.260 g, 80%), which were suitable for X-ray analysis. ^{1}H NMR (C_6D_6): δ = 0.52 (s, 6H, $SiMe_2$), 1.10 (d, 6H, $CH\underline{Me}_2$), 1.19 (d, 6H, $CH\underline{Me}_2$), 2.63 (sept, 2H, $C\underline{H}Me_2$), 3.53 (m, 2H, CH-α of Cp), 4.31 (M, 2H, CH-β of Cp), 4.46 ppm (m, 2H, CH-β of Cp); ^{13}C NMR (C_6D_6): δ = -0.12 ($SiCH_3$), 21.58 [$CH(\underline{C}H_3)CH_3$], 27.76 [$CH(CH_3)\underline{C}H_3$], 28.98 [$\underline{C}H(CH_3)_2$], 31.65 (*ipso*-Cp, Si), 73.32 (C-β of Cp), 76.51 (C-β of Cp), 80.55 (C-α of Cp), 104.66 ppm (*ipso*-Cp, *i*Pr); UV/Vis (hexanes): λ_{max} (ε) = 480 nm (250 L mol^{-1} cm^{-1}); MS (70 eV): *m/z* (%): 326 (100) [M^+]; HRMS (70 eV): *m/z* calcd for $C_{18}H_{26}FeSi$: 326.1153; found: 326.1147; elemental anal. calcd (%) for $C_{18}H_{26}FeSi$ (326.330): C 66.25, H 8.03; found: C 65.53, H, 8.29.

4.32. Synthesis of the [1]FCP 141[164]

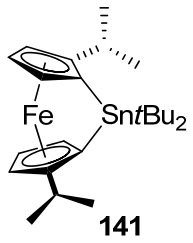

141

Species **120** (0.428 g, 1.00 mmol) was dissolved in a solvent mixture (10 mL of hexanes : thf, 9 : 1) and cooled to 0 °C. A solution of *n*BuLi (2.5 M in hexanes, 0.84 mL, 2.10 mmol) was added dropwise and the reaction mixture was stirred at 0 °C for 30 min. tBu$_2$SnCl$_2$ (0.315 g, 1.04 mmol) was dissolved in diethyl ether (10 mL) and added dropwise within 1 min via cannula tubing and the cold bath was removed. The color of the reaction mixture immediately changed from orange to red, along with formation of a colorless precipitate. The cold bath was removed and the reaction was strirred for 5 min at r. t. All volatiles were removed and the resulting red residue was dissolved in hexanes (10 mL). After removal of all solids through filtration, solvent was removed under vacuum, and the product sublimed (55 °C oil bath temperature; p ~ 10^{-2} mbar) to give red crystals (0.440 g, 88%), which were suitable for X-ray analysis. ^{1}H NMR (C_6D_6): δ = 1.16 (d, 6H, CH_3), 1.35 (d, 6H, CH_3), 1.46 (s, 18H, *t*Bu), 2.68 (sept, 2H, CH), 4.02 (m, 2H, CH-α of Cp), 4.27 (m, 2H, CH-β of Cp), 4.45 ppm (m, 2H, CH-β of Cp); ^{13}C NMR (C_6D_6): δ = 21.77 [CH($\underline{C}H_3$)CH_3], 27.94 [CH(CH_3)$\underline{C}H_3$], 30.67 [$\underline{C}H(CH_3)_2$], 32.17 [C($\underline{CH_3}$)$_3$], 33.77 [$\underline{C}(CH_3)_3$], 36.72 (*ipso*-Cp, Sn), 71.11 (C-β of Cp), 75.92 (C-β of Cp), 80.56 (C-α of Cp), 106.20 ppm (*ipso*-Cp, *i*Pr); UV/Vis (hexanes): λ_{max} (ε) = 474 nm (148 L mol^{-1} cm^{-1}); MS (70 eV): *m/z* (%): 502 (35) [M$^+$], 446 (12) [M$^+$ - *t*Bu], 388 (100) [M$^+$ - 2*t*Bu], 446 (55) [M$^+$ - SntBu$_2$]; HRMS (70 eV): *m/z* calcd for $C_{24}H_{38}FeSn$: 502.1345; found: 502.1348; elemental anal. calcd (%) for $C_{24}H_{38}FeSn$ (501.114): C 57.52, H 7.64; found: C 55.83, H 7.48.

4.33. Synthesis of the [1]FCP 142

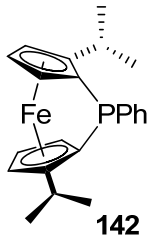

142

*n*BuLi (2.5 M in hexanes, 1.81 mL, 4.51 mmol) was added dropwise to a cold (0 ºC) solution of **120** (0.920 g, 2.15 mmol) in a mixture of thf (2 mL) and hexanes (18 mL). The reaction mixture was stirred at 0 ºC for 30 min, resulting in an orange solution. The reaction mixture was warmed up to r.t. and $PhPCl_2$ (0.400 g, 2.24 mmol) was added dropwise within 2 min via syringe. The reaction color changed from orange to dark-red along with formation of a white precipitate. After the reaction mixture was stirred at r.t. for 20 min, it was transferred to a column packed with silica gel (hexanes/EtOAc 9:1, 10% Et_3N) under N_2 atmosphere. The dark-red fraction was collected from the column and further purified by sublimation at 80 ºC as dark-red crystals (0.470 g 56%).^{1}H NMR (C_6D_6): δ = 0.90 [d, 3H, CH(C$\underline{H}_3$)$_2$], 1.02 [d, 3H, CH(C$\underline{H}_3$)$_2$], 1.19 [d, 3H, CH(C$\underline{H}_3$)$_2$], 1.31 [d, 3H, CH(C$\underline{H}_3$)$_2$], 2.14 [sept, 1H, C$\underline{H}$(CH$_3$)$_2$], 3.50 [sept, 1H, C$\underline{H}$(CH$_3$)$_2$], 4.11 (m, 2H, CH of Cp), 4.17 (m, 1H, CH of Cp), 4.26 (m, 2H, CH of Cp), 4.38 (m, 1H, CH of Cp), 7.01 (m, 1H, *p*-Ph), 7.12 (m, 2H, *m*-Ph), 7.75 (m, 2H, *o*-Ph). ^{13}C NMR (C_6D_6): δ = 15.86 [d, $\underline{C}$-PPh, J(^{13}C/^{31}P) = 51 Hz], 18.65 [d, $\underline{C}$-PPh, J(^{13}C/^{31}P) = 63 Hz], 21.46 [d, $\underline{C}$H(CH$_3$)$_2$, J(^{13}C/^{31}P) = 37 Hz], 27.05 [s, $\underline{C}$H(CH$_3$)$_2$], 27.13 [s, CH($\underline{C}$H$_3$)$_2$], 27.22 [s, CH($\underline{C}$H$_3$)$_2$], 27.27 [s, CH($\underline{C}$H$_3$)$_2$], 27.51 [s, CH($\underline{C}$H$_3$)$_2$], 74.32 (s, Cp), 74.47 (s, Cp), 75.24 [d, Cp, J(^{13}C/^{31}P) = 11 Hz], 76.53 (s, Cp), 83.60 [d, Cp, J(^{13}C/^{31}P) = 19 Hz], 83.77 [d, Cp, J(^{13}C/^{31}P) = 14 Hz], 105.81 [d, $\underline{C}$-*i*Pr, J(^{13}C/^{31}P) = 26 Hz], 107.36 [d, $\underline{C}$-*i*Pr, J(^{13}C/^{31}P) = 9.1 Hz], 127.62 (s, *p*-Ph), 128.56 [d, *m*-Ph, J(^{13}C/^{31}P) = 3.8 Hz], 130.37 [d, *o*-Ph, J(^{13}C/^{31}P) = 16 Hz], 138.17 [d, *ipso*-Ph, J(^{13}C/^{31}P) = 13 Hz]. ^{31}P{^{1}H} NMR (C_6D_6): δ = 8.77. MS (70 eV): *m/z* (%) 376 (100) [M$^+$], 333 (10) [M$^+$ - *i*Pr],

268 (6) [M^+ - PPh]. HRMS (70 eV; m/z): calcd for $C_{22}H_{25}FeP$, 376.104329; found, 376.104292. Elemental Anal. Calcd for $C_{19}H_{27}FeP$ (376.10): C, 70.23; H, 6.70. Found: C, 70.00; H, 7.00.

4.34. Synthesis of the [1]FCP 143

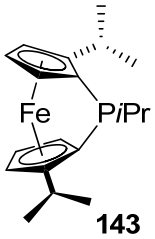

143

*n*BuLi (2.5 M in hexanes, 2.50 mL, 6.24 mmol) was added dropwise to a cold (0 ºC) solution of **120** (1.273 g, 2.97 mmol) in a mixture of thf (3 mL) and hexanes (27 mL). The reaction mixture was stirred at 0 ºC for 30 min, resulting in an orange solution. The reaction mixture was warmed up to r.t. and *i*PrPCl$_2$ (0.448 g, 3.09 mmol) was added dropwise within 2 min via syringe. The reaction color changed from orange to dark-red along with formation of a white precipitate. After the reaction mixture was stirred at r.t. for 20 min, it was transferred to a column packed with silica gel (hexanes, 10% Et_3N) under N_2 atmosphere. The dark-red fraction was collected from the column and further purified by sublimation at 60 ºC as dark-red crystals (0.530 g 52%).^{1}H NMR (C_6D_6): δ = 1.08 [d, 3H, CH(C$\underline{H}_3$)$_2$], 1.16 [d, 3H, CH(C$\underline{H}_3$)$_2$], 1.17 – 1.34 [m, 12H, CH(C$\underline{H}_3$)$_2$], 2.69 [sept, 1H, C$\underline{H}$(CH$_3$)$_2$], 2.78 [sept, 1H, C$\underline{H}$(CH$_3$)$_2$], 3.43 [sept, 1H, C$\underline{H}$(CH$_3$)$_2$], 3.93 (m, 1H, CH of Cp), 3.95 (m, 1H, CH of Cp), 4.16 (m, 1H, CH of Cp), 4.22 (m, 1H, CH of Cp), 4.25 (m, 1H, CH of Cp), 4.37 (m, 1H, CH of Cp). ^{13}C NMR (C_6D_6): δ = 18.28 [d, $\underline{C}$-P*i*Pr, J(^{13}C/^{31}P) = 51 Hz], 18.63 [d, $\underline{C}$H(CH$_3$)$_2$, J(^{13}C/^{31}P) = 13 Hz], 18.64 [d, PCH($\underline{C}$H$_3$)$_2$, J(^{13}C/^{31}P) = 62 Hz], 19.78 [d, $\underline{C}$-P*i*Pr, J(^{13}C/^{31}P) = 62 Hz], 21.68 [d, $\underline{C}$H(CH$_3$)$_2$, J(^{13}C/^{31}P) = 9.1 Hz], 21.72 [d, PCH($\underline{C}$H$_3$)$_2$, J(^{13}C/^{31}P) = 87 Hz], 27.05 [d, $\underline{C}$H(CH$_3$)$_2$, J(^{13}C/^{31}P) = 10 Hz], 27.53 [s, CH($\underline{C}$H$_3$)$_2$], 27.84 [s, CH($\underline{C}$H$_3$)$_2$], 28.57 [s, 2C, CH($\underline{C}$H$_3$)$_2$], 73.80 [d, Cp, J(^{13}C/^{31}P) = 3.4 Hz],

74.06 [d, Cp, $J(^{13}C/^{31}P)$ = 3.4 Hz], 74.96 [d, Cp, $J(^{13}C/^{31}P)$ = 10 Hz], 76.15 (s, Cp), 81.27 [d, Cp, $J(^{13}C/^{31}P)$ = 7.7 Hz], 84.13 [d, Cp, $J(^{13}C/^{31}P)$ = 37 Hz], 105.72 [d, C-*i*Pr, $J(^{13}C/^{31}P)$ = 23 Hz], 106.25 [d, C-*i*Pr, $J(^{13}C/^{31}P)$ = 10 Hz]. $^{31}P\{^{1}H\}$ NMR (C_6D_6): δ = -155.1. MS (70 eV): *m/z* (%) 342 (100) [M^+], 299 (19) [M^+ - *i*Pr], 256 (11) [M^+ - 2*i*Pr]. HRMS (70 eV; m/z): calcd for $C_{19}H_{27}FeP$, 342.119979; found, 342.118604. Elemental Anal. Calcd for $C_{19}H_{27}FeP$ (407.24): C, 66.68; H, 7.95. Found: C, 67.01; H, 8.11.

4.35. Synthesis of the [1]FCP 144

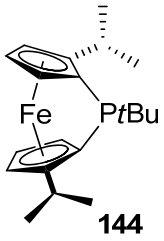

144

*n*BuLi (2.5 M in hexanes, 1.68 mL, 4.21 mmol) was added dropwise to a cold (0 ºC) solution of **120** (0.857 g, 2.00 mmol) in a mixture of thf (2 mL) and hexanes (18 mL). The reaction mixture was stirred at 0 ºC for 30 min, resulting in an orange solution. The reaction mixture was warmed up to r.t. and *t*BuPCl$_2$ (1.0 M in diethylether, 2.10 mL, 2.10 mmol) was added dropwise within 2 min via syringe. The reaction color changed from orange to dark-red along with formation of a white precipitate. After the reaction mixture was stirred at r.t. for 20 min, it was transferred to a column packed with silica gel (hexanes/EtOAc 9:1, 10% Et_3N) under N_2 atmosphere. The dark-red fraction was collected from the column and further purified by flask-to-flask condensation at 80 ºC as dark-red oil (0.514 g 67%). ^{1}H NMR (C_6D_6): δ = 1.09 [d, 3H, $CH(C\underline{H}_3)_2$], 1.16 [d, 3H, $CH(C\underline{H}_3)_2$], 1.27 [m, 6H, $CH(C\underline{H}_3)_2$], 1.42 [d, 9H $C(C\underline{H}_3)_3$], 2.86 [sept, 1H, $C\underline{H}(CH_3)_2$], 3.55 [sept, 1H, $C\underline{H}(CH_3)_2$], 4.00 (m, 1H, CH of Cp), 4.08 (m, 1H, CH of Cp), 4.18 (m, 1H, CH of Cp), 4.22 (m, 2H, CH of Cp), 4.40 (m, 1H, CH of Cp). ^{13}C NMR (C_6D_6): δ = 21.08 [d, C-P*t*Bu,

$J(^{13}C/^{31}P)$ = 57 Hz], 21.58 [d, C$H(CH_3)_2$, $J(^{13}C/^{31}P)$ = 38 Hz], 25.24 [d, C-P*t*Bu, $J(^{13}C/^{31}P)$ = 70 Hz], 26.88 [d, C$H(CH_3)_2$, $J(^{13}C/^{31}P)$ = 14 Hz], 27.56 [s, CH(C$H_3)_2$], 27.57 [s, CH(C$H_3)_2$], 29.00 [s, 2C, CH(C$H_3)_2$], 30.18 [d, 3C, C(C$H_3)_3$, $J(^{13}C/^{31}P)$ = 20 Hz], 31.38 [d, *C*$(CH_3)_3$, $J(^{13}C/^{31}P)$ = 23 Hz], 73.28 [d, Cp, $J(^{13}C/^{31}P)$ = 3.8 Hz], 73.57 [d, Cp, $J(^{13}C/^{31}P)$ = 2.3 Hz], 74.82 [d, Cp, $J(^{13}C/^{31}P)$ = 13 Hz], 76.17 [d, Cp, $J(^{13}C/^{31}P)$ = 1.1 Hz], 84.03 [d, Cp, $J(^{13}C/^{31}P)$ = 7.7 Hz], 85.73 [d, Cp, $J(^{13}C/^{31}P)$ = 48 Hz], 106.02 [d, C-*i*Pr, $J(^{13}C/^{31}P)$ = 11 Hz], 107.21 [d, C-*i*Pr, $J(^{13}C/^{31}P)$ = 27 Hz]. $^{31}P\{^{1}H\}$ NMR (C_6D_6): δ = 29.02. MS (70 eV): *m/z* (%) 356 (100) [M^+], 299 (31) [M^+ - *t*Bu], 256 (17) [M^+ - *i*Pr - *t*Bu]. HRMS (70 eV; m/z): calcd for $C_{20}H_{29}FeP$, 357.130565; found, 357.136799. As **144** was obtained as a viscous oil, a CHN analysis was not measured.

REFERENCES

1. Rinehart, K. L., Jr.; Curby, R. J.,Jr. *J. Am. Chem. Soc.* **1957**, 3290-3291.

2. Rinehart, K. L., Jr.; Frerichs, A. K.; Kittle, P. A.; Westman, L. F.; Gustafson, D. H.; Pruett, R. L.; McMahon, J. E. *J. Am. Chem. Soc.* **1960**, 4111-4112.

3. Osborne, A. G.; Whiteley, R. H. *J. Organomet. Chem.* **1975***, 2,* C27-C28.

4. Braunschweig, H.; Damme, A.; Kupfer, T. *Eur. J. Inorg. Chem.* **2010***, 28,* 4423-4426.

5. Berenbaum, A.; Braunschweig, H.; Dirk, R.; Englert, U.; Green, J. C.; Jäkle, F.; Lough, A. J.; Manners, I. *J. Am. Chem. Soc.* **2000***, 24,* 5765-5774.

6. Schachner, J. A.; Lund, C. L.; Quail, J. W.; Müller, J. *Organometallics* **2005***, 5,* 785-787.

7. Fischer, A. B.; Kinney, J. B.; Staley, R. H.; Wrighton, M. S. *J. Am. Chem. Soc.* **1979***, 22,* 6501-6506.

8. Seyferth, D.; Withers, H. P.,Jr. *J. Organomet. Chem.* **1980***, 1,* C1-C5.

9. Stoeckli-Evans, H.; Osborne, A. G.; Whiteley, R. H. *J. Organomet. Chem.* **1980***, 1,* 91-101.

10. Pudelski, J. K.; Gates, D. P.; Rulkens, R.; Lough, A. J.; Manners, I. *Angew. Chem., Int. Ed.* **1995***, 13,* 1506-1508.

11. Rulkens, R.; Gates, D. P.; Balaishis, D.; Pudelski, J. K.; McIntosh, D. F.; Lough, A. J.; Manners, I. *J. Am. Chem. Soc.* **1997***, 45,* 10976-10986.

12. Foucher, D. A.; Manners, I. *Macromol. Rapid Commun.* **1993***, 2,* 63-66.

13. Jäkle, F.; Rulkens, R.; Zech, G.; Foucher, D. A.; Lough, A. J.; Manners, I. *Chem.–Eur. J.* **1998***, 11,* 2117-2128.

14. Barlow, S.; Drewitt, M. J.; Dijkstra, T.; Green, J. C.; O'Hare, D.; Whittingham, C.; Wynn, H. H.; Gates, D. P.; Manners, I.; Nelson, J. M.; Pudelski, J. K. *Organometallics* **1998***, 10,* 2113-2120.

15. Manners, I. *Adv. Organomet. Chem.* **1995**, 131-168.

16. Wrighton, M. S.; Palazzotto, M. C.; Bocarsly, A. B.; Bolts, J. M.; Fischer, A. B.; Nadjo, L. *J. Am. Chem. Soc.* **1978***, 23,* 7264-7271.

17. Herberhold, M.; Hofmann, T.; Weinberger, S.; Wrackmeyer, B. *Z. Naturforsch., B: Chem. Sci.* **1997***, 9,* 1037-1042.

18. Foucher, D. A.; Tang, B. Z.; Manners, I. *J. Am. Chem. Soc.* **1992***, 15,* 6246-6248.

19. Arsenault, A. C.; Puzzo, D. P.; Manners, I.; Ozin, G. A. *Nat. Photonics* **2007***, 8,* 468-472.

20. MacLachlan, M. J.; Ginzburg, M.; Coombs, N.; Coyle, T. W.; Raju, N. P.; Greedan, J. E.; Ozin, G. A.; Manners, L. *Science* **2000***, 5457,* 1460-1463.

21. Ma, Y.; Dong, W.; Hempenius, M. A.; Moehwald, H.; Vancso, G. J. *Nat. Mater.* **2006***, 9,* 724-729.

22. Rupar, P. A.; Cambridge, G.; Winnik, M. A.; Manners, I. *J. Am. Chem. Soc.* **2011***, 42,* 16947-16957.

23. Rupar, P. A.; Chabanne, L.; Winnik, M. A.; Manners, I. *Science* **2012***, 6094,* 559-562.

24. Patra, S. K.; Ahmed, R.; Whittell, G. R.; Lunn, D. J.; Dunphy, E. L.; Winnik, M. A.; Manners, I. *J. Am. Chem. Soc.* **2011***, 23,* 8842-8845.

25. He, F.; Gädt, T.; Manners, I.; Winnik, M. A. *J. Am. Chem. Soc.* **2011***, 23,* 9095-9103.

26. Qiu, H.; Cambridge, G.; Winnik, M. A.; Manners, I. *J. Am. Chem. Soc.* **2013***, 33,* 12180-12183.

27. Herbert, D. E.; Mayer, U. F. J.; Manners, I. *Angew. Chem., Int. Ed.* **2007***, 27,* 5060-5081.

28. Bellas, V.; Rehahn, M. *Angew. Chem., Int. Ed.* **2007***, 27,* 5082-5104.

29. Musgrave, R. A.; Russell, A. D.; Manners, I. *Organometallics* **2013***, 20,* 5654-5667.

30. Braunschweig, H.; Dirk, R.; Müller, M.; Nguyen, P.; Resendes, R.; Gates, D. P.; Manners, I. *Angew. Chem., Int. Ed.* **1997***, 21,* 2338-2340.

31. Schachner, J. A.; Lund, C. L.; Quail, J. W.; Müller, J. *Organometallics* **2005***, 18,* 4483-4488.

32. Lund, C. L.; Schachner, J. A.; Quail, J. W.; Müller, J. *Organometallics* **2006***, 24,* 5817-5823.

33. Bagh, B.; Gilroy, J. B.; Staubitz, A.; Müller, J. *J. Am. Chem. Soc.* **2010***, 6,* 1794-1795.

34. Bagh, B.; Schatte, G.; Green, J. C.; Müller, J. *J. Am. Chem. Soc.* **2012***, 18,* 7924-7936.

35. Braunschweig, H.; Burschka, C.; Clentsmith, G. K. B.; Kupfer, T.; Radacki, K. *Inorg. Chem.* **2005***, 14,* 4906-4908.

36. Schachner, J. A.; Orlowski, G. A.; Quail, J. W.; Kraatz, H. B.; Müller, J. *Inorg. Chem.* **2006***, 1,* 454-459.

37. Schachner, J. A.; Lund, C. L.; Burgess, I. J.; Quail, J. W.; Schatte, G.; Müller, J. *Organometallics* **2008***, 18,* 4703-4710.

38. Blake, A. J.; Mayers, F. R.; Osborne, A. G.; Rosseinsky, D. R. *J. Chem. Soc., Dalton Trans.* **1982***, 12,* 2379-2383.

39. Calleja, G.; Carre, F.; Cerveau, G.; Corriu, R. J. P. *C. R. Acad. Sci., Ser. IIc.* **1998***, 4,* 285-291.

40. Foucher, D.; Ziembinski, R.; Petersen, R.; Pudelski, J.; Edwards, M.; Ni, Y.; Massey, J.; Jaeger, C. R.; Vancso, G. J.; Manners, I. *Macromolecules* **1994***, 14,* 3992-3999.

41. Zechel, D. L.; Hultszch, K. C.; Rulkens, R.; Balaishis, D.; Ni, Y.; Pudelski, J. K.; Lough, A. J.; Manners, I.; Foucher, D. A. *Organometallics* **1996***, 8,* 1972-1978.

42. Nguyen, P.; Lough, A. J.; Manners, I. *Macromol. Rapid Commun.* **1997***, 11,* 953-959.

43. Berenbaum, A.; Lough, A. J.; Manners, I. *Organometallics* **2002***, 21,* 4415-4424.

44. Jäkle, F.; Vejzovic, E.; Power-Billard, K. N.; MacLachlan, M. J.; Lough, A. J.; Manners, I. *Organometallics* **2000***, 15,* 2826-2828.

45. Hatanaka, Y.; Okada, S.; Minami, T.; Goto, M.; Shimada, K. *Organometallics* **2005***, 6,* 1053-1055.

46. Masson, G.; Herbert, D. E.; Whittell, G. R.; Holland, J. P.; Lough, A. J.; Green, J. C.; Manners, I. *Angew. Chem., Int. Ed.* **2009***, 27,* 4961-4964.

47. Osborne, A. G.; Whiteley, R. H.; Meads, R. E. *J. Organomet. Chem.* **1980***, 3,* 345-357.

48. MacLachlan, M. J.; Lough, A. J.; Geiger, W. E.; Manners, I. *Organometallics* **1998***, 9,* 1873-1883.

49. Masson, G.; Beyer, P.; Cyr, P. W.; Lough, A. J.; Manners, I. *Macromolecules* **2006***, 11,* 3720-3730.

50. Peckham, T. J.; Foucher, D. A.; Lough, A. J.; Manners, I. *Can. J. Chem.* **1995***, 11,* 2069-2078.

51. Pudelski, J. K.; Foucher, D. A.; Honeyman, C. H.; Lough, A. J.; Manners, I.; Barlow, S.; O'Hare, D. *Organometallics* **1995***, 5,* 2470-2479.

52. Schultz, M.; Sofield, C. D.; Walter, M. D.; Andersen, R. A. *New J. Chem.* **2005***, 7,* 919-927.

53. Foucher, D. A.; Edwards, M.; Burrow, R. A.; Lough, A. J.; Manners, I. *Organometallics* **1994***, 12,* 4959-4966.

54. Kapoor, R. N.; Crawford, G. M.; Mahmoud, J.; Dementiev, V. V.; Nguyen, M. T.; Diaz, A. F.; Pannell, K. H. *Organometallics* **1995***, 10,* 4944-4947.

55. Zurcher, S.; Gramlich, V.; Togni, A. *Inorg. Chim. Acta* **1999***, 1-2,* 355-364.

56. Rulkens, R.; Lough, A. J.; Manners, I. *Angew. Chem., Int. Ed.* **1996***, 16,* 1805-1807.

57. Sharma, H. K.; Cervantes-Lee, F.; Mahmoud, J. S.; Pannell, K. H. *Organometallics* **1999***, 3,* 399-403.

58. Clearfield, A.; Simmons, C. J.; Withers, H. P., Jr.; Seyferth, D. *Inorg. Chim. Acta* **1983***, 1,* 139-144.

59. Berenbaum, A.; Jäkle, F.; Lough, A. J.; Manners, I. *Organometallics* **2002***, 12,* 2359-2361.

60. Baumgartner, T.; Jäkle, F.; Rulkens, R.; Zech, G.; Lough, A. J.; Manners, I. *J. Am. Chem. Soc.* **2002***, 34,* 10062-10070.

61. Butler, I. R.; Cullen, W. R.; Einstein, F. W. B.; Rettig, S. J.; Willis, A. J. *Organometallics* **1983***, 1,* 128-135.

62. Brunner, H.; Klankermayer, J.; Zabel, M. *J. Organomet. Chem.* **2000***, 2,* 211-219.

63. Honeyman, C. H.; Foucher, D. A.; Dahmen, F. Y.; Rulkens, R.; Lough, A. J.; Manners, I. *Organometallics* **1995***, 12,* 5503-5512.

64. Patra, S. K.; Whittell, G. R.; Nagiah, S.; Ho, C.; Wong, W.; Manners, I. *Chem.–Eur. J.* **2010***, 10,* 3240-3250.

65. Mizuta, T.; Yamasaki, T.; Nakazawa, H.; Miyoshi, K. *Organometallics* **1996***, 4,* 1093-1100.

66. Mizuta, T.; Yamasaki, T.; Miyoshi, K. *Chem. Lett.* **2000***, 8,* 924-925.

67. Peckham, T. J.; Lough, A. J.; Manners, I. *Organometallics* **1999***, 6,* 1030-1040.

68. Evans, C. E. B.; Lough, A. J.; Grondey, H.; Manners, I. *New J. Chem.* **2000***, 6,* 447-453.

69. F. A. Cotton, G. Wilkinson *Advanced Inorganic Chemistry. A Comprehensive Text,* 5th ed. Wiley-Interscience, New York, **1988**.

70. Bishop, J. J.; Davison, A.; Katcher, M. L.; Lichtenberg, D. W.; Merrill, R. E.; Smart, J. C. *J. Organometal. Chem.* **1971***, 2,* 241-249.

71. Arimoto, F. S.; Haven, A. C.,Jr. *J. Am. Chem. Soc.* **1955**, 6295-6297.

72. Abd-El-Aziz, A. S. *Macromol. Rapid Commun.* **2002***, 17,* 995-1031.

73. Andres, P. R.; Schubert, U. S. *Adv. Mater. (Weinheim, Ger.)* **2004***, 13,* 1043-1068.

74. Hofmeier, H.; Schubert, U. S. *Chem. Soc. Rev.* **2004***, 6,* 373-399.

75. Manners, I. *Science* **2001***, 5547,* 1664-1666.

76. Withers, H. P., Jr.; Seyferth, D.; Fellmann, J. D.; Garrou, P. E.; Martin, S. *Organometallics* **1982***, 10,* 1283-1288.

77. Brandt, P. F.; Rauchfuss, T. B. *J. Am. Chem. Soc.* **1992***, 5,* 1926-1927.

78. Manners, I. *Can. J. Chem.* **1998***, 4,* 371-381.

79. Rosenberg, H.; Rausch, M. D. US Patent 3060215, **1962**.

80. Rosenberg, H. US Patent 3426053, **1969**.

81. Rehahn, M. *Acta Polym.* **1998***, 5,* 201-224.

82. Roesky, H. W.; Lücke, M. *J. Chem. Soc., Chem. Commun.* **1989***, 11,* 748.

83. Roesky, H. W.; Lücke, M. *Angew. Chem., Int. Ed.* **1989***, 4,* 493-494.

84. Rulkens, R.; Lough, A. J.; Manners, I. *J. Am. Chem. Soc.* **1994***, 2,* 797-798.

85. Rulkens, R.; Lough, A. J.; Manners, I.; Lovelace, S. R.; Grant, C.; Geiger, W. E. *J. Am. Chem. Soc.* **1996***, 50,* 12683-12695.

86. Ni, Y.; Rulkens, R.; Manners, I. *J. Am. Chem. Soc.* **1996***, 17,* 4102-4114.

87. Mizuta, T.; Onishi, M.; Miyoshi, K. *Organometallics* **2000***, 24,* 5005-5009.

88. Mizuta, T.; Imamura, Y.; Miyoshi, K.; Yorimitsu, H.; Oshima, K. *Organometallics* **2005***, 5,* 990-996.

89. Tanabe, M.; Manners, I. *J. Am. Chem. Soc.* **2004***, 37,* 11434-11435.

90. Tanabe, M.; Vandermeulen, G. W. M.; Chan, W. Y.; Cyr, P. W.; Vanderark, L.; Rider, D. A.; Manners, I. *Nat. Mater.* **2006***, 6,* 467-470.

91. Reddy, N. P.; Yamashita, H.; Tanaka, M. *J. Chem. Soc., Chem. Commun.* **1995***, 22,* 2263-2264.

92. Ni, Y.; Rulkens, R.; Pudelski, J. K.; Manners, I. *Macromol. Rapid Commun.* **1995***, 9,* 637-641.

93. Gomez-Elipe, P.; Macdonald, P. M.; Manners, I. *Angew. Chem., Int. Ed.* **1997***, 7,* 762-764.

94. Sheridan, J. B.; Temple, K.; Lough, A. J.; Manners, I. *J. Chem. Soc., Dalton Trans.* **1997***, 5,* 711-713.

95. Temple, K.; Jäkle, F.; Sheridan, J. B.; Manners, I. *J. Am. Chem. Soc.* **2001***, 7,* 1355-1364.

96. Temple, K.; Massey, J. A.; Chen, Z.; Vaidya, N.; Berenbaum, A.; Foster, M. D.; Manners, I. *J. Inorg. Organomet. Polym.* **1999***, 4,* 189-198.

97. Heilmann, J. B.; Scheibitz, M.; Qin, Y.; Sundararaman, A.; Jäkle, F.; Kretz, T.; Bolte, M.; Lerner, H.; Holthausen, M. C.; Wagner, M. *Angew. Chem., Int. Ed.* **2006***, 6,* 920-925.

98. Schachner, J. A.; Lund, C. L.; Quail, J. W.; Müller, J. *Acta Crystallogr., Sect. E: Struct. Rep. Online* **2005***, 4,* m682-m684.

99. Schachner, J. A.; Tockner, S.; Lund, C. L.; Quail, J. W.; Rehahn, M.; Müller, J. *Organometallics* **2007***, 18,* 4658-4662.

100. Nelson, J. M.; Rengel, H.; Manners, I. *J. Am. Chem. Soc.* **1993***, 15,* 7035-7036.

101. Lentzner, H. L.; Watts, W. E. *Tetrahedron* **1971***, 18,* 4343-4351.

102. Buretea, M. A.; Tilley, T. D. *Organometallics* **1997***, 7,* 1507-1510.

103. Arisandy, C.; Cowley, A. R.; Barlow, S. *J. Organomet. Chem.* **2004***, 4,* 775-780.

104. Heo, R. W.; Somoza, F. B.; Lee, T. R. *J. Am. Chem. Soc.* **1998***, 7,* 1621-1622.

105. Heo, R. W.; Park, J.; Lee, T. R. *Macromolecules* **2005***, 7,* 2564-2573.

106. Hempenius, M. A.; Brito, F. F.; Vancso, G. J. *Macromolecules* **2003***, 17,* 6683-6688.

107. Ieong, N. S.; Manners, I. *Macromol. Chem. Phys.* **2009***, 13,* 1080-1086.

108. Peckham, T. J.; Massey, J. A.; Edwards, M.; Manners, I.; Foucher, D. A. *Macromolecules* **1996***, 7,* 2396-2403.

109. Gädt, T.; Ieong, N. S.; Cambridge, G.; Winnik, M. A.; Manners, I. *Nat. Mater.* **2009***, 2,* 144-150.

110. Mochida, K.; Shibayama, N.; Goto, M. *Chem. Lett.* **1998***, 4,* 339-340.

111. Cao, L.; Winnik, M. A.; Manners, I. *J. Inorg. Organomet. Polym.* **1998***, 4,* 215-224.

112. Blaser, H.; Brieden, W.; Pugin, B.; Spindler, F.; Studer, M.; Togni, A. *Top. Catal.* **2002***, 1,* 3-16.

113. Blaser, H.; Pugin, B.; Spindler, F. *J. Mol. Catal. A: Chem.* **2005***, 1,* 1-20.

114. Kagan, H. B.; Diter, P.; Gref, A.; Guillaneux, D.; Masson-Szymczak, A.; Rebiere, F.; Riant, O.; Samuel, O.; Taudien, S. *Pure Appl. Chem.* **1996***, 1,* 29-36.

115. Richards, C. J.; Locke, A. J. *Tetrahedron: Asymmetry* **1998***, 14,* 2377-2407.

116. Atkinson, R. C. J.; Gibson, V. C.; Long, N. J. *Chem. Soc. Rev.* **2004***, 5,* 313-328.

117. Stepnicka, P.; Lamac, M.; Cisarova, I. *J. Organomet. Chem.* **2008***, 3,* 446-456.

118. Benkeser, R. A.; Bach, J. L. *J. Am. Chem. Soc.* **1964***, 5,* 890-895.

119. Snieckus, V. *Chem. Rev.* **1990***, 6,* 879-933.

120. Haag, B.; Mosrin, M.; Ila, H.; Malakhov, V.; Knochel, P. *Angew. Chem., Int. Ed.* **2011***, 42,* 9794-9824.

121. Benkeser, R. A.; Fitzgerald, W. P.; Melzer, M. S. *J. Org. Chem.* **1961**, 2569-2571.

122. Slocum, D. W.; Rockett, B. W.; Hauser, C. R. *J. Am. Chem. Soc.* **1965***, 6,* 1241-1246.

123. Behrens, U. *J. Organomet. Chem.* **1979***, 1,* 89-98.

124. Koridze, A. A.; Astakhova, N. M.; Petrovskii, P. V. *J. Organomet. Chem.* **1983***, 3,* 345-360.

125. Xiao, L.; Mereiter, K.; Weissensteiner, W.; Widhalm, M. *Synthesis* **1999***, 8,* 1354-1362.

126. Schaarschmidt, D.; Lang, H. *Organometallics* **2013***, 20,* 5668-5704.

127. Garcia-Alvarez, J.; Kennedy, A. R.; Klett, J.; Mulvey, R. E. *Angew. Chem., Int. Ed.* **2007***, 7,* 1105-1108.

128. Blair, V. L.; Carrella, L. M.; Clegg, W.; Klett, J.; Mulvey, R. E.; Rentschler, E.; Russo, L. *Chem.–Eur. J.* **2009***, 4,* 856-863.

129. Clegg, W.; Conway, B.; Garcia-Alvarez, P.; Kennedy, A. R.; Klett, J.; Mulvey, R. E.; Russo, L. *J. Chem. Soc., Dalton Trans.* **2010***, 1,* 62-65.

130. Mongin, F.; Harrison-Marchand, A. *Chem. Rev.* **2013***, 10,* 7563-7727.

131. Stoll, A. H.; Mayer, P.; Knochel, P. *Organometallics* **2007***, 27,* 6694-6697.

132. Dayaker, G.; Sreeshailam, A.; Chevallier, F.; Roisnel, T.; Krishna, P. R.; Mongin, F. *J. Chem. Soc., Chem. Commun.* **2010***, 16,* 2862-2864.

133. Aratani, T.; Gonda, T.; Nozaki, H. *Tetrahedron Lett.* **1969***, 27,* 2265-2268.

134. Aratani, T.; Gonda, T.; Nozaki, H. *Tetrahedron* **1970***, 23,* 5453-5464.

135. Marquarding, D.; Klusacek, H.; Gokel, G.; Hoffmann, P.; Ugi, I. *J. Am. Chem. Soc.* **1970***, 18,* 5389-5393.

136. Battelle, L. F.; Bau, R.; Gokel, G. W.; Oyakawa, R. T.; Ugi, I. *Angew. Chem., Int. Ed.* **1972***, 2,* 138-140.

137. Battelle, L. F.; Bau, R.; Gokel, G. W.; Oyakawa, R. T.; Ugi, I. K. *J. Am. Chem. Soc.* **1973***, 2,* 482-486.

138. Hayashi, T.; Mise, T.; Fukushima, M.; Kagotani, M.; Nagashima, N.; Hamada, Y.; Matsumoto, A.; Kawakami, S.; Konishi, M.; et al. *Bull. Chem. Soc. Jpn.* **1980***, 4,* 1138-1151.

139. Hayashi, T.; Yamamoto, A.; Hojo, M.; Ito, Y. *J. Chem. Soc., Chem. Commun.* **1989***, 8,* 495-496.

140. Hayashi, T.; Yamamoto, A.; Hojo, M.; Kishi, K.; Ito, Y.; Nishioka, E.; Miura, H.; Yanagai, K. *J. Organomet. Chem.* **1989***, 1-3,* 129-139.

141. Schwink, L.; Knochel, P. *Tetrahedron Lett.* **1996***, 1,* 25-28.

142. Schwink, L.; Knochel, P. *Chem.–Eur. J.* **1998***, 5,* 950-968.

143. Gleiter, R.; Bleiholder, C.; Rominger, F. *Organometallics* **2007***, 20,* 4850-4859.

144. Gokel, G. W.; Marquarding, D.; Ugi, I. K. *J. Org. Chem.* **1972***, 20,* 3052-3058.

145. Mernyi, A.; Kratky, C.; Weissensteiner, W.; Widhalm, M. *J. Organomet. Chem.* **1996***, 1,* 209-218.

146. Valkovich, P. B.; Gokel, G. W.; Ugi, I. K. *Tetrahedron Lett.* **1973***, 31,* 2947-2950.

147. Lotz, M.; Ireland, T.; Tappe, K.; Knochel, P. *Chirality* **2000***, 5,* 389-395.

148. Kloetzing, R. J.; Lotz, M.; Knochel, P. *Tetrahedron: Asymmetry* **2003***, 2,* 255-264.

149. Kealy, T. J.; Pauson, P. L. *Nature* **1951**, 1039-1040.

150. Miller, S. A.; Tebboth, J. A.; Tremaine, J. F. *J. Chem. Soc.* **1952**, 632-635.

151. Woodward, R. B.; Rosenblum, M.; Whiting, M. C. *J. Am. Chem. Soc.* **1952**, 3458-3459.

152. Itsuno, S.; Ito, K.; Hirao, A.; Nakahama, S. *J. Chem. Soc., Chem. Commun.* **1983***, 8,* 469-470.

153. Corey, E. J.; Bakshi, R. K.; Shibata, S. *J. Am. Chem. Soc.* **1987***, 18,* 5551-5553.

154. Corey, E. J.; Bakshi, R. K.; Shibata, S.; Chen, C. P.; Singh, V. K. *J. Am. Chem. Soc.* **1987***, 25,* 7925-7926.

155. Nefedova, M. N.; Mamed'yarova, I. A.; Petrovskii, P. P.; Sokolov, V. I. *J. Organomet. Chem.* **1992***, 1,* 125-130.

156. Wright, J.; Frambes, L.; Reeves, P. *J. Organomet. Chem.* **1994***, 2,* 215-217.

157. Ohno, A.; Yamane, M.; Hayashi, T.; Oguni, N.; Hayashi, M. *Tetrahedron: Asymmetry* **1995***, 10,* 2495-2502.

158. Woltersdorf, M.; Kranich, R.; Schmalz, H. *Tetrahedron* **1997***, 21,* 7219-7230.

159. Soai, K.; Hayase, T.; Takai, K.; Sugiyama, T. *J. Org. Chem.* **1994***, 25,* 7908-7909.

160. Kang, J.; Lee, J. H.; Choi, J. S. *Tetrahedron: Asymmetry* **2001***, 1,* 33-35.

161. Kang, J.; Lee, J. H.; Im, K. S. *J. Mol. Catal. A: Chem.* **2003***, 2,* 55-63.

162. Bailey, W. F.; Luderer, M. R.; Jordan, K. P. *J. Org. Chem.* **2006***, 7,* 2825-2828.

163. Matsumoto, T.; Tanaka, K.; Chujo, Y. *J. Am. Chem. Soc.* **2013***, 11,* 4211-4214.

164. Sadeh, S.; Schatte, G.; Müller, J. *Chem.–Eur. J.* **2013***, 40,* 13408-13417.

165. Baerends, E. J.; Ellis, D. E.; Ros, P. *Chem. Phys.* **1973***, 1,* 41-51.

166. Te Velde, G.; Baerends, E. J. *J. Comput. Phys.* **1992***, 1,* 84-98.

167. Matas, I.; Whittell, G. R.; Partridge, B. M.; Holland, J. P.; Haddow, M. F.; Green, J. C.; Manners, I. *J. Am. Chem. Soc.* **2010***, 38,* 13279-13289.

168. Bagh, B.; Sadeh, S.; Green, J. C.; Müller, J. *Chem.–Eur. J.* **2014***, 8,* 2318-2327.

169. Lorbach, A.; Huebner, A.; Wagner, M. *J. Chem. Soc., Dalton Trans.* **2012***, 20,* 6048-6063.

170. Tanaka, K.; Chujo, Y. *Macromol. Rapid Commun.* **2012***, 15,* 1235-1255.

171. Jäkle, F. *Chem. Rev.* **2010***, 7,* 3985-4022.

172. Honeyman, C. H.; Peckham, T. J.; Massey, J. A.; Manners, I. *J. Chem. Soc., Chem. Commun.* **1996***, 22,* 2589-2590.

173. Mizuta, T.; Imamura, Y.; Miyoshi, K. *J. Am. Chem. Soc.* **2003***, 8,* 2068-2069.

174. Braunschweig, H.; von Koblinski, C.; Englert, U. *J. Chem. Soc., Chem. Commun.* **2000***, 12,* 1049-1050.

175. Paetzold, P. *Adv. Inorg. Chem.* **1987**, 123-170.

176. Sadeh, S.; Bhattacharjee, H.; Khozeimeh Sarbisheh, E.; Quail, J. W.; Müller, J. *Chem.–Eur. J.* **2014** DOI: 10.1002/chem.201404222.

177. Finckh, W.; Tang, B. Z.; Foucher, D. A.; Zamble, D. B.; Ziembinski, R.; Lough, A.; Manners, I. *Organometallics* **1993***, 3,* 823-829.

178. Peckham, T. J.; Massey, J. A.; Honeyman, C. H.; Manners, I. *Macromolecules* **1999***, 9,* 2830-2837.

179. Khozeimeh Sarbisheh, E.; Green, J. C.; Müller, J. *Organometallics* **2014***, 13,* 3508-3513.

180. Brown, D. S.; Decken, A.; Cowley, A. H. *J. Am. Chem. Soc.* **1995***, 19,* 5421-5422.

181. Cowley, A. H.; Gabbai, F. P.; Isom, H. S.; Decken, A.; Culp, R. D. *Main Group Chem.* **1995***, 1,* 9-19.

182. Butler, I. R.; Cullen, W. R.; Ni, J.; Rettig, S. J. *Organometallics* **1985***, 12,* 2196-2201.

183. Niedenzu, K.; Dawson, J. W. *J. Am. Chem. Soc.* **1959**, 3561-3564.

184. Neilson, R. H.; Wells, R. L. *Syn. Inorg. Metal-Org. Chem.* **1973***, 3,* 283-289.

185. Massey, J. A.; Kulbaba, K.; Winnik, M. A.; Manners, I. *J. Polym. Sci., Part B: Polym. Phys.* **2000***, 23,* 3032-3041.

186. Burchard, W. *Adv. Polym. Sci.* **1999***, Branched Polymers II,* 113-194.

187. Versluis, L.; Ziegler, T. *J. Chem. Phys.* **1988***, 1,* 322-328.

188. Snijders, J. G.; Baerends, E. J.; Ros, P. *Mol. Phys.* **1979***, 6,* 1909-1929.

189. Ziegler, T.; Baerends, E. J.; Snijders, J. G.; Ravenek, W.; Tschinke, V. *J. Phys. Chem.* **1989***, 8,* 3050-3056.

190. Vosko, S. H.; Wilk, L.; Nusair, M. *Can. J. Phys.* **1980***, 8,* 1200-1211.

191. Becke, A. D. *Phys. Rev. A: Gen. Phys.* **1988***, 6,* 3098-3100.

192. Farrugia, L. J. *J. Appl. Crystallogr.* **1997***, 5, 30,* 565.